THE ROLE OF IMMUNE CELLS IN HEPATIC ISCHEMIA REPERFUSION

EDITED BY: Tao Qiu, Helong Dai, Zhiyong Guo, Bibo Ke and Qiang Wei
PUBLISHED IN: Frontiers in Immunology

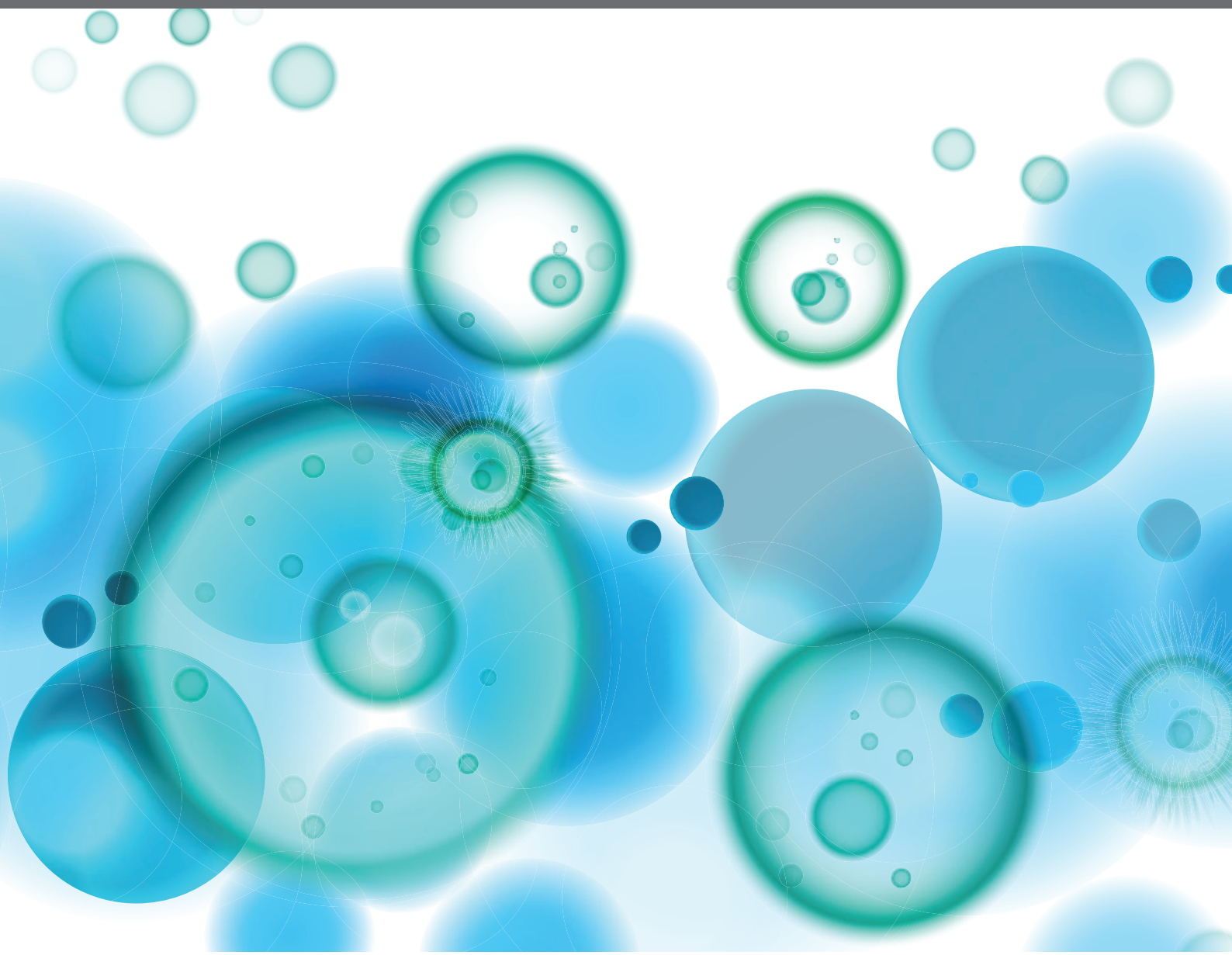

frontiers Research Topics

frontiers

ISSN 1664-8714
ISBN 978-2-83250-817-6
DOI 10.3389/978-2-83250-817-6

About Frontiers

Frontiers is more than just an open-access publisher of scholarly articles: it is a pioneering approach to the world of academia, radically improving the way scholarly research is managed. The grand vision of Frontiers is a world where all people have an equal opportunity to seek, share and generate knowledge. Frontiers provides immediate and permanent online open access to all its publications, but this alone is not enough to realize our grand goals.

Frontiers Journal Series

The Frontiers Journal Series is a multi-tier and interdisciplinary set of open-access, online journals, promising a paradigm shift from the current review, selection and dissemination processes in academic publishing. All Frontiers journals are driven by researchers for researchers; therefore, they constitute a service to the scholarly community. At the same time, the Frontiers Journal Series operates on a revolutionary invention, the tiered publishing system, initially addressing specific communities of scholars, and gradually climbing up to broader public understanding, thus serving the interests of the lay society, too.

Dedication to Quality

Each Frontiers article is a landmark of the highest quality, thanks to genuinely collaborative interactions between authors and review editors, who include some of the world's best academicians. Research must be certified by peers before entering a stream of knowledge that may eventually reach the public - and shape society; therefore, Frontiers only applies the most rigorous and unbiased reviews.
Frontiers revolutionizes research publishing by freely delivering the most outstanding research, evaluated with no bias from both the academic and social point of view. By applying the most advanced information technologies, Frontiers is catapulting scholarly publishing into a new generation.

What are Frontiers Research Topics?

Frontiers Research Topics are very popular trademarks of the Frontiers Journals Series: they are collections of at least ten articles, all centered on a particular subject. With their unique mix of varied contributions from Original Research to Review Articles, Frontiers Research Topics unify the most influential researchers, the latest key findings and historical advances in a hot research area! Find out more on how to host your own Frontiers Research Topic or contribute to one as an author by contacting the Frontiers Editorial Office: frontiersin.org/about/contact

THE ROLE OF IMMUNE CELLS IN HEPATIC ISCHEMIA REPERFUSION

Topic Editors:
Tao Qiu, Renmin Hospital of Wuhan University, China
Helong Dai, Central South University, China
Zhiyong Guo, The First Affiliated Hospital of Sun Yat-sen University, China
Bibo Ke, University of California, Los Angeles, United States
Qiang Wei, Zhejiang University School of Medicine, China

Citation: Qiu, T., Dai, H., Guo, Z., Ke, B., Wei, Q., eds. (2022). The Role of Immune Cells in Hepatic Ischemia Reperfusion. Lausanne: Frontiers Media SA.
doi: 10.3389/978-2-83250-817-6

Table of Contents

frontiers | Frontiers in Immunology

TYPE Editorial
PUBLISHED 04 November 2022
DOI 10.3389/fimmu.2022.1075984

OPEN ACCESS

EDITED AND REVIEWED BY
Kojiro Nakamura,
Kyoto University, Japan

*CORRESPONDENCE
Tao Qiu
qiutao@whu.edu.cn

SPECIALTY SECTION
This article was submitted to Molecular Innate Immunity, a section of the journal Frontiers in Immunology

RECEIVED 21 October 2022
ACCEPTED 26 October 2022
PUBLISHED 04 November 2022

CITATION
Ke B, Dai H, Wei Q, Guo Z and Qiu T (2022) Editorial: The role of immune cells in hepatic ischemia reperfusion. *Front. Immunol.* 13:1075984. doi: 10.3389/fimmu.2022.1075984

Editorial: The role of immune cells in hepatic ischemia reperfusion

Bibo Ke[1], Helong Dai[2], Qiang Wei[3], Zhiyong Guo[4] and Tao Qiu[5]*

[1]The Dumont-UCLA Transplant Center, Division of Liver and Pancreas Transplantation, Department of Surgery, David Geffen School of Medicine at the University of California at Los Angeles, Los Angeles, CA, United States, [2]Department of Kidney Transplantation, The Second Xiangya Hospital of Central South University, Changsha, China, [3]Department of Hepatobiliary and Pancreatic Surgery, The Center for Integrated Oncology and Precision Medicine, Affiliated Hangzhou First People's Hospital, Zhejiang University School of Medicine, Hangzhou, China, [4]Organ Transplant Center, the First Affiliated Hospital, Sun Yat-sen University, Guangzhou, China, [5]Department of Organ Transplantation, Renmin Hospital of Wuhan University, Wuhan, China

KEYWORDS

liver, ischemia reperfusion injury, immune cells, macrophages, innate lymphoid cells, natural killer cells, hepatic stellate cells

Editorial of the Research Topic
The role of immune cells in hepatic ischemia reperfusion

We are honored to accept twelve articles on the Research Topic of "*The role of immune cells in hepatic ischemia-reperfusion*," which have received widespread interest. Hepatic ischemia-reperfusion (I/R) injury is a pathological process involved in oxidative stress-induced cellular damage and immune activation during liver resection and transplantation. We have known that the generation of reactive oxygen species (ROS) from oxidative stress may be critical mediators during hepatic IR. However, there is growing interest in the roles of immune cells in IR-triggered liver inflammation and injury.

Liver resection and transplantation are the most effective treatments for patients with hepatocellular carcinoma. However, there is still a high recurrence rate after surgery, of which liver IR injury is closely related to liver cancer recurrence. Immune activation is crucial in the inflammatory damage process of liver I/R. The intense and sustained inflammatory response promotes tumor recurrence by activating tumor cell proliferation, adhesion, invasion, angiogenesis, and immune escape by many key inflammatory components. Targeting critical immune and inflammatory signaling pathways reduces I/R-induced liver inflammation and injury and prevents tumor recurrence after liver surgery, suggesting a promising win-win strategy (Chen et al.). The severity of I/R injury in the liver is primarily determined by the ratio of M1 to M2 macrophages. Hepatic I/R injury triggers the release of Damage-associated molecular patterns (DAMPs) that strongly activate the NLRP3 inflammasome. This essential molecule functions as a critical component of the innate immune response in hepatic macrophages. Increasing autophagy in

hepatic macrophages can effectively alleviate liver I/R injury with depressed NLRP3 inflammasome activation (Wu et al.).

Moreover, macrophages are partially differentiated into M2 macrophages toward an anti-inflammatory phenotype and maintain environmental homeostasis. A novel study by Zhang et al. found that group 2 innate lymphoid cells (ILC2s) could induce polarization of M2-type $CD45^{+}CD11B^{+}F4/80^{high}$ macrophages and that ILC2s proliferation was regulated by stimulation of exogenous IL-33 to exert a protective effect during hepatic I/R. This regulatory mechanism was found in the liver and the spleen. M1 macrophages are pro-inflammatory and play an essential role in activating liver inflammation during I/R. Liraglutide, a glucagon-like peptide-1 analogue, significantly inhibited the polarization of M1-type macrophages during hepatic I/R injury *via* the GLP-1 receptor, thereby improving hepatic I/R injury (Li et al.). The metabolic roles of intestinal microorganisms can produce substances with anti-hepatic I/R injury. Intestinal microorganisms break down inulin into short-chain fatty acids, one of the metabolites of which, propionic acid (PA), has a pro-inflammatory effect on macrophages. Inulin helps to regulate the gut microbes to maximize their effect. PA enters the portal vein to ameliorate I/R injury in the liver effectively. More importantly, PA directly inhibits TLR-4-HMGB1-mediated inflammatory responses in macrophages (Kawasoe et al.).

During hepatic I/R, DAMPs eventually lead to neutrophil activation and infiltration into the liver. The formation of neutrophil extracellular traps (NETs) released by neutrophils is critical in triggering an inflammatory response by releasing related enzymes and activating the complement system. NETs can also activate platelets leading to systemic immune thrombosis and organ damage. Neutrophils and NETs interact with other immune components of the tumor microenvironment in the transplanted liver to promote tumor progression (Kaltenmeier et al.).

Natural killer (NK) cells play a pivotal role in activating liver immune cells after reperfusion. NK cells can be recruited to the liver, increasing pro-inflammatory cytokine secretion and inducing early infiltration of neutrophils to exacerbate an inflammatory injury. Donor-derived NK cells are also gradually replaced by recipient NK cells after allogeneic liver transplantation, eventually exerting the negative effect of immunological rejection. NK cell depletion, inhibition of NK cell activation receptors, or blockade of signaling pathways for NK cell maturation can effectively reduce liver I/R injury (Huang et al.).

Hepatic stellate cells (HSCs) regulate liver I/R injury during the injury and repair/regeneration phases, depending on regulating different pathways and molecules. HSCs are activated and respond to signals from Kupffer cells during hepatic I/R. HSCs promote early I/R-induced injury by activating the ROCK-mediated hepatic microenvironment, ET-1 signaling, and the TNF-α-triggered inflammatory cascade. HSC-derived MMPs exacerbate injury by destroying ECM and recruiting leukocytes. However, the role of HSCs in the repair and regeneration phase deserves attention. The induction of HSC activation and proliferation by hepatic Kupffer cells also has a vital role in this process (Peng et al.). HSCs are the primary source of repairing myofibroblasts after injury. Shi et al. first reveal that phosphorylation of mixed lineage kinase domain-like protein (p-MLKL) is expressed in the periportal area. Activation of p-MLKL induces necroptotic cell death after liver transplant reperfusion. They also demonstrate that p-MLKL activates fibroblasts, a primary cell type that can effectively predict early graft injury during hepatic I/R.

The therapeutic effect of bio-nanomaterials on I/R injury of the liver has shown advantages over conventional molecules in various aspects and has good efficacy. Huang et al. showed that the Prussian blue (PB) is a good scavenger of ROS, which can reduce ROS production in hepatocytes and macrophages caused by various stimuli. PB reduces neutrophil infiltration, promotes M2 macrophage polarization, and ameliorates Hepatic I/R injury. Moreover, PB has good biocompatibility compared to other nanomaterials, suggesting that PB may be a potential therapeutic agent in managing hepatic I/R injury. Liggett et al. showed that steatotic donor livers are more susceptible to I/R-induced liver damage during transplantation. Type 1 Natural Killer T-cells (NKT1 cells) responses to endogenous lipid antigens mediate the exacerbation of I/R injury in the liver. Oral administration of N-acetylcysteine significantly reduced liver steatosis and downregulated CD1d to block NKT cell activation and reduce IFN-γ levels by using a reliable high-fat diet mouse model of liver I/R injury, thereby reducing damage. This study provides novel insights into the interplay between liver metabolism, I/R injury, and immune cells. In another study of steatotic donor livers, mice on a high-fat diet were found to significantly increase in type 1 Innate lymphoid cells (ILC1s) populations but not conventional natural killer cells after I/R injury, and ILC1 promotes inflammatory injury through T-bet-dependent forms of IFN-γ and TNF-α secretion. Furthermore, ILC1s is an intrinsic inflammatory effector subgroup in fatty liver. Targeting this immune subgroup provides evidence of the future use of marginal donor liver transplantation in the steatotic liver (Kang et al.).

The role of immune cells in hepatic I/R injury has been increasingly appreciated, particularly affecting innate immunity and adaptive immunity during hepatic I/R injury. However, the complex regulatory mechanisms between immune cells and hepatocytes in IR-triggered liver inflammation and injury are still unclear. Under this research theme, we have gained an initial understanding of the function of immune cells. Further study needs to identify the molecular regulators of immune activation and provide novel therapeutic approaches targeting immune cells for treating I/R-induced liver inflammatory injury.

Author contributions

TQ: writing the original manuscript. BK: writing and revising the manuscript. HD, QW, and ZG: supervision.

All authors contributed to the article and approved the submitted version.

Conflict of interest

The authors declare that the research was conducted in the absence of any commercial or financial relationships that could be construed as a potential conflict of interest.

Publisher's note

frontiers in Immunology

REVIEW
published: 28 March 2022
doi: 10.3389/fimmu.2022.870038

Natural Killer Cells in Hepatic Ischemia-Reperfusion Injury

Miao Huang[1,2†], *Hao Cai*[1†], *Bing Han*[1†], *Yuhan Xia*[1], *Xiaoni Kong*[2*] *and Jinyang Gu*[1*]

[1] Department of Transplantation, Xinhua Hospital Affiliated to Shanghai Jiao Tong University School of Medicine, Shanghai, China, [2] Central Laboratory, Department of Liver Diseases, Shuguang Hospital Affiliated to Shanghai University of Traditional Chinese Medicine, Shanghai, China

Ischemia-reperfusion injury can be divided into two phases, including insufficient supply of oxygen and nutrients in the first stage and then organ injury caused by immune inflammation after blood flow recovery. Hepatic ischemia-reperfusion is an important cause of liver injury post-surgery, consisting of partial hepatectomy and liver transplantation, and a central driver of graft dysfunction, which greatly leads to complications and mortality after liver transplantation. Natural killer (NK) cells are the lymphocyte population mainly involved in innate immune response in the human liver. In addition to their well-known role in anti-virus and anti-tumor defense, NK cells are also considered to regulate the pathogenesis of liver ischemia-reperfusion injury under the support of more and more evidence recently. The infiltration of NK cells into the liver exacerbates the hepatic ischemia-reperfusion injury, which could be significantly alleviated after depletion of NK cells. Interestingly, NK cells may contribute to both liver graft rejection and tolerance according to their origins. In this article, we discussed the development of liver NK cells, their role in ischemia-reperfusion injury, and strategies of inhibiting NK cell activation in order to provide potential possibilities for translation application in future clinical practice.

Keywords: NK, natural killer, ischemia-reperfusion injury, liver transplantation, inflammation, immune tolerance

OPEN ACCESS

Edited by:
Qiang Wei,
Zhejiang University, China

Reviewed by:
Haiyang Xie,
Zhejiang University, China
Qifa Ye,
Wuhan University, China

***Correspondence:**
Jinyang Gu
gjynyd@126.com
Xiaoni Kong
xiaoni-kong@126.com

†*These authors have contributed equally to this work*

Specialty section:
This article was submitted to Molecular Innate Immunity, a section of the journal Frontiers in Immunology

Received: *05 February 2022*
Accepted: *07 March 2022*
Published: *28 March 2022*

Citation:
Huang M, Cai H, Han B, Xia Y, Kong X and Gu J (2022) Natural Killer Cells in Hepatic Ischemia-Reperfusion Injury. Front. Immunol. 13:870038. doi: 10.3389/fimmu.2022.870038

INTRODUCTION

Ischemia-reperfusion (I/R) injury is a two-stage pathophysiological process, characterized by hypoxia-induced cell damage in the ischemia phase and by immune inflammation after blood flow restoration (1). The ischemic insult exposes hepatic cells to oxygen deprivation, ATP depletion, and pH changes as well as cellular metabolic stress, all leading to initial cell injury or death (2). During subsequent reperfusion injury, the liver metabolism is disturbed and interconnected inflammatory cascades are induced, thereby further aggravating hepatocellular damage (1). In addition, hepatic I/R can result from both warm and cold ischemia types. Warm I/R occurs in vascular occlusion of liver tissues associated with liver resection, hemorrhagic shock, trauma, cardiac arrest, or hepatic sinusoidal obstruction syndrome (3, 4). However, cold I/R is obviously

Abbreviations: AAGM1, anti-asialo monosialotetrahexosylganglioside; AhR, aryl hydrocarbon receptor; CCL, C-C motif chemokine ligand; GM-CSF, granulocyte-macrophage colony-stimulating factor; IFN, interferon; IL, Interleukin; I/R, ischemia-reperfusion; KIR, killer cell immunoglobulin receptor; NK, natural killer; PLZF, promyelocytic leukemia zinc finger; TNF, tumor necrosis factor.

dominant during liver transplantation, where the donated liver graft is preserved in a hypothermic and anoxic environment before implantation into the recipient (3). Although these two types of liver I/R are involved in different disease models, they share similar characteristics in the mechanism of cell injury, such as activation of liver immune cells after reperfusion (5), among which natural killer (NK) cells play a quite vital role.

NK cells originate from bone marrow, develop in lymphoid tissue, and migrate into the bloodstream and tissues to play a fundamental role in the innate immune response. Discovered in 1975, NK cells are identified to take part in the early defense against virus-infected or tumor cells *via* secretion of granzymes and perforin, or expression of ligands for death receptors without prior immunization (6). In addition, NK cells could also contribute to immunoregulation through producing various cytokines, such as granulocyte-macrophage colony-stimulating factor (GM-CSF), Interleukin (IL) -10, IL-2, C-C motif chemokine ligand (CCL) 3, CCL4, CCL5, Interferon (IFN) -γ, and Tumor Necrosis Factor (TNF) -α (7, 8). It has been previously discussed that NK cells play an important role in other liver diseases, including autoimmune diseases (autoimmune hepatitis, primary biliary cirrhosis, and primary sclerosing cholangitis), non-alcoholic fatty liver disease, and liver fibrosis (9). However, how NK cells affect hepatic I/R is still understood limitedly. Herein, we aim to shed light on the current knowledge in the characteristics of NK cells, their function in hepatic I/R pathogenesis, and the potential mechanism of intervening NK cell activation.

DEVELOPMENT OF HEPATIC NK CELLS

Hepatic NK cells could be mainly divided into circulation NK (c-NK) and liver-resident NK (lr-NK) cell subtypes, which are distinguished by molecular markers, such as ($CD27^{-}CD11b^{+}$ and $CD27^{+}CD11b$-) in mouse liver, and $CD56^{dim}$ and $CD56^{bright}$ in human liver (8, 10). In addition, CD49a and CD49b are frequently used to distinguish c-NK ($CD49a^{-}CD49b^{+}Eomes^{+}$) and lr-NK ($CD49a^{+}CD49b^{-}Eomes^{-}$) cells in the mouse liver (6). Compared with c-NK, activated lr-NK cells partially retain cytotoxic function to target cells, manifested by reduced expression levels of perforin and granzyme B, but are more efficient in the secretion of TNF-α, IL-2, and GM-CSF (6, 11). In mice, the development of hepatic lr-NK and c-NK cells depends on many different transcription factors, although they are jointly dependent on IL-15 signaling (12). For example, T-bet deficiency only modestly affects peripheral c-NK cell, but has a more severe influence on hepatic lr-NK cells (12, 13). Mice lacking *Nfil3* have a quantitatively significant decrease in the bone marrow NK progenitor and mature NK cells, however, *Nfil3* is dispensable for lr-NK (14–17). Moreover, in contrast to *Eomes* deficiency reducing bone marrow and peripheral c-NK cell numbers, *Eomes* are not required for hepatic lr-NK development (18, 19). Promyelocytic leukemia zinc finger (PLZF) and aryl hydrocarbon receptor (AhR) have been reported to promote the development of different lr-NK cells, while these two transcription factors are not critical for c-NK development (20, 21). In other words, mice lacking PLZF or AhR have reduced hepatic lr-NK numbers, but c-NK are not significantly altered.

Some murine NK cell markers do not correspond one-to-one with their human counterparts, which largely explains the lack of phenotypic matching between murine and human lr-NK cells. Overall, c-NK cells rely mainly on T-bet and Eomes for humans, which has some similarities to the developmental process of mice, whereas lr-NK cells are regulated by a wide range of transcription factors including Eomes, Hobit, etc (11, 22). Compared with mice, human lr-NK cells express high levels of Eomes but not T-bet (11, 23, 24). Specifically, human lr-NK cells have few positive expressions of T-bet and are all positive in Hobit (25, 26). It is worth noting that lr-NK cells are probably dependent on the expression of surface adhesion molecules such as CD69, CD103, CD49a, CCR5, CXCR3, and CXCR6 to support their residence in the liver sinusoids (27, 28).

FUNCTION OF NK CELLS IN HEPATIC I/R

NK cell signaling in hepatic I/R is primarily mediated by engagement of their activating receptors (mainly including CD16, NKG2C:CD94, NKG2D, NKp46, NKp44, NKp30, CD226, and natural killer granule 7) and inhibitory receptors (largely composed of CD96, TIGIT, LAG3, killer cell immunoglobulin receptor (KIR) (Ly49 receptor in mice), and NKG2A:CD94), and the dynamic balance between them determines the responsiveness of NK cells (29, 30). Notably, the human KIR (Ly49 molecule in mice) and NKG2A:CD94 could recognize MHC class I molecules that are abundantly expressed on normal cells, thereby inhibiting NK cell function to ensure perfect tolerance to their own healthy cells (29, 31). In warm I/R, such as liver resection and hemorrhagic shock, NK cells mainly play the role of aggravating liver injury and promoting inflammatory cell infiltration (**Figure 1**). Whereas in cold I/R (primarily liver transplantation), NK cells not only participate in the inflammatory response, but also produce a marked effect in post-transplant immune tolerance (**Figure 2**).

NK Cells and Inflammatory Response in Hepatic I/R

It has been previously reported that depletion of NK cells had no significant effect on hepatic I/R injury, as demonstrated by unchanged liver function assays and infiltrated MPO content into the liver, suggesting that NK cells are not recruited to the liver after reperfusion (32). However, there is accumulating direct evidence that NK cells are involved in the development of the pathophysiology of hepatic I/R. In an experiment in which a rat was subjected to 1 hour of right hepatic lobe ischemia and the remaining liver was excised, a significant increase in NK cell infiltration into the rat liver parenchyma was detected after reperfusion for 2 hours (33), and depletion of NK cells could significantly decrease hepatic CXCL-2 expression, reduce neutrophil infiltration into the liver, and attenuate hepatic I/R

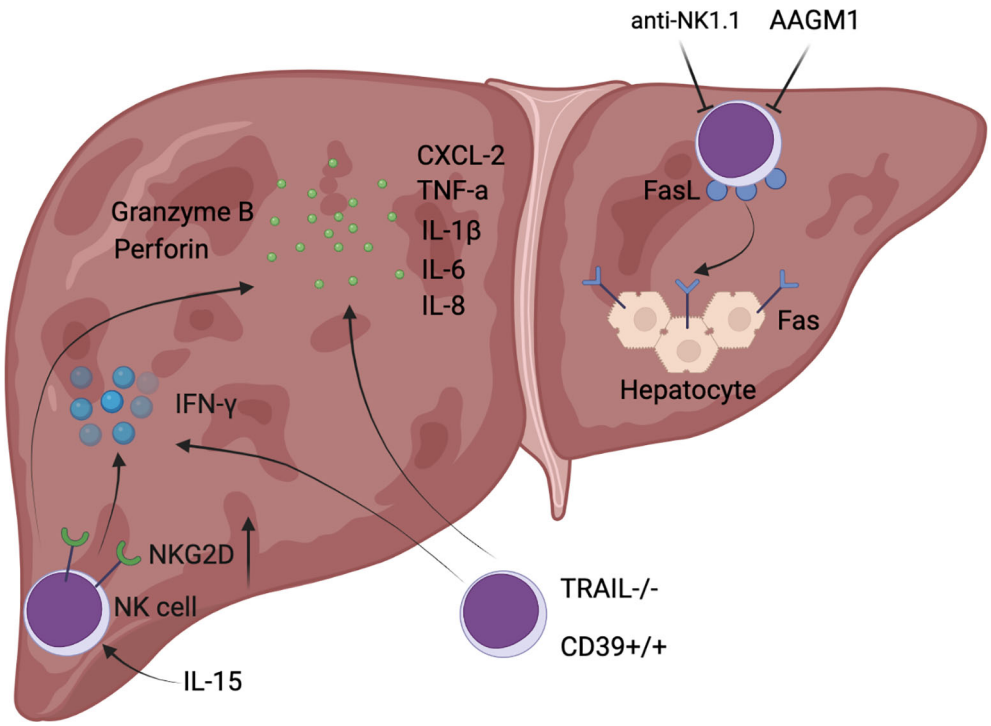

FIGURE 1 | Diagrammatic sketch of NK cell-mediated exacerbated liver injury during hepatic I/R.

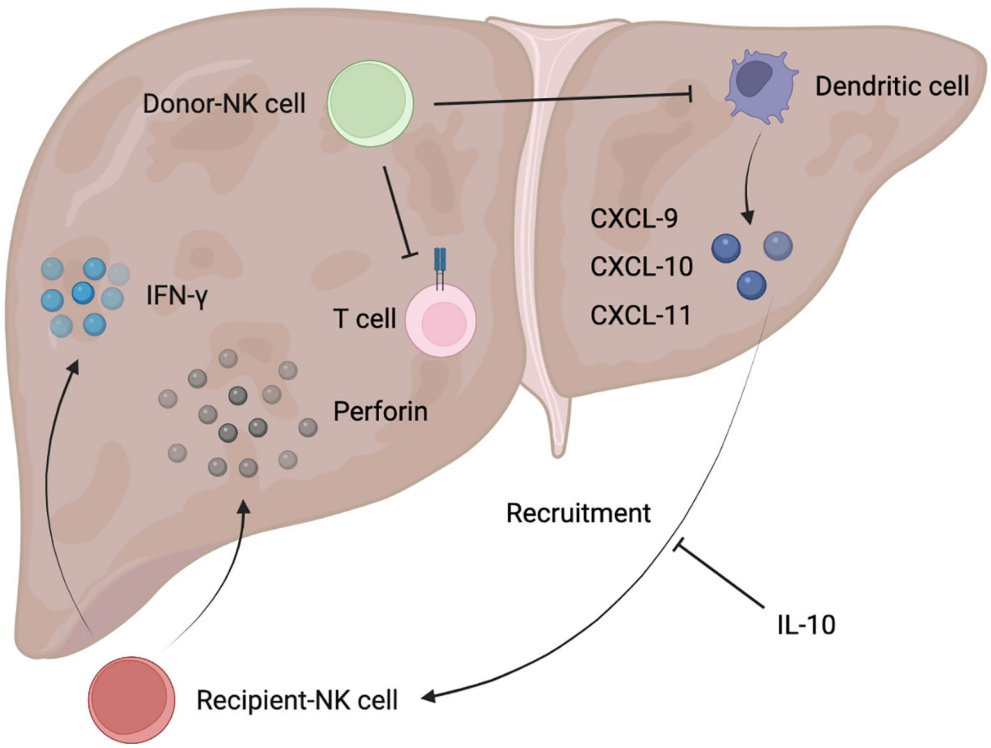

FIGURE 2 | Schematic diagram of donor/recipient-derived NK cells in immune tolerance after liver transplantation.

injury levels (34). Similarly, the mRNA level of *NKG2D*, an activating receptor for NK cells, rapidly increased in allografts (LEW to SD rats), indicating a significant activation of NK cells, while donor livers that were pretreated with anti-asialo monosialotetrahexosylganglioside (AAGM1) to deplete NK cells, showed a significant decrease in not only NKG2D expression levels but also hepatic cytokines (TNF-α, IL-1 β, IL-6, and IL-8) as well as secretion levels of cytolytic molecules (perforin, granzyme B), along with a reduction in early neutrophil infiltration (31). In contrast to the depletion of NK cells described above, administration of soluble pro-inflammatory IL-15/IL-15Rα complexes increased the absolute number of NK cells in the liver of *IRF-1* knockout mice after orthotopic liver transplantation, accompanied by increased expression of cytotoxic effector molecules (NKG2D, granzyme B, and perforin) and inflammatory cytokines (IFN-γ, IL-6, and TNF-α), eventually resulting in worsening liver injury and decreased survival (35). NK cell activation in hepatic I/R relied on the hydrolysis of ADP to AMP by CD39, and *CD39* deletion reduces IFN-γ secreted by NK cells to limit hepatic I/R injury (5). To be specific, *CD39*-deficient mice exhibited reduced pro-inflammatory cytokines in serum 3 hours after reperfusion, and also showed reduced hepatocyte injury and necrosis area after 24 hours of reperfusion (5). In addition, TRAIL expression on NK cells was upregulated following hepatic I/R in mice and exerted marked protective effects such as reduced serum transaminases, histological necrosis, neutrophil infiltration, and IL-6 levels in serum, whereas TRAIL-null NK cells exhibited higher cytotoxicity and significantly increased secretion of IFN-γ, indicating that TRAIL could confine further liver injury by blocking NK cell activation (36). IFN-γ secreted by NK cells can upregulate the expression of Fas in hepatocytes, while IL-18 released by injured Kupffer cells in hepatic I/R injury could increase the expression level of FasL (Fas ligand) in NK cells (37, 38). Therefore, the inflammation and liver damage are further amplified under this complex positive feedback. As can be seen from the above literature, IFN-γ secretion by NK cells plays a pivotal role in hepatic I/R, and the mechanism of its secretion is largely regulated by Tbox transcription factors such as T-bet and Eomes (39), which is tightly associated with NK cell development. NK cells can not only aggravate hepatic I/R injury by producing IFN-γ, but also increase the synthesis of IL-17, which could enhance the recruitment of neutrophils into the injured liver (34). This study provided strong proof that neutralization of IL-17 attenuated hepatic I/R injury in *Rag1* knockout mice (34).

NK Cells and Immune Tolerance in Hepatic I/R

The immunological process of donor NK cells entering the recipient bloodstream and recipient NK cells flowing into the donor graft with the bloodstream occurs early after liver transplantation, where donor NK cells migrate out of the liver and are detected in the recipient's circulation generally for 2 weeks, but there are also possibilities that graft NK cells will persist for decades (40). Thirteen genes were found to be significantly overexpressed in NK cells from immune-tolerant recipients of liver transplantation, suggesting that NK cells may be involved in the induction of immune tolerance (41). In fact, recipient-derived NK cells and donor-derived NK cells could play opposed roles in liver graft tolerance, with the former tending to reject allografts and the latter mainly promoting tolerance (40, 42). Recipient-derived NK cells produced IFN-γ after entering liver grafts, which predisposed to graft non-function (43). Correspondingly, either depletion of NK cells or reduction of IFN-γ production could be capable of promoting increased graft survival rate (43). According to clinical trials, recipient hypertension can further activate NK cells and lead to moderate to severe I/R injury, which may markedly increase the incidence of early allograft dysfunction and reduce the 6-month survival rate of grafts (44, 45). In contrast, after liver transplantation, treatment with anti-inflammatory factor IL-10 given to the recipient reduced the NK recruitment of chemokines CXCL-9, CXCL-10, and CXCL-11 produced by activated Dendritic cells, leading to a decrease in the number of recipient NK cells entering the liver graft in a clinical study (46). Meanwhile, a decrease of pro-inflammatory IL-12 also induced a shift in recipient NK cells to a tolerogenic phenotype with concomitant downregulation of NK-activating receptors, and reduction of cytotoxicity and cytokine production (47), which further limits the rejection of transplanted liver mediated by recipient NK cells. Of note, the rejection of ABO-incompatible liver transplantation by NK cells was particularly pronounced in clinical practice. It has been reported that a large number of NK cells in recipient peripheral blood was the only risk factor for the induction of ischemic biliary tract disease after ABO-incompatible adult living donor liver transplantation. This may be explained that recipient NK cells could recognize various NK cell ligands on the donor endothelial cells after flowing into the liver graft, and the ABO antigen was abundantly expressed on the endothelial cells of the transplant graft, thereby directly producing cytotoxicity and resulting in decreased graft survival (48, 49). Besides, there is a clinical study suggesting that recipient-derived NK cells are reduced but retain the robust expression of NK cell receptors such as NKG2D in the early stage of pediatric liver transplantation, which may be closely related to the increase of acute graft rejection episode (50).

As previously reported, infusion of donor liver NK cells can alleviate acute rejection of rat liver allografts and prolong graft survival (51), revealing the important function of donor NK cells in immune tolerance. It has also been reported in clinical research that bone marrow-derived mesenchymal stromal cell infusion induces the increase of donor-derived NK cells, which promotes the establishment of a pro-tolerance graft environment that persists in a long time (52). Hepatic NK cells from the donors played a major role in promoting graft tolerance, possibly through direct killing of recipient activated T cells and immature Dendritic cells recruited to the transplanted liver (40, 53). But this requires more experimental evidence to further confirm.

STRATEGIES TO INHIBIT NK CELLS IN HEPATIC I/R

On the one hand, NK cells play a pro-inflammatory and pro-injury role during hepatic I/R. On the other hand, donor NK cells

will be gradually replaced by recipient NK cells after liver transplantation, which predominantly exerts the negative effect of mediating graft liver rejection. Therefore, it is necessary to intervene in NK cells during the occurrence of I/R in the liver and at the stage of immune rejection that follows. Currently, possible approaches are NK cell depletion, inhibition of NK cell activation receptor signaling, and blockade of NK cell developmental signaling.

NK Cell Depletion

In general, there were two commonly used depletion antibodies for NK cells, AAGM1 and anti-NK1.1 (34, 54). AAGM1 causes certain membrane damage that gives rise to loss of NK function, and is effective in depleting NK cells in various mouse strains, but it may also interfere with other lymphocyte subsets that express GM1 (54). Treatment with the anti-NK1.1 antibody PK136 depletes NK cells in the liver and in a subset of NKT and γδ T cells (34). However, anti-NK1.1-mediated NK cell depletion is still the mainstay of analysis of NK cells in the liver (34). In a phase I/II trial, NK cells are depleted by a combination of anti-CD3 and anti-CD7 antibodies to treat acute graft-versus-host disease (55).

NK Cell Activating Receptor Blockade

It has been reported that transforming growth factor-β, IL-10, tryptophan catabolites, prostaglandin E_2, dickkopf-related protein 2, indoleamine 2,3-dioxygenase, soluble HLA-G, soluble NKG2D ligands, and galactin-3 (soluble inhibitory receptor for NKp30) could be viewed as the inhibitors of NK cells and their receptors, downregulating cytotoxic activity and the capabilities of secreting IFN-γ (56). For example, corticosteroids are utilized to significantly downregulate the expression of activated receptors NKp30 and NKp46 in clinical research, and NKG2D blockade can also reduce the incidence of allograft rejection (55). However, there are still many aspects of validation necessary to apply the above methods to the clinic.

Blockade of NK Cell Developmental Signaling

It has been reported that multiple signaling pathways are involved in the activation of NK cells and mediate the important role of NK cells in liver I/R. For example, activated AMPK, deletion of *FoxO1* gene, and inhibition of SREBP all could downregulate the number of mature terminally differentiated NK cells, inhibit NK cell cytotoxicity, and reduce granzyme B and IFN-γ production expression levels (57, 58). But these pathways are far from well-studied and full of controversy and contradictions. At present, the mTOR pathways have been widely and relatively well studied, and the metabolic signaling mediated by it is generally considered to be an important node in NK cell development. mTOR is a ubiquitous serine/threonine kinase that requires two regulatory proteins, raptor and rictor, to form functionally distinct mTOR complexes 1 and 2 (mTORC1 and 2), respectively (59). mTORC1 plays a major role among mTOR pathways, whereas mTORC2 can negatively regulate mTORC1 activity to some extent by inhibiting STAT5-mediated expression of the amino acid transporter SLC7A5 (60, 61). IL-15 stimulated mTORC1 through the Jak1 and PI3K/Akt signaling axes, and activated mTORC1 promoted NK precursor development (62, 63). Moreover, mTOR activated by the kinase PDK1, downstream of IL-15 signaling, was found to be required for E4BP4 expression in bone marrow NK cells, and E4BP4 can promote *Eomes* transcription, thereby playing an indispensable role in NK cell development (15). Since mTOR activity was inhibited after knockdown of *PDK1* in NK cells, NK development was impeded at an early stage (64). When *mTOR* was specifically knocked out in NK cells, the number of NK cells in peripheral blood was drastically reduced (65). Moreover, the use of the mTOR-selective inhibitor rapamycin broadly inhibited the expression levels of IFN-γ, perforin, and granzyme B secreted by NK cells (66, 67). In a rat I/R study, rapamycin significantly reduced parenchymal infiltration of NK cells, liver histological damage, and mortality (33), which formed strong support for the above observations.

CONCLUSIONS AND FUTURE PERSPECTIVES

In clinical practice, an important factor affecting the prognosis of partial hepatectomy and liver transplantation is liver I/R. The former is mainly manifested as severe liver injury caused by I/R, while the latter is also associated with graft rejection. Considering the inevitability of I/R in this type of liver surgery, mitigating the hazards caused by I/R to patients becomes the key. Accumulating evidence indicates that NK cells can be recruited to the liver, activate inflammation and worsen liver injury in I/R, and enhance rejection of grafts by recipient NK cells, thereby reducing graft survival. Using NK cell depletion, inhibiting NK cell activating receptors, or blocking the signaling pathway of NK cell maturation will become an effective approach for the intervention of hepatic I/R, which may show great potential for the clinical application. Collectively, an understanding of the pro-inflammatory effects of NK cells, as well as the donor/recipient-derived immune tolerance/rejection, may aid in liver protection in liver transplantation and partial hepatectomy, providing a rationale for further clinical treatments in the future.

AUTHOR CONTRIBUTIONS

JG and XK conceived the topic of this review article. MH, HC, BH, and YX searched reference articles and extracted key information for this review article. MH and XK wrote this manuscript. All authors listed have made a substantial, direct, and intellectual contribution to the work, and approved it for publication.

FUNDING

This work was supported by the National Natural Science Foundation of China (82130020, 82072646, and 81772507 to JG, 81873582 and 82070633 to X Kong). Clinical Research Plan of SHDC (No. SHDC2020CR3005A), Shanghai "Rising Stars of Medical Talent" Youth Development Program "Outstanding Youth Medical Talents" (No. SHWSRS (2021)

_099), Shanghai Municipal Education Commission–Gaofeng Clinical Medicine Grant Support (No. 20191910) to JG. Program of Shanghai Academic/Technology Research Leader (20XD1403700) to XK.

ACKNOWLEDGMENTS

The authors are grateful to Biorender.com for providing diagram support.

REFERENCES

1. Hirao H, Nakamura K, Kupiec-Weglinski JW. Liver Ischaemia-Reperfusion Injury: A New Understanding of the Role of Innate Immunity. *Nat Rev Gastroenterol Hepatol* (2021). doi: 10.1038/s41575-021-00549-8. Epub ahead of print
2. Ye L, He S, Mao X, Zhang Y, Cai Y, Li S. Effect of Hepatic Macrophage Polarization and Apoptosis on Liver Ischemia and Reperfusion Injury During Liver Transplantation. *Front Immunol* (2020) 11:1193. doi: 10.3389/fimmu.2020.01193
3. Papadopoulos D, Siempis T, Theodorakou E, Tsoulfas G. Hepatic Ischemia and Reperfusion Injury and Trauma: Current Concepts. *Arch Trauma Res* (2013) 2(2):63–70. doi: 10.5812/atr.12501
4. Mao XL, Cai Y, Chen YH, Wang Y, Jiang XX, Ye LP, et al. Novel Targets and Therapeutic Strategies to Protect Against Hepatic Ischemia Reperfusion Injury. *Front Med (Lausanne)* (2021) 8:757336. doi: 10.3389/fmed.2021.757336
5. Zhai Y, Petrowsky H, Hong JC, Busuttil RW, Kupiec-Weglinski JW. Ischaemia-Reperfusion Injury in Liver Transplantation–From Bench to Bedside. *Nat Rev Gastroenterol Hepatol* (2013) 10(2):79–89. doi: 10.1038/nrgastro.2012.225
6. Valero-Pacheco N, Beaulieu AM. Transcriptional Regulation of Mouse Tissue-Resident Natural Killer Cell Development. *Front Immunol* (2020) 11:309. doi: 10.3389/fimmu.2020.00309
7. Zhou J, Tian Z, Peng H. Tissue-Resident Nk Cells and Other Innate Lymphoid Cells. *Adv Immunol* (2020) 145:37–53. doi: 10.1016/bs.ai.2019.11.002
8. Crinier A, Narni-Mancinelli E, Ugolini S, Vivier E. Snapshot: Natural Killer Cells. *Cell* (2020) 180(6):1280– e1. doi: 10.1016/j.cell.2020.02.029
9. Highton AJ, Schuster IS, Degli-Esposti MA, Altfeld M. The Role of Natural Killer Cells in Liver Inflammation. *Semin Immunopathol* (2021) 43(4):519–33. doi: 10.1007/s00281-021-00877-6
10. Abel AM, Yang C, Thakar MS, Malarkannan S. Natural Killer Cells: Development, Maturation, and Clinical Utilization. *Front Immunol* (2018) 9:1869. doi: 10.3389/fimmu.2018.01869
11. Mikulak J, Bruni E, Oriolo F, Di Vito C, Mavilio D. Hepatic Natural Killer Cells: Organ-Specific Sentinels of Liver Immune Homeostasis and Physiopathology. *Front Immunol* (2019) 10:946. doi: 10.3389/fimmu.2019.00946
12. Bi J, Wang X. Molecular Regulation of Nk Cell Maturation. *Front Immunol* (2020) 11:1945. doi: 10.3389/fimmu.2020.01945
13. Huang C, Bi J. Expression Regulation and Function of T-Bet in Nk Cells. *Front Immunol* (2021) 12:761920. doi: 10.3389/fimmu.2021.761920
14. Yu X, Wang Y, Deng M, Li Y, Ruhn KA, Zhang CC, et al. The Basic Leucine Zipper Transcription Factor Nfil3 Directs the Development of a Common Innate Lymphoid Cell Precursor. *Elife* (2014) 3:e04406. doi: 10.7554/eLife.04406
15. Male V, Nisoli I, Kostrzewski T, Allan DS, Carlyle JR, Lord GM, et al. The Transcription Factor E4bp4/Nfil3 Controls Commitment to the Nk Lineage and Directly Regulates Eomes and Id2 Expression. *J Exp Med* (2014) 211(4):635–42. doi: 10.1084/jem.20132398
16. Seillet C, Huntington ND, Gangatirkar P, Axelsson E, Minnich M, Brady HJ, et al. Differential Requirement for Nfil3 During Nk Cell Development. *J Immunol* (2014) 192(6):2667–76. doi: 10.4049/jimmunol.1302605
17. Sojka DK, Plougastel-Douglas B, Yang L, Pak-Wittel MA, Artyomov MN, Ivanova Y, et al. Tissue-Resident Natural Killer (Nk) Cells Are Cell Lineages Distinct From Thymic and Conventional Splenic Nk Cells. *Elife* (2014) 3:e01659. doi: 10.7554/eLife.01659
18. Weizman OE, Adams NM, Schuster IS, Krishna C, Pritykin Y, Lau C, et al. Ilc1 Confer Early Host Protection at Initial Sites of Viral Infection. *Cell* (2017) 171(4):795–808 e12. doi: 10.1016/j.cell.2017.09.052
19. Wu SY, Fu T, Jiang YZ, Shao ZM. Natural Killer Cells in Cancer Biology and Therapy. *Mol Cancer* (2020) 19(1):120. doi: 10.1186/s12943-020-01238-x
20. Zhang LH, Shin JH, Haggadone MD, Sunwoo JB. The Aryl Hydrocarbon Receptor Is Required for the Maintenance of Liver-Resident Natural Killer Cells. *J Exp Med* (2016) 213(11):2249–57. doi: 10.1084/jem.20151998
21. Constantinides MG, McDonald BD, Verhoef PA, Bendelac A. A Committed Precursor to Innate Lymphoid Cells. *Nature* (2014) 508(7496):397–401. doi: 10.1038/nature13047
22. Marcenaro E, Notarangelo LD, Orange JS, Vivier E. Editorial: Nk Cell Subsets in Health and Disease: New Developments. *Front Immunol* (2017) 8:1363. doi: 10.3389/fimmu.2017.01363
23. Harmon C, Robinson MW, Fahey R, Whelan S, Houlihan DD, Geoghegan J, et al. Tissue-Resident Eomes(Hi) T-Bet(Lo) Cd56(Bright) Nk Cells With Reduced Proinflammatory Potential Are Enriched in the Adult Human Liver. *Eur J Immunol* (2016) 46(9):2111–20. doi: 10.1002/eji.201646559
24. Stegmann KA, Robertson F, Hansi N, Gill U, Pallant C, Christophides T, et al. Cxcr6 Marks a Novel Subset of T-Bet(Lo)Eomes(Hi) Natural Killer Cells Residing in Human Liver. *Sci Rep* (2016) 6:26157. doi: 10.1038/srep26157
25. Marquardt N, Beziat V, Nystrom S, Hengst J, Ivarsson MA, Kekalainen E, et al. Cutting Edge: Identification and Characterization of Human Intrahepatic Cd49a+ Nk Cells. *J Immunol* (2015) 194(6):2467–71. doi: 10.4049/jimmunol.1402756
26. Lunemann S, Martrus G, Goebels H, Kautz T, Langeneckert A, Salzberger W, et al. Hobit Expression by a Subset of Human Liver-Resident Cd56(Bright) Natural Killer Cells. *Sci Rep* (2017) 7(1):6676. doi: 10.1038/s41598-017-06011-7
27. Freud AG, Mundy-Bosse BL, Yu J, Caligiuri MA. The Broad Spectrum of Human Natural Killer Cell Diversity. *Immunity* (2017) 47(5):820–33. doi: 10.1016/j.immuni.2017.10.008
28. Hudspeth K, Donadon M, Cimino M, Pontarini E, Tentorio P, Preti M, et al. Human Liver-Resident Cd56(Bright)/Cd16(Neg) Nk Cells Are Retained Within Hepatic Sinusoids *via* the Engagement of Ccr5 and Cxcr6 Pathways. *J Autoimmun* (2016) 66:40–50. doi: 10.1016/j.jaut.2015.08.011
29. Jacquelot N, Seillet C, Souza-Fonseca-Guimaraes F, Sacher AG, Belz GT, Ohashi PS. Natural Killer Cells and Type 1 Innate Lymphoid Cells in Hepatocellular Carcinoma: Current Knowledge and Future Perspectives. *Int J Mol Sci* (2021) 22(16):9044. doi: 10.3390/ijms22169044
30. Zhang C, Wang H, Li J, Hou X, Li L, Wang W, et al. Involvement of Tigit in Natural Killer Cell Exhaustion and Immune Escape in Patients and Mouse Model With Liver Echinococcus Multilocularis Infection. *Hepatology* (2021) 74(6):3376–93. doi: 10.1002/hep.32035
31. Kimura S, Ozaki KS, Ueki S, Zhang M, Yokota S, Stolz DB, et al. Contribution of Alloantigens to Hepatic Ischemia/Reperfusion Injury: Roles of Natural Killer Cells and Innate Immune Recognition of Nonself. *Liver Transpl* (2016) 22(1):80–90. doi: 10.1002/lt.24330
32. Kuboki S, Sakai N, Tschop J, Edwards MJ, Lentsch AB, Caldwell CC. Distinct Contributions of Cd4+ T Cell Subsets in Hepatic Ischemia/Reperfusion Injury. *Am J Physiol Gastrointest Liver Physiol* (2009) 296(5):G1054–9. doi: 10.1152/ajpgi.90464.2008
33. Arias-Diaz J, Ildefonso JA, Munoz JJ, Zapata A, Jimenez E. Both Tacrolimus and Sirolimus Decrease Th1/Th2 Ratio, and Increase Regulatory T Lymphocytes in the Liver After Ischemia/Reperfusion. *Lab Invest* (2009) 89(4):433–45. doi: 10.1038/labinvest.2009.3
34. Feng M, Li G, Qian X, Fan Y, Huang X, Zhang F, et al. Il-17a-Producing Nk Cells Were Implicated in Liver Injury Induced by Ischemia and Reperfusion. *Int Immunopharmacol* (2012) 13(2):135–40. doi: 10.1016/j.intimp.2012.03.007
35. Yokota S, Yoshida O, Dou L, Spadaro AV, Isse K, Ross MA, et al. Irf-1 Promotes Liver Transplant Ischemia/Reperfusion Injury *via* Hepatocyte Il-15/Il-15ralpha Production. *J Immunol* (2015) 194(12):6045–56. doi: 10.4049/jimmunol.1402505

36. Fahrner R, Trochsler M, Corazza N, Graubardt N, Keogh A, Candinas D, et al. Tumor Necrosis Factor-Related Apoptosis-Inducing Ligand on Nk Cells Protects From Hepatic Ischemia-Reperfusion Injury. *Transplantation* (2014) 97(11):1102–9. doi: 10.1097/TP.0000000000000101
37. Tsutsui H, Matsui K, Okamura H, Nakanishi K. Pathophysiological Roles of Interleukin-18 in Inflammatory Liver Diseases. *Immunol Rev* (2000) 174:192–209. doi: 10.1034/j.1600-0528.2002.017418.x
38. Nakajima H, Mizuta N, Fujiwara I, Sakaguchi K, Ogata H, Magae J, et al. Blockade of the Fas/Fas Ligand Interaction Suppresses Hepatocyte Apoptosis in Ischemia-Reperfusion Rat Liver. *Apoptosis* (2008) 13(8):1013–21. doi: 10.1007/s10495-008-0234-5
39. Eggenhofer E, Sabet-Rashedi M, Lantow M, Renner P, Rovira J, Koehl GE, et al. Rorgammat(+) Il-22-Producing Nkp46(+) Cells Protect From Hepatic Ischemia Reperfusion Injury in Mice. *J Hepatol* (2016) 64(1):128–34. doi: 10.1016/j.jhep.2015.08.023
40. Jiang Y, Que W, Zhu P, Li XK. The Role of Diverse Liver Cells in Liver Transplantation Tolerance. *Front Immunol* (2020) 11:1203. doi: 10.3389/fimmu.2020.01203
41. Huang H, Lu Y, Zhou T, Gu G, Xia Q. Innate Immune Cells in Immune Tolerance After Liver Transplantation. *Front Immunol* (2018) 9:2401. doi: 10.3389/fimmu.2018.02401
42. Harmon C, Sanchez-Fueyo A, O'Farrelly C, Houlihan DD. Natural Killer Cells and Liver Transplantation: Orchestrators of Rejection or Tolerance? *Am J Transplant* (2016) 16(3):751–7. doi: 10.1111/ajt.13565
43. Fahrner R, Dondorf F, Ardelt M, Settmacher U, Rauchfuss F. Role of Nk, Nkt Cells and Macrophages in Liver Transplantation. *World J Gastroenterol* (2016) 22(27):6135–44. doi: 10.3748/wjg.v22.i27.6135
44. Ito T, Naini BV, Markovic D, Aziz A, Younan S, Lu M, et al. Ischemia-Reperfusion Injury and Its Relationship With Early Allograft Dysfunction in Liver Transplant Patients. *Am J Transplant* (2021) 21(2):614–25. doi: 10.1111/ajt.16219
45. Jayaram A, Deer E, Amaral LM, Campbell N, Vaka VR, Cunningham M, et al. The Role of Tumor Necrosis Factor in Triggering Activation of Natural Killer Cell, Multi-Organ Mitochondrial Dysfunction and Hypertension During Pregnancy. *Pregnancy Hypertens* (2021) 24:65–72. doi: 10.1016/j.preghy.2021.02.006
46. Ingelsten M, Gustafsson K, Olausson M, Haraldsson B, Karlsson-Parra A, Nystrom J. Rapid Increase of Interleukin-10 Plasma Levels After Combined Auxiliary Liver-Kidney Transplantation in Presensitized Patients. *Transplantation* (2014) 98(2):208–15. doi: 10.1097/TP.0000000000000038
47. Jamil KM, Hydes TJ, Cheent KS, Cassidy SA, Traherne JA, Jayaraman J, et al. Stat4-Associated Natural Killer Cell Tolerance Following Liver Transplantation. *Gut* (2017) 66(2):352–61. doi: 10.1136/gutjnl-2015-309395
48. Lee CY, Lotfi-Emran S, Erdinc M, Murata K, Velidedeoglu E, Fox-Talbot K, et al. The Involvement of Fcr Mechanisms in Antibody-Mediated Rejection. *Transplantation* (2007) 84(10):1324–34. doi: 10.1097/01.tp.0000287457.54761.53
49. Bang JB, Kim BW, Kim YB, Wang HJ, Lee HY, Sim J, et al. Risk Factor for Ischemic-Type Biliary Lesion After Abo-Incompatible Living Donor Liver Transplantation. *World J Gastroenterol* (2016) 22(30):6925–35. doi: 10.3748/wjg.v22.i30.6925
50. Pham B, Piard-Ruster K, Silva R, Gallo A, Esquivel CO, Martinez OM, et al. Changes in Natural Killer Cell Subsets in Pediatric Liver Transplant Recipients. *Pediatr Transplant* (2012) 16(2):176–82. doi: 10.1111/j.1399-3046.2012.01653.x
51. Yu JD, Long TZ, Li GL, Lv LH, Lin HM, Huang YH, et al. Donor Liver Natural Killer Cells Alleviate Liver Allograft Acute Rejection in Rats. *Hepatobil Pancreat Dis Int* (2011) 10(4):386–92. doi: 10.1016/s1499-3872(11)60065-9
52. Casiraghi F, Perico N, Podesta MA, Todeschini M, Zambelli M, Colledan M, et al. Third-Party Bone Marrow-Derived Mesenchymal Stromal Cell Infusion Before Liver Transplantation: A Randomized Controlled Trial. *Am J Transplant* (2021) 21(8):2795–809. doi: 10.1111/ajt.16468
53. Cerboni C, Zingoni A, Cippitelli M, Piccoli M, Frati L, Santoni A. Antigen-Activated Human T Lymphocytes Express Cell-Surface Nkg2d Ligands *via* an Atm/Atr-Dependent Mechanism and Become Susceptible to Autologous Nk-Cell Lysis. *Blood* (2007) 110(2):606–15. doi: 10.1182/blood-2006-10-052720
54. Nishikado H, Mukai K, Kawano Y, Minegishi Y, Karasuyama H. Nk Cell-Depleting Anti-Asialo Gm1 Antibody Exhibits a Lethal Off-Target Effect on Basophils *In Vivo*. *J Immunol* (2011) 186(10):5766–71. doi: 10.4049/jimmunol.1100370
55. Groth C, van Groningen LFJ, Matos TR, Bremmers ME, Preijers F, Dolstra H, et al. Phase I/Ii Trial of a Combination of Anti-Cd3/Cd7 Immunotoxins for Steroid-Refractory Acute Graft-Versus-Host Disease. *Biol Blood Marrow Transplant* (2019) 25(4):712–9. doi: 10.1016/j.bbmt.2018.10.020
56. Khan M, Arooj S, Wang H. Nk Cell-Based Immune Checkpoint Inhibition. *Front Immunol* (2020) 11:167. doi: 10.3389/fimmu.2020.00167
57. Muller-Durovic B, Lanna A, Covre LP, Mills RS, Henson SM, Akbar AN. Killer Cell Lectin-Like Receptor G1 Inhibits Nk Cell Function Through Activation of Adenosine 5'-Monophosphate-Activated Protein Kinase. *J Immunol* (2016) 197(7):2891–9. doi: 10.4049/jimmunol.1600590
58. Assmann N, O'Brien KL, Donnelly RP, Dyck L, Zaiatz-Bittencourt V, Loftus RM, et al. Srebp-Controlled Glucose Metabolism Is Essential for Nk Cell Functional Responses. *Nat Immunol* (2017) 18(11):1197–206. doi: 10.1038/ni.3838
59. Sengupta S, Peterson TR, Sabatini DM. Regulation of the Mtor Complex 1 Pathway by Nutrients, Growth Factors, and Stress. *Mol Cell* (2010) 40(2):310–22. doi: 10.1016/j.molcel.2010.09.026
60. Yang C, Tsaih SW, Lemke A, Flister MJ, Thakar MS, Malarkannan S. Mtorc1 and Mtorc2 Differentially Promote Natural Killer Cell Development. *Elife* (2018) 7:e35619. doi: 10.7554/eLife.35619
61. Wang F, Meng M, Mo B, Yang Y, Ji Y, Huang P, et al. Crosstalks Between Mtorc1 and Mtorc2 Variagate Cytokine Signaling to Control Nk Maturation and Effector Function. *Nat Commun* (2018) 9(1):4874. doi: 10.1038/s41467-018-07277-9
62. Nandagopal N, Ali AK, Komal AK, Lee SH. The Critical Role of Il-15-Pi3k-Mtor Pathway in Natural Killer Cell Effector Functions. *Front Immunol* (2014) 5:187. doi: 10.3389/fimmu.2014.00187
63. Wang S, Xia P, Huang G, Zhu P, Liu J, Ye B, et al. Foxo1-Mediated Autophagy Is Required for Nk Cell Development and Innate Immunity. *Nat Commun* (2016) 7:11023. doi: 10.1038/ncomms11023
64. Yang M, Li D, Chang Z, Yang Z, Tian Z, Dong Z. Pdk1 Orchestrates Early Nk Cell Development Through Induction of E4bp4 Expression and Maintenance of Il-15 Responsiveness. *J Exp Med* (2015) 212(2):253–65. doi: 10.1084/jem.20141703
65. Marcais A, Cherfils-Vicini J, Viant C, Degouve S, Viel S, Fenis A, et al. The Metabolic Checkpoint Kinase Mtor Is Essential for Il-15 Signaling During the Development and Activation of Nk Cells. *Nat Immunol* (2014) 15(8):749–57. doi: 10.1038/ni.2936
66. Viel S, Marcais A, Guimaraes FS, Loftus R, Rabilloud J, Grau M, et al. Tgf-Beta Inhibits the Activation and Functions of Nk Cells by Repressing the Mtor Pathway. *Sci Signal* (2016) 9(415):ra19. doi: 10.1126/scisignal.aad1884
67. Abel AM, Tiwari AA, Gerbec ZJ, Siebert JR, Yang C, Schloemer NJ, et al. Iq Domain-Containing Gtpase-Activating Protein 1 Regulates Cytoskeletal Reorganization and Facilitates Nkg2d-Mediated Mechanistic Target of Rapamycin Complex 1 Activation and Cytokine Gene Translation in Natural Killer Cells. *Front Immunol* (2018) 9:1168. doi: 10.3389/fimmu.2018.01168

Conflict of Interest: The authors declare that the research was conducted in the absence of any commercial or financial relationships that could be construed as a potential conflict of interest.

frontiers | Frontiers in Immunology

ORIGINAL RESEARCH
published: 05 April 2022
doi: 10.3389/fimmu.2022.869050

Liraglutide Attenuates Hepatic Ischemia–Reperfusion Injury by Modulating Macrophage Polarization

Shang-Lin Li[1,2†], Zhi-Min Wang[3†], Cong Xu[1,2], Fu-Heng Che[1,2], Xiao-Fan Hu[1,2], Rui Cao[1,2], Ya-Nan Xie[1,2], Yang Qiu[1,2], Hui-Bo Shi[1,2], Bin Liu[1,2], Chen Dai[1,2†] and Jun Yang[1,2*†]*

[1] Institute of Organ Transplantation, Tongji Hospital, Tongji Medical College, Huazhong University of Science and Technology, Wuhan, China, [2] Key Laboratory of Organ Transplantation, Ministry of Education, NHC Key Laboratory of Organ Transplantation, Key Laboratory of Organ Transplantation, Chinese Academy of Medical Sciences, Wuhan, China, [3] Department of Pediatrics, Tongji Hospital, Tongji Medical College, Huazhong University of Science and Technology, Wuhan, China

OPEN ACCESS

Edited by:
Tao Qiu,
Renmin Hospital of Wuhan University, China

Reviewed by:
Kang He,
Shanghai JiaoTong University, China
Moufida Ben Nasr,
University of Milan, Italy
Benhua Zhao,
Xiamen University, China

***Correspondence:**
Chen Dai
cdai26@tjh.tjmu.edu.cn
Jun Yang
jy@tjh.tjmu.edu.cn

[†]These authors have contributed equally to this work

Specialty section:
This article was submitted to Molecular Innate Immunity, a section of the journal Frontiers in Immunology

Received: 03 February 2022
Accepted: 09 March 2022
Published: 05 April 2022

Citation:
Li S-L, Wang Z-M, Xu C, Che F-H, Hu X-F, Cao R, Xie Y-N, Qiu Y, Shi H-B, Liu B, Dai C and Yang J (2022) Liraglutide Attenuates Hepatic Ischemia–Reperfusion Injury by Modulating Macrophage Polarization. Front. Immunol. 13:869050. doi: 10.3389/fimmu.2022.869050

Ischemia-reperfusion injury (IRI) is a common complication associated with liver surgery, and macrophages play an important role in hepatic IRI. Liraglutide, a glucagon-like peptide-1 (GLP-1) analog primarily used to treat type 2 diabetes and obesity, regulates intracellular calcium homeostasis and protects the cardiomyocytes from injury; however, its role in hepatic IRI is not yet fully understood. This study aimed to investigate whether liraglutide can protect the liver from IRI and determine the possible underlying mechanisms. Our results showed that liraglutide pretreatment significantly alleviated the liver damage caused by ischemia-reperfusion (I/R), as evidenced by H&E staining, serum aspartate aminotransferase (AST) and alanine aminotransferase (ALT) levels, and TUNEL staining. Furthermore, the levels of inflammatory cytokines elicited by I/R were distinctly suppressed by liraglutide pretreatment, accompanied by significant reduction in TNF-α, IL-1β, and IL-6 levels. Furthermore, pretreatment with liraglutide markedly inhibited macrophage type I (M1) polarization during hepatic IRI, as revealed by the significant reduction in $CD68^+$ levels in Kupffer cells (KCs) detected *via* flow cytometry. However, the protective effects of liraglutide on hepatic IRI were partly diminished in GLP-1 receptor-knockout ($GLP\text{-}1R^{-/-}$) mice. Furthermore, in an *in vitro* study, we assessed the role of liraglutide in macrophage polarization by examining the expression profiles of M1 in bone marrow-derived macrophages (BMDMs) from $GLP\text{-}1R^{-/-}$ and C57BL/6J mice. Consistent with the results of the *in vivo* study, liraglutide treatment attenuated the LPS-induced M1 polarization and reduced the expression of M1 markers. However, the inhibitory effect of liraglutide on LPS-induced M1 polarization was largely abolished in BMDMs from $GLP\text{-}1R^{-/-}$ mice. Collectively, our study indicates that liraglutide can ameliorate hepatic IRI by inhibiting macrophage polarization towards an inflammatory phenotype *via* GLP-1R. Its protective effect against liver IRI suggests that liraglutide may serve as a potential drug for the clinical treatment of liver IRI.

Keywords: acute liver injury, ischemia-reperfusion, liraglutide, macrophage polarization, glucagon-like peptide-1 receptor

INTRODUCTION

Hepatic IRI is a common clinical, pathophysiological phenomenon that often occurs during trauma, shock, liver surgery, and liver transplantation. It is the main factor affecting the complications associated with liver surgery and the survival and prognosis of patients (1, 2). In addition, liver dysfunction caused by hepatic ischemia-reperfusion injury can further affect distal organs and cause systemic damage (3). Although liver IRI involves a variety of molecular mechanisms and results from the joint action of various cells, its underlying mechanism has not yet been fully elucidated.

Recent studies have shown that macrophages play an important role in hepatic IRI (4, 5). Hepatic IRI can be divided into early and late stages. The early stage of IRI involves the rapid activation of KC cells after reperfusion, and the late stage is characterized by the recruitment of neutrophils to the liver (6). As the largest immune organ in the human body, the liver contains various immune cells such as resident macrophages (KCs), dendritic cells (DCs), natural killer cells (NKs), and natural killer T cells (NKTs) (7). In these cells, the macrophage-mediated inflammatory response is considered an important factor in hepatic IRI. Liver macrophages are divided into M1- and M2-type macrophages according to their phenotype and function. M1 macrophages promote the development of inflammation, whereas M2 macrophages inhibit inflammation. The proportion of M1/M2 macrophages in the liver affects the pathological outcome of hepatic IRI (8).

Liraglutide, a glucagon-like peptide-1 (GLP-1) analog that binds to and activates GLP-1R, is primarily used to treat type 2 diabetes and obesity (9, 10). Recent studies have shown that GLP-1R is distributed in the pancreas and organs such as the heart, lung, liver, and kidney (11, 12). In addition to regulating blood sugar levels, liraglutide has other biological activities as well. For example, it can regulate intracellular calcium homeostasis to protect cardiomyocytes from injury (13). In addition, liraglutide has been reported to play a role in liver protection by reducing inflammation in a liver/nonalcoholic steatohepatitis (NAFLD/NASH) model (14).

This study aimed to examine the protective effect of liraglutide on hepatic IRI and its effects on macrophages and explore the possible underlying mechanism using a partial hepatic IRI mouse model. The outcomes of this study could provide a new direction for the clinical treatment of HIRI.

MATERIALS AND METHODS

Mice

C57BL/6J (B6) mice were purchased from Beijing HFK Bioscience Co. Ltd. (Beijing, China). GLP-1R$^{-/-}$ mice were purchased from Beijing Biocytogen Co. Ltd. (Beijing, China). All mice were 6–8 weeks of age and housed under specific pathogen-free conditions at the Tongji Medical School Facilities for Animal Care and Housing. All animal studies were performed in accordance with the guidelines of the Chinese Council on Animal Care and approved by the Tongji Medical College Committees on Animal Experimentation.

Reagents and Experimental Design

Liraglutide was purchased from Novo Nordisk (Copenhagen, Denmark) and diluted in 0.9% normal saline before administration. Each 200 μg/kg dose of liraglutide was subcutaneously administered every 12 h for three consecutive days to the mice. The dose of liraglutide was based on our previous study (15).

In the $GdCl_3$ treatment group, mice were injected intravenously with $GdCl_3$ at 10 mg/kg (Sigma-Aldrich, USA) 24 h before the onset of liver ischemia. For NK and NKT cell depletion, anti-NK1.1 MAb (PK136, BioLegend, USA) was intraperitoneally injected (200 ug per mouse) on day -2, -1, 0 before the procedure. For depletion of NK cells alone, 50 μg of anti-asialoGM1 Ab (Sigma-Aldrich, USA) was intraperitoneally injected twice on day -3 and -1 before liver IRI. In addition, anti-Gr-1 (BioLegend, USA) was intraperitoneally injected (10 mg/kg) 24 h prior to hepatic IRI.

Liver IRI Model

Male C57BL/6J wild-type and GLP-1R$^{-/-}$ mice (6–8 weeks of age) were used in these experiments. The partial liver I/R animal model was established as described in our previous publication, with some modifications (16). Briefly, mice were anesthetized with sodium pentobarbital (80 mg/kg, intraperitoneally) (Sigma, MO, USA), and after midline laparotomy, the arterial and portal venous blood supplies to the left and middle liver lobes were interrupted with an atraumatic clip (using an operating microscope) for 60 min of partial hepatic warm ischemia, and the clamp was then removed. Body temperature was maintained at 32°C using a warming pad. The sham animals underwent the same procedures but were not subjected to hepatic ischemia. After a certain time (2, 6, or 24 h) of reperfusion, the mice were sacrificed for tissue analysis.

Isolation of Kupffer Cells (KCs)

KCs were isolated as previously described by Li et al. (17). Briefly, livers were perfused with 10 mL of calcium-free Hank balanced salt solution (HyClone Laboratories, USA) *via* the portal vein, followed by 0.27% type IV collagenase (Sigma-Aldrich, USA) in a water bath at 37°C for 20 min. The perfused liver was dissected, and a 70 mm cell filter was used to produce a single-cell suspension. Next, KCs were obtained by discontinuous density gradient centrifugation. After 2 h of incubation at 37°C and 5% CO_2, the isolated KCs were purified by removing the non-adherent cells.

Extraction and Culture of Bone Marrow-Derived Macrophages (BMDMs)

BMDMs were obtained from fresh BM cells of C57BL/6J mice or GLP-1R$^{-/-}$ mice. These cells were then cultured in a DMEM medium (Gibco, China) containing 10% heat-inactivated fetal bovine serum (FBS) and granulocyte-macrophage colony-stimulating factor (GM-CSF, PeproTech, USA, 10 ng/ml). The medium was replaced every two days. Five days later, the cells were pretreated with liraglutide (50 μM) for 24 h and then treated with LPS (100ng/ml) for 24 h.

Serum Transaminase Level Measurement

Blood samples were collected at a particular time, and serum alanine aminotransferase (ALT) and aspartate aminotransferase (AST) levels were measured using an automated biochemical analyzer BS-200 (Mindray, Shenzhen, China).

Histopathology Assay

Harvested liver tissues were fixed in 4% formalin and embedded in paraffin blocks. Four-micrometer sections were stained with hematoxylin and eosin (H&E), and liver damage caused by I/R was scored by a pathologist blindly using Suzuki criteria (18) on a scale from 0–4.

Immunofluorescence and Immunohistochemical Assays

For immunofluorescence analysis, paraffin-embedded liver sections were incubated with primary antibodies against F4/80 (1:3000, Servicebio, China) and iNOS (1:200, Abcam, USA), followed by incubation with a secondary antibody (Servicebio, Wuhan, China). Apoptotic cells were evaluated using the terminal deoxynucleotidyl transferase (TdT) dUTP nick-end labeling (TUNEL) assay kit (Roche Applied Science) according to a standard protocol. Liver myeloperoxidase (MPO) activity was assessed using immunohistochemistry. The sections were incubated with primary antibodies against MPO (Servicebio, Wuhan, China), followed by the application of the appropriate secondary antibody (Servicebio, Wuhan, China). Five microscopic fields were examined for each section and used for calculations.

Flow Cytometric Analysis

BMDMs and KCs were stained with monoclonal antibodies against F4/80 APC, CD11b BV421, CD68 FITC and CD86 BV605 (eBioscience, San Diego, CA, USA) at 4°C for 30 min, washed with phosphate-buffered saline and fixed with 1% formalin. Flow cytometry analysis was performed using a FACSCaliber system (BD Biosciences, USA) and analyzed using the FlowJo software.

Western Blotting

Proteins were extracted from the I/R liver and cultured BMDMs for western blotting. The primary antibody used was anti-STAT1 (1:1000; CST, USA), anti-Bax (1:1000; ABclonal, Wuhan, China), anti-Bcl-2 (1:1000; ABclonal, China), and anti-β-actin (1:10000; ProteinTech, USA). Membranes were then incubated with horseradish peroxidase-conjugated goat anti-rabbit polyclonal secondary antibodies (1:1000; Servicebio, Wuhan, China). The protein bands were visualized using GeneGnome XRQ (SYNGENE, UK), and data were obtained from three independent experiments.

Quantitative Reverse Transcription-PCR (qRT-PCR)

Total RNA was extracted from mouse livers or BMDMs using TRIzol reagent (Ambion) and reverse-transcribed into cDNA templates using a PrimeScriptTM RT reagent kit (Takara, Japan). RT-qPCR was performed using SYBR® Premix Ex TaqTM II (Tli RNaseH Plus) (Takara, Japan) with the following primers: iNOS (forward: 5′-ATTCACAGCTCATCCGGTACG-3′; reverse: 5′-GGATCTTGACCATCAGCTTGC-3′), TNF-α (forward: 5′-TATGGCTCAGGGTCCAACTC-3′, reverse: 5′-GGAAAGCCCATTTGAGTCCT-3′), IL-6 (forward: 5′-ACCAGAGGAAATTTTCAATAGGC-3′, reverse: 5′-TGATGCACTTGCAGAAAACA-3′), IL-1β (forward: 5′-GGTCAAAGGTTTGGAAGCAG-3′, reverse: 5′-TGTGAAATGCCACCTTTTGA-3′), and GLP-1R (forward: 5′-ACAGTGGGGTACGCACTTTC-3′, reverse: 5′-CGGAGGATGAAGGATGCAAAC-3′), and GAPDH (forward: 5′-AGGTCGGTGTGAACGGATTTG-3′, reverse: 5′-TGTAGACCATGTAGTTGAGGTCA-3′). Samples were analyzed in triplicate using StepOne Software v2.3 (Thermo Fisher Scientific, USA). For quantitative analysis, all samples were analyzed using the ΔΔCT method.

Statistical Analysis

All data are expressed as mean ± standard deviation (SD). Student's unpaired t-test was used to compare the differences in the means between two groups, and one-way analysis of variance (ANOVA) followed by Bonferroni's *post hoc* test was used to perform multiple statistical comparisons. Statistical significance was set at $P < 0.05$. All statistical analyses were performed using GraphPad Prism 8.

RESULTS

Liraglutide Pretreatment Ameliorates I/R-Induced Liver Damage in Mice

A mouse partial liver IRI model with different reperfusion time intervals was established to investigate the protective effects of liraglutide on hepatic IRI. Serum and liver specimens were harvested 2, 6, and 24 h after reperfusion, and liver injury was assessed by hematoxylin and eosin (H&E) staining (**Figure 1A**), serum ALT (**Figure 1B**), and AST (**Figure 1C**) levels. As shown in **Figure 1B**, ALT and AST levels gradually increased 2 and 6 h after reperfusion in the I/R group. However, liver function gradually recovered 24 h after reperfusion, and ALT and AST values were significantly attenuated in the liraglutide pretreatment group at different reperfusion times (**Figures 1B, C**, $P < 0.01$ or $P < 0.001$). Consistent with these results, H&E staining (**Figure 1A**) showed that the hepatic sinusoids were severely congested and swollen with extensive necrosis and a large number of infiltrating lymphocytes after reperfusion. Liraglutide pre-treatment distinctly improved these pathological changes at different reperfusion time intervals, verified by the Suzuki score (**Figure 1D**, $P < 0.01$). Overall, our results demonstrated that liraglutide pre-treatment protected against hepatic IRI.

Liraglutide Pretreatment Attenuates the Apoptosis of Liver Cells Caused by I/R

Hepatocyte apoptosis in I/R-induced liver injury was assessed using TUNEL staining and western blotting. As demonstrated in **Figure 2A**, the number of TUNEL-positive cells significantly

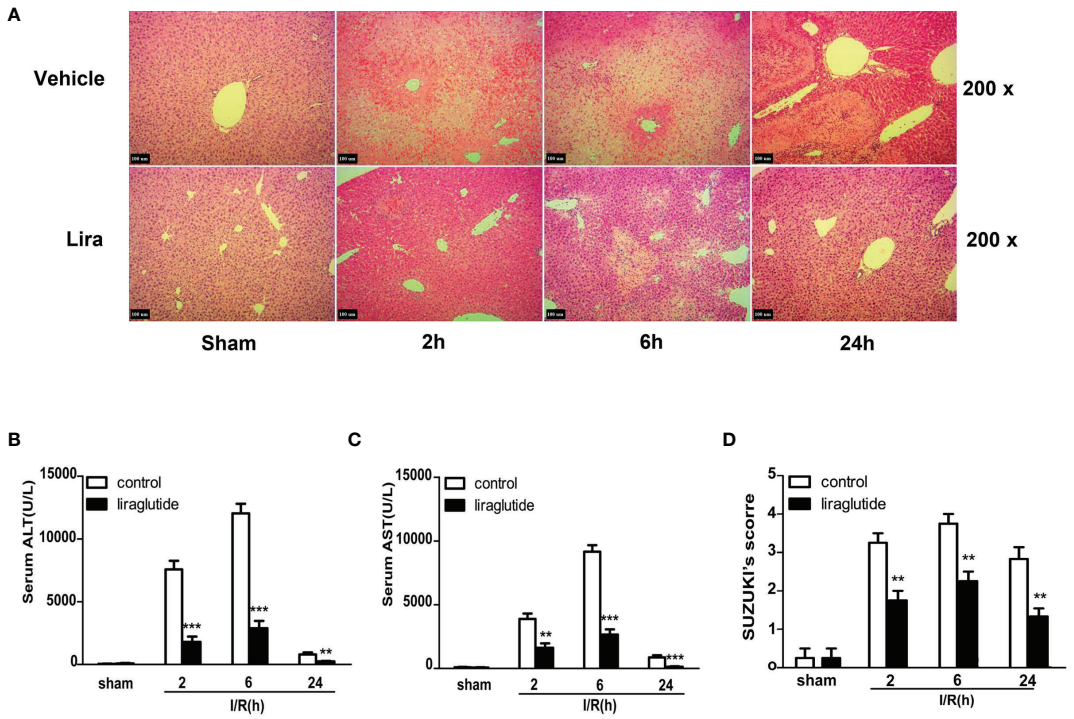

FIGURE 1 | Liraglutide pretreatment ameliorates I/R-induced liver damage. Mice were subjected to 60 min of hepatic ischemia, followed by 2, 6, and 24 h of reperfusion. **(A)** H&E staining was performed to assess live injury in mice (original magnification 200×). **(B, C)** Serum ALT and AST levels of the control and liraglutide-treated mice were detected after hepatic IRI (n = 4–6 per group). **(D)** The degree of liver injury was assessed by Suzuki's injury score (n = 3 per group). These results were obtained from at least three independent experiments. Values are presented as mean ± SD. **P < 0.01, ***P < 0.001 vs. the control group.

increased 6 h after reperfusion, whereas apoptosis was distinctly reduced in the liraglutide treatment group (P < 0.05). The balance between the pro-apoptotic protein Bax and anti-apoptotic protein Bcl-2 determines whether cells survive or undergo apoptosis. Hepatic IRI caused a significant increase in Bax expression and a marked reduction in Bcl-2 at the protein level, and liraglutide pretreatment partially reversed these changes (**Figures 2B–D**, P < 0.01 or P < 0.001). These results indicate that liraglutide pretreatment alleviated I/R-induced apoptosis in the liver.

The Protective Effect of Liraglutide Against Hepatic IRI May Be Realized Through Its Action on Macrophages

The liver contains many immune cells such as resident macrophages (KCs), neutrophils, natural killer cells (NKs), and natural killer T cells (NKTs). To investigate the effect of liraglutide on liver IRI, we eliminated these cells from mice. Surprisingly, liraglutide exerted hepatoprotective effects after the depletion of NKs (**Figure 3A**), NKTs (**Figure 3B**), and neutrophils (**Figure 3C**). However, after removing macrophages (**Figure 3D**, P < 0.01), the protective effects of liraglutide on liver IRI were largely abolished. These results demonstrated that macrophages might mediate the protective effect of liraglutide against liver IRI.

Liraglutide Pretreatment Inhibits I/R-Elicited M1 Polarization of Kupffer Cells in the Liver

Previous studies have shown that macrophage polarization plays an important role in hepatic IRI (19). Activated M1 macrophages can aggravate the inflammatory response by secreting various pro-inflammatory cytokines such as TNF-α, IL-1β, and IL-6. Therefore, we further investigated the effects of liraglutide on macrophages during liver IRI. First, macrophage phenotyping was performed by dual immunofluorescence using the macrophage markers F4/80 and M1-induced nitric oxide synthase (iNOS) markers. As presented in **Figure 4A**, more macrophages in the I/R group showed M1-type macrophages, as evidenced by an increase in $F4/80^+/iNOS^+$ positive cells, whereas liraglutide pretreatment markedly suppressed M1 polarization induced by I/R (P < 0.001). Next, we evaluated neutrophil infiltration and M1 markers using MPO staining and qRT-PCR, respectively. In the I/R group, MPO-positive cells, TNF-α, IL-1β and IL-6 levels were increased in the liver. In contrast, liraglutide treatment significantly reduced these I/R-induced elevations (**Figures 4B–E**, P < 0.05 or P < 0.001).

KCs were isolated from the liver to verify these results, and $CD68^+$ positive cells in the $F4/80^+$ and $CD11b^+$ subsets were calculated by flow cytometry. According to immunohistochemical

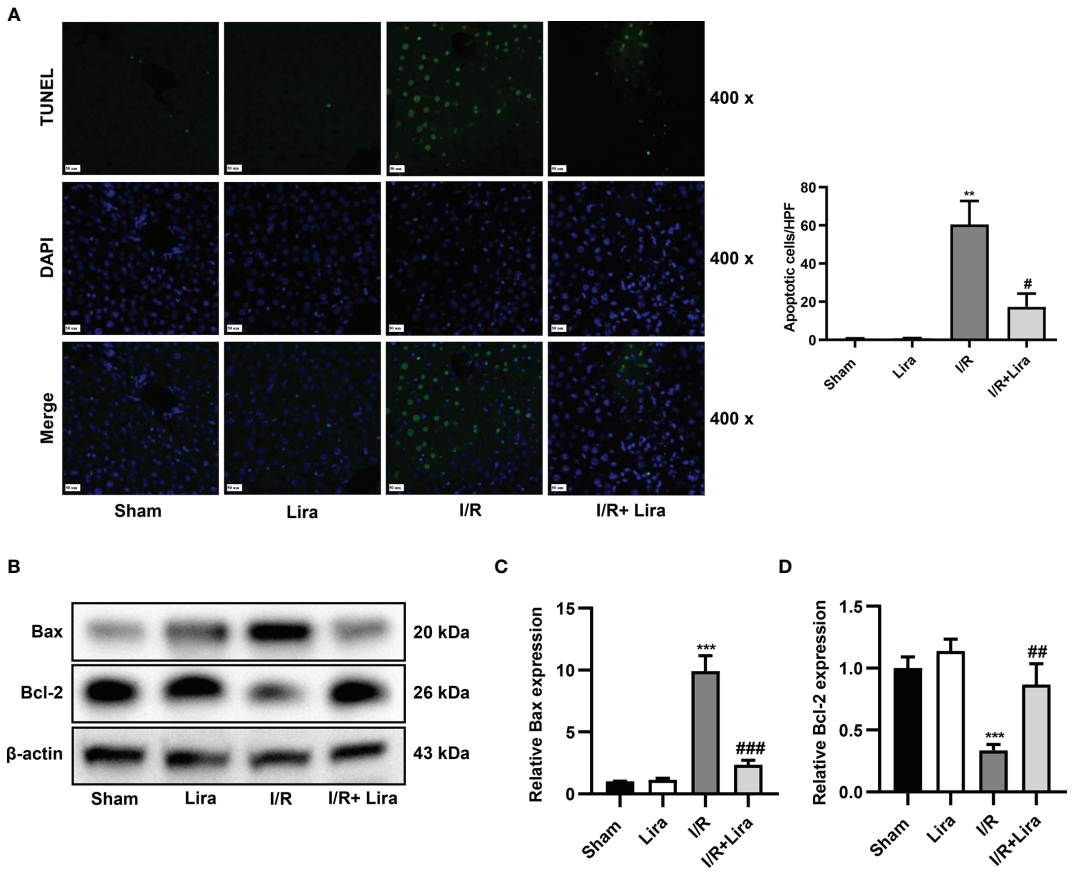

FIGURE 2 | Liraglutide pretreatment attenuates the apoptosis of liver cells caused by I/R. Mice were subjected to 60 min of hepatic ischemia, followed by 6 h of reperfusion. **(A)** TUNEL staining was performed, and TUNEL-positive cells were calculated (original magnification 400×). **(B)** The expression of Bax and Bcl-2 was determined *via* western blotting. Densitometric analysis of the Bax/β-actin **(C)**, Bcl-2/β-actin **(D)** ratios is shown. All the results were obtained from at least three independent experiments. Data are presented as mean ± SD, n = 3 per group. $^{**}P < 0.01$, $^{***}P < 0.001$ vs. the Sham group; $^{\#}P < 0.05$, $^{\#\#}P < 0.01$, and $^{\#\#\#}P < 0.001$ vs. the I/R group.

staining results, liraglutide significantly decreased M1 polarization during liver IRI. As shown in **Figure 4F**, the percentage of $CD68^+$ cells was significantly lower in the I/R+Lira group than in the I/R group (52.4.0% vs. 19.3%, $P < 0.001$). However, in GLP-$1R^{-/-}$ mice, the decrease in $CD68^+$ cells was suppressed (28.0% vs. 19.3%, $P < 0.01$). These results confirmed our findings that liraglutide pretreatment reduced M1 macrophages during hepatic IRI, and GLP-1R probably mediated the protective effects of liraglutide on liver IRI. Overall, these results showed that liraglutide pretreatment reduced the inflammatory response by inhibiting I/R-elicited M1 polarization in the liver.

Liraglutide Pretreatment Reduces LPS-Induced M1 Polarization *In Vitro*

Next, we investigated the role of liraglutide in regulating macrophage M1 polarization. BMDMs from GLP-$1R^{-/-}$ and C57BL/6J mice were isolated and cultured for *in vitro* studies. After stimulation with LPS for 24 h, the expression profiles of M1 in BMDMs were analyzed using flow cytometry and qRT-PCR. As shown in **Figure 5A**, the ratio of $CD86^+$ positive cells was significantly increased in the LPS-treated group, while M1 phenotypic transformation was reduced by liraglutide pretreatment (**Figure 5A**, second row: 82.3% vs. 60.9%, $P < 0.01$), and this inhibitory effect was partly diminished in BMDMs from GLP-$1R^{-/-}$ mice (**Figure 5A**, second row, 77.0% vs. 60.9%, $P < 0.01$). Pursuant to the above results, the expression profiles of LPS-induced M1, such as iNOS (**Figure 5B**, $P < 0.01$), TNF-α (**Figure 5C**, $P < 0.01$), IL-1β (**Figure 5D**, $P < 0.01$), and IL-6 (**Figure 5E**, $P < 0.01$), were obviously decreased by liraglutide pretreatment. However, the inhibitory effect of liraglutide on LPS-induced M1 phenotypic transformation was reversed in BMDMs from GLP-$1R^{-/-}$ mice (**Figures 5B–E**, $P < 0.05$).

Macrophage polarization is a complex process involving stimulus recognition and the activation of transcription factors (20). Recent studies have suggested that the STAT1 signaling pathway is involved in M1 macrophage polarization (21). To investigate whether liraglutide affects these cascades, we examined STAT1 phosphorylation by western blotting.

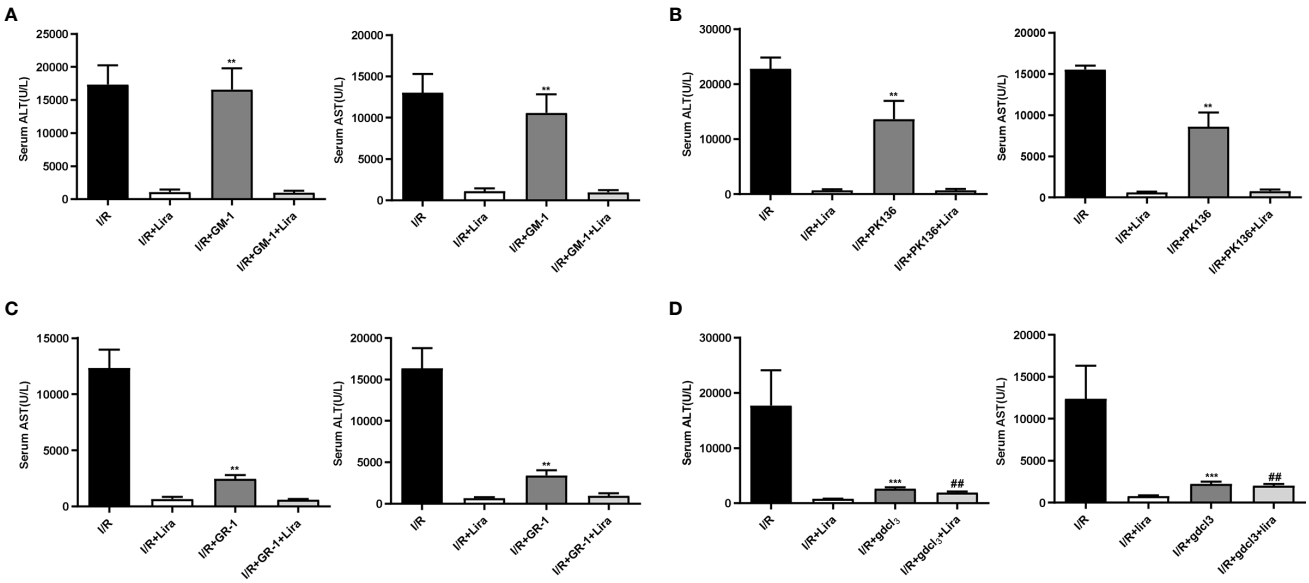

FIGURE 3 | The protective effect of liraglutide on hepatic IRI may be realized through its action on macrophages. NKs, NKTs, neutrophils, and macrophages were eliminated before liver IRI. Serum ALT and AST levels of each group after NK **(A)**, NKT **(B)**, neutrophil **(C),** and macrophage **(D)** depletion. Similar results were obtained from at least three independent experiments. Data are shown as mean ± SD, n = 3–6 per group. **P < 0.01, ***P < 0.001 vs. the I/R+Lira group; ##P < 0.01 vs. the I/R+Lira group. NKs, natural killer cells; NKTs, natural killer T cells.

Compared to unstimulated cells, the phosphorylation of STAT1 was increased in response to LPS stimulation. However, liraglutide pretreatment significantly inhibited LPS-induced phosphorylation of STAT1, and this inhibitory effect of liraglutide on LPS-induced phosphorylation of STAT1 was partly abolished in BMDMs from GLP-1R$^{-/-}$ mice (**Figure 5F**, P < 0.01). In summary, our results derived from GLP-1R-KO and C57BL/6J mice clearly indicated that the regulation of macrophage polarization by liraglutide is dependent on the GLP-1R receptor.

The Protective Effects of Liraglutide Against Hepatic IRI Are Partly Diminished in *GLP-1R*-Knockout Mice

The biological effects of liraglutide, a GLP-1R agonist, are mainly mediated by GLP-1R (22). Therefore, we examined the expression of GLP-1R in KCs exposed or unexposed to I/R using qRT-PCR. As expected, there is a certain expression of GLP-1R in the sham and liraglutide treatment groups (**Figure 6A**), whereas a significant reduction in GLP-1R expression was detected in the I/R group. However, liraglutide pretreatment markedly prevented the decrease in KC expression of GLP-1R at 6 h after reperfusion (**Figure 6A**, P < 0.05).

To determine whether the protective effects of liraglutide on hepatic IRI depended on GLP-1R, a mouse liver partial IRI model was used in C57BL/6J and GLP-1R$^{-/-}$ mice. Compared with the I/R group, liraglutide pretreatment significantly reduced the serum ALT and AST levels (**Figures 6B, C**, P < 0.001). However, when subjected to the same liraglutide treatment and hepatic I/R procedure, GLP-1R$^{-/-}$ mice showed moderately elevated serum ALT and AST levels (**Figures 6B, C**, P < 0.01). In addition, the inhibitory effects of liraglutide on liver injury, neutrophil infiltration, hepatocyte apoptosis, and M1 polarization were partly diminished in GLP-1R$^{-/-}$ mice (**Figures 6D–H**).

Overall, these results indicate that the protective effects of liraglutide on hepatic IRI were partly dependent on GLP-1R.

DISCUSSION

Hepatic IRI widely exists in clinical environments, such as liver resection, liver transplantation, and trauma, and is a key factor affecting postoperative liver function, leading to liver dysfunction and even failure (23). Therefore, the prevention and treatment of hepatic IRI are common concerns for many clinicians. With an in-depth study of hepatic IRI, the role of macrophage polarization in hepatic IRI has gradually been recognized. In the early stage of liver IRI, liver macrophages mainly show the M1-dominated pro-inflammatory response, while in the late stage of liver IRI, liver macrophages primarily exhibit M2-dominated promotion of tissue repair (24). Considering the different functions of different macrophage phenotypes, hepatic IRI can be improved by regulating macrophage polarization. In this study, we found that liraglutide reduced hepatic IRI and inhibited the inflammatory response during IRI. This protective effect was achieved *via* the regulation of macrophage polarization by GLP-1R.

The liver, the largest immune organ in the human body, contains metabolically active hepatocytes, non-hepatocyte

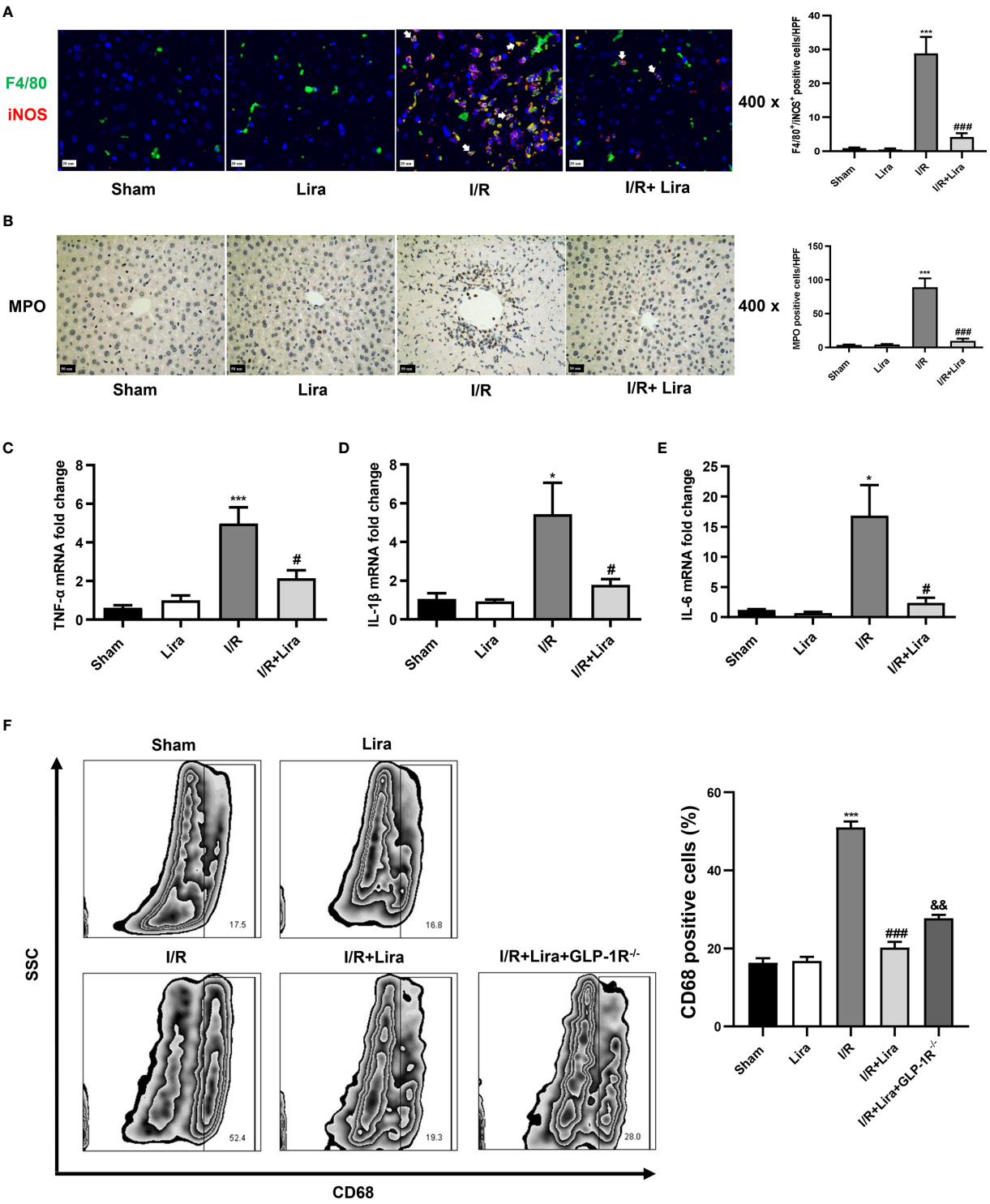

FIGURE 4 | Liraglutide pretreatment inhibits I/R-elicited M1 polarization of KCs in the liver. Mice underwent 60 min of liver ischemia and 6 h of reperfusion; liver tissues were harvested for immunofluorescence staining **(A)** and MPO staining **(B)** (original magnification 400×), and the number of F4/80$^+$/iNOS$^+$ positive cells and MPO-positive cells was calculated. The expression of pro-inflammatory cytokines, including TNF-α **(C)**, IL-1β **(D)**, and IL-6 **(E),** in the liver was detected *via* qRT-PCR. **(F)** The number of CD68$^+$-positive cells of KCs under F4/80$^+$ and CD11b$^+$ subsets was calculated *via* flow cytometry. The results represent the means from at least 3 independent experiments. Values are shown as mean ± SD, n = 3 per group. *P < 0.05, ***P < 0.001 vs. the Sham group; $^{\#}$P < 0.05, $^{\#\#\#}$P < 0.001 vs. the I/R group. $^{\&\&}$P < 0.01 vs. the I/R+Lira group. KCs, resident macrophages; MPO, myeloperoxidase.

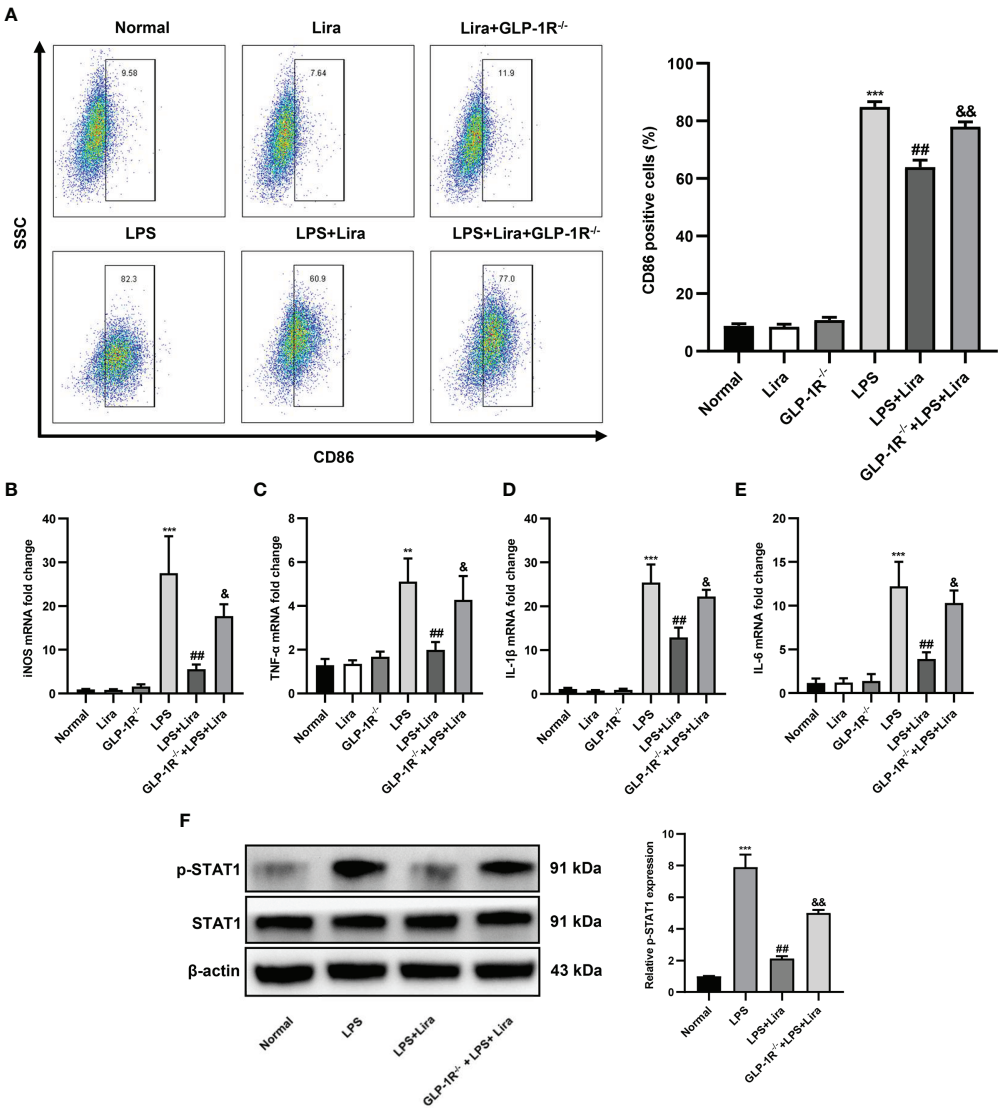

FIGURE 5 | Liraglutide pretreatment reduces LPS-induced M1 polarization *in vitro*. BMDMs from GLP-1R$^{-/-}$ and C57BL/6J mice were isolated and cultured for *in vitro* study. The cells were pretreated with liraglutide (50 μm) for 24 h, stimulated with LPS (100 nm) for 24 h, and the expression profiles of M1 in BMDMs in each group were analyzed *via* flow cytometry, RT-PCR, and western blotting. **(A)** The number of CD86^{+}-positive cells of BMDMs under F4/80^{+} and CD11b^{+} subsets was calculated *via* flow cytometry. The mRNA levels of iNOS **(B)**, TNF-α **(C)**, IL-1β **(D)**, and IL-6 **(E)** were measured *via* qRT-PCR. **(F)** The phosphorylation of STAT1 was analyzed *via* western blotting. Similar results were obtained from at least three independent experiments. Data are expressed as mean ± SD, n = 3 per group. $^{**}P < 0.01$, $^{***}P < 0.001$ vs. the Normal group; $^{\#\#}P < 0.01$ vs. the LPS group. $^{\&}P < 0.05$, $^{\&\&}P < 0.01$ vs. the LPS+Lira group. BMDMs, bone marrow derived macrophages.

parenchymal cells, and various immune cell populations. These cells play an important role in hepatic IRI (25, 26). To confirm the cells on which liraglutide acts, we first investigated the effect of liraglutide on hepatocytes *in vitro*. However, liraglutide did not show any protective effect against hypoxia-induced hepatocyte apoptosis (data not shown), which may be attributed to the lack of GLP-1R expression in hepatocytes (27, 28). Next, we removed KCs, NKs, NKTs, and neutrophils from a mouse hepatic IRI model. Interestingly, the protective effect of liraglutide on hepatic IRI disappeared after macrophage depletion; however, after the removal of NKs, NKTs, and neutrophils, liraglutide still exerted a good liver protection effect. These results indicate that the protective effect of liraglutide against hepatic IRI may be achieved through their action on macrophages.

The liver contains the largest proportion of macrophages among parenchymal organs, and macrophages play a crucial role in maintaining liver homeostasis and pathology (29, 30). Macrophages can change their phenotype according to changes in the surrounding microenvironment, and phenotypic variation in

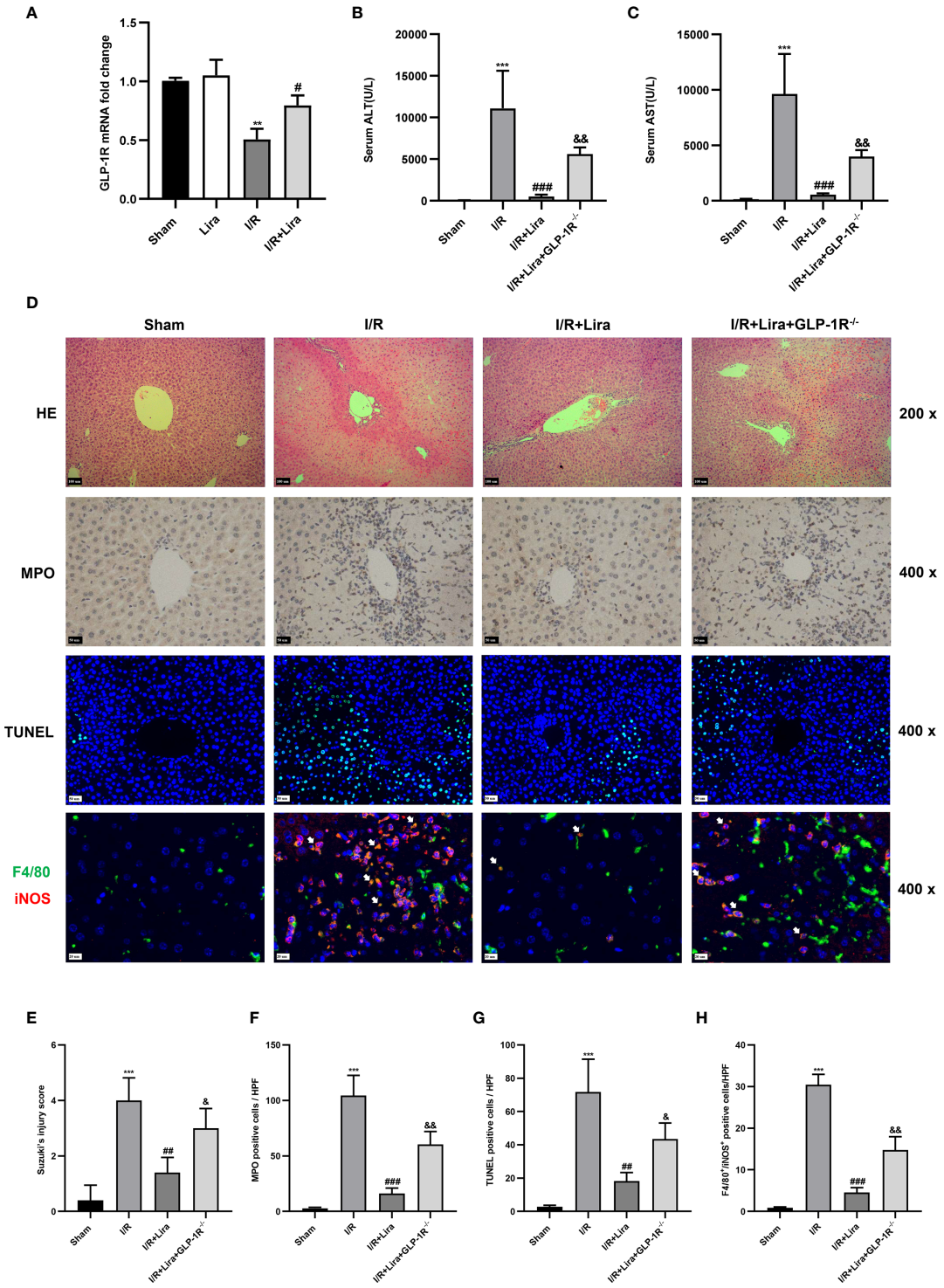

FIGURE 6 | The protective effects of liraglutide on hepatic IRI are partly diminished in *GLP-1R*- knockout mice. A mouse liver partial IRI model was established using C57BL/6J mice and GLP-1R$^{-/-}$ mice. **(A)**qRT-PCT was performed to detect GLP-1R expression in KCs from sham-operated, Lira-treated, I/R, and I/R+ Lira-treated groups (n = 3 per group). Serum levels of ALT **(B)** and AST **(C)** in each group (n = 4–6 per group). **(D)** Liver injury, neutrophil infiltration, hepatocyte apoptosis, and macrophage phenotyping were assessed *via* H&E staining, MPO, TUNEL assays, and immunofluorescence staining, respectively. Quantitation of liver injury **(E)**, neutrophil infiltration **(F)**, hepatocyte apoptosis **(G)**, and macrophage phenotyping **(H)** in each group (n = 3 per group). These results were obtained from at least three independent experiments. All values are expressed as mean ± SD. $^{**}P < 0.01$, $^{***}P < 0.001$ vs. the Sham group; $^{\#}P < 0.05$, $^{\#\#}P < 0.01$, and $^{\#\#\#}P < 0.001$ vs. the I/R group. $^{\&}P < 0.05$, $^{\&\&}P < 0.01$ vs. the I/R+Lira group.

macrophages affects their ability to secrete a variety of cytokines (31). Both phenotypes can modulate sterile liver inflammation and play important roles in initiating, maintaining, and ameliorating hepatic IRI. Macrophages can be induced to differentiate into the M1 type upon lipopolysaccharide stimulation. M1 macrophages highly express CD80, CD86, MHC II, and iNOS and secrete pro-inflammatory factors (30–32). In this study, the serum levels of ALT, AST, and pro-inflammatory cytokines, including TNF-α, IL-1β, and IL-6, significantly decreased after liraglutide treatment. Next, we examined macrophage polarization markers in liver tissues *via* flow cytometry. As expected, liraglutide treatment reduced the I/R-induced activation and recruitment of M1 macrophages. M2 macrophages play a crucial role in hepatic IRI as an anti-inflammatory phenotype. Therefore, we investigated the effects of liraglutide on M2 macrophages. Unfortunately, liraglutide treatment did not promote the growth of M2 macrophages (data not shown).

Most of the effects of liraglutide are mediated by GLP-1R, which is expressed in different cells and tissues. In the heart, GLP-1R is expressed on cardiac graft endothelial cells, and by activating the GLP-1R receptor on endothelial cells, it can delay the occurrence of graft CVD in a mouse heart transplant model (15). GLP-1R activation in tubular epithelial cells in the kidney reduces HMGB1 release during renal IRI, thereby attenuating renal injury (33). Recent studies have shown that GLP-1R is expressed in the liver (12). In a model of nonalcoholic fatty liver disease (NAFLD), liraglutide could regulate the transformation of macrophages, thereby reducing lipid accumulation and steatosis (34). However, little research has been conducted on the relationship between liraglutide pretreatment and macrophage polarity. Therefore, we speculate that liraglutide may attenuate hepatic IRI by modulating the phenotype of macrophages *via* acting on GLP-1R. Our study found that in GLP-1R$^{-/-}$ mice, the protective effect of liraglutide against hepatic IRI was partly diminished. In the *in vitro* study, we assessed the role of liraglutide in macrophage polarization by examining the expression profiles of M1 in BMDMs from GLP-1R$^{-/-}$ and C57BL/6J mice. Consistent with the *in vivo* study, liraglutide attenuated LPS-induced M1 polarization and decreased the expression of M1 markers. However, the inhibitory effect of liraglutide on LPS-induced M1 polarization was largely abolished in BMDMs from GLP-1R$^{-/-}$ mice, and the regulatory effect of liraglutide on macrophages may be mediated by the STAT1 signaling pathway. Our data derived from GLP-1R-/- and C57BL/6J mice clearly indicated that the regulation of macrophage polarization by liraglutide is dependent on the GLP-1R receptor.

However, our study has some limitations. First, as the largest immune organ in the human body, the liver contains many immune cells; however, we only investigated the effects of liraglutide on neutrophils, NKs, NKTs, and macrophages during hepatic IRI, and whether liraglutide affects other cells in the liver remains to be determined. Second, the protective effects of liraglutide on liver IRI were partially reversed in GLP-1R$^{-/-}$ mice, indicating that liraglutide may act through non-receptor pathways. Third, a recent study indicated that metabolic reprogramming is involved in macrophage polarization, and metabolic and intrinsic hormonal changes were observed in ischemic patients (35, 36); whether liraglutide, as an intrinsic hormone analog, affects macrophages by regulating metabolic reprogramming needs further investigation. These limitations should be addressed in future studies.

In summary, our study shows that liraglutide inhibits macrophage polarization towards an inflammatory phenotype *via* the GLP-1R receptor. Furthermore, our findings indicate that liraglutide pretreatment attenuates hepatic IRI and improves liver function. These results may provide a new direction for the clinical treatment of HIRI.

DATA AVAILABILITY STATEMENT

The original contributions presented in the study are included in the article/supplementary material. Further inquiries can be directed to the corresponding authors.

ETHICS STATEMENT

The animal study was reviewed and approved by Tongji Medical College Committees on Animal Experimentation.

AUTHOR CONTRIBUTIONS

Author contributions: JY had full access to all the data in the study and was responsible for the integrity of the data and accuracy of the data analysis. Study design: CD, S-LL, and Z-MW. Acquisition of data: CD, CX, and F-HC. Analysis and interpretation of data: CD, X-FH, and RC. Drafting of the manuscript: S-LL, Z-MW, CD, H-BS, Y-NX, and YQ. Critical revision of the manuscript for important intellectual content: CD and JY. Statistical analysis: S-LL, Z-MW, and JY. Obtaining funding: JY, CD, and Z-MW. Administrative, technical, or material support: H-BS and BL. Supervision: JY. All authors contributed to the article and approved the submitted version.

FUNDING

This study was supported by the National Natural Science Foundation of China (grant numbers 81873624, 81900368, and 82100800).

ACKNOWLEDGMENTS

We would like to thank the Institute of Organ Transplantation, Tongji Hospital, Tongji Medical College, Huazhong University of Science and Technology, Key Laboratory of Organ Transplantation, Ministry of Education, NHC Key Laboratory of Organ Transplantation, and Key Laboratory of Organ Transplantation, Chinese Academy of Medical Sciences, Wuhan, China 430030 and thank the colleagues there.

REFERENCES

1. Serracino-Inglott F, Habib NA, Mathie RT. Hepatic Ischemia-Reperfusion Injury. *Am J Surg* (2001) 181:160–6. doi: 10.1016/S0002-9610(00)00573-0
2. Saidi RF, Kenari SKH. Liver Ischemia/Reperfusion Injury: An Overview. *J Invest Surg* (2014) 27:366–79. doi: 10.3109/08941939.2014.932473
3. Nastos C, Kalimeris K, Papoutsidakis N, Tasoulis MK, Lykoudis PM, Theodoraki K, et al. Global Consequences of Liver Ischemia/Reperfusion Injury. *Oxid Med Cell Longev* (2014) 2014:906965. doi: 10.1155/2014/906965
4. Zheng L, Ling W, Zhu D, Li Z, Kong L. Roquin-1 Regulates Macrophage Immune Response and Participates in Hepatic Ischemia-Reperfusion Injury. *J Immunol Baltimore Md* (2020) 204:1322–33. doi: 10.4049/jimmunol.1900053
5. Wu S, Yang J, Sun G, Hu J, Zhang Q, Cai J, et al. Macrophage Extracellular Traps Aggravate Iron Overload-Related Liver Ischaemia/Reperfusion Injury. *Br J Pharmacol* (2021) 178:3783–96. doi: 10.1111/bph.15518
6. Konishi T, Lentsch AB. Hepatic Ischemia/Reperfusion: Mechanisms of Tissue Injury, Repair, and Regeneration. *Gene Expr* (2017) 17:277–87. doi: 10.3727/105221617X15042750874156
7. Dong Z, Wei H, Sun R, Tian Z. The Roles of Innate Immune Cells in Liver Injury and Regeneration. *Cell Mol Immunol* (2007) 4:241–52.
8. Lu TF, Yang TH, Zhong CP, Shen C, Lin WW, Gu GX, et al. Dual Effect of Hepatic Macrophages on Liver Ischemia and Reperfusion Injury During Liver Transplantation. *Immune Netw* (2018) 18:e24. doi: 10.4110/in.2018.18.e24
9. Jacobsen LV, Flint A, Olsen AK, Ingwersen SH. Liraglutide in Type 2 Diabetes Mellitus: Clinical Pharmacokinetics and Pharmacodynamics. *Clin Pharmacokinet* (2016) 55:657–72. doi: 10.1007/s40262-015-0343-6
10. Burcelin R, Gourdy P. Harnessing Glucagon-Like Peptide-1 Receptor Agonists for the Pharmacological Treatment of Overweight and Obesity. *Obes Rev* (2017) 18:86–98. doi: 10.1111/obr.12465
11. Knudsen LB, Lau J. The Discovery and Development of Liraglutide and Semaglutide. *Front Endocrinol (Lausanne)* (2019) 10:155. doi: 10.3389/fendo.2019.00155
12. Valdecantos MP, Pardo V, Ruiz L, Castro-Sánchez L, Lanzón B, Fernández-Millán E, et al. A Novel Glucagon-Like Peptide 1/Glucagon Receptor Dual Agonist Improves Steatohepatitis and Liver Regeneration in Mice. *Hepatology* (2017) 65:950–68. doi: 10.1002/hep.28962
13. Hu SY, Zhang Y, Zhu PJ, Zhou H, Chen YD. Liraglutide Directly Protects Cardiomyocytes Against Reperfusion Injury Possibly *via* Modulation of Intracellular Calcium Homeostasis. *J Geriatr Cardiol* (2017) 14:57–66. doi: 10.11909/j.issn.1671-5411.2017.01.008
14. Somm E, Montandon SA, Loizides-Mangold U, Gaïa N, Lazarevic V, De Vito C, et al. The Glp-1r Agonist Liraglutide Limits Hepatic Lipotoxicity and Inflammatory Response in Mice Fed a Methionine-Choline Deficient Diet. *Transl Res* (2021) 227:75–88. doi: 10.1016/j.trsl.2020.07.008
15. Li Y, Ma D, Wang Z, Yang J. Microrna-155 Deficiency in Kupffer Cells Ameliorates Liver Ischemia-Reperfusion Injury in Mice. *Transplantation* (2017) 101:1600–8. doi: 10.1097/TP.0000000000001765
16. Li PZ, Li JZ, Li M, Gong JP, He K. An Efficient Method to Isolate and Culture Mouse Kupffer Cells. *Immunol Lett* (2014) 158:52–6. doi: 10.1016/j.imlet.2013.12.002
17. Li SL, Cao R, Hu XF, Xiong P, Zhao GY, Xie YN, et al. Daidzein Ameliorated Concanavalin A-Induced Liver Injury Through the Akt/GSK-3β/Nrf2 Pathway in Mice. *Ann Transl Med* (2021) 9:1228. doi: 10.21037/atm-21-378
18. Shang L, Ren H, Wang S, Liu H, Hu A, Gou P, et al. Ss-31 Protects Liver From Ischemia-Reperfusion Injury *via* Modulating Macrophage Polarization. *Oxid Med Cell Longev* (2021) 2021:6662156. doi: 10.1155/2021/6662156
19. Biswas SK, Mantovani A. Macrophage Plasticity and Interaction With Lymphocyte Subsets: Cancer as a Paradigm. *Nat Immunol* (2010) 11:889–96. doi: 10.1038/ni.1937
20. Mosser DM, Edwards JP. Exploring the Full Spectrum of Macrophage Activation. *Nat Rev Immunol* (2008) 8:958–69. doi: 10.1038/nri2448
21. Li YK, Ma DX, Wang ZM, Hu XF, Li SL, Tian HZ, et al. The Glucagon-Like Peptide-1 (Glp-1) Analog Liraglutide Attenuates Renal Fibrosis. *Pharmacol Res* (2018) 131:102–11. doi: 10.1016/j.phrs.2018.03.004
22. Cannistrà M, Ruggiero M, Zullo A, Gallelli G, Serafini S, Maria M, et al. Hepatic Ischemia Reperfusion Injury: A Systematic Review of Literature and the Role of Current Drugs and Biomarkers. *Int J Surg* (2016) 33 Suppl 1:S57–70. doi: 10.1016/j.ijsu.2016.05.050
23. Wang H, Xi Z, Deng L, Pan Y, He K, Xia Q. Macrophage Polarization and Liver Ischemia-Reperfusion Injury. *Int J Med Sci* (2021) 18:1104–13. doi: 10.7150/ijms.52691
24. Zhai Y, Busuttil RW, Kupiec-Weglinski JW. Liver Ischemia and Reperfusion Injury: New Insights Into Mechanisms of Innate-Adaptive Immune-Mediated Tissue Inflammation. *Am J Transplant* (2011) 11:1563–9. doi: 10.1111/j.1600-6143.2011.03579.x
25. Fahrner R, Dondorf F, Ardelt M, Settmacher U, Rauchfuss F. Role of Nk, Nkt Cells and Macrophages in Liver Transplantation. *World J Gastroenterol* (2016) 22:6135–44. doi: 10.3748/wjg.v22.i27.6135
26. Byun S, Seok S, Kim YC, Zhang Y, Yau P, Iwamori N, et al. Fasting-Induced FGF21 Signaling Activates Hepatic Autophagy and Lipid Degradation *via* Jmjd3 Histone Demethylase. *Nat Commun* (2020) 11:807. doi: 10.1038/s41467-020-14384-z
27. Boland ML, Laker RC, Mather K, Nawrocki A, Oldham S, Boland BB, et al. Resolution of Nash and Hepatic Fibrosis by the Glp-1r/Gcgr Dual-Agonist Cotadutide *via* Modulating Mitochondrial Function and Lipogenesis. *Nat Metab* (2020) 2:413–31. doi: 10.1038/s42255-020-0209-6
28. Krenkel O, Tacke F. Liver Macrophages in Tissue Homeostasis and Disease. *Nat Rev Immunol* (2017) 17:306–21. doi: 10.1038/nri.2017.11
29. Sica A, Invernizzi P, Mantovani A. Macrophage Plasticity and Polarization in Liver Homeostasis and Pathology. *Hepatology* (2014) 59:2034–42. doi: 10.1002/hep.26754
30. Funes SC, Rios M, Escobar-Vera J, Kalergis AM. Implications of Macrophage Polarization in Autoimmunity. *Immunology* (2018) 154:186–95. doi: 10.1111/imm.12910
31. Tugal D, Liao X, Jain MK. Transcriptional Control of Macrophage Polarization. *Arterioscler Thromb Vasc Biol* (2013) 33:1135–44. doi: 10.1161/ATVBAHA.113.301453
32. Wang Z, Wang M, Hu X, Li Y, Ma D, Li S, et al. Liraglutide, a Glucagon-Like Peptide-1 Receptor Agonist, Attenuates Development of Cardiac Allograft Vasculopathy in a Murine Heart Transplant Model. *Transplantation* (2019) 103:502–11. doi: 10.1097/TP.0000000000002448
33. Li Y, Xu B, Yang J, Wang L, Tan X, Hu X, et al. Liraglutide Protects Against Lethal Renal Ischemia-Reperfusion Injury by Inhibiting High-Mobility Group Box 1 Nuclear-Cytoplasmic Translocation and Release. *Pharmacol Res* (2021) 173:105867. doi: 10.1016/j.phrs.2021.105867
34. Li Z, Feng PP, Zhao ZB, Zhu W, Gong JP, Du HM. Liraglutide Protects Against Inflammatory Stress in Non-Alcoholic Fatty Liver by Modulating Kupffer Cells M2 Polarization *via* Camp-Pka-Stat3 Signaling Pathway. *Biochem Biophys Res Commun* (2019) 510:20–6. doi: 10.1016/j.bbrc.2018.12.149
35. Usuelli V, Ben Nasr M, D'Addio F, Liu K, Vergani A, El Essawy B, et al. Mir-21 Antagonism Reprograms Macrophage Metabolism and Abrogates Chronic Allograft Vasculopathy. *Am J Transplant* (2021) 21:3280–95. doi: 10.1111/ajt.16581
36. Fiorina P, Lattuada G, Ponari O, Silvestrini C, Dallaglio P. Impaired Nocturnal Melatonin Excretion and Changes of Immunological Status in Ischaemic Stroke Patients. *Lancet* (1996) 347:692–3. doi: 10.1016/S0140-6736(96)91246-5

Conflict of Interest: The authors declare that the research was conducted in the absence of any commercial or financial relationships that could be construed as a potential conflict of interest.

frontiers | Frontiers in Immunology

ORIGINAL RESEARCH
published: 22 April 2022
doi: 10.3389/fimmu.2022.862503

Propionic Acid, Induced in Gut by an Inulin Diet, Suppresses Inflammation and Ameliorates Liver Ischemia and Reperfusion Injury in Mice

Junya Kawasoe[1,2], Yoichiro Uchida[1,2], Hiroshi Kawamoto[1,2], Tomoyuki Miyauchi[2], Takeshi Watanabe[3], Kenichi Saga[1,2], Kosuke Tanaka[1,2], Shugo Ueda[2], Hiroaki Terajima[1,2], Kojiro Taura[1] and Etsuro Hatano[1]*

[1] Department of Surgery, Graduate School of Medicine, Kyoto University, Kyoto, Japan, [2] Department of Gastroenterological Surgery and Oncology, Kitano Hospital Medical Research Institute, Osaka, Japan, [3] Division of Immunology, Institute for Frontier Life and Medical Sciences, Kyoto University, Kyoto, Japan

OPEN ACCESS

Edited by:
Bibo Ke,
University of California, Los Angeles, United States

Reviewed by:
Hirofumi Hirao,
University of California, Los Angeles, United States
Arun Prakash,
University of California, San Francisco, United States

***Correspondence:**
Yoichiro Uchida
uchiday@kuhp.kyoto-u.ac.jp

Specialty section:
This article was submitted to Molecular Innate Immunity, a section of the journal Frontiers in Immunology

Received: 26 January 2022
Accepted: 28 March 2022
Published: 22 April 2022

Citation:
Kawasoe J, Uchida Y, Kawamoto H, Miyauchi T, Watanabe T, Saga K, Tanaka K, Ueda S, Terajima H, Taura K and Hatano E (2022) Propionic Acid, Induced in Gut by an Inulin Diet, Suppresses Inflammation and Ameliorates Liver Ischemia and Reperfusion Injury in Mice. Front. Immunol. 13:862503. doi: 10.3389/fimmu.2022.862503

Liver ischemia and reperfusion injury (IRI) is one of the obstacles in liver surgery such as liver resection and transplantation. In this study, we investigated the preventive effect on mouse liver IRI by feeding mice with inulin, which is a heterogeneous blend of indigestible fructose polymer. Mice were fed either a control ordinary diet (CD) or an inulin diet (ID) containing 5% inulin in the CD, for 14 days before the ischemia and reperfusion (IR) maneuver. IR induced-liver damages were significantly ameliorated in the ID group, compared with those in the CD group. Feeding mice with an ID, but not a CD, elevated levels of *Bacteroidetes* among gut microbiota, and especially increased *Bacteroides acidifaciens* in mouse feces, which resulted in significant elevation of short-chain fatty acids (SCFAs) in the portal vein of mice. Among SCFAs, propionic acid (PA) was most significantly increased. The microbial gene functions related to PA biosynthesis were much higher in the fecal microbiome of the ID group compared to the CD. However, the action of PA on liver IRI has not been yet clarified. Direct intraperitoneal administration of PA alone prior to the ischemia strongly suppressed liver cell damages as well as inflammatory responses caused by liver IR. Furthermore, PA suppressed the secretion of inflammatory cytokines from peritoneal macrophages stimulated *in vitro* through TLR-4 with high-mobility group box 1 protein (HMGB-1), known to be released from apoptotic liver cells during the IR insult. The present study shows that PA may play a key role in the inulin-induced amelioration of mouse liver IRI.

Keywords: liver ischemia-reperfusion injury, inulin diet, short-chain fatty acid, gut microbiota, propionic acid

Abbreviations: CD, control ordinary diet; DAMPs, damage-associated molecular patterns; ELISA, enzyme-linked immunosorbent assay; ERAS, Enhanced Recovery After Surgery; F/B, Bacteroidetes-to-Firmicutes; FOXO1, Forkhead box protein O1; GPR, G protein-coupled receptor; HDAC, histone deacetylase; HMGB-1, high-mobility group box 1 protein; HO-1, heme oxygenase-1; ID, inulin diet; IR, ischemia and reperfusion; IRI, ischemia and reperfusion injury; PA, propionic acid; ROS, reactive oxygen species; sALT, serum alanine aminotransferase; SCFA, short-chain fatty acid; STAT, signal transducer and activator of transcription; TLR-4, Toll-like receptor 4; TNF-α, tumor necrosis factor-α; Treg cells, regulatory T cells; TUNEL, terminal deoxynucleotidyl transferase-mediated deoxyuridine triphosphate nick-end labeling; WT, wild-type.

INTRODUCTION

Liver ischemia and reperfusion injury (IRI) is an inevitable event in the field of liver surgery including liver transplantation, and it has been a major cause of postoperative liver dysfunction and failure (1, 2). IRI is caused by various mechanisms, including the release of inflammatory cytokines and chemokines that results in the activation of neutrophils and macrophages. As to liver IRI, damage-associated molecular patterns (DAMPs) such as high-mobility group box 1 (HMGB-1) proteins, free fatty acids, and heat shock proteins are released from damaged liver sinusoidal endothelial cells and hepatocytes (3). These molecules increase and amplify ischemia and reperfusion (IR)-induced liver injury. Reactive oxygen species (ROS) generated by activated Kupffer cells are also a major mediator in liver IRI (4). So far, we have reported various approaches to overcome liver IRI (5–7). It has been shown that HMGB-1 released from an IR-injured liver acts through the Toll-like receptor 4 (TLR-4) on hepatocytes and macrophages, which results in the apoptotic cell death of hepatocytes and induction of severe inflammatory responses by macrophages (8). Blocking the interaction between HMGB-1 and TLR-4 could prevent liver IRI in a TLR-4 dependent manner (5, 6). Recently, the Enhanced Recovery After Surgery (ERAS) protocol is advocated in the field of liver surgery. ERAS is a multifaceted pathway, including a preoperative nutritional approach, and has been developed to overcome the deleterious effect of perioperative stress after surgery (9). We recently reported a finding that pretreatment of mice by the short-term (12 h) restriction of feeding remarkably ameliorates IR-induced liver damage and inflammation (7).

Inulin is a water-soluble fermentable dietary fiber, belonging to a group of nondigestible carbohydrates called fructans (10). Inulin cannot be absorbed by the human intestinal tract, and is decomposed by gut microbiota into degradation products, such as short-chain fatty acids (SCFAs) (11, 12). SCFAs interact with various receptors, such as G protein-coupled receptors (GPRs), GPR41, GPR43, and GPR109A, expressed on the gut epithelium and immune cells (13). The interaction between SCFAs and GPRs is related to the activity of immune cells and the induction of regulatory T cells. Butyrate is one of the SCFAs and has been reported to induce the differentiation of regulatory T cells and to ameliorate the development of colitis (14). The effects of SCFAs, such as butyric acid, propionic acid (PA), and valeric acid, have been reported to show a negative correlation with the immunostimulatory M1 macrophages, but a positive correlation with the immunoinhibitory M2 macrophages (15). In a mouse alcoholic liver disease model, feeding mice with inulin ameliorates the inflammation by inducing the suppression of M1 and facilitating M2 macrophages *via* SCFAs (15). Various previous reports suggest the efficacy of SCFAs, especially butyric acid, against IR-induced organ injury (16–22). In the present study, we show, for the first time, that feeding mice with an inulin-rich enteral diet significantly reduced mouse liver IR insult, suggesting the efficacy of preoperative inulin-rich enteral diets against liver IRI as a novel means of ERAS. PA among the SCFAs, was most significantly increased in the portal vein of mice fed with an inulin-rich diet, suggesting that inulin diet efficiently promoted the production of PA by gut microbiota. Although few studies thus far have reported the efficacy of PA on liver IRI, the present study clearly shows that the intraperitoneal administration of PA alone resulted in remarkable amelioration of liver injury through not only the protection from liver cell death caused by IR but also the suppression of proinflammatory responses induced in macrophages activated by HMGB-1. PA might play a key role in the inulin diet-induced suppression of liver IRI.

MATERIALS AND METHODS

Animals

Male C57BL/6 mice (8-10 weeks old, weighing 20-25 g) were purchased from Shimizu Laboratory Supplies (Kyoto, Japan). All animals were maintained in specific pathogen-free conditions and received humane care according to the Guide for Care and Use of Laboratory Animals. All experimental protocols were approved by the Animal Research Committee of The Tazuke Kofukai Medical Research Institute, Kitano Hospital, Osaka, Japan.

Mouse Diets

The control ordinary diet (CD) was AIN-93G (23). The inulin diet (ID) was the CD supplemented with 5% inulin. We determined the content of inulin based on the previous studies (24, 25). Both diet reagents were provided by EN Otsuka Pharmaceutical Co., Ltd. (Hanamaki, Iwate, Japan). The compositions of both diets are shown in **Table 1**.

Liver IRI Model

We used the established mouse model of partial warm liver IRI (5, 6). Mice were anesthetized under isoflurane and injected with heparin (100 U/kg). An atraumatic clip was used to interrupt the artery and portal venous supply and the bile duct to the left and middle liver lobes. After 60 minutes of ischemia at room temperature, the clamp was removed, and reperfusion was initiated. After 6 hours of reperfusion, mice were sacrificed. Liver samples were immediately fixed overnight in 10% formaldehyde or frozen in liquid nitrogen until the extraction procedure. Sham-operated mice underwent the same procedure, but without vascular occlusion.

Hepatocyte Function

Serum alanine aminotransferase (sALT) levels, used as a measure of liver injury, were determined by a standard spectrophotometric method with an automated clinical analyzer (JCABM9030, JEOL Ltd., Tokyo, Japan).

Treatment of Mice With Propionic Acid

Propionic acid (PA) solution was purchased from FUJIFILM Wako Pure Chemical Corporation (Osaka, Japan) and diluted with saline. After sterilization by filter, PA (at 5 mmol/kg, 100μM per a mouse of 20 grams weight, in saline) was administered intraperitoneally 2 hours before the ischemic insult. The dosage of PA was determined based on the previous report (26).

TABLE 1 | Compositions of the Control ordinary diet and Inulin diet.

	Control ordinary diet (AIN-93G) (377 kcal/100g) (%)	Inulin diet (366 kcal/100g) (%)
Casein	20.0000	20.0000
L-cystine	0.3000	0.3000
Corn starch	**39.7486**	**34.7486**
αcorn starch	13.2000	13.2000
Sucrose	10.0000	10.0000
Soybean oil	7.0000	7.0000
Cellulose powder	5.0000	5.0000
Minerals	3.5000	3.5000
Vitamins	1.0000	1.0000
Choline Bitartrate	0.2500	0.2500
t-butylhydroquinone	0.0015	0.0014
inulin	**0.0000**	**5.0000**

The bold values mean our intention to emphasize the difference between the two groups.

Histology

Liver paraffin sections (5 μm thick) were stained with hematoxylin and eosin (H&E). The severity of liver IRI (necrosis, sinusoidal congestion, and centrilobular ballooning) was graded on a scale from 0 to 4 by an investigator who was blinded to the experimental conditions using the modified Suzuki's criteria (27). In the modified Suzuki's criteria, scores are determined by the presence of congestion (from a value of 0 to a value of 4 depending on the severity), vacuolization (from 0 to 4) and necrosis (from 0 to 4). Ten fields were examined for each sample.

Enzyme-Linked Immunosorbent Assay (ELISA)

The serum HMGB-1 level was quantified with the HMGB-1 ELISA Kit II (Shino-Test, Tokyo, Japan). The medium from peritoneal macrophage culture was analyzed for tumor necrosis factor (TNF)-α using an ELISA kit as per the manufacturer's instructions (R&D Systems, Minneapolis, MN, USA).

Western Blot Assay

Western immunoblotting was performed using standard techniques as described previously (7). Primary antibodies used are listed in **Table S1**.

Quantitative Reverse-Transcription Polymerase Chain Reaction (qRT-PCR)

Total RNA was extracted from liver tissues with the RNeasy Mini Kit (QIAGEN, Venlo, the Netherlands). Complementary DNA was prepared using a PrimeScript RT Reagent Kit (TAKARA BIO, Kusatsu, Japan). qRT-PCR was performed using the StepOnePlus$_{TM}$ Real-Time PCR System (Life Technologies, Tokyo, Japan). Primers used to amplify specific gene fragments are listed in **Table S2**. Target gene expression was calculated using the ratio of that gene to the housekeeping gene, β-actin.

Apoptosis Assay

Apoptosis in 5-μm-thick liver paraffin sections was detected by the terminal deoxynucleotidyl transferase-mediated deoxyuridine triphosphate nick-end labeling (TUNEL) method using an *in situ* Apoptosis Detection Kit (Takara Bio, Kyoto, Japan), according to the manufacturer's instructions.

Analyses of Gut Microbiota in Mice

Mice were divided into two groups. Mice in each group were fed a CD or an ID for 14 days before feces collection. On day 15, all fecal samples obtained from mice of both groups were collected and stored at -80 °C until analyses of the gut microbial flora. A two-step tailed PCR method was used for the preparation of dsDNA libraries. Library concentrations were measured with a Synergy H1 microplate reader (BioTek) and a QuantiFluor dsDNA System (Promega). The library quality was assessed using a Fragment Analyzer (Advanced Analytical Technologies, Ankeny, IA, USA) with a dsDNA 915 Reagent Kit (Agilent, Santa Clara, CA, USA). Paired-end sequencing (2 × 300 bp) was performed on the Illumina MiSeq platform (Illumina, San Diego, CA, USA) with the MiSeq Reagent Kit v3 (Illumina). A sequence that completely matched the primer used was extracted by using the fast barcode splitter tool. After the trimming of the primer sequence, denoized sequences were analyzed using Qiime2.0 (2019.4). The EzBioCloud 16S database (28) was used to classify the bacterial species. These analysis procedures were performed at Bioengineering Lab. Co., Ltd. (Sagamihara, Kanagawa, Japan).

Predictive Function Analysis

Phylogenetic Investigation of Communities by Reconstruction of Unobserved States (PICRUSt) (29) provided a number of scripts in fecal microbiome, that could be useful for analyzing both 16S rRNA gene relative abundances and the predicted metabolic data.

Quantification of SCFAs in the Portal Vein

After mice were fed with a CD or an ID for 14 days, the blood in the portal vein of mice in both groups were sampled with 27-gauge needles. After centrifugation at 2000 × g for 10 minutes at room temperature, serum samples were collected and stored at -80°C until the detection of SCFAs. The SCFA extraction

procedure and analysis methods were the same as those described previously by the Kyoto Institute of Nutrition and Pathology (Kyoto, Japan) (30, 31).

Cell Cultures

Thioglycollate-elicited peritoneal macrophages, which were collected using a method described previously (5), were plated into 24-well cell culture plates, at 2.0×10^5 cells/well at a volume of 0.5 mL/well, and the plates were incubated in a humidified atmosphere of 5% CO_2 and 95% air. After 3 hours, adherent cells were recovered and washed three times with phosphate-buffered saline to remove non-adherent cells. Resultant peritoneal macrophages were then incubated with various concentrations of PA (n = 3 in each group) for 30 minutes. Then, bovine HMGB-1 (Chondrex, Redmond, WA, USA) (1 μg/mL) was added to the macrophages. Forty-eight hours after treatment, supernatants were collected and stored at -80°C until measurements of TNF-α were performed by ELISA. Plated macrophages were collected by dissolving in cell lysis buffer with protease and phosphorylation inhibitors. Cell lysates were stored at -80°C until western blotting analyses.

Flow Cytometry

The ratio of Foxp3-positive T cells to CD4-positive cells was assessed by flow cytometry using CytoFLEX (Beckman Coulter, Brea, CA, USA). The FOXP3 Fix/Perm Buffer Set (BioLegend, San Diego, CA, USA) was used for the intracellular staining of Foxp3. Anti-CD4 monoclonal antibody (FITC) and anti-Foxp3 monoclonal antibody (APC) were purchased from eBioscience (San Diego, CA, USA).

Statistical Analyses

All data are presented as the means ± standard deviations. Differences between experimental groups were analyzed using the one-way analysis of variance of Student's t-test for unpaired data. All differences were considered statistically significant at a P-value less than 0.05.

RESULTS

Two Weeks of Feeding With an ID Suppressed Liver IRI

The control ordinary diet (CD) was AIN-93G (23). The inulin diet (ID) was the CD supplemented with 5% inulin (**Table 1**). We determined the content of inulin based on the previous studies (24, 25). It has been reported that feeding with AIN-93G plus 5% inulin could reduce the presence of Clostridium XI in mouse intestinal microbiota (25). The two groups of mice were fed either a CD or an ID, in addition to water ad libitum, for 14 days prior to IR stimulation. Then, mice in both groups received the liver IR treatment (**Figure 1A**). The body weights of the mice in both groups before IR were measured on days 1 and 15 after feeding them with the CD or ID. No significant difference in body weight was observed in the two groups (**Figure 1B**). The sALT titers of mice in the ID group after liver IR insult were decreased significantly compared with those in the CD group (**Figure 1C**). As **Figure 1D** shows, liver histology displayed prominent hepatocellular necrosis, in addition to congestion and ballooning, among the mice in the CD group after IR stimulation. By contrast, the livers from the ID group subjected to IR stimulation revealed significantly less pathology, as shown in **Figure 1D**. Suzuki's score was also significantly lower in the ID group (**Figure 1E**). As IR stimulation has been reported to promote the production of ROS and hepatocyte apoptosis (4, 32, 33), we examined liver tissues from both groups using the TUNEL assay to assess apoptosis. The numbers of TUNEL-positive cells induced by IR were diminished significantly in the ID group compared with the CD group (**Figures 1F, G**). It has been reported that inflammatory cytokines and chemokines play a key role in liver IRI (34, 35). Feeding mice with an ID resulted in a significant decrease in the expression of proinflammatory cytokines, such as TNF-α and IL-6. As to chemokines, CXCL-2 expression was strongly suppressed in the ID group (**Figure 1H**), suggesting that the infiltration of neutrophils into the liver may also be reduced. However, no significant increase was observed in the expression of immunosuppressive cytokines, such as IL-10, in liver tissues from the ID group (**Figure 1H**). The ratio of Foxp3-positive T cells in the mesenteric lymph nodes showed no significant difference between both groups (**Figure S1**). These results indicated that the inulin-enriched diet could exhibit the amelioration of liver injury induced by IR through the suppression of proinflammatory cytokines and the prevention of apoptosis. However, either immunosuppressive cytokines, such as IL-10 or Foxp3-positive regulatory T cells appeared not to play a crucial role in the suppression of inflammation as well as in the improvement of liver cell survival during IRI.

Effects of ID on Distribution of Gut Microbiota and SCFA Concentration in the Portal Vein

It has been reported that inulin is fermented by gut microbiota into degradation products such as SCFAs. To investigate first whether the ID affects the changes in gut microbiota, fecal samples collected from both groups of CD and ID were examined by sequencing the conserved 16S rRNA gene. Among the various changes in gut microbiota, elevated levels of *Bacteroidetes* (from 41% to 56% of the gut microbiota) and reduced levels of *Firmicutes* (from 45% to 40% of the gut microbiota) were observed in the ID group compared with the CD group (**Figure 2A**). Furthermore, the ratio of *Bacteroides acidifaciens*, a potential inulin utilizer (36), was significantly increased in feces of the ID group (from 0.6% to 17% of the gut microbiota) (**Figure 2B**). It has been reported that feeding mice with an inulin-rich diet resulted in the increase of *Bacteroides acidifaciens* in their feces (37). The decreased ratio of *Firmicutes* to *Bacteroidetes* (F/B) might affect SCFA production in the intestinal tract of mice. The majority of SCFAs is produced mainly by gut microbiota through the saccharolytic fermentation of carbohydrates (38). A decrease in the F/B ratio has been reported to be positively correlated with the fecal concentration of SCFAs, such as acetic acid, PA, and

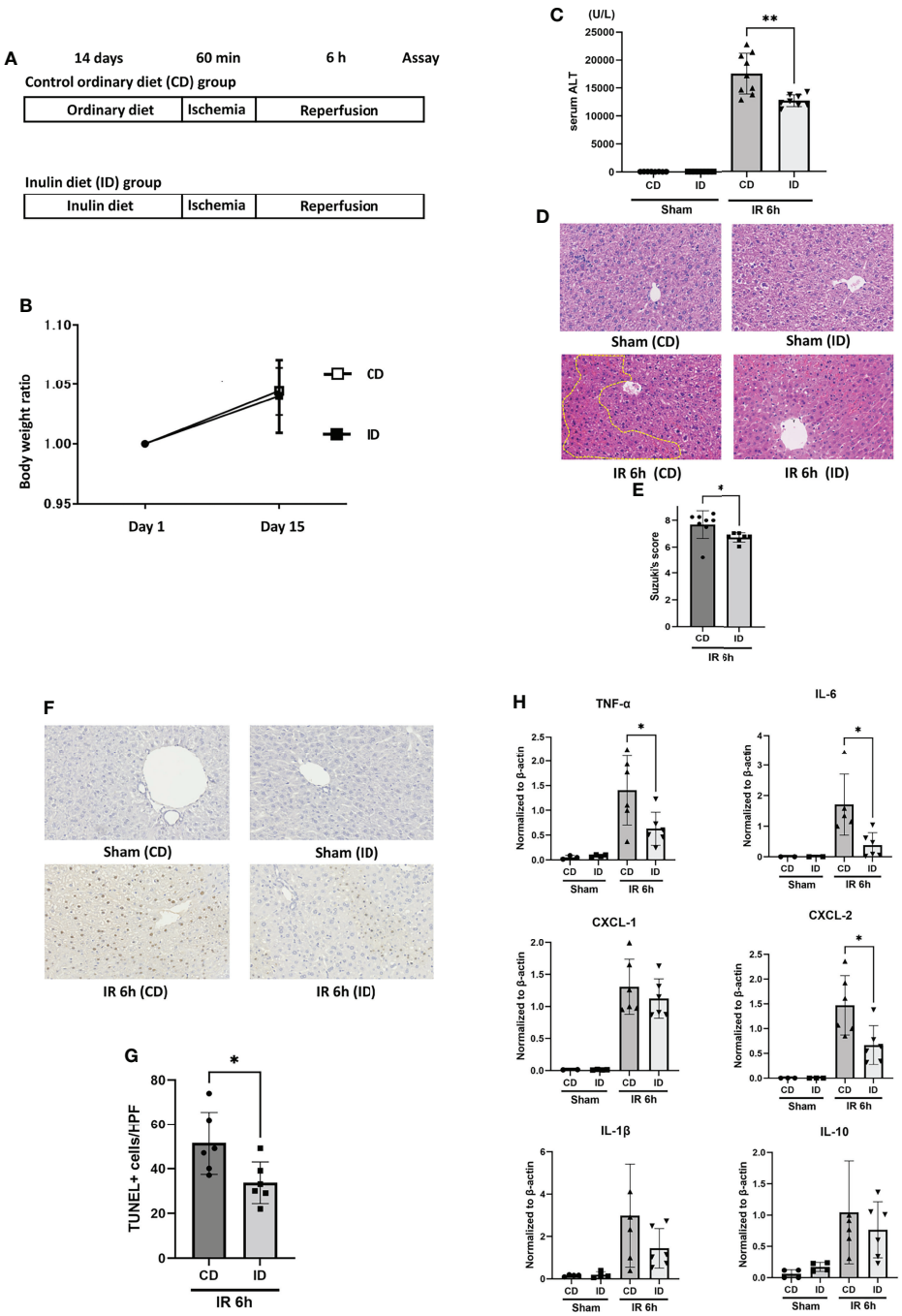

FIGURE 1 | Feeding with an inulin diet ameliorates liver ischemia and reperfusion injury in mice. **(A)** Wild-type (WT) mice were divided into two groups. They were fed a CD or an ID for 14 days prior to IR stimulation. Then, mice in both groups were subjected to liver IRI treatment which means 60 min of liver ischemia, followed by 6 h of reperfusion. After 6 h of reperfusion, the serum and liver tissue of each mouse was collected for assays. Sham-operated mice underwent the same procedure, but without vascular occlusion. **(B)** The body weight of each mouse was monitored on days 1 and 15. **(C)** The sALT level after 6 h of reperfusion (n = 8 mice/group; **P < .01) (Power calculation: 1.000). **(D)** Representative liver histology (H&E staining) after IR insult (magnification ×400). Congestion area was shown in circle by yellow dot. **(E)** Suzuki's histological grading in each group (n = 8 mice/group; *P < .05). **(F)** Representative TUNEL-assisted detection of hepatic apoptosis in liver tissues after IR (magnification ×400). **(G)** Quantification of hepatic apoptosis by counting TUNEL-positive cells. (n = 8 mice/group; *P < .05). (Power calculation: 0.981) **(H)** Quantitative RT-PCR detection of inflammatory cytokines (TNF-α, IL-6, CXCL-1, CXCL-2, IL-1β, and IL-10) at 6 h of reperfusion. Data were normalized to β-actin gene expression (n = 6 mice/group; *P < .05) (Power calculation: TNF-α; 0.968, IL-6; 0.984, CXCL-2; 0.990).

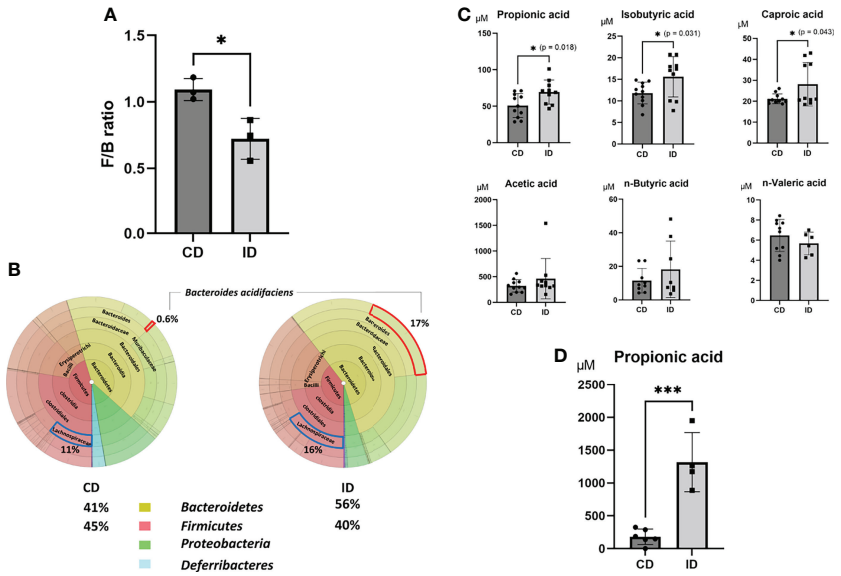

FIGURE 2 | Effects of an inulin diet on the distribution of gut microbiota and the concentrations of short-chain fatty acids in the portal vein. The feces obtained from mice fed a CD or an ID were collected and analyzed by sequencing of the conserved 16S ribosomal RNA (rRNA) gene to examine gut microbiota. **(A)** The decreased ratio of *Firmicutes* (F) to *Bacteroidetes* (B) (F/B ratio) in the CD and ID groups (n = 3 mice/group) (Power calculation: 0.912). **(B)** The average value of the distribution of gut microbiota in the CD and ID groups (n = 3 mice/group). **(C)** The concentrations of various fatty acids in the portal vein in mice of both groups were measured (n = 10-11 mice/group; *P < .05) (Power calculation: Propionic acid; 1.000, Isobutyric acid; 0.998, Caproic acid; 0.996). **(D)** The concentration of propionic acid in the cecal contents in mice of both groups was measured (n = 4 mice/group; ***P < .01) (Power calculation: 1.000).

butyric acid (39). These SCFAs are supposed to be absorbed from the intestinal mucosa into the portal vein. Therefore, the concentrations of various fatty acids in the portal vein were measured in both groups (**Figure 2C**). Among the SCFAs examined, levels of propionic acid (PA) ($p = 0.018$) as well as isobutyric acid ($p = 0.031$), and caproic acid ($p = 0.043$) were elevated significantly in the portal vein of mice in the ID group compared to that in the CD group. On the other hand, among *Firmicutes* genus, the increase of *Lachnospiraceae* in feces was also evident upon the inulin diet (**Figure 2B**). It has been reported that the enhancement of propionate is correlated with favorable increases of *Lachnospiraceae* (40), suggesting they might also contribute to the increment of propionate induced by inulin diet. In fact, the concentration of PA in the cecal content obtained from mice fed with ID for 14 days was significantly higher than that from mice fed with CD (**Figure 2D**).

PICRUSt (Phylogenetic Investigation of Communities by Reconstruction of Unobserved States) analysis (29) was used to predict the abundances of functional genes in fecal microbiota of CD and ID groups of mice. In the Kyoto Encyclopedia of Genes and Genomes (KEGG) pathways, the microbial gene functions related to PA biosynthesis were much higher in the fecal microbiome of the ID group ($p < 0.05$, **Figure S2**). From these analyses, although the effect of butyric acid on the suppression of liver IRI has been well examined previously (17, 19, 21), we focused in the present study especially on the action of PA, which showed the most significant elevation in the portal vein in the ID group, as another possible candidate for the amelioration of mouse liver IRI.

Intraperitoneal PA Administration Strongly Improved Liver IRI by Suppressing Inflammatory Cytokines

In order to clarify whether or not the effect of PA plays a crucial role in the ID-induced amelioration of liver IRI, PA (at 5 mmol/kg, 100μM per a mouse of 20 grams weight, in saline) was administered intraperitoneally 2 hours before the ischemic insult as shown in **Figure 3A**. As a control, mice were intraperitoneally administered saline only instead of PA at the same time point. The sALT level was significantly improved in the PA group (**Figure 3B**). Macroscopically (**Figure 3C**) and microscopically (**Figure 3D**), PA-pretreated mice clearly showed less liver damage caused by IR insult, than saline-pretreated mice. Pathological findings (Suzuki's score, **Figure 3E**) were also improved in the PA group. The expression of inflammatory cytokines and chemokines in liver tissues after IR stimulation was clearly suppressed in the PA group, that is, IL-6, TNF-α, IL-1β, and CXCL-2 but not CXCL-1 were remarkably reduced in the PA-treated group than in the saline-treated group (**Figure 3F**). However, similarly to the results of inulin-diet fed mice as shown in **Figure 1H**, the expression of IL-10, which is known as one of the immunosuppressive cytokines, was not affected by PA treatment, suggesting that immunoregulatory effect may not be involved in the suppression of inflammation induced by PA as well as the inulin. HMGB-1 has been reported as one of the DAMPs released from necrotic cells and hepatocytes in the case of liver IR insult, which leads to the activation of macrophages, followed by the production of

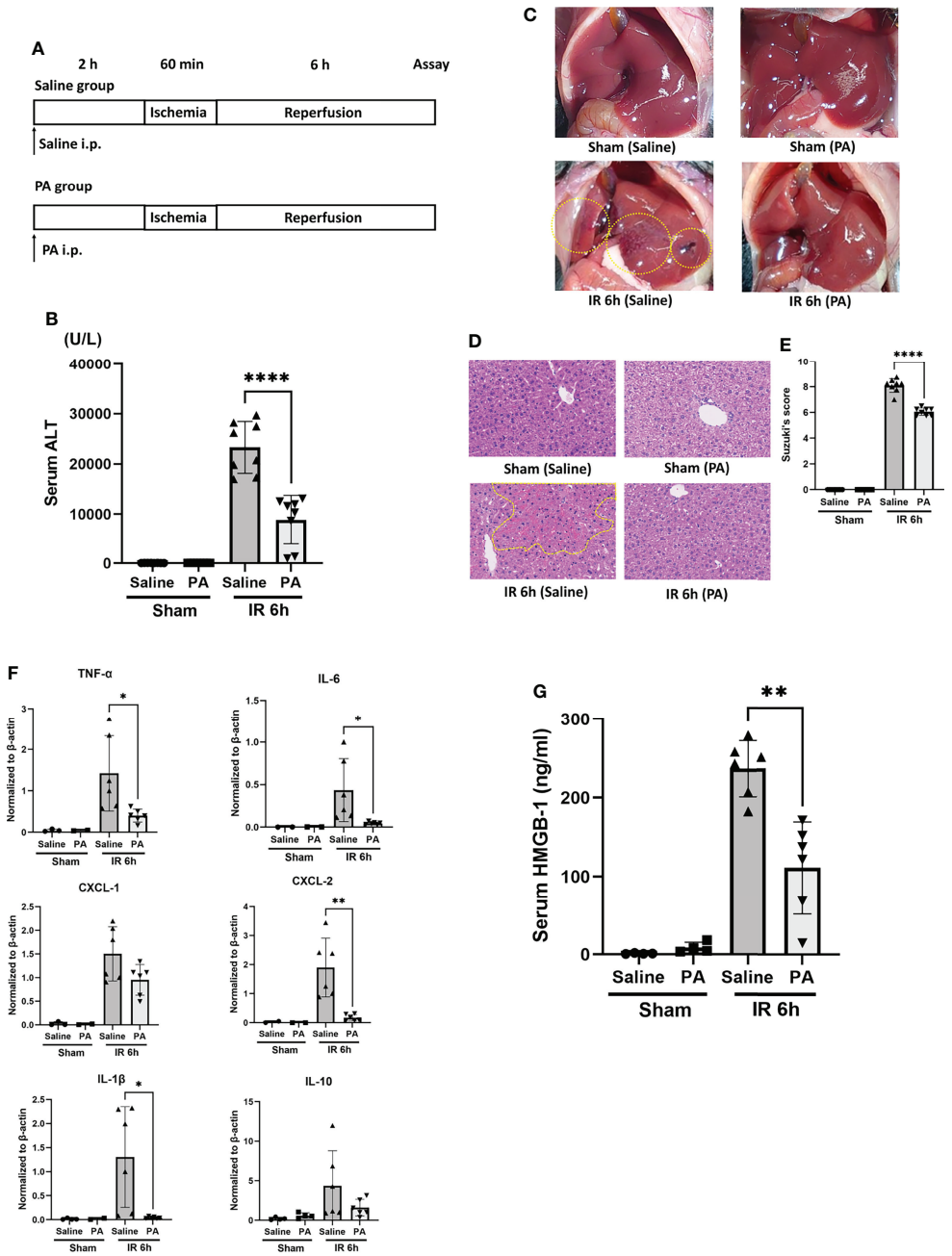

FIGURE 3 | Intraperitoneal pretreatment with propionic acid ameliorates liver IRI in mice. **(A)** WT mice were divided into two groups. Mice in the PA group were intraperitoneally pretreated with PA (5 mmol/kg in saline) 2 h prior to liver ischemia, whereas mice in the saline group were pretreated with saline. Then, mice in both groups were performed liver IRI model. **(B)** The sALT level after 6 h of reperfusion (n = 8 mice/group; ****P < .0001) (Power calculation: 1.000). **(C)** Macroscopic findings after 6 h of reperfusion in saline- and PA -pretreated mice. Regions (bleeding and swelling) of macroscopic changes induced by IR insult are circled by dotted lines. **(D)** Representative liver histology (H&E staining) after IR insult (magnification ×400). Congestion area was shown in circle by yellow dot. **(E)** Suzuki's histological grading (26) in each group (n = 8 mice/group; ****P < .0001) (Power calculation: 1.000). **(F)** Quantitative RT-PCR detection of inflammatory cytokines (TNF-α, IL-6, CXCL-1, CXCL-2, IL-1β, and IL-10) at 6 h of reperfusion. Data were normalized to β-actin gene expression (n = 6 mice/group; *P < .05, **P < .01) (Power calculation: TNF-α; 0.998, IL-6; 0.980, CXCL-2; 1.000, IL-1β; 0.996). The reduction of CXCL-1 and IL-10 in PA-treated group compared to saline-treated group was not significant. **(G)** The levels of serum HMGB-1 at 6 h after reperfusion in saline- and PA -pretreated mice (n = 8 mice/group; **P < .01) (Power calculation: 1.000).

proinflammatory cytokines (3, 8). Our previous study revealed that the HMGB-1/TLR-4 pathway played a critical role in the process of liver IRI (5, 6). To clarify how intraperitoneal PA administration affects the HMGB-1/TLR-4 pathway, HMGB-1 levels after the IR treatment were measured in the sera of PA and saline-injected mice. The serum HMGB-1 level was significantly increased 6 hours after reperfusion, whereas the level of HMGB-1 after IR was markedly reduced in the PA group (**Figure 3G**). The reduction of serum HMGB-1 by PA pretreatment might downregulate the further activation of immune cells through the TLR-4 pathway, resulting in the lowered expression of inflammatory cytokines and chemokines. These data indicate that PA reduces the release of HMGB-1 by suppressing liver cell injury or death caused by the IR insult, which results in the downregulation of the TLR-4 pathway, followed by the reduction of proinflammatory cytokines.

PA Strongly Increased Acetylation of Histone-3 and Expression of Antioxidant Enzyme HO-1 in Liver Tissues After IR Stimulation

Forkhead box protein O1 (FOXO1) is involved in the transcriptional regulation of antioxidant enzymes such as heme oxygenase 1 (HO-1) (41). It has been reported that HO-1 overexpressing cells increased survival against oxidative stress (42). As shown in **Figure 4**, at 6 hours after reperfusion, FOXO1 expression in the liver of PA (5 mmol/kg in saline)-pretreated mice was slightly higher than that of saline-pretreated mice. HO-1 expression increased more clearly in the liver of the PA-pretreated group. Besides, the increased expression of acetylated histone-3 was observed in the liver of the PA pretreated-group, indicating that the increase of histone-3 acetylation induced FOXO1 expression, followed by HO-1 upregulation, which increased liver cell survival against the ischemia-induced oxidative stress. As a result, the increased expression level of cleaved caspase-3 after IR was strongly downregulated and almost diminished by PA pretreatment. These results indicate that PA pretreatment exhibited antioxidative effects and suppressed the liver cell death caused by an IR insult.

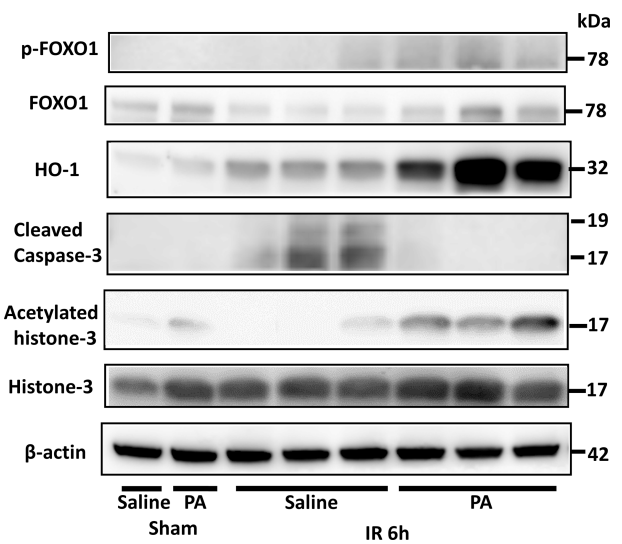

FIGURE 4 | An antioxidative effect of PA on liver tissues after IR insult by inducing the acetylation of histone-3 and the expression of HO-1. Western blot assisted analyses of the total and phosphorylated protein levels of FOXO1, acetylated histone-3, histone-3, HO-1, and cleaved caspase-3 in liver tissues after 6 h of reperfusion. β-actin was used as the internal control.

Preconditioning With PA Suppressed TNF-α Production *In Vitro* From Mouse Peritoneal Macrophages Stimulated by HMGB-1

To clarify the direct effect of PA on HMGB-1-induced production of proinflammatory cytokines such as TNF-α from immune cells, the mouse peritoneal macrophages were stimulated *in vitro* with HMGB-1 in the presence or absence of PA. At first, peritoneal macrophages from wild-type mice were cultured in RPMI 1640 medium containing various concentrations of PA (0-10 mM). Thirty minutes after the pretreatment with PA, bovine HMGB-1 (1 μg/mL) was added. As shown in **Figure 5A**, in the case of macrophages without PA pretreatment, the stimulation with HMGB-1 resulted in the significant elevation of TNF-α secretion. By contrast, in the case of macrophages pretreated with PA, the TNF-α secretion was markedly downregulated in a PA dose-dependent manner from 1 mM. As shown in **Figure 5B**, the expressions of canonical nuclear factor kappa B (NF-κB) signaling and mitogen-activated protein kinase (MAPK) signaling molecules, such as IκBα, Erk1/2, p-Erk1/2, and p-p38, were markedly decreased in the PA-pretreated macrophages. These results indicate that PA not only causes the reduction of HMGB-1 released from IR-affected cells but could also directly inhibit the TLR-4 mediated inflammatory responses in macrophages.

DISCUSSION

It is now well known that gut flora affects the host's overall health. The human gut microbiota includes two major phyla, *Bacteroidetes* (B) and *Firmicutes* (F). As reported previously, the fecal concentration of propionate, one of SCFAs, is correlated positively with *Bacteroidetes* (43) and the F/B ratio was negatively correlated with fecal levels of propionate and butyrate in healthy humans (44). Another report showed that in case of mice, aging increases the relative abundance of *Firmicutes* while decreasing that of *Bacteroidetes*. Young mice transplanted with the supernatant of fecal suspensions from aged mice with high F/B ratio had a greater increase in proinflammatory cytokines following a stroke, compared to the aged mice transplanted with microbiota from young mouse fecal suspension of low F/B ratio (45). These reports suggest that manipulating the gut microbiota results in the changes of SCFA production and affects the activities of immune cells. SCFAs absorbed from the intestinal mucosa are supposed to flow into the portal vein stream further into liver. It has been reported that

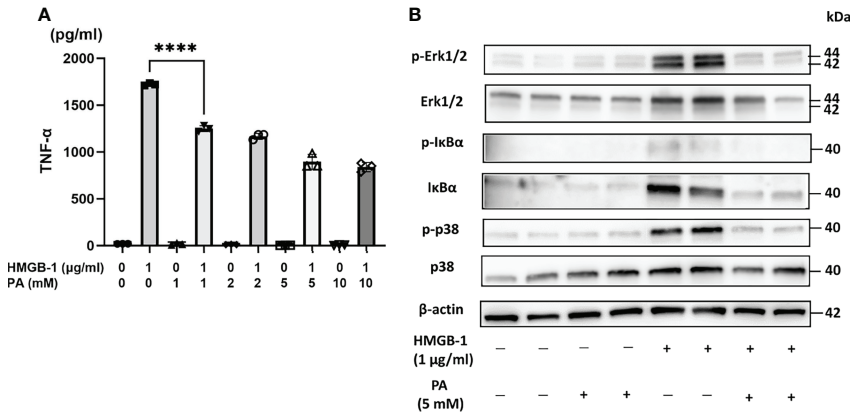

FIGURE 5 | PA suppressed HMGB-1-mediated activation of peritoneal macrophages. Peritoneal macrophages from WT mice stimulated by HMGB-1 (1 μg/mL) were cultured with or without the pretreatment with PA (1, 2, 5, and 10 mM, respectively) for 48 h. **(A)** TNF-α release was measured by ELISA (n = 3 samples/group; ****P < .0001) (Power calculation: 1.000). **(B)** Western blot assisted analyses of NF-κB signaling and MAPK signaling molecules in the macrophages stimulated by HMGB-1 (1 μg/mL) 30 min after the pretreatment with PA (5 mM). β-actin was used as the internal control.

gut microbiota-derived propionate reduced cancer cell proliferation in the liver (13, 46). It was reported that feeding mice with an inulin-rich diet resulted in the increase of *Bacteroides acidifaciens* in their feces and in the increased radiosensitivity of the mouse tumors (37).

The present study showed that diet of inulin, a water-soluble nondigestible carbohydrate dietary fiber, elevated levels of *Bacteroidetes* and reduced levels of *Firmicutes*. Inulin diet resulted also in the increase of *Bacteroides acidifaciens* in feces (**Figure 2**). This result is consistent with a previous report which demonstrated that inulin-rich diet elevated levels of acetic, propionic and butyric acids in mouse feces and increased plasma PA levels in mice (47). The present study provides clear evidence that inulin diet significantly increased propionate, one of the SCFAs, and showed a protective effect against warm liver IRI in mice. Further, it was clearly shown that the direct intraperitoneal administration of PA alone also efficiently ameliorated liver IRI in mice by preventing apoptotic cell death of hepatocytes as well inflammatory responses. PA also strongly suppressed *in vitro* activation of macrophages induced by HMGB-1 through TLR-4. As demonstrated in **Figure 4**, intraperitoneal PA administration remarkably increased the upregulation of acetylated histone-3, FOXO1, and HO-1. It has been reported that sodium propionate inhibited histone deacetylases (HDACs) 2 and 8 activity in bovine mammary epithelial cells, which led to the increase of histone-3 acetylation (48). The intraperitoneal administration of PA in mice might result in the inhibition of HDACs, followed by the increased acetylation of histone-3 in liver tissues, which protected mice from liver injury caused by IR. It has been reported that acetylated histone induced by the HDAC inhibitor increases the FOXO1 protein level and its target gene (49). FOXO1 regulates the expression of HO-1 by binding to the promoter of HO-1 (41). HO-1 is a member of the heat shock protein family, which is associated with cellular antioxidant defense and antiapoptotic functions. HO-1 knockdown is reported to enhance heat stress-induced ROS generation and apoptosis, which reduces the antioxidative responses (50). Furthermore, it has been reported that postoperative but not preoperative liver HO-1 expression correlates negatively with IRI severity in patients with orthotopic liver transplantation (51). Thus, the upregulation of HO-1 expression in liver tissues pretreated with PA as shown in **Figure 4** may play an essential role in the amelioration of liver IRI. Antioxidative nutrient-rich diets, including vitamins C and E, could partially suppress liver injury by reducing ROS production (52). An inulin-rich diet could similarly and more efficiently ameliorate IR-induced liver damage by antioxidative effects by modulating gut microbiota and increasing PA in the portal vein.

HMGB-1 is a molecule released from necrotic cells. It has been reported that the blockade of HMGB-1 by anti-HMGB-1 antibody could protect liver IRI (53, 54). We have reported that recombinant thrombomodulin and its derivative lectin-like domain could inhibit the HMGB-1 and TLR-4 interaction, which resulted in the suppression of mouse liver IRI (5, 6). As shown in **Figure 3G**, serum HMGB-1 upregulated by liver IR was decreased significantly by the PA pretreatment probably because of the suppression of liver cell death, as stated above. This reduction of serum HMGB-1 might result in the reduction of inflammatory responses transmitted through the HMGB-1 and TLR-4 signal pathway.

The question arises as to whether PA exhibits a suppressive effect on the HMGB-1/TLR-4 pathway in mouse liver IRI not only by the reduction of TLR-4 ligand, HMGB-1, but also through a direct action on the TLR-4 signal cascade. High-dose propionate has been reported to reduce LPS-induced inflammatory response in mouse endothelial cells and alveolar macrophages in a TLR-4 dependent manner (55). Another report showed the protective effect of PA against IκBα degradation and p65 translocation in LPS-treated IEC-6 cells

(56), which suggests the suppression of the NF-κB/TLR-4 pathway by PA. In the present study, PA directly suppressed the HMGB-1 triggered TLR-4 activation in macrophages and suppressed TNF-α production. The amelioration of liver IRI by the pretreatment with inulin or PA might be achieved not only by blocking the death of liver cells but also by the suppression of the inflammation in macrophages through downregulation of TLR-4/NF-κB as well as MAPK pathways. It has been reported that propionate showed an immune-modulatory role against hypertensive cardiac damages and significantly attenuated cardiac hypertrophy, fibrosis, vascular dysfunction, and hypertension (57).

In conclusion, inulin pretreatment can alleviate liver IRI in mice. This protective effect is achieved firstly by the antioxidative and antiapoptotic effects on liver cells through the increase of PA in the portal vein, which activated the acetylated histone-3/FOXO-1/HO-1 pathway. This resulted in the inhibition of cell death and the reduction of HMGB-1 released from necrotic cells. Besides, the suppression of inflammatory cytokines through the direct action of PA on inflammatory cells such as macrophages also contributed to the amelioration of mouse liver IRI.

DATA AVAILABILITY STATEMENT

The original contributions presented in the study are publicly available. This data can be found here: NCBI, BioProject, PRJDB13048.

ETHICS STATEMENT

The animal study was reviewed and approved by the Animal Research Committee of The Tazuke Kofukai Medical Research Institute, Kitano Hospital, Osaka, Japan.

AUTHOR CONTRIBUTIONS

JK, TM, and HK performed experiments. JK, YU, TM, and TW planned the study and analyzed data. JK, YU, HK, and TW wrote the manuscript. All authors contributed to, read and approved the final manuscript.

FUNDING

This study was supported by a Grant-in-Aid for Scientific Research C: 18K08609, B: 20H03743 and Research Activity Start-up: 19K24019 from the Ministry of Education, Culture, Science and Sports, Japan and by the Kitano Research Grant from The Tazuke Kofukai Medical Research Institute, Kitano Hospital.

ACKNOWLEDGMENTS

We thank Yuya Sasaki, Megumi Sadakata, and Hiroyuki Kuzuoka of Research and Development Laboratories, EN Otsuka Pharmaceutical Co., Ltd. (Hanamaki, Iwate, Japan) for providing us with scientific and technical advice concerning the analysis of gut microbiota. We thank Koichi Hirano for caring for the animals at The Tazuke Kofukai Medical Research Institute, Kitano Hospital, Osaka, Japan.

SUPPLEMENTARY MATERIAL

The Supplementary Material for this article can be found online at: https://www.frontiersin.org/articles/10.3389/fimmu.2022.862503/full#supplementary-material

Supplementary Figure 1 | The ratio of Foxp3-positive cells to CD4-positive cells in mesenteric lymph nodes in CD and ID group mice. (n = 5 mice/group).

Supplementary Figure 2 | PICRUSt2 analysis in the MetaCyc pathways for the fecal microbiome (24). Significant MetaCyc pathways for the fecal microbiome of the ID group and the CD group were identified by STAMP software. Rounded square highlights data showing the enhanced propionate biosynthesis from pyruvate in the gut microbiome of the ID group. PICRUSt, Phylogenetic Investigation of Communities by Reconstruction of Unobserved States; STAMP, Statistical Analysis of Metagenomic Profiles.

Supplementary Table 1 | List of antibodies used for western blotting analysis.

Supplementary Table 2 | List of primer couples generated for qRT-PCR.

REFERENCES

1. Zhai Y, Petrowsky H, Hong JC, Busuttil RW, Kupiec-Weglinski JW. Ischaemia-Reperfusion Injury in Liver Transplantation–from Bench to Bedside. *Nat Rev Gastroenterol Hepatol* (2013) 10(2):79–89. doi: 10.1038/nrgastro.2012.225
2. Zhou J, Chen J, Wei Q, Saeb-Parsy K, Xu X. The Role of Ischemia/Reperfusion Injury in Early Hepatic Allograft Dysfunction. *Liver Transpl* (2020) 26 (8):1034–48. doi: 10.1002/lt.25779
3. Dar WA, Sullivan E, Bynon JS, Eltzschig H, Ju C. Ischaemia Reperfusion Injury in Liver Transplantation: Cellular and Molecular Mechanisms. *Liver Int* (2019) 39(5):788–801. doi: 10.1111/liv.14091
4. Zhang W, Wang M, Xie HY, Zhou L, Meng XQ, Shi J, et al. Role of Reactive Oxygen Species in Mediating Hepatic Ischemia-Reperfusion Injury and Its Therapeutic Applications in Liver Transplantation. *Transplant Proc* (2007) 39 (5):1332–7. doi: 10.1016/j.transproceed.2006.11.021
5. Kadono K, Uchida Y, Hirao H, Miyauchi T, Watanabe T, Iida T, et al. Thrombomodulin Attenuates Inflammatory Damage Due to Liver Ischemia and Reperfusion Injury in Mice in Toll-Like Receptor 4-Dependent Manner. *Am J Transplant* (2017) 17(1):69–80. doi: 10.1111/ajt.13991
6. Kawasoe J, Uchida Y, Miyauchi T, Kadono K, Hirao H, Saga K, et al. The Lectin-Like Domain of Thrombomodulin Is a Drug Candidate for Both Prophylaxis and Treatment of Liver Ischemia and Reperfusion Injury in Mice. *Am J Transplant* (2021) 21(2):540–51. doi: 10.1111/ajt.16269
7. Miyauchi T, Uchida Y, Kadono K, Hirao H, Kawasoe J, Watanabe T, et al. Up-Regulation of Foxo1 and Reduced Inflammation by β-Hydroxybutyric Acid Are Essential Diet Restriction Benefits Against Liver Injury. *Proc Natl Acad Sci USA* (2019) 116(27):13533–42. doi: 10.1073/pnas.1820282116

8. Nace GW, Huang H, Klune JR, Eid RE, Rosborough BR, Korff S, et al. Cellular-Specific Role of Toll-Like Receptor 4 in Hepatic Ischemia-Reperfusion Injury in Mice. *Hepatology* (2013) 58(1):374–87. doi: 10.1002/hep.26346
9. Melloul E, Hübner M, Scott M, Snowden C, Prentis J, Dejong CH, et al. Guidelines for Perioperative Care for Liver Surgery: Enhanced Recovery After Surgery (Eras) Society Recommendations. *World J Surg* (2016) 40(10):2425–40. doi: 10.1007/s00268-016-3700-1
10. Shoaib M, Shehzad A, Omar M, Rakha A, Raza H, Sharif HR, et al. Inulin: Properties, Health Benefits and Food Applications. *Carbohydr Polym* (2016) 147:444–54. doi: 10.1016/j.carbpol.2016.04.020
11. Le Bastard Q, Chapelet G, Javaudin F, Lepelletier D, Batard E, Montassier E. The Effects of Inulin on Gut Microbial Composition: A Systematic Review of Evidence From Human Studies. *Eur J Clin Microbiol Infect Dis* (2020) 39 (3):403–13. doi: 10.1007/s10096-019-03721-w
12. Roberfroid M, Slavin J. Nondigestible Oligosaccharides. *Crit Rev Food Sci Nutr* (2000) 40(6):461–80. doi: 10.1080/10408690091189239
13. Sivaprakasam S, Prasad PD, Singh N. Benefits of Short-Chain Fatty Acids and Their Receptors in Inflammation and Carcinogenesis. *Pharmacol Ther* (2016) 164:144–51. doi: 10.1016/j.pharmthera.2016.04.007
14. Furusawa Y, Obata Y, Fukuda S, Endo TA, Nakato G, Takahashi D, et al. Commensal Microbe-Derived Butyrate Induces the Differentiation of Colonic Regulatory T Cells. *Nature* (2013) 504(7480):446–50. doi: 10.1038/nature12721
15. Wang Z, Zhang X, Zhu L, Yang X, He F, Wang T, et al. Inulin Alleviates Inflammation of Alcoholic Liver Disease *Via* Scfas-Inducing Suppression of M1 and Facilitation of M2 Macrophages in Mice. *Int Immunopharmacol* (2020) 78:106062. doi: 10.1016/j.intimp.2019.106062
16. Aguilar-Nascimento JE, Salomão AB, Nochi RJ Jr, Nascimento M, Neves Jde S. Intraluminal Injection of Short Chain Fatty Acids Diminishes Intestinal Mucosa Injury in Experimental Ischemia-Reperfusion. *Acta Cir Bras* (2006) 21(1):21–5. doi: 10.1590/s0102-86502006000100006
17. Liu B, Qian J, Wang Q, Wang F, Ma Z, Qiao Y. Butyrate Protects Rat Liver Against Total Hepatic Ischemia Reperfusion Injury With Bowel Congestion. *PloS One* (2014) 9(8):e106184. doi: 10.1371/journal.pone.0106184
18. Qiao Y, Qian J, Lu Q, Tian Y, Chen Q, Zhang Y. Protective Effects of Butyrate on Intestinal Ischemia-Reperfusion Injury in Rats. *J Surg Res* (2015) 197 (2):324–30. doi: 10.1016/j.jss.2015.04.031
19. Qiao YL, Qian JM, Wang FR, Ma ZY, Wang QW. Butyrate Protects Liver Against Ischemia Reperfusion Injury by Inhibiting Nuclear Factor Kappa B Activation in Kupffer Cells. *J Surg Res* (2014) 187(2):653–9. doi: 10.1016/j.jss.2013.08.028
20. Sun J, Wang F, Li H, Zhang H, Jin J, Chen W, et al. Neuroprotective Effect of Sodium Butyrate Against Cerebral Ischemia/Reperfusion Injury in Mice. *BioMed Res Int* (2015) 2015:395895. doi: 10.1155/2015/395895
21. Sun J, Wu Q, Sun H, Qiao Y. Inhibition of Histone Deacetylase by Butyrate Protects Rat Liver From Ischemic Reperfusion Injury. *Int J Mol Sci* (2014) 15 (11):21069–79. doi: 10.3390/ijms151121069
22. Suzuki M, Suzuki M, Kitamura Y, Mori S, Sato K, Dohi S, et al. Beta-Hydroxybutyrate, A Cerebral Function Improving Agent, Protects Rat Brain Against Ischemic Damage Caused by Permanent and Transient Focal Cerebral Ischemia. *Jpn J Pharmacol* (2002) 89(1):36–43. doi: 10.1254/jjp.89.36
23. Reeves PG. Components of the AIN-93 Diets as Improvements in the AIN-76A Diet. *J Nutr* (1997) 127(5 Suppl):838s–41s. doi: 10.1093/jn/127/5/838S
24. Sugatani J, Wada T, Osabe M, Yamakawa K, Yoshinari K, Miwa M. Dietary Inulin Alleviates Hepatic Steatosis and Xenobiotics-Induced Liver Injury in Rats Fed a High-Fat and High-Sucrose Diet: Association With the Suppression of Hepatic Cytochrome P450 and Hepatocyte Nuclear Factor 4alpha Expression. *Drug Metab Dispos* (2006) 34(10):1677–87. doi: 10.1124/dmd.106.010645
25. Zheng W, Wang K, Sun Y, Kuo SM. Dietary or Supplemental Fermentable Fiber Intake Reduces the Presence of Clostridium Xi in Mouse Intestinal Microbiota: The Importance of Higher Fecal Bacterial Load and Density. *PloS One* (2018) 13(10):e0205055. doi: 10.1371/journal.pone.0205055
26. Tirosh A, Calay ES, Tuncman G, Claiborn KC, Inouye KE, Eguchi K, et al. The Short-Chain Fatty Acid Propionate Increases Glucagon and Fabp4 Production, Impairing Insulin Action in Mice and Humans. *Sci Transl Med* (2019) 11(489):eaav0120. doi: 10.1126/scitranslmed.aav0120
27. Suzuki S, Toledo-Pereyra LH, Rodriguez FJ, Cejalvo D. Neutrophil Infiltration as an Important Factor in Liver Ischemia and Reperfusion Injury. Modulating Effects of Fk506 and Cyclosporine. *Transplantation* (1993) 55(6):1265–72. doi: 10.1097/00007890-199306000-00011
28. Yoon SH, Ha SM, Kwon S, Lim J, Kim Y, Seo H, et al. Introducing Ezbiocloud: A Taxonomically United Database of 16s Rrna Gene Sequences and Whole-Genome Assemblies. *Int J Syst Evol Microbiol* (2017) 67(5):1613–7. doi: 10.1099/ijsem.0.001755
29. Langille MG, Zaneveld J, Caporaso JG, McDonald D, Knights D, Reyes JA, et al. Predictive Functional Profiling of Microbial Communities Using 16s Rrna Marker Gene Sequences. *Nat Biotechnol* (2013) 31(9):814–21. doi: 10.1038/nbt.2676
30. Kawase T, Hatanaka K, Kono M, Shirahase Y, Ochiai K, Takashiba S, et al. Simultaneous Determination of 7 Short-Chain Fatty Acids in Human Saliva by High-Sensitivity Gas Chromatography-Mass Spectrometry. *Chromatography* (2020) 41(2):63–71. doi: 10.15583/jpchrom.2019.025
31. Tsukahara T, Matsukawa N, Tomonaga S, Inoue R, Ushida K, Ochiai K. High-Sensitivity Detection of Short-Chain Fatty Acids in Porcine Ileal, Cecal, Portal and Abdominal Blood by Gas Chromatography-Mass Spectrometry. *Anim Sci J* (2014) 85(4):494–8. doi: 10.1111/asj.12188
32. Kohli V, Selzner M, Madden JF, Bentley RC, Clavien PA. Endothelial Cell and Hepatocyte Deaths Occur by Apoptosis After Ischemia-Reperfusion Injury in the Rat Liver. *Transplantation* (1999) 67(8):1099–105. doi: 10.1097/00007890-199904270-00003
33. Rüdiger HA, Clavien PA. Tumor Necrosis Factor Alpha, But Not Fas, Mediates Hepatocellular Apoptosis in the Murine Ischemic Liver. *Gastroenterology* (2002) 122(1):202–10. doi: 10.1053/gast.2002.30304
34. Colletti LM, Kunkel SL, Walz A, Burdick MD, Kunkel RG, Wilke CA, et al. The Role of Cytokine Networks in the Local Liver Injury Following Hepatic Ischemia/Reperfusion in the Rat. *Hepatology* (1996) 23(3):506–14. doi: 10.1002/hep.510230315
35. Lentsch AB, Yoshidome H, Cheadle WG, Miller FN, Edwards MJ. Chemokine Involvement in Hepatic Ischemia/Reperfusion Injury in Mice: Roles for Macrophage Inflammatory Protein-2 and Kupffer Cells. *Hepatology* (1998) 27(2):507–12. doi: 10.1002/hep.510270226
36. Chijiiwa R, Hosokawa M, Kogawa M, Nishikawa Y, Ide K, Sakanashi C, et al. Single-Cell Genomics of Uncultured Bacteria Reveals Dietary Fiber Responders in the Mouse Gut Microbiota. *Microbiome* (2020) 8(1):5. doi: 10.1186/s40168-019-0779-2
37. Then CK, Paillas S, Wang X, Hampson A, Kiltie AE. Association of Bacteroides Acidifaciens Relative Abundance With High-Fibre Diet-Associated Radiosensitisation. *BMC Biol* (2020) 18(1):102. doi: 10.1186/s12915-020-00836-x
38. Macfarlane S, Macfarlane GT. Regulation of Short-Chain Fatty Acid Production. *Proc Nutr Soc* (2003) 62(1):67–72. doi: 10.1079/pns2002207
39. Zhu L, Sha L, Li K, Wang Z, Wang T, Li Y, et al. Dietary Flaxseed Oil Rich in Omega-3 Suppresses Severity of Type 2 Diabetes Mellitus *Via* Anti-Inflammation and Modulating Gut Microbiota in Rats. *Lipids Health Dis* (2020) 19(1):20. doi: 10.1186/s12944-019-1167-4
40. Ezequias Castillo-Lopez, Andreas Haselmann, Renee M, Petri, Wilhelm Knaus, Qendrim Zebeli. Evaluation of Fecal Fermentation Profile and Bacterial Community in Organically Fed Dairy Cows Consuming Forage-Rich Diets With Different Particle Sizes. *J Dairy Sci* (2020) 103:8020–33. doi: 10.3168/jds.2019-18036
41. Liu X, Cui Y, Li M, Xu H, Zuo J, Fang F, et al. Cobalt Protoporphyrin Induces Ho-1 Expression Mediated Partially by Foxo1 and Reduces Mitochondria-Derived Reactive Oxygen Species Production. *PloS One* (2013) 8(11):e80521. doi: 10.1371/journal.pone.0080521
42. Lee PJ, Alam J, Wiegand GW, Choi AM. Overexpression of Heme Oxygenase-1 in Human Pulmonary Epithelial Cells Results in Cell Growth Arrest and Increased Resistance to Hyperoxia. *Proc Natl Acad Sci USA* (1996) 93 (19):10393–8. doi: 10.1073/pnas.93.19.10393
43. Salonen A, Lahti L, Salojärvi J, Holtrop G, Korpela K, Duncan SH, et al. Impact of Diet and Individual Variation on Intestinal Microbiota Composition and Fermentation Products in Obese Men. *Isme J* (2014) 8 (11):2218–30. doi: 10.1038/ismej.2014.63
44. Rodríguez-Carrio J, López P, Sánchez B, González S, Gueimonde M, Margolles A, et al. Intestinal Dysbiosis Is Associated With Altered Short-

Chain Fatty Acids and Serum-Free Fatty Acids in Systemic Lupus Erythematosus. *Front Immunol* (2017) 8:23. doi: 10.3389/fimmu.2017.00023
45. Spychala MS, Venna VR, Jandzinski M, Doran SJ, Durgan DJ, Ganesh BP, et al. Age-Related Changes in the Gut Microbiota Influence Systemic Inflammation and Stroke Outcome. *Ann Neurol* (2018) 84(1):23–36. doi: 10.1002/ana.25250
46. Bindels LB, Porporato P, Dewulf EM, Verrax J, Neyrinck AM, Martin JC, et al. Gut Microbiota-Derived Propionate Reduces Cancer Cell Proliferation in the Liver. *Br J Cancer* (2012) 107(8):1337–44. doi: 10.1038/bjc.2012.409
47. Igarashi M, Morimoto M, Suto A, Nakatani A, Hayakawa T, Hara K, et al. Synthetic Dietary Inulin, Fuji Ff, Delays Development of Diet-Induced Obesity by Improving Gut Microbiota Profiles and Increasing Short-Chain Fatty Acid Production. *PeerJ* (2020) 8:e8893. doi: 10.7717/peerj.8893
48. Silva LG, Ferguson BS, Avila AS, Faciola AP. Sodium Propionate and Sodium Butyrate Effects on Histone Deacetylase (Hdac) Activity, Histone Acetylation, and Inflammatory Gene Expression in Bovine Mammary Epithelial Cells. *J Anim Sci* (2018) 96(12):5244–52. doi: 10.1093/jas/sky373
49. Zhang J, Ng S, Wang J, Zhou J, Tan SH, Yang N, et al. Histone Deacetylase Inhibitors Induce Autophagy Through Foxo1-Dependent Pathways. *Autophagy* (2015) 11(4):629–42. doi: 10.1080/15548627.2015.1023981
50. Wang Y, Yang C, Elsheikh NAH, Li C, Yang F, Wang G, et al. Ho-1 Reduces Heat Stress-Induced Apoptosis in Bovine Granulosa Cells by Suppressing Oxidative Stress. *Aging (Albany NY)* (2019) 11(15):5535–47. doi: 10.18632/aging.102136
51. Hirao H, Dery KJ, Kageyama S, Nakamura K, Kupiec-Weglinski JW. Heme Oxygenase-1 in Liver Transplant Ischemia-Reperfusion Injury: From Bench-To-Bedside. *Free Radic Biol Med* (2020) 157:75–82. doi: 10.1016/j.freeradbiomed.2020.02.012
52. Miyauchi T, Uchida Y, Kadono K, Hirao H, Kawasoe J, Watanabe T, et al. Preventive Effect of Antioxidative Nutrient-Rich Enteral Diet Against Liver Ischemia and Reperfusion Injury. *JPEN J Parenter Enteral Nutr* (2019) 43(1):133–44. doi: 10.1002/jpen.1308
53. Tsung A, Sahai R, Tanaka H, Nakao A, Fink MP, Lotze MT, et al. The Nuclear Factor Hmgb1 Mediates Hepatic Injury After Murine Liver Ischemia-Reperfusion. *J Exp Med* (2005) 201(7):1135–43. doi: 10.1084/jem.20042614
54. Watanabe T, Kubota S, Nagaya M, Ozaki S, Nagafuchi H, Akashi K, et al. The Role of Hmgb-1 on the Development of Necrosis During Hepatic Ischemia and Hepatic Ischemia/Reperfusion Injury in Mice. *J Surg Res* (2005) 124(1):59–66. doi: 10.1016/j.jss.2004.10.019
55. Tian X, Hellman J, Horswill AR, Crosby HA, Francis KP, Prakash A. Elevated Gut Microbiome-Derived Propionate Levels Are Associated With Reduced Sterile Lung Inflammation and Bacterial Immunity in Mice. *Front Microbiol* (2019) 10:159. doi: 10.3389/fmicb.2019.00159
56. Yang R, Hu X, Xie X, Chen H, Fang H, Zhu L, et al. Propionic Acid Targets the Tlr4/Nf-κb Signaling Pathway and Inhibits Lps-Induced Intestinal Barrier Dysfunction: *In Vitro* and *In Vivo* Studies. *Front Pharmacol* (2020) 11:573475. doi: 10.3389/fphar.2020.573475
57. Bartolomaeus H, Balogh A, Yakoub M, Homann S, Markó L, Höges S, et al. Short-Chain Fatty Acid Propionate Protects From Hypertensive Cardiovascular Damage. *Circulation* (2019) 139(11):1407–21. doi: 10.1161/circulationaha.118.036652

Conflict of Interest: The authors declare that the research was conducted in the absence of any commercial or financial relationships that could be construed as a potential conflict of interest.

Publisher's Note: All claims expressed in this article are solely those of the authors and do not necessarily represent those of their affiliated organizations, or those of the publisher, the editors and the reviewers. Any product that may be evaluated in this article, or claim that may be made by its manufacturer, is not guaranteed or endorsed by the publisher.

frontiers | Frontiers in Immunology

MINI REVIEW
published: 11 May 2022
doi: 10.3389/fimmu.2022.879552

One Shoot, Two Birds: Alleviating Inflammation Caused by Ischemia/Reperfusion Injury to Reduce the Recurrence of Hepatocellular Carcinoma

Hao Chen[1,2,3†], *Di Lu*[1,2,3†], *Xinyu Yang*[1,2,3], *Zhihang Hu*[1,2,3], *Chiyu He*[1,2,3,4], *Huigang Li*[1,2,3], *Zuyuan Lin*[1,2,3], *Modan Yang*[1,2,3] *and Xiao Xu*[1,2,3,5*]

[1] *Key Laboratory of Integrated Oncology and Intelligent Medicine of Zhejiang Province, Department of Hepatobiliary and Pancreatic Surgery, Affiliated Hangzhou First People's Hospital, Zhejiang University School of Medicine, Hangzhou, China,* [2] *National Health Commission (NHC) Key Laboratory of Combined Multi-organ Transplantation, The First Affiliated Hospital, School of Medicine, Zhejiang University, Hangzhou, China,* [3] *Institute of Organ Transplantation, Zhejiang University, Hangzhou, China,* [4] *Department of Hepatobiliary and Pancreatic Surgery, Shulan (Hangzhou) Hospital, Hangzhou, China,* [5] *Westlake Laboratory of Life Sciences and Biomedicine, Westlake University, Hangzhou, China*

OPEN ACCESS

Edited by:
Tao Qiu,
Renmin Hospital of Wuhan University, China

Reviewed by:
Arshi Khanam,
University of Maryland, United States

***Correspondence:**
Xiao Xu
zjxu@zju.edu.cn

[†]*These authors have contributed equally to this work*

Specialty section:
This article was submitted to Molecular Innate Immunity, a section of the journal Frontiers in Immunology

Received: *19 February 2022*
Accepted: *15 April 2022*
Published: *11 May 2022*

Citation:
Chen H, Lu D, Yang X, Hu Z, He C, Li H, Lin Z, Yang M and Xu X (2022) One Shoot, Two Birds: Alleviating Inflammation Caused by Ischemia/Reperfusion Injury to Reduce the Recurrence of Hepatocellular Carcinoma. Front. Immunol. 13:879552. doi: 10.3389/fimmu.2022.879552

Inflammation is crucial to tumorigenesis and the development of metastasis. Hepatic ischemia/reperfusion injury (IRI) is an unresolved problem in liver resection and transplantation which often establishes and remodels the inflammatory microenvironment in liver. More and more experimental and clinical evidence unmasks the role of hepatic IRI and associated inflammation in promoting the recurrence of hepatocellular carcinoma (HCC). Meanwhile, approaches aimed at alleviating hepatic IRI, such as machine perfusion, regulating the gut-liver axis, and targeting key inflammatory components, have been proved to prevent HCC recurrence. This review article highlights the underlying mechanisms and promising therapeutic strategies to reduce tumor recurrence through alleviating inflammation induced by hepatic IRI.

Keywords: hepatic, ischemia/reperfusion injury, inflammation, hepatocellular carcinoma, liver transplantation, liver resection

INTRODUCTION

Hepatocellular carcinoma (HCC) is one of the most prevalent malignancies and the third leading cause of cancer-related mortality in the world (1). Surgical therapies, including hepatectomy and liver transplantation (LT), are the most efficient treatments for patients with HCC (2). However, the prognosis of HCC patients remains dismal due to the high incidence of metastasis and recurrence after surgery, with 5-year recurrence rates reaching up to 70% after liver resection (LR) and 40% after LT (3, 4). Ischemia/reperfusion injury (IRI) refers to the pathophysiological process in which ischemic tissue injury is accentuated following the restoration of blood flow after a period of ischemia (5). Hepatic IRI is an inevitable consequence of LR and LT, which is usually accompanied by intense inflammatory cascade and subsequent damage repair (5). In the mid-19th century, the link between inflammation and cancer was firstly suggested by Rudolf Virchow, based on

discovering leukocyte infiltration in neoplastic tissues (6). Nowadays, inflammation has been demonstrated to be strongly associated with tumorigenesis and metastasis of most types of cancer. Targeting inflammation associated with tumor progress has gradually become a critical anti-cancer treatment (7). Currently, multiple preclinical and clinical studies suggest that inflammation induced by hepatic IRI promoted tumor relapse and metastasis after LR or LT (8–12). Meanwhile, alleviating inflammation induced by hepatic IRI is emerging as a promising therapeutic strategy for reducing liver damage and simultaneously suppressing tumor recurrence for HCC patients (13). In this review, we summarize the clinical evidence that hepatic IRI promotes tumor relapse and metastasis. Furthermore, we review recent advances in therapeutic strategies which suppress tumor recurrence through alleviating inflammation induced by hepatic IRI. These avenues of killing two birds with one stone may provide new insights into preventing HCC relapse.

HEPATIC IRI PROMOTES THE RECURRENCE OF HCC: CLINICAL EVIDENCE IN LT

LT, which removes the tumor and the diseased liver at the same time, is a radical treatment modality for HCC. However, tumor relapse is still the most severe threat to the survival of HCC patients after LT (14). Hepatic IRI is a common but thorny problem in different clinical settings such as LT, LR, trauma surgery, and shock. As essential procedures during LT, cold preservation of liver graft and subsequent warm reperfusion when implanted into the recipients result in hepatic IRI, which can be stratified into warm IRI and cold IRI (15). The severity of IRI and subsequent inflammation is positively correlated with ischemia time, which can also be partitioned into warm ischemia time (WIT) and cold ischemia time (CIT) (16).

Clinically, HCC patients with prolonged WIT and CIT are more likely to relapse after transplantation, revealing the links between hepatic IRI and HCC recurrence (8–12). The details of relevant clinical studies are listed in **Table 1**. A retrospective study that enrolled 391 patients found that CIT >10 hours and WIT >50 minutes were associated with significantly increased recurrence (P=0.015 and 0.036, respectively) (8). Another single-center study from Germany also showed that WIT>50 min was an independent risk factor for HCC recurrence (OR=15.5; P <0.001) (9). Orci et al. analyzed the data of 9724 HCC patients from the American Scientific Registry of Transplant Recipients (SRTR). They found that WIT >19 minutes was associated with an increased HCC recurrence risk (P = 0.025) (11). In 2018, our team reached a similar conclusion in HCC patients of China, where hepatitis-B constitutes the main cause of HCC. We recognized CIT >12 hours as the independent donor prognostic factor for predicting HCC recurrence (HR=2.23; P=0.007) (10). In addition to ischemia time, post-reperfusion serum aspartate transaminase (AST) and lactate dehydrogenase (LDH), important indicators reflecting the degree of hepatic inflammatory injury, have also been shown to correlate with the risk of tumor recurrence in patients within the Milan criteria (12).

These findings provide the clinical evidence that inflammation induced by hepatic IRI promoted HCC recurrence and indicate that minimizing ischemia time may be beneficial to alleviating inflammatory injury and reducing the risk of HCC recurrence. However, reducing ischemia time might be difficult in clinical practice, which depends on many factors such as organ allocation system, organ transport, surgery complexity, and experience of transplant teams. Therefore, repair of liver injury or targeting inflammatory mechanisms of hepatic IRI may be more practical solutions in the existing clinical context.

INFLAMMATION-TARGETING CANCER THERAPY: HIT TWO BIRDS WITH ONE STONE

Alleviating Hepatic IRI and Subsequent Inflammation From the Source: Machine Perfusion

Currently, cold static storage (CS) is still the most commonly utilized method for liver preservation in LT. Meanwhile, due to the shortage of donor livers, extended criteria donor (ECD) liver grafts such as steatotic grafts, livers from older donors and donors after cardiac death (DCD) are utilized to expand the scarce donor pool (17). These ECD liver grafts are more susceptible to hepatic IRI and are linked to inferior post-transplant outcomes (18). Besides, the use of organs from DCD donors with prolonged WIT and severe steatotic donor livers was proved to increase the risk of HCC recurrence post LT (11, 19). In such a context, the limitations of CS become more obvious. As a future direction of graft preservation, there is increasing attention to machine perfusion (MP) due to its ability to preserve, evaluate and recondition such donor livers prior to transplantation (20).

Oldani et al. found that the use of ischemic rat liver graft accompanied by an increased serum pro-inflammatory cytokine profile increased the risk of cancer recurrence (21). Investigators approximated an *in vivo* normothermic perfusion by reperfusing the liver *in vivo* (animal alive) for two hours before flushing and retrieving. This method attenuated liver injury, measured by the release of liver enzymes (AST and ALT). Besides, prior-to-retrieval reperfusion decreased the recurrence and growth of HCC after transplantation. These effects were partly attributed to the improvement of serum inflammatory cytokine profile. In clinical practice, normothermic extracorporeal membrane oxygenation (NECMO) or NECMO-based normothermic regional perfusion (NRP) is the closest procedure to reproduce the studied model (22). As a technique that allows the *in-situ* perfusion of organs with oxygenated blood in DCD donors, NRP can reduce warm ischemia time and improve graft function (23). This investigation further revealed the possible potential of NRP in preventing hepatic IRI-associated HCC recurrence.

Hypothermic oxygenated perfusion (HOPE) is an emerging organ preservation strategy for marginal grafts (20). The use of

TABLE 1 | The clinical evidence of hepatic IRI promoting recurrence of HCC after LT.

Study	Data sources	N	Underlying liver disease	Milan status	Donor type	Definition of WIT	Definition of CIT	Conclusion
Nagai et al. (8)	Two centers (USA)	391	NA	NA	DBD	Removal of the graft from the cold preservation solution to portal reperfusion	Donor cross-clamping to the removal of the graft from the cold preservation solution	CIT>10 h (HR=1.9; P=0.03) and WIT>50 min (HR=2. 84; P=0.003) were independent risk factors for HCC recurrence
Kornberg et al. (9)	Single center (Germany)	103	Alcoholic (55.3%) Viral (28.2%) Autoimmune (9.7%) Other(6.8%)	In (61.2%) Out (38.8%)	DBD	Removal of the graft from the cold preservation solution to portal reperfusion	In situ cold liver flushing to the removal of the graft from the cold preservation solution	WIT>50 min was an independent risk factor for HCC recurrence (OR=15.5; P <0.001)
Ling et al. (10)	CLTR (China)	673	Hepatitis B cirrhosis (88.9%) Other (11.1%)	In (54.7%) Out (45.3%)	DBD (14.0%) DCD (41.5%) DBCD (44.4%)	Removal of the graft from the cold preservation solution to portal reperfusion	Perfusion of the cold perfusate to the removal of the graft from the cold preservation solution	CIT>12 h was the independent donor prognostic factor for predicting HCC recurrence (HR=2. 234; P=0.007)
Orci et al. (11)	SRTR (USA)	486	NA	NA	DCD	Removal of life support to aortic perfusion with cold preservation solution	In situ aortic cold perfusion to the removal of the graft from the cold preservation solution	WIT>19 min was associated with an increased HCC recurrence risk (HR=4.26; P=0.025)
Grąt et al. (12)	Single center (Poland)	195	Hepatitis C virus infection (67.7%) Hepatitis B virus infection (45.6%)	In (57.9%) Out (42.1%)	DBD	Removal of the graft from the cold preservation solution to portal reperfusion	Clamping of the donor aorta to the removal of the graft from the cold preservation solution	Post-reperfusion AST≥1896 U/L(HR=5.99; P=0.039) and LDH≥4670 U/L (HR=6.08; P=0.04) increased the risk of HCC recurrence after LT in patients within Milan criteria

IRI, ischemia/ reperfusion injury; HCC, hepatocellular carcinoma; LT, liver transplantation; NA, not available; DBD, donation after brain death; DCD, donation after cardiac death; DBCD, donation after brain death followed by circulatory death; WIT, warm ischemia time; CIT, cold ischemia time; HR, hazard ratio; OR, Odds Ratio; CLTR, China Liver Transplant Registry; SRTR, Scientific Registry of Transplant Recipients; AST, aspartate transferase; LDH, lactate dehydrogenase

artificial, cooled perfusion solutions with oxygenation applied in HOPE has been demonstrated to decrease oxidative stress and inflammatory damage in LT (24). To validate the protective effect of HOPE in HCC recurrence, Mueller et al. compared tumor recurrence rate between HOPE-treated DCD and unperfused DBD liver recipients after liver LT for HCC (25). The results showed that HOPE alleviated general inflammation (measured through plasma CRP of the recipient) and recovered liver functions. He also observed a significantly lower recurrence rate in patients who received end-ischemic HOPE treatment (5.7%, n = 4/70) compared to an unperfused DBD cohort (25.7%, 18/70), despite the use of high-risk DCD grafts (P=0.002). Besides, HOPE treatment improved recurrence-free survival and reduced tumor load significantly compared to an external, nonperfused DCD and DBD liver recipient cohort. HOPE before implantation protected the liver from reperfusion injury and subsequently prevented ongoing tissue inflammation and hypoxia, making the environment less favorable for tumor recurrence and metastasis.

Despite the ability to decrease damage and improve outcomes, hepatic IRI cannot be completely avoided using the techniques above. With the innovations of surgical techniques and NMP, the technique named ischemia-free liver transplantation (IFLT) has been created. Its application is able to procure, preserve, and implant liver grafts from DBD donors without stopping the blood and oxygen supply, thus entirely preventing hepatic IRI (26). A recent propensity-matched cohort study showed that IFLT recipients had a higher RFS rate at 1 and 3 years (92.2% and 86.7%) than conventional LT recipients (88.1% and 53.6%), with much lower liver damage (27). Though the oncological benefit of IFLT needs further observation and validation in a larger sample, this technique shows enormous potential not only for completely avoiding IRI but also for preventing associated HCC recurrence. However, this technique is not applicable to LDLT and DCD LT, which occupy the major types of LT.

Gut-Liver Axis as a Target in Inflammation-Associated Cancer Recurrence Induced by Hepatic IRI

The close interplay between the intestine and liver in anatomy and function is known as the gut-liver axis. In the liver, two-thirds of total blood flow originates from the portal circulation, which contains gut-derived bacterial products (28). As a "microbial organ", gut microbiota is involved in the development of many liver disorders through the gut-liver axis (29, 30). During LT and LR, portal vein clamping usually results in venous congestion and hypoperfusion of the intestines,

followed by intestinal mucosa damage and increased permeability (31). In these cases, endotoxin/lipopolysaccharide (LPS), a cell wall component of Gram-negative bacteria, could translocate to the portal blood through the impaired intestinal mucosal barrier and intensify hepatic IRI (32).

A recent study has revealed the connection between hepatic IRI and HCC recurrence from a brand-new perspective of the gut-liver axis. The study found that pedicle clamping induced the congestive injury of the bowel wall and subsequent increase of LPS in portal circulation. Upon re-establishment of portal blood flow, bacterial LPS activated the Toll-like receptor 4 (TLR4) signaling pathway in the liver, leading to aggravated IRI, exacerbated inflammatory response, and increased tumor burden (33). In this process, hyperactivation of TLR4 by LPS results in the activation and over-expression of pro-inflammatory transcription factors (TFs) such as nuclear factor-kappaB (NF-κB), activator protein 1 (AP-1) and interferon regulatory factor 3 (IRF3) (34). Increased production of pro-inflammatory cytokines (IL-6, TNF-α, etc.) and chemokines (CXCL1, CXCL10, etc.) intensify hepatic IRI and upregulate the components involved in the progression and metastasis of HCC including angiogenesis cytokines and immunosuppressive cells such as Tregs (35).

The researchers also explored several therapeutic approaches to suppress tumor growth by targeting the gut–liver axis (33). They found that remote ischemic preconditioning (RIPC) induced by brief and repeated sequences of femoral vascular bundle clamping and declamping could prevent liver injury and associated HCC recurrence through dampening small bowel venous ischemia and preventing bacterial translocation. Despite promising animal evidence supporting the protective effect of RIPC on hepatic IRI, the results of several clinical trials are inconsistent, indicating that RIPC's clinical role remains to be further confirmed (36–39). Besides RIPC, the study also showed that gut decontamination (antibiotics) and pharmacological TLR4 inhibition confer systemic protection against inflammation-mediated accelerated HCC growth. Their results indicated that modulating the gut–liver axis during liver surgery could be a potential target in combating HCC recurrence. Predictably, gut microecological therapy will gradually become an emerging treatment modality in preventing inflammation-induced HCC recurrence. **Figure 1** displays the schematic diagram of the gut-liver axis as a target in inflammation-associated cancer recurrence induced by hepatic IRI.

Targeting Key Inflammatory Components in the Tumor Microenvironment

Hepatic IRI is a dynamic process including two related stages: ischemic injury and inflammation-mediated reperfusion injury (40). In the phase of ischemia, hepatocytes are exposed to oxygen deprivation, ATP depletion, and pH decreasement (41). These changes result in the accumulation of reactive oxygen species (ROS), increasement of intracellular calcium concentrations which lead to hepatocyte damage and different cell death programs such as apoptosis, necrosis, ferroptosis and pyroptosis (13, 42). The following reperfusion triggers inflammatory cascade that aggravates hepatocyte injury through multiple mechanisms. In addition to cell death programs and metabolic disorders, innate immune activation plays a major role in this process (5). After sensing damage-associated molecular patterns (DAMPs) released from damaged or dead cells, Kupffer cells become activated through pattern-recognition receptors (PRRs) and release chemokines and cytokines to initiate a pro-inflammatory response (43).

The inflammatory cascade after reperfusion involves multiple inflammatory components and their interactions. Activated Kupffer cells release cytokines like IL-1β and chemokines such as CXCL1 and CXCL2 to activate and recruit neutrophils in damaged site (44). Platelets activated by DAMPs also serve as immune mediators which express CXCL4 and P-selectin and promote the recruitment of monocytes and neutrophils to the inflammation site (45–47). The expression of NKG2D (an activating receptor for NK cells) is significantly upregulated in the reperfused liver (48). Increased NK cells recruited to the liver can not only exacerbate IRI by producing IFNγ but also increase the production of IL-17, which promotes the recruitment of neutrophils (49, 50). Hepatic IRI also elicits a robust adaptive immune response in which CD4+ T cells mediate aggravated inflammatory damage (40).

The balance of pro-inflammatory and anti-inflammatory components determines the outcome of inflammation during IRI (44). Multiple clinical and experimental studies have suggested that intense and continuous inflammation induced by hepatic IRI promoted tumor recurrence *via* activating cellular signaling for tumor cell proliferation, adhesion, invasion and angiogenesis (8, 51). Hypoxia-inducible factor 1α (HIF1α), matrix metalloproteinase 9 (MMP9), vascular endothelial growth factor (VEGF) and other key molecules play important roles in this process (52).

After the initiation of inflammation, some anti-inflammatory components and repair factors will be recruited into the inflammatory microenvironment to inhibit the progress of inflammation and promote injury repair. Anti-inflammatory cytokines, such as IL-4 or IL-13, and apoptotic cells promote *in situ* macrophage polarization and reprogramming and then initiate the resolution phase of inflammation (53–55). Some anti-inflammatory neutrophil subtypes exert anti-inflammatory and repair functions through inhibiting cytotoxic T cells (CTLs), promoting macrophage polarization and angiogenesis (44, 56). Besides, regulatory T cells (Tregs), myeloid-derived suppressor cells (MDSCs), endothelial progenitor cells (EPCs), platelets and many other factors also play critical roles in regulating inflammation and its resolution (44, 57, 58).

However, in the setting of oncology, these beneficial components may also result in worsened oncologic outcomes. Some components responding to inflammation have been proved to promote HCC recurrence through different mechanisms, including mediating the immune escape and angiogenesis of tumor as well as causing tumor cells to be more aggressive by triggering tumor cell adhesion, migration, and invasion (13). Targeting key inflammatory components in the tumor microenvironment may suppress tumor recurrence. Compared to machine perfusion, this method provides more

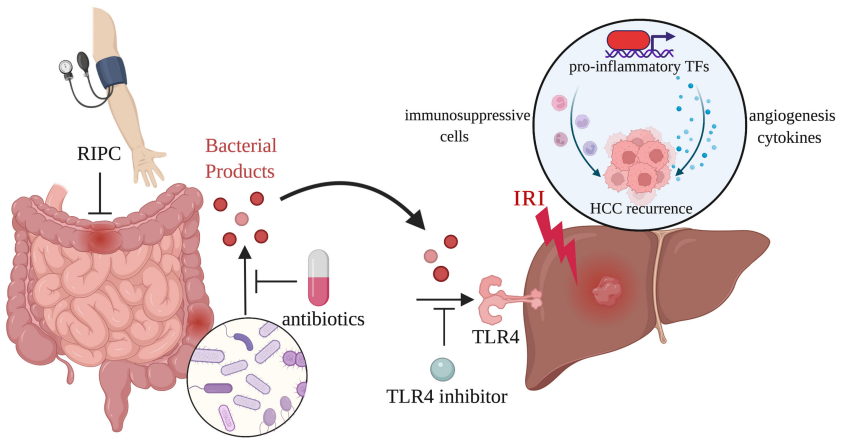

FIGURE 1 | The gut-liver axis as a target in inflammation-associated cancer recurrence induced by hepatic IRI. Portal vein clamping during LT and LR leads to venous congestion and hypoperfusion of the intestines. Bacterial products released through damaged intestinal mucosa activate TLR4 signaling pathway in the liver, resulting in the exacerbated inflammatory response and increased tumor burden. RIPC, antibiotics, and TLR4 inhibition are able to act on the gut-liver axis to reduce inflammation-associated HCC recurrence.

targeted treatment for HCC patients and can be applied to both LR and LT. **Figure 2** displays the key inflammatory components in the tumor microenvironment and relevant therapies.

Immune escape is a crucial characteristic during tumor growth and metastasis. MDSCs and Tregs have been identified as key immune cell subsets that mediate tumor immune escape (59). Of them, MDSCs are a heterogeneous population of immunosuppressive cells derived from myeloid progenitors, which can be upregulated by inflammatory mediators such as IL-2, GCSF, and so on (57). MDSCs suppress the immune system by various mechanisms including (i) inhibiting CTLs proliferation and activation by increased nitric oxide (NO), nitrotyrosine and ROS secretion, and decreased l-arginine production (ii) inducing immunosuppressive cells like T helper (Th) 17 cells and Tregs (60); Tregs are crucial suppressors of immune responses and are essential for maintaining immunological tolerance and controlling inflammatory diseases (61, 62). In the process of tumor immune escape, Tregs can suppress antigen presentation by DCs, CD4+ Th cell function and promote intratumoral T cell exhaustion through secreting TGF-β, IL-10 and IL-35 (63, 64). Recent findings also demonstrated the crosstalk between Tregs and MDSCs, which found that Tregs regulate MDSCs differentiation and function through TGF-β and the programmed death ligand 1 (B7-H1) (65, 66). In HCC patients, MDSCs and Tregs were found to be significantly elevated in the peripheral blood and tumor (67, 68). Besides, emerging tumor immunotherapy targeting MDSC and Tregs has effectively inhibited the progression of HCC (63, 69).

In addition to immune escape, tumor angiogenesis also plays a key role in tumor recurrence. EPCs are a kind of vascular progenitor with high proliferative potential that are derived from bone marrow (70). Inflammatory endothelial injury can trigger mobilization, homing, and transdifferentiation of EPCs, thereby contributing to the repair of injured endothelium (71). Recent studies have found that EPCs participate in neovascularization during acute ischemic injury (58). However, mobilization of EPCs also occurs in response to low oxygenation during tumor growth (72). They are able to facilitate the release of proangiogenic cytokines and promote vessel incorporation and stabilization (73). Multiple studies have shown that mobilization of circulating EPC results in tumor neovascularization and accelerates tumor growth and metastasis (74, 75). Besides, the inhibition of EPCs mobilization restrained angiogenesis and tumor progression (76).

In the inflammatory cascade triggered by hepatic IRI, chemokines and chemokine receptors are involved in the recruitment of inflammation-responsive components discussed above (77). Selectively targeting these pathways has been heralded as a promising avenue for suppressing these cell subsets. Through a series of clinical analyses, *in vitro* and *in vivo* experiments, Liu et al. found that MDSCs recruited by CXCL10/TLR4 during acute phase inflammation played a critical role in tumor recurrence after LT. Targeting MDSC mobilization *via* CXCL10/TLR4 signaling could not only protect the liver graft from IRI but also reduce tumor recurrence after transplantation (78). Ling et al. identified that post-transplant enhanced CXCL10/CXCR3 signaling in small-for-size liver grafts directly induced EPC mobilization, differentiation, and neovessel formation, which further promotes tumor growth (79). Besides, CXCL10/CXCR3 signaling upregulated at liver graft injury directly induced the mobilization and intragraft recruitment of Tregs, which further promoted HCC recurrence after transplantation (80). Targeting CXCL10/CXCR3 signaling inhibited the mobilization of Treg and EPC, attenuated early-phase liver graft injury, and prevented late-phase tumor recurrence/metastasis after transplantation (79, 80).

In addition to genetic approaches and pharmacological inhibitors, some drugs can also act through the above pathways. FTY720 (fingolimod) is a sphingosine-1-phosphate (S1P) receptor agonist that has been approved by FDA as a treatment for multiple

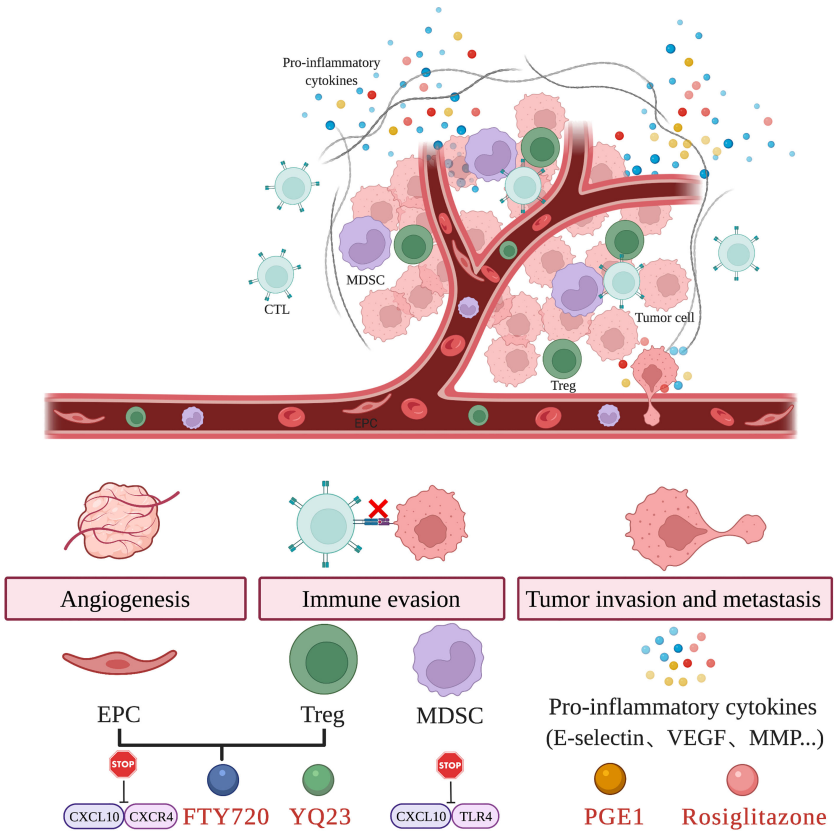

FIGURE 2 | Targeting key inflammatory components in the tumor microenvironment. Hepatic IRI results in the recruitment of EPC, Treg, and MDSC as well as the release of pro-inflammatory cytokines. These changes in the tumor microenvironment induce tumor angiogenesis, immune evasion and promote tumor invasion and metastasis. The use of agents such as FTY720, YQ23, PGE1, Rosiglitazone and targeting key inflammatory pathways are able to attenuate hepatic IRI and prevent tumor recurrence.

sclerosis (MS) (81). In models of lung, kidney, and liver IRI, FTY720 unfolds a demonstrated anti-inflammatory effect (82–84). Furthermore, FTY720 has exhibited a strong anti-tumor activity in liver cancer, breast cancer, bladder cancer, and so on (85–88). Li et al. found that FTY720 significantly attenuated hepatic IRI and tumor metastasis after LR through the downregulating CXCL10/CXCR3 signaling pathway. In their study, FTY720 treatment reduced the population of circulating EPCs and Tregs and thereby limited tumor angiogenesis and enhanced antitumor immune response (89, 90). A novel oxygen carrier called YQ23 played a similar role in suppressing liver tumor metastasis after major hepatectomy and partial hepatic I/R injury through increasing liver oxygenation and reducing the number of circulating EPCs and Tregs (91).

A number of studies have indicated that proinflammatory cytokines such as E-selectin, VEGF and MMP activated by hepatic IRI promoted tumor invasion and metastasis (92–94). Ligands of PPARγ, such as rosiglitazone can downregulate the expression of proinflammatory cytokines that are associated with tumor metastases through inhibiting the NF-κB signaling pathway (95–97). In an experimental mouse model of hepatic IRI-induced HCC metastasis, rosiglitazone exerts a protective effect on hepatic IRI and significantly inhibits tumor metastasis following that. As reported in this article, the dual action may be attributed to inhibited NF-κB signaling and reduced expression of proinflammatory cytokines in liver (98).

Prostaglandins (PGs) are products of arachidonic acid metabolism *via* the cyclooxygenase pathway, which are produced primarily by activated Kupfer cells during hepatic IRI (99). PGs exert anti-inflammatory effects by prevention of leucocyte migration and down-regulation of pro-inflammatory cytokines (100). The administration of alprostadil, a synthetic stable form of prostaglandin E1(PGE1), was shown to attenuate hepatic IRI and improve liver graft function (101). In a retrospective clinical study, Kornberg et al. found that treating hepatic IRI with alprostadil reduced systemic inflammation levels and the risk of early HCC recurrence following LT (102).

Besides these mentioned strategies above, glutathione peroxidase 3, thymoquinone, and zinc finger protein A20 also show the potential to be "one stone for two birds" strategies that attenuate hepatic IR injury and prevent tumor recurrence after liver surgery (103–105). However, their inhibition of hepatic IRI-

associated recurrence needs further experimental research and clinical verification.

CONCLUSION AND PROSPECT

Collectively, the inflammation induced by hepatic IRI plays a crucial role in the development and progression of HCC, which contributes to several hallmarks of HCC, such as promoting proliferative and survival signaling, inducing angiogenesis, evading immune surveillance, and activating invasion and metastasis. Besides, alleviating inflammation such as machine perfusion, regulating the gut-liver axis and targeting key inflammatory components or inflammatory pathways is believed to be an attractive therapeutic strategy. However, current evidence mainly comes from animal models. More clinical studies with larger numbers of patients will be required. Moreover, not all measures are applicable to LT or LR due to the differences in surgical procedures, use of immunosuppressive agents and postoperative management. Additional validation is needed in different models and patient populations. In the future, we advocate using advanced techniques such as single-cell multi-omics and spatial omics to explore the mechanism and targets for therapeutic intervention comprehensively. Meanwhile, we believe that combining different approaches at different time points should yield better outcomes for patients.

AUTHOR CONTRIBUTIONS

XX and DL designed and supervised the study. HC and XY performed the article searching and wrote the manuscript. ZH, CH, HL, ZL and MY revised the manuscript. All authors contributed to the article and approved the submitted version.

FUNDING

This work was supported by grants from The Major Research Plan of the National Natural Science Foundation of China (92159202), Key Program, National Natural Science Foundation of China (81930016), National Key Research and Development Program of China (2021YFA1100500), Key Research & Development Plan of Zhejiang Province (No. 2019C03050), and Young Program of National Natural Science Funds (No. 82000617).

ACKNOWLEDGMENTS

We thank all members of Key Laboratory of Integrated Oncology and Intelligent Medicine of Zhejiang Province for helpful suggestions regarding the manuscript. Figures were created with BioRender.

REFERENCES

1. Torre LA, Bray F, Siegel RL, Ferlay J, Lortet-Tieulent J, Jemal A. Global Cancer Statistics, 2012. *CA Cancer J Clin* (2015) 65(2):87–108. doi: 10.3322/caac.21262
2. Kawaguchi Y, Honda G, Endo I, Cherqui D, Kokudo N. Current Technical Issues for Surgery of Primary Liver Cancer. *Liver Cancer* (2016) 6(1):51–8. doi: 10.1159/000449345
3. El-Serag HB. Hepatocellular Carcinoma. *N Engl J Med* (2011) 365(12):1118–27. doi: 10.1056/NEJMra1001683
4. Xia YX, Zhang F, Li XC, Kong LB, Zhang H, Li DH, et al. Surgical Treatment of Primary Liver Cancer: A Report of 10 966 Cases. *Zhonghua Wai Ke Za Zhi* (2021) 59(1):6–17. doi: 10.3760/cma.j.cn112139-20201110-00791
5. Zhou J, Chen J, Wei Q, Saeb-Parsy K, Xu X. The Role of Ischemia/Reperfusion Injury in Early Hepatic Allograft Dysfunction. *Liver Transpl* (2020) 26(8):1034–48. doi: 10.1002/lt.25779
6. Mollinedo F. Neutrophil Degranulation, Plasticity, and Cancer Metastasis. *Trends Immunol* (2019) 40(3):228–42. doi: 10.1016/j.it.2019.01.006
7. Lazennec G, Richmond A. Chemokines and Chemokine Receptors: New Insights Into Cancer-Related Inflammation. *Trends Mol Med* (2010) 16 (3):133–44. doi: 10.1016/j.molmed.2010.01.003
8. Nagai S, Yoshida A, Facciuto M, Moonka D, Abouljoud MS, Schwartz ME, et al. Ischemia Time Impacts Recurrence of Hepatocellular Carcinoma After Liver Transplantation. *Hepatology* (2015) 61(3):895–904. doi: 10.1002/hep.27358
9. Kornberg A, Witt U, Kornberg J, Friess H, Thrum K. Extended Ischemia Times Promote Risk of Hcc Recurrence in Liver Transplant Patients. *Dig Dis Sci* (2015) 60(9):2832–9. doi: 10.1007/s10620-015-3541-z
10. Ling Q, Liu J, Zhuo J, Zhuang R, Huang H, He X, et al. Development of Models to Predict Early Post-Transplant Recurrence of Hepatocellular Carcinoma That Also Integrate the Quality and Characteristics of the Liver Graft: A National Registry Study in China. *Surgery* (2018) 164 (1):155–164. doi: 10.1016/j.surg.2018.01.022
11. Orci LA, Berney T, Majno PE, Lacotte S, Oldani G, Morel P, et al. Donor Characteristics and Risk of Hepatocellular Carcinoma Recurrence After Liver Transplantation. *Br J Surg* (2015) 102(10):1250–7. doi: 10.1002/bjs.9868
12. Grąt M, Krawczyk M, Wronka KM, Stypułkowski J, Lewandowski Z, Wasilewicz M, et al. Ischemia-Reperfusion Injury and the Risk of Hepatocellular Carcinoma Recurrence After Deceased Donor Liver Transplantation. *Sci Rep* (2018) 8(1):8935. doi: 10.1038/s41598-018-27319-y
13. Liu H, Man K. New Insights in Mechanisms and Therapeutics for Short- and Long-Term Impacts of Hepatic Ischemia Reperfusion Injury Post Liver Transplantation. *Int J Mol Sci* (2021) 22(15):8210. doi: 10.3390/ijms22158210
14. Bruix J, Sherman M. Management of Hepatocellular Carcinoma. *Hepatology* (2005) 42(5):1208–36. doi: 10.1002/hep.20933
15. Heylen L, Pirenne J, Naesens M, Sprangers B, Jochmans I. "Time Is Tissue"-A Minireview on the Importance of Donor Nephrectomy, Donor Hepatectomy, and Implantation Times in Kidney and Liver Transplantation. *Am J Transplant* (2021) 21(8):2653–61. doi: 10.1111/ajt.16580
16. Ito T, Naini BV, Markovic D, Aziz A, Younan S, Lu M, et al. Ischemia-Reperfusion Injury and Its Relationship With Early Allograft Dysfunction in Liver Transplant Patients. *Am J Transplant* (2021) 21(2):614–25. doi: 10.1111/ajt.16219
17. Ceresa CDL, Nasralla D, Pollok JM, Friend PJ. Machine Perfusion of the Liver: Applications in Transplantation and Beyond. *Nat Rev Gastroenterol Hepatol* (2022) 19(3):199–209. doi: 10.1038/s41575-021-00557-8
18. Vodkin I, Kuo A. Extended Criteria Donors in Liver Transplantation. *Clin Liver Dis* (2017) 21(2):289–301. doi: 10.1016/j.cld.2016.12.004
19. Orci LA, Lacotte S, Oldani G, Slits F, De Vito C, Crowe LA, et al. Effect of Ischaemic Preconditioning on Recurrence of Hepatocellular Carcinoma in an Experimental Model of Liver Steatosis. *Br J Surg* (2016) 103(4):417–26. doi: 10.1002/bjs.10080
20. van Rijn R, Schurink IJ, de Vries Y, van den Berg AP, Cortes Cerisuelo M, Darwish Murad S, et al. Hypothermic Machine Perfusion in Liver

Transplantation - A Randomized Trial. *N Engl J Med* (2021) 384(15):1391–401. doi: 10.1056/NEJMoa2031532
21. Oldani G, Crowe LA, Orci LA, Slits F, Rubbia-Brandt L, de Vito C, et al. Pre-Retrieval Reperfusion Decreases Cancer Recurrence After Rat Ischemic Liver Graft Transplantation. *J Hepatol* (2014) 61(2):278–85. doi: 10.1016/j.jhep.2014.03.036
22. Oldani G, Lacotte S, Orci L, Toso C. Reply To: Pre-Retrieval Reperfusion Decreases Cancer Recurrence After Rat Ischemic Liver Graft Transplantation. *J Hepatol* (2014) 61(4):962–3. doi: 10.1016/j.jhep.2014.06.011
23. Watson CJE, Hunt F, Messer S, Currie I, Large S, Sutherland A, et al. *In Situ* Normothermic Perfusion of Livers in Controlled Circulatory Death Donation May Prevent Ischemic Cholangiopathy and Improve Graft Survival. *Am J Transplant* (2019) 19(6):1745–58. doi: 10.1111/ajt.15241
24. Czigany Z, Lurje I, Schmelzle M, Schöning W, Öllinger R, Raschzok N, et al. Ischemia-Reperfusion Injury in Marginal Liver Grafts and the Role of Hypothermic Machine Perfusion: Molecular Mechanisms and Clinical Implications. *J Clin Med* (2020) 9(3):846. doi: 10.3390/jcm9030846
25. Mueller M, Kalisvaart M, O'Rourke J, Shetty S, Parente A, Muller X, et al. Hypothermic Oxygenated Liver Perfusion (Hope) Prevents Tumor Recurrence in Liver Transplantation From Donation After Circulatory Death. *Ann Surg* (2020) 272(5):759–65. doi: 10.1097/sla.0000000000004258
26. Guo Z, Zhao Q, Huang S, Huang C, Wang D, Yang L, et al. Ischaemia-Free Liver Transplantation in Humans: A First-In-Human Trial. *Lancet Reg Health West Pac* (2021) 16:100260. doi: 10.1016/j.lanwpc.2021.100260
27. Tang Y, Wang T, Ju W, Li F, Zhang Q, Chen Z, et al. Ischemic-Free Liver Transplantation Reduces the Recurrence of Hepatocellular Carcinoma After Liver Transplantation. *Front Oncol* (2021) 11:773535. doi: 10.3389/fonc.2021.773535
28. Tripathi A, Debelius J, Brenner DA, Karin M, Loomba R, Schnabl B, et al. The Gut-Liver Axis and the Intersection With the Microbiome. *Nat Rev Gastroenterol Hepatol* (2018) 15(7):397–411. doi: 10.1038/s41575-018-0011-z
29. Yang X, Lu D, Zhuo J, Lin Z, Yang M, Xu X. The Gut-Liver Axis in Immune Remodeling: New Insight Into Liver Diseases. *Int J Biol Sci* (2020) 16 (13):2357–66. doi: 10.7150/ijbs.46405
30. Dapito DH, Mencin A, Gwak GY, Pradere JP, Jang MK, Mederacke I, et al. Promotion of Hepatocellular Carcinoma by the Intestinal Microbiota and Tlr4. *Cancer Cell* (2012) 21(4):504–16. doi: 10.1016/j.ccr.2012.02.007
31. Dello SA, Reisinger KW, van Dam RM, Bemelmans MH, van Kuppevelt TH, van den Broek MA, et al. Total Intermittent Pringle Maneuver During Liver Resection Can Induce Intestinal Epithelial Cell Damage and Endotoxemia. *PloS One* (2012) 7(1):e30539. doi: 10.1371/journal.pone.0030539
32. Colletti LM, Green M. Lung and Liver Injury Following Hepatic Ischemia/Reperfusion in the Rat Is Increased by Exogenous Lipopolysaccharide Which Also Increases Hepatic Tnf Production in Vivo and in Vitro. *Shock* (2001) 16(4):312–9. doi: 10.1097/00024382-200116040-00014
33. Orci LA, Lacotte S, Delaune V, Slits F, Oldani G, Lazarevic V, et al. Effects of the Gut-Liver Axis on Ischaemia-Mediated Hepatocellular Carcinoma Recurrence in the Mouse Liver. *J Hepatol* (2018) 68(5):978–85. doi: 10.1016/j.jhep.2017.12.025
34. Yamamoto M, Sato S, Hemmi H, Hoshino K, Kaisho T, Sanjo H, et al. Role of Adaptor Trif in the Myd88-Independent Toll-Like Receptor Signaling Pathway. *Science* (2003) 301(5633):640–3. doi: 10.1126/science.1087262
35. Sepehri Z, Kiani Z, Kohan F, Alavian SM, Ghavami S. Toll Like Receptor 4 and Hepatocellular Carcinoma; a Systematic Review. *Life Sci* (2017) 179:80–7. doi: 10.1016/j.lfs.2017.04.025
36. Kanoria S, Robertson FP, Mehta NN, Fusai G, Sharma D, Davidson BR. Effect of Remote Ischaemic Preconditioning on Liver Injury in Patients Undergoing Major Hepatectomy for Colorectal Liver Metastasis: A Pilot Randomised Controlled Feasibility Trial. *World J Surg* (2017) 41(5):1322–30. doi: 10.1007/s00268-016-3823-4
37. Rakić M, Patrlj L, Amić F, Aralica G, Grgurević I. Comparison of Hepatoprotective Effect From Ischemia-Reperfusion Injury of Remote Ischemic Preconditioning of the Liver Vs Local Ischemic Preconditioning of the Liver During Human Liver Resections. *Int J Surg* (2018) 54(Pt A):248–53. doi: 10.1016/j.ijsu.2018.05.001
38. Robertson FP, Goswami R, Wright GP, Imber C, Sharma D, Malago M, et al. Remote Ischaemic Preconditioning in Orthotopic Liver Transplantation (Ripcolt Trial): A Pilot Randomized Controlled Feasibility Study. *HPB (Oxford)* (2017) 19(9):757–67. doi: 10.1016/j.hpb.2017.05.005
39. Teo JY, Ho AFW, Bulluck H, Gao F, Chong J, Koh YX, et al. Effect of Remote Ischemic Preconditioning on Liver Injury in Patients Undergoing Liver Resection: The Eric-Liver Trial. *HPB (Oxford)* (2020) 22(9):1250–7. doi: 10.1016/j.hpb.2019.12.002
40. Zhai Y, Petrowsky H, Hong JC, Busuttil RW, Kupiec-Weglinski JW. Ischaemia-Reperfusion Injury in Liver Transplantation–from Bench to Bedside. *Nat Rev Gastroenterol Hepatol* (2013) 10(2):79–89. doi: 10.1038/nrgastro.2012.225
41. Selzner M, Selzner N, Jochum W, Graf R, Clavien PA. Increased Ischemic Injury in Old Mouse Liver: An Atp-Dependent Mechanism. *Liver Transpl* (2007) 13(3):382–90. doi: 10.1002/lt.21100
42. Lentsch AB, Kato A, Yoshidome H, McMasters KM, Edwards MJ. Inflammatory Mechanisms and Therapeutic Strategies for Warm Hepatic Ischemia/Reperfusion Injury. *Hepatology* (2000) 32(2):169–73. doi: 10.1053/jhep.2000.9323
43. Li P, He K, Li J, Liu Z, Gong J. The Role of Kupffer Cells in Hepatic Diseases. *Mol Immunol* (2017) 85:222–9. doi: 10.1016/j.molimm.2017.02.018
44. Hirao H, Nakamura K, Kupiec-Weglinski JW. Liver Ischaemia-Reperfusion Injury: A New Understanding of the Role of Innate Immunity. *Nat Rev Gastroenterol Hepatol* (2021) 19(4):239–56. doi: 10.1038/s41575-021-00549-8
45. Suzuki J, Hamada E, Shodai T, Kamoshida G, Kudo S, Itoh S, et al. Cytokine Secretion From Human Monocytes Potentiated by P-Selectin-Mediated Cell Adhesion. *Int Arch Allergy Immunol* (2013) 160(2):152–60. doi: 10.1159/000339857
46. Singh MV, Davidson DC, Jackson JW, Singh VB, Silva J, Ramirez SH, et al. Characterization of Platelet-Monocyte Complexes in Hiv-1-Infected Individuals: Possible Role in Hiv-Associated Neuroinflammation. *J Immunol* (2014) 192(10):4674–84. doi: 10.4049/jimmunol.1302318
47. Hwaiz R, Rahman M, Zhang E, Thorlacius H. Platelet Secretion of Cxcl4 Is Rac1-Dependent and Regulates Neutrophil Infiltration and Tissue Damage in Septic Lung Damage. *Br J Pharmacol* (2015) 172(22):5347–59. doi: 10.1111/bph.13325
48. Kimura S, Ozaki KS, Ueki S, Zhang M, Yokota S, Stolz DB, et al. Contribution of Alloantigens to Hepatic Ischemia/Reperfusion Injury: Roles of Natural Killer Cells and Innate Immune Recognition of Nonself. *Liver Transpl* (2016) 22(1):80–90. doi: 10.1002/lt.24330
49. Nakajima H, Mizuta N, Fujiwara I, Sakaguchi K, Ogata H, Magae J, et al. Blockade of the Fas/Fas Ligand Interaction Suppresses Hepatocyte Apoptosis in Ischemia-Reperfusion Rat Liver. *Apoptosis* (2008) 13 (8):1013–21. doi: 10.1007/s10495-008-0234-5
50. Feng M, Li G, Qian X, Fan Y, Huang X, Zhang F, et al. Il-17a-Producing Nk Cells Were Implicated in Liver Injury Induced by Ischemia and Reperfusion. *Int Immunopharmacol* (2012) 13(2):135–40. doi: 10.1016/j.intimp.2012.03.007
51. Man K, Ng KT, Lo CM, Ho JW, Sun BS, Sun CK, et al. Ischemia-Reperfusion of Small Liver Remnant Promotes Liver Tumor Growth and Metastases–Activation of Cell Invasion and Migration Pathways. *Liver Transpl* (2007) 13 (12):1669–77. doi: 10.1002/lt.21193
52. Orci LA, Lacotte S, Oldani G, Morel P, Mentha G, Toso C. The Role of Hepatic Ischemia-Reperfusion Injury and Liver Parenchymal Quality on Cancer Recurrence. *Dig Dis Sci* (2014) 59(9):2058–68. doi: 10.1007/s10620-014-3182-7
53. Blander JM. The Many Ways Tissue Phagocytes Respond to Dying Cells. *Immunol Rev* (2017) 277(1):158–73. doi: 10.1111/imr.12537
54. Bosurgi L, Cao YG, Cabeza-Cabrerizo M, Tucci A, Hughes LD, Kong Y, et al. Macrophage Function in Tissue Repair and Remodeling Requires Il-4 or Il-13 With Apoptotic Cells. *Science* (2017) 356(6342):1072–6. doi: 10.1126/science.aai8132
55. Soehnlein O, Lindbom L. Phagocyte Partnership During the Onset and Resolution of Inflammation. *Nat Rev Immunol* (2010) 10(6):427–39. doi: 10.1038/nri2779
56. Wang J. Neutrophils in Tissue Injury and Repair. *Cell Tissue Res* (2018) 371 (3):531–9. doi: 10.1007/s00441-017-2785-7
57. Scalea JR, Lee YS, Davila E, Bromberg JS. Myeloid-Derived Suppressor Cells and Their Potential Application in Transplantation. *Transplantation* (2018) 102(3):359–67. doi: 10.1097/tp.0000000000002022

58. Minami E, Laflamme MA, Saffitz JE, Murry CE. Extracardiac Progenitor Cells Repopulate Most Major Cell Types in the Transplanted Human Heart. *Circulation* (2005) 112(19):2951–8. doi: 10.1161/circulationaha.105.576017
59. Kerkar SP, Restifo NP. Cellular Constituents of Immune Escape Within the Tumor Microenvironment. *Cancer Res* (2012) 72(13):3125–30. doi: 10.1158/0008-5472.Can-11-4094
60. De Cicco P, Ercolano G, Ianaro A. The New Era of Cancer Immunotherapy: Targeting Myeloid-Derived Suppressor Cells to Overcome Immune Evasion. *Front Immunol* (2020) 11:1680. doi: 10.3389/fimmu.2020.01680
61. Kwon HK, Chen HM, Mathis D, Benoist C. Different Molecular Complexes That Mediate Transcriptional Induction and Repression by Foxp3. *Nat Immunol* (2017) 18(11):1238–48. doi: 10.1038/ni.3835
62. Faustino LD, Griffith JW, Rahimi RA, Nepal K, Hamilos DL, Cho JL, et al. Interleukin-33 Activates Regulatory T Cells to Suppress Innate γδ T Cell Responses in the Lung. *Nat Immunol* (2020) 21(11):1371–83. doi: 10.1038/s41590-020-0785-3
63. Li C, Jiang P, Wei S, Xu X, Wang J. Regulatory T Cells in Tumor Microenvironment: New Mechanisms, Potential Therapeutic Strategies and Future Prospects. *Mol Cancer* (2020) 19(1):116. doi: 10.1186/s12943-020-01234-1
64. Sullivan JA, Tomita Y, Jankowska-Gan E, Lema DA, Arvedson MP, Nair A, et al. Treg-Cell-Derived Il-35-Coated Extracellular Vesicles Promote Infectious Tolerance. *Cell Rep* (2020) 30(4):1039–51.e5. doi: 10.1016/j.celrep.2019.12.081
65. Fujimura T, Ring S, Umansky V, Mahnke K, Enk AH. Regulatory T Cells Stimulate B7-H1 Expression in Myeloid-Derived Suppressor Cells in Ret Melanomas. *J Invest Dermatol* (2012) 132(4):1239–46. doi: 10.1038/jid.2011.416
66. Lee CR, Kwak Y, Yang T, Han JH, Park SH, Ye MB, et al. Myeloid-Derived Suppressor Cells Are Controlled by Regulatory T Cells *Via* Tgf-B During Murine Colitis. *Cell Rep* (2016) 17(12):3219–32. doi: 10.1016/j.celrep.2016.11.062
67. Hoechst B, Ormandy LA, Ballmaier M, Lehner F, Krüger C, Manns MP, et al. A New Population of Myeloid-Derived Suppressor Cells in Hepatocellular Carcinoma Patients Induces Cd4(+)Cd25(+)Foxp3(+) T Cells. *Gastroenterology* (2008) 135(1):234–43. doi: 10.1053/j.gastro.2008.03.020
68. Viguier M, Lemaître F, Verola O, Cho MS, Gorochov G, Dubertret L, et al. Foxp3 Expressing Cd4+Cd25(High) Regulatory T Cells Are Overrepresented in Human Metastatic Melanoma Lymph Nodes and Inhibit the Function of Infiltrating T Cells. *J Immunol* (2004) 173(2):1444–53. doi: 10.4049/jimmunol.173.2.1444
69. Shimizu J, Yamazaki S, Sakaguchi S. Induction of Tumor Immunity by Removing Cd25+Cd4+ T Cells: A Common Basis Between Tumor Immunity and Autoimmunity. *J Immunol* (1999) 163(10):5211–8.
70. Reinisch A, Hofmann NA, Obenauf AC, Kashofer K, Rohde E, Schallmoser K, et al. Humanized Large-Scale Expanded Endothelial Colony-Forming Cells Function in Vitro and in Vivo. *Blood* (2009) 113(26):6716–25. doi: 10.1182/blood-2008-09-181362
71. Inoue T, Sata M, Hikichi Y, Sohma R, Fukuda D, Uchida T, et al. Mobilization of Cd34-Positive Bone Marrow-Derived Cells After Coronary Stent Implantation: Impact on Restenosis. *Circulation* (2007) 115(5):553–61. doi: 10.1161/circulationaha.106.621714
72. de la Puente P, Muz B, Azab F, Azab AK. Cell Trafficking of Endothelial Progenitor Cells in Tumor Progression. *Clin Cancer Res* (2013) 19(13):3360–8. doi: 10.1158/1078-0432.Ccr-13-0462
73. Gao D, Nolan D, McDonnell K, Vahdat L, Benezra R, Altorki N, et al. Bone Marrow-Derived Endothelial Progenitor Cells Contribute to the Angiogenic Switch in Tumor Growth and Metastatic Progression. *Biochim Biophys Acta* (2009) 1796(1):33–40. doi: 10.1016/j.bbcan.2009.05.001
74. Ruzinova MB, Schoer RA, Gerald W, Egan JE, Pandolfi PP, Rafii S, et al. Effect of Angiogenesis Inhibition by Id Loss and the Contribution of Bone-Marrow-Derived Endothelial Cells in Spontaneous Murine Tumors. *Cancer Cell* (2003) 4(4):277–89. doi: 10.1016/s1535-6108(03)00240-x
75. Peters BA, Diaz LA, Polyak K, Meszler L, Romans K, Guinan EC, et al. Contribution of Bone Marrow-Derived Endothelial Cells to Human Tumor Vasculature. *Nat Med* (2005) 11(3):261–2. doi: 10.1038/nm1200
76. Lyden D, Hattori K, Dias S, Costa C, Blaikie P, Butros L, et al. Impaired Recruitment of Bone-Marrow-Derived Endothelial and Hematopoietic Precursor Cells Blocks Tumor Angiogenesis and Growth. *Nat Med* (2001) 7(11):1194–201. doi: 10.1038/nm1101-1194
77. Colletti LM, Kunkel SL, Walz A, Burdick MD, Kunkel RG, Wilke CA, et al. The Role of Cytokine Networks in the Local Liver Injury Following Hepatic Ischemia/Reperfusion in the Rat. *Hepatology* (1996) 23(3):506–14. doi: 10.1002/hep.510230315
78. Liu H, Ling CC, Yeung WHO, Pang L, Liu J, Zhou J, et al. Monocytic Mdsc Mobilization Promotes Tumor Recurrence After Liver Transplantation *Via* Cxcl10/Tlr4/Mmp14 Signaling. *Cell Death Dis* (2021) 12(5):489. doi: 10.1038/s41419-021-03788-4
79. Ling CC, Ng KT, Shao Y, Geng W, Xiao JW, Liu H, et al. Post-Transplant Endothelial Progenitor Cell Mobilization *Via* Cxcl10/Cxcr3 Signaling Promotes Liver Tumor Growth. *J Hepatol* (2014) 60(1):103–9. doi: 10.1016/j.jhep.2013.08.017
80. Li CX, Ling CC, Shao Y, Xu A, Li XC, Ng KT, et al. Cxcl10/Cxcr3 Signaling Mobilized-Regulatory T Cells Promote Liver Tumor Recurrence After Transplantation. *J Hepatol* (2016) 65(5):944–52. doi: 10.1016/j.jhep.2016.05.032
81. Strader CR, Pearce CJ, Oberlies NH. Fingolimod (Fty720): A Recently Approved Multiple Sclerosis Drug Based on a Fungal Secondary Metabolite. *J Nat Prod* (2011) 74(4):900–7. doi: 10.1021/np2000528
82. Stone ML, Sharma AK, Zhao Y, Charles EJ, Huerter ME, Johnston WF, et al. Sphingosine-1-Phosphate Receptor 1 Agonism Attenuates Lung Ischemia-Reperfusion Injury. *Am J Physiol Lung Cell Mol Physiol* (2015) 308(12):L1245–52. doi: 10.1152/ajplung.00302.2014
83. Foster AD, Vicente D, Clark N, Leonhardt C, Elster EA, Davis TA, et al. Fty720 Effects on Inflammation and Liver Damage in a Rat Model of Renal Ischemia-Reperfusion Injury. *Mediators Inflammation* (2019) 2019:3496836. doi: 10.1155/2019/3496836
84. Man K, Ng KT, Lee TK, Lo CM, Sun CK, Li XL, et al. Fty720 Attenuates Hepatic Ischemia-Reperfusion Injury in Normal and Cirrhotic Livers. *Am J Transplant* (2005) 5(1):40–9. doi: 10.1111/j.1600-6143.2004.00642.x
85. Lee TK, Man K, Ho JW, Wang XH, Poon RT, Xu Y, et al. Fty720: A Promising Agent for Treatment of Metastatic Hepatocellular Carcinoma. *Clin Cancer Res* (2005) 11(23):8458–66. doi: 10.1158/1078-0432.Ccr-05-0447
86. Azuma H, Takahara S, Horie S, Muto S, Otsuki Y, Katsuoka Y. Induction of Apoptosis in Human Bladder Cancer Cells *in Vitro* and *in Vivo* Caused by Fty720 Treatment. *J Urol* (2003) 169(6):2372–7. doi: 10.1097/01.ju.0000064938.32318.91
87. Azuma H, Takahara S, Ichimaru N, Wang JD, Itoh Y, Otsuki Y, et al. Marked Prevention of Tumor Growth and Metastasis by a Novel Immunosuppressive Agent, Fty720, in Mouse Breast Cancer Models. *Cancer Res* (2002) 62(5):1410–9.
88. Zhou C, Ling MT, Kin-Wah Lee T, Man K, Wang X, Wong YC. Fty720, a Fungus Metabolite, Inhibits Invasion Ability of Androgen-Independent Prostate Cancer Cells Through Inactivation of Rhoa-Gtpase. *Cancer Lett* (2006) 233(1):36–47. doi: 10.1016/j.canlet.2005.02.039
89. Li CX, Shao Y, Ng KT, Liu XB, Ling CC, Ma YY, et al. Fty720 Suppresses Liver Tumor Metastasis by Reducing the Population of Circulating Endothelial Progenitor Cells. *PloS One* (2012) 7(2):e32380. doi: 10.1371/journal.pone.0032380
90. Li CX, Yang XX, Wang HW, Li XC, Ng KT, Lo CM, et al. Fty720 Suppresses Liver Tumor Growth and Metastasis by Reducing Circulating Regulating T Cells and Enhancing the Anti-Tumor Effect of Rapamycin. *Onco Targets Ther* (2020) 13:4743–54. doi: 10.2147/ott.S234394
91. Li CX, Wong BL, Ling CC, Ma YY, Shao Y, Geng W, et al. A Novel Oxygen Carrier "Yq23" Suppresses the Liver Tumor Metastasis by Decreasing Circulating Endothelial Progenitor Cells and Regulatory T Cells. *BMC Cancer* (2014) 14:293. doi: 10.1186/1471-2407-14-293
92. Uotani H, Yamashita I, Nagata T, Kishimoto H, Kashii Y, Tsukada K. Induction of E-Selectin After Partial Hepatectomy Promotes Metastases to Liver in Mice. *J Surg Res* (2001) 96(2):197–203. doi: 10.1006/jsre.2001.6095
93. Tamagawa K, Horiuchi T, Uchinami M, Doi K, Yoshida M, Nakamura T, et al. Hepatic Ischemia-Reperfusion Increases Vascular Endothelial Growth Factor and Cancer Growth in Rats. *J Surg Res* (2008) 148(2):158–63. doi: 10.1016/j.jss.2007.12.787

94. Cuzzocrea S. Peroxisome Proliferator-Activated Receptors Gamma Ligands and Ischemia and Reperfusion Injury. *Vascul Pharmacol* (2004) 41(6):187–95. doi: 10.1016/j.vph.2004.10.004
95. Wu QD, Wang JH, Condron C, Bouchier-Hayes D, Redmond HP. Human Neutrophils Facilitate Tumor Cell Transendothelial Migration. *Am J Physiol Cell Physiol* (2001) 280(4):C814–22. doi: 10.1152/ajpcell.2001.280.4.C814
96. Baud V, Karin M. Is Nf-Kappab a Good Target for Cancer Therapy? Hopes and Pitfalls. *Nat Rev Drug Discovery* (2009) 8(1):33–40. doi: 10.1038/nrd2781
97. Rogers AB, Fox JG. Inflammation and Cancer. I. Rodent Models of Infectious Gastrointestinal and Liver Cancer. *Am J Physiol Gastrointest Liver Physiol* (2004) 286(3):G361–6. doi: 10.1152/ajpgi.00499.2003
98. Liu YI, Liu Z, Chen Y, Xu K, Dong J. Pparγ Activation Reduces Ischemia/Reperfusion-Induced Metastasis in a Murine Model of Hepatocellular Carcinoma. *Exp Ther Med* (2016) 11(2):387–96. doi: 10.3892/etm.2015.2934
99. Nishizawa N, Ito Y, Eshima K, Ohkubo H, Kojo K, Inoue T, et al. Inhibition of Microsomal Prostaglandin E Synthase-1 Facilitates Liver Repair After Hepatic Injury in Mice. *J Hepatol* (2018) 69(1):110–20. doi: 10.1016/j.jhep.2018.02.009
100. Hossain MA, Wakabayashi H, Izuishi K, Okano K, Yachida S, Maeta H. The Role of Prostaglandins in Liver Ischemia-Reperfusion Injury. *Curr Pharm Des* (2006) 12(23):2935–51. doi: 10.2174/138161206777947678
101. Hsieh CC, Hsieh SC, Chiu JH, Wu YL. Protective Effects of N-Acetylcysteine and a Prostaglandin E1 Analog, Alprostadil, Against Hepatic Ischemia: Reperfusion Injury in Rats. *J Tradit Complement Med* (2014) 4(1):64–71. doi: 10.4103/2225-4110.124351
102. Kornberg A, Witt U, Kornberg J, Friess H, Thrum K. Treating Ischaemia-Reperfusion Injury With Prostaglandin E1 Reduces the Risk of Early Hepatocellular Carcinoma Recurrence Following Liver Transplantation. *Aliment Pharmacol Ther* (2015) 42(9):1101–10. doi: 10.1111/apt.13380
103. Qi X, Ng KT, Shao Y, Li CX, Geng W, Ling CC, et al. The Clinical Significance and Potential Therapeutic Role of Gpx3 in Tumor Recurrence After Liver Transplantation. *Theranostics* (2016) 6(11):1934–46. doi: 10.7150/thno.16023
104. Bimonte S, Albino V, Barbieri A, Tamma ML, Nasto A, Palaia R, et al. Dissecting the Roles of Thymoquinone on the Prevention and the Treatment of Hepatocellular Carcinoma: An Overview on the Current State of Knowledge. *Infect Agent Cancer* (2019) 14:10. doi: 10.1186/s13027-019-0226-9
105. Yi PS, Shu Y, Bi WX, Zheng XB, Feng WJ, He LY, et al. Emerging Role of Zinc Finger Protein A20 as a Suppressor of Hepatocellular Carcinoma. *J Cell Physiol* (2019) 234(12):21479–84. doi: 10.1002/jcp.28877

Conflict of Interest: The authors declare that the research was conducted in the absence of any commercial or financial relationships that could be construed as a potential conflict of interest.

Publisher's Note: All claims expressed in this article are solely those of the authors and do not necessarily represent those of their affiliated organizations, or those of the publisher, the editors and the reviewers. Any product that may be evaluated in this article, or claim that may be made by its manufacturer, is not guaranteed or endorsed by the publisher.

frontiers | Frontiers in Immunology

ORIGINAL RESEARCH
published: 17 May 2022
doi: 10.3389/fimmu.2022.890353

Liver Ischemia and Reperfusion Induce Periportal Expression of Necroptosis Executor pMLKL Which Is Associated With Early Allograft Dysfunction After Transplantation

Shaojun Shi[1], Eliano Bonaccorsi-Riani[2,3†], Ivo Schurink[1†], Thierry van den Bosch[4], Michael Doukas[4], Karishma A. Lila[4], Henk P. Roest[1], Daela Xhema[3], Pierre Gianello[3], Jeroen de Jonge[1], Monique M. A. Verstegen[1] and Luc J. W. van der Laan[1]*

[1] Department of Surgery, Erasmus MC Transplant Institute, University Medical Center, Rotterdam, Netherlands, [2] Abdominal Transplant Unit, Cliniques Universitaires Saint-Luc, Université Catholique de Louvain, Brussels, Belgium, [3] Pôle de Chirurgie Expérimentale et Transplantation Institute de Recherche Expérimentale et Clinique, Université Catholique de Louvain, Brussels, Belgium, [4] Department of Pathology, Erasmus MC-University Medical Center, Rotterdam, Netherlands

Background: Early allograft dysfunction (EAD) following liver transplantation (LT) remains a major threat to the survival of liver grafts and recipients. In animal models, it is shown that hepatic ischemia-reperfusion injury (IRI) triggers phosphorylation of Mixed Lineage Kinase domain-like protein (pMLKL) inducing necroptotic cell death. However, the clinical implication of pMLKL-mediated cell death in human hepatic IRI remains largely unexplored. In this study, we aimed to investigate the expression of pMLKL in human liver grafts and its association with EAD after LT.

Methods: The expression of pMLKL was determined by immunohistochemistry in liver biopsies obtained from both human and rat LT. Human liver biopsies were obtained at the end of preservation (T0) and ~1 hour after reperfusion (T1). The positivity of pMLKL was quantified electronically and compared in rat and human livers and post-LT outcomes. Multiplex immunofluorescence staining was performed to characterize the pMLKL-expressing cells.

Results: In the rat LT model, significant pMLKL expression was observed in livers after IRI as compared to livers of sham-operation animals. Similarly, the pMLKL score was highest after IRI in human liver grafts (in T1 biopsies). Both in rats and humans, the pMLKL expression is mostly observed in the portal triads. In grafts who developed EAD after LT (n=24), the pMLKL score at T1 was significantly higher as compared to non-EAD grafts (n=40). ROC curve revealed a high predictive value of pMLKL score at T1 (AUC 0.70) and the ratio of pMLKL score at T1 and T0 (pMLKL-index, AUC 0.82) for EAD. Liver grafts with a high pMLKL index (>1.64) had significantly higher levels of serum ALT, AST, and LDH 24 hours after LT compared to grafts with a low pMLKL index. Multivariate logistical

OPEN ACCESS

Edited by:
Bibo Ke,
University of California, Los Angeles, United States

Reviewed by:
Keri E. Lunsford,
Rutgers, The State University Of New Jersey, United States
Haoming Zhou,
Nanjing Medical University, China
Mingwei Sheng,
Tianjin First Central Hospital, China

***Correspondence:**
Luc J. W. van der Laan
l.vanderlaan@erasmusmc.nl

[†]These authors have contributed equally to this work

Specialty section:
This article was submitted to Molecular Innate Immunity, a section of the journal Frontiers in Immunology

Received: 05 March 2022
Accepted: 13 April 2022
Published: 17 May 2022

Citation:
Shi S, Bonaccorsi-Riani E, Schurink I, van den Bosch T, Doukas M, Lila KA, Roest HP, Xhema D, Gianello P, de Jonge J, Verstegen MMA and van der Laan LJW (2022) Liver Ischemia and Reperfusion Induce Periportal Expression of Necroptosis Executor pMLKL Which Is Associated With Early Allograft Dysfunction After Transplantation. Front. Immunol. 13:890353. doi: 10.3389/fimmu.2022.890353

regression analysis identified the pMLKL-index (Odds ratio=1.3, 95% CI 1.1-1.7) as a predictor of EAD development. Immunohistochemistry on serial sections and multiplex staining identified the periportal pMLKL-positive cells as portal fibroblasts, fibrocytes, and a minority of cholangiocytes.

Conclusion: Periportal pMLKL expression increased significantly after IRI in both rat and human LT. The histological score of pMLKL is predictive of post-transplant EAD and is associated with early liver injury after LT. Periportal non-parenchymal cells (i.e. fibroblasts) appear most susceptible to pMLKL-mediated cell death during hepatic IRI.

Keywords: ischemia-reperfusion injury, programmed cell death, non-parenchymal cell, myofibroblast, liver transplantation

INTRODUCTION

Liver transplantation (LT) is the only curative intervention for patients with end-stage liver diseases or hepatic malignancies (1). Procurement of the liver graft is associated with hepatic ischemia-reperfusion injury (IRI) in the donor, during storage and transportation, and after transplantation in the recipient. Though the extent of IRI varies per graft, overall, it has a negative impact on LT outcome (2). Early allograft dysfunction (EAD), defining the initial inferior function of the implanted liver is a critical determinant of graft survival and recipient outcome following both cadaveric and living donor LT (3–5). Risk factors associated with EAD development after LT include donor and recipient characteristics (age, BMI, and lifestyle), and intraoperative events such as prolonged cold or warm ischemia time, macrovesicular steatosis, and intra-operative transfusion requirements, and prolonged operation time (6–8). Secondary to IRI, these combined factors contribute to EAD by inducing hepatocellular damage, oxidative stress, accidental or programmed cell death, and severe inflammatory responses, which were clinically observed and confirmed in histological studies (7, 9–12).

The two major types of cell death caused by IRI are apoptosis and necrosis. This has been extensively studied in both animal models and human tissue biopsies (13). Gujral et al. (14) demonstrated that hepatocyte death in IRI was mainly caused by necrosis, especially during the reperfusion stage. Only a small population of sinusoidal endothelial cells and hepatocytes underwent apoptosis. Another study described that apoptosis in hepatocytes found in donor liver biopsies collected at the end of organ procurement predicted EAD after LT (10). However, studies unraveling the role of the particular types of cell death in the development of EAD are scarce.

Recent studies have shown that liver cells affected by IRI, including parenchymal and non-parenchymal cells, could die not only as a result of apoptosis or necrosis but also by several non-apoptotic forms of programmed cell death, also known as "regulated necrosis" (15). Of those, necroptosis is one of the most studied and incorporates the characteristics of both apoptosis and necrosis (16). Necroptosis and apoptosis share the same upstream mechanism which is induced by cell death receptors. Upon the inhibition of caspase 8 or Fas-associated *via* death domain, the complex of receptor-interacting protein kinase 1 (RIPK1) and RIPK3 is formed and switches the apoptosis machinery into necroptosis. The mixed lineage kinase domain-like protein (MLKL) is phosphorylated and oligomerized subsequently, translocating to the cell membrane and mediating the cell rupture to execute necroptosis (17). Although pMLKL has been widely regarded as the hallmark of necroptosis, the activation of pMLKL has been observed in endoplasmic reticulum stress-related apoptosis (18), hinting that pMLKL-mediated cells death might not be not exclusively necroptosis. In the case of pMLKL-mediated necroptosis, the leakage of the damage-associated molecular patterns from ruptured cells further contributes to inflammatory response, also known as sterile inflammation or necroinflammation, which is a critical pathological process during hepatic IRI.

The emerging role of necroptosis in hepatic IRI has been reported in a few experimental studies. Based on murine IRI models, necroptosis has been found to not only result in hepatic damage during IRI in healthy livers (19, 20) but also aggravate IRI in both aging (21) and steatotic (22, 23) livers. On the contrary, there are also studies demonstrating that necroptosis does not play a critical role in murine hepatic IRI (24, 25). This contradiction may arise from the difference in the animal model used. Of note, the necroptosis machinery varies between species and can therefore lead to a potential discrepancy in experimental and clinical studies (15, 26). However, clinical evidence of the involvement of necroptosis mediators, such as pMLKL, in human liver IRI is lacking.

We have previously shown that necroptosis is involved in various human liver diseases in an etiology-dependent manner (27). Interestingly, although based on only a few cases, we found extensive expression of pMLKL in human liver biopsies during LT, implying the potential existence of pMLKL-mediated cell death in human liver IRI. The pMLKL expression as previously published was mostly found in the portal triad area, which was different from that in other biopsies obtained from patients with chronic liver diseases. The portal triad consists of the bile duct, hepatic artery, and portal vein, supported by numerous non-parenchymal cells with distinct molecular features (28). Myofibroblasts represent one of the major stromal and extracellular matrix (ECM) producing cells in the portal triads, and originate from hepatic stellate cells (HSCs), portal fibroblasts

(PFs), and fibrocytes, which serve a variety of functions in the response to acute and chronic insults (29–31). We hypothesized that the non-parenchymal cells, possibly the myofibroblasts, present in the portal triads might be the major cell population co-expressing pMLKL during liver transplantation. In the present study, we aim to investigate the pMLKL expression in both rat and human liver biopsies and whether the histological score of pMLKL is associated with the development of EAD after transplantation. Furthermore, we characterized the molecular phenotype of the liver cells expressed pMLKL.

PATIENTS AND METHODS

Patient Selection and Data Collection

We performed a retrospective study using liver biopsies from patients undergoing orthotopic liver transplantation (OLT) between April 2008 and March 2012 at the Erasmus University Medical Center, Rotterdam, the Netherlands. Of 83 cases enrolled in our previous prospective study (32), 64 patients were included in this study. Due to incomplete biopsy retrieval from the pathology biobank, 19 patients were excluded. The main demographic and clinical characteristics of included recipients and donors were listed in **Table S1**. Postoperative laboratory data were collected for the first 7 days after OLT. This study was approved by the Erasmus MC medical ethics council (MEC-2014-060). All patients gave informed consent for the use of material for research purposes.

Definitions of Post-Transplant Complications

Early allograft dysfunction (EAD) was defined according to the criteria of Olthoff et al. (33) by the presence of one or more of the following: (i) bilirubin ≥ 10 mg/dL on a postoperative day (POD) 7; (ii) INR ≥ 1.6 on POD7; (iii) alanine aminotransferase (ALT) or aspartate aminotransferase (AST) > 2000 IU/mL within the first 7 postoperative days. According to the criteria of Verhoeven C et al. (34), the definition of ischemic-type biliary lesions (ITBL) in this study includes (i) intrahepatic or hilar bile duct(s) strictures and dilatation after OLT, which (ii) were confirmed by cholangiography and in the absence of hepatic artery thrombosis as demonstrated by Doppler ultrasonography, and (iii) which required endoscopic or percutaneous management in the biliary tract or liver retransplantation in recipients. Postoperative rejection was diagnosed according to the histological assessment.

Sample Collection and Processing

All graft livers were procured following a standard procurement protocol (32, 34). After procurement and initial flush, the graft liver was stored in cold University of Wisconsin (UW) solution (Viaspan, Duramed Pharm Inc, Pomona, NY) or histidine tryptophan ketoglutarate (HTK) solution (Custodial HTK, Essential Pharmaceuticals, LLC, Pennsylvania, USA), and then transported to our center. Upon the arrival of the liver, a conventional back table procedure was performed by the surgeon. Briefly, an additional *ex situ* perfusion of the portal venous system was performed *via* gravity with 1000 ml of UW or HTK. A secondary flush was done under normal hydrostatic pressure with 500 ml of 4% human albumin solution (Albuman, Sanquin, The Netherlands), immediately before implantation. Liver biopsies were obtained at the end of the back table procedure (T0) and ~1 hour after portal reperfusion (T1).

Rat Liver Transplantation Model

An established rat orthotopic liver transplantation method, which was approved by the institutional review board and the animal procedures, was conducted at the Laboratory of Experimental Surgery and Transplantation, Institute of Research Experimental and Clinic at the University Catholic of Louvain, Brussels, Belgium. For standardization and reproducibility purposes only male rats were used. Additionally, we need to infuse fluids intravenously through the penile vein during liver transplantation. Therefore male Lewis rats, purchased from Janvier Labs (Le Genest-Saint-Isle, France), weighing between 200 and 250 g at the time of the transplantation, were used as donors and recipients. Organ procurement and liver implantation were performed according to the full-vascularized technique, which included graft re-arterialization, previously described by Aiyakhagorn et al. (35). Rat livers (n=4) were procured and stored cold in Belzer UW® preservation solution (Bridge to LifeTM – IL - USA) for 22 h before implantation. Before implantation, liver grafts were rinsed with 10 ml of 0.9% saline through the portal vein. Anastomosis of the suprahepatic vena cava, the portal vein, and the intrahepatic vena cava was performed with continuous suture using 7/0 polypropylene (Prolene® - Ethicon - OH – USA) for the first and 8/0 for the last two. Graft arterialization was performed using a plastic stent telescoped into the donor celiac trunk and the recipient's common hepatic artery. Biliary reconstruction was performed using a segment of 8 mm of a venous catheter 22g (Becton, Dickinson, and Company – NJ – USA) telescoped into the donor and recipient common bile duct and secured with 7/0 silk ligatures. Euthanasia was performed 24 hours after graft implantation for samples collection. Sham operations were conducted on rats (n=4) by performing a midline laparotomy under the same conditions as the liver recipients. Samples were collected 24 hours after the procedure.

Histological Analyses

The liver specimens were routinely fixed with 4% paraformaldehyde for 24 hours, embedded in paraffin, and cut into 4μm sections. Sections were stained with hematoxylin and eosin (H&E) according to standard procedures. Immunostaining was performed as previously described (27). In short, sections were dewaxed and rehydrated *via* gradient ethanol washes. Antigen retrieval was then performed by heating the sections at 100°C in 10mM citrate acid buffer (pH 6.0). Incubation with 1% bovine serum albumin (BSA) and 10% normal goat serum (both from Sigma-Aldrich) in phosphate-buffered saline (PBS) were performed to prevent a-specific staining. The sections were then incubated with pMLKL (Thermofisher) antibody diluted in 1% BSA/0.025% Triton X100/ 1% normal goat serum (antibody diluent), at 4°C overnight.

Information on all the primary antibodies used is listed in **Table S2**. Irrelevant rabbit IgG (Thermofisher) was applied as a negative isotype control. For immunohistochemistry, sections were incubated with 0.3% hydrogen peroxide for 15 min and by a 1-hour incubation with secondary goat anti-rabbit Immunoglobulins/HRP (Dako, Glostrup, Denmark) at room temperature. The reaction products were visualized using a 3,3'-Diaminobenzidine (DAB) substrate kit (Dako). Subsequently, the slides were counterstained with Mayer's s hematoxylin and mounted in Pertex mounting medium. Whole-slide immunohistochemistry images were acquired on NanoZoomer (Hamamatsu, Iwata City, Japan).

Automated multiplex immunofluorescent staining was further performed using the Ventana Benchmark Discovery (Ventana Medical Systems Inc.) to determine the markers co-expressed with pMLKL. In brief, following deparaffinization and heat-induced antigen retrieval with CC1 (#950-500, Ventana) for 64 minutes at 97°C, the tissue samples were incubated with primary antibodies at 37°C in a step-by-step manner. The antibody denature step was performed between every antibody incubation and visualization using CC2 (#950-123, Ventana) for 20 minutes at 100˚C. pMLKL was incubated for 32 min, detected with Universal HQ kit (#760-275, Ventana), and visualization with R6G (#760-244, Ventana) for 4 minutes. CD90 was incubated for 60 minutes, detected with a Universal HQ kit, and visualized with DCC (#760-240, Ventana). Fibulin-2 was incubated for 32 minutes, detected with Universal HQ kit (#760-275, Ventana), and visualized with Red610 (#760-245, Ventana). CD45 was incubated for 32 minutes, detected with omnimap anti-mouse HRP (#760-4310, Ventana), and visualized with Cy5 (#760-238, Ventana) for 4 minutes. CD34 was incubated for 32 minutes, detected with omnimap anti-mouse HRP, and visualized with FAM (#760-243, Ventana) for 4 minutes. Slides were incubated in PBS with DAPI for 15 minutes and covered with an anti-fading medium (DAKO, S3023). Slides were scanned using the ZEISS Axio Imager 2.0 and analyzed using Qupath.

Information on the antibodies used can be found in **Table S2**.

Immunohistochemistry Scoring

Immunohistochemistry scoring of pMLKL staining was performed electronically using the software ImageJ (imagej.nih.gov/ij) and the whole procedure was shown in **Figure S1A**. Considering pMLKL positivity was predominantly detected in the portal triad, at least 8 high-power fields (200X magnification) of portal triad areas were blindly selected for each section from the whole-slide images (representative images are shown in **Figure S1B**). The related clinical data belonging to the images was unknown at that time. After color deconvolution, the pixel intensity of cytoplasmic pMLKL staining, visualized by DAB, was automatically determined using the plugin IHC Profiler (36–38) and ImageJ software, in which high-positive, moderate-positive, low-positive, and negative zones were calculated. The threshold assignment was encoded in the plugin and performed automatically (38). We calculated the H-Score [scale 0 to 300, exemplified images were shown in **Figure S1C**)] for each image based on the generated products of the percentage contribution of positive zones and the intensity of labeling (0=negative; 1 = weak positive; 2 = moderate positive; 3 = high positive) using the following equation (36, 37, 39):

H-score= (percentage contribution of high-positive zone×3) + (percentage contribution moderate-positive zone×2) + (percentage contribution of low-positive zone)

Median H-scores in the selected fields were designated as the pMLKL positivity for each section. The pMLKL index for each graft liver was calculated by dividing the H-score in the T1 sample by the H-score in the T0 sample.

Statistical Analysis

Statistical analysis was performed using SPSS statistics 25 (SPSS Inc, Chicago, IL, USA) and Prism software (GraphPad Software Inc., San Diego, USA). Data were presented as the median and interquartile range (IQR). Group comparisons were performed using the Mann-Whitney U test or Wilcoxon matched-pairs signed-rank test for continuous values and the chi-square test for categorical data. Spearman's rank correlation test was conducted to estimate the linear relationship between variables. To identify risk factors for EAD, a logistic regression model was applied for multivariate analysis. A p-value of <0.05 was considered significant.

RESULTS

MLKL Phosphorylation in Rat Hepatic IRI

To determine whether the activation of pMLKL is involved in rat hepatic IRI, rat liver biopsies were collected after 22 hours of cold storage and 24 hours of reperfusion or sham operation (**Figure 1A**), followed by immunohistochemistry staining of pMLKL using a validated antibody (27, 40, 41). Compared to sham-operated rats, a significant increase of serum ALT (1153.0 (441.5-1652.0) vs 10.0 (10.0-17.5), p=0.029) and AST (1294.0 (654.5-1497.0) vs 66.5 (47.0-94.0), p=0.029) levels was observed in rats after LT (**Figure 1B**). The pMLKL expression in the liver after IRI is shown in **Figure 1C**. No positive staining was observed in rat liver biopsies incubated with negative isotype control antibody, confirming the specificity of the pMLKL and secondary antibodies. As shown in **Figure 1D**, The pMLKL positivity was barely observed in rat livers collected after the sham operation, suggesting that the increased expression of pMLKL was possibly associated with IRI. Clear pMLKL expression is detected in the portal triads but not in the liver parenchyma. As shown in **Figure 1E**, automated quantification of the histological score (H-Score) of pMLKL staining showed a significant increase in the IRI group versus sham group (1.524 (1.80) *vs* 0.014 (0.01), p=0.029).

Post-Reperfusion pMLKL Score Correlates With The Development of EAD After LT

To investigate the expression of pMLKL in human liver grafts, a retrospective study was performed (**Figure 2A**). Out of 64 included LT patients, 24 recipients developed EAD (38%). (**Table S1**). Representative H&E and pMLKL stained images of T0 and T1 biopsies are shown in **Figures 2B, C**. The pMLKL$^+$

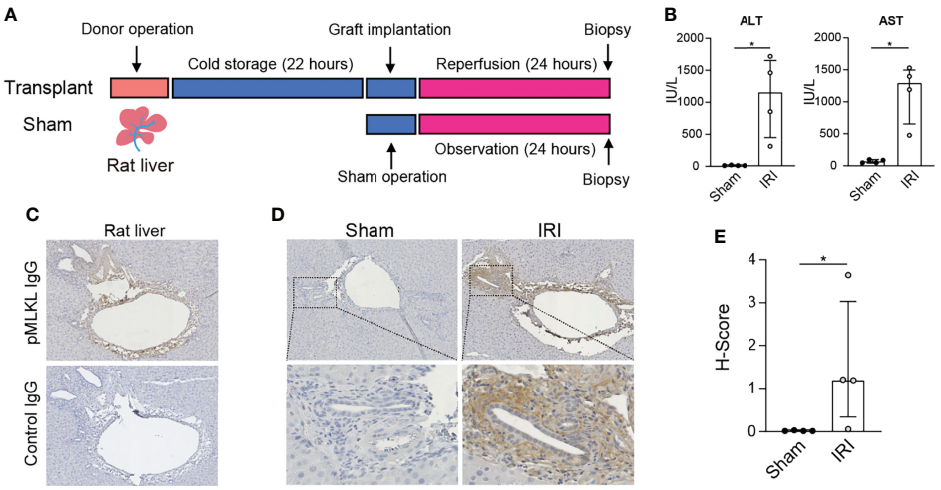

FIGURE 1 | Expression of pMLKL in graft livers from the rat LT model. **(A)** Schematic representation of the timeline. Rat livers were procured and stored in cold preservation solution for 22 hours and then transplanted. Liver biopsies (n=4) were taken after 24 hours of reperfusion. **(B)** Serum ALT and AST in recipient rats after 24 hours of reperfusion were determined. The levels of both ALT and AST increased significantly in the IRI group compared with sham-operated rats. **(C)** Immunohistochemistry was performed on collected rat liver after IRI. Serial sections were stained with either pMLKL or a negative isotype control antibody. Shown is a representative microscopic image (magnification, 100X) confirming the specificity of the pMLKL antibody and the secondary antibody. **(D)** Representative microscopic images of pMLKL staining on rat livers undergoing either IRI or sham operation were shown (magnification, 100X). Enlarged images from the boxed area are shown in the bottom panel (magnification, 400X). Clear pMLKL was detected in the portal triads of rat liver undergoing IRI, but not in the sham-operated rats. **(E)** The H-Score of pMLKL staining was compared in rat donor liver undergoing hepatic IRI or sham operation (Mann-Whitney test), in which a significant increase in the IRI group was observed. *p < 0.05.

cells mainly had a periportal localization, distributed within the stroma of the portal triad adjacent to the wall of the portal vein, hepatic artery, and biliary epithelium. The paired analysis further showed that pMLKL-T1 was significantly higher than pMLKL-T0 in recipients that developed EAD (1.88 (0.85- 7.55) vs. 0.70 (0.21-2.97), p=0.008) rather than the non-EAD group (0.75 (0.35- 2.74) vs. 1.14 (0.37-2.78), p=0.289) (**Figures 2D, E**). The pMLKL index was significantly higher in the EAD group versus the non-EAD group (2.77 (1.75-6.65) vs. 0.95 (0.39-1.62), p<0.0001) (**Figure 2F**). Interestingly, also a significantly higher pMLKL index was observed in DCD liver grafts compared to DBD livers (3.44 (1.06-6.71) vs. 1.10 (0.42-2.21), p=0.019) (**Figure 2G**). Moreover, based on the receiver operating characteristic (ROC) curve, the pMLKL index outperformed the pMLKL-T1 in predicting the development of EAD (**Figure 2H**). We further found an optimal cut-off value of 1.64 of the pMLKL index displaying the most optimized sum of sensitivity (83.3%) and specificity (77.7%).

Based on the cut-off value of the pMLKL index, 64 grafts were allocated to a low pMLKL index (<1.64; n=35) and a high pMLKL index (≥1.64; n=29) group. Demographics of donors and recipients with low pMLKL index grafts versus high pMLKL index grafts are shown in **Table 1**. The high-pMLKL index group showed a higher trend in the last serum AST of the donor before procurement. Interestingly, a higher portion of ITBL occurrence was observed in the high-pMLKL index group though the difference was not significant. The distribution of the pMLKL index in high and low groups is shown in **Figure 3A**. As shown in **Figure 3B**, the high pMLKL index group had a significantly higher serum ALT level at POD1-4 (p<0.05). Also, the AST level at POD1 (**Figure 3C**, p<0.05), and LDH level at POD1 (**Figure 3D**, p<0.05) were elevated in this group. Correlation analysis based on the entire cohort revealed a relatively weak correlation between serum ALT at POD1 and pMLKL index (rs=0.400, p<0.01) and between serum AST at POD1 and pMLKL index (rs=0.312, p<0.05) (data not shown).

pMLKL Index Is a Predictor Factor for EAD

To determine whether the pMLKL-T1 score or pMLKL index are independent predictors for EAD, we conducted a multivariate analysis (**Table 2**). Univariate analysis indicates the EAD risk factors in this cohort, including higher pMLKL-T1 score (1.88 (0.85- 7.55) vs. 0.75 (0.35- 2.74), p = 0.059), higher pMLKL index, DCD grafts (38% vs. 18%, p=0.079) and male donors (67% vs. 45%, p=0.096) (**Table S1**). On multivariate analysis, only the high pMLKL index was identified as an independent predictive factor for EAD (odds ratio = 1.348; 95% CI, 1.066-1.703; p = 0.013). In this model, the discriminative power of the pMLKL index is indicated as a C-statistics calculation that reached up to 0.932 and was not below 0.705.

Activation of pMLKL in Multiple Non-Parenchymal Cells in the Portal Triad

Considering periportal non-parenchymal cells seem to be the major source of pMLKL$^+$ cells, we aim to characterize the cellular populations in portal triads with pMLKL positivity. ECM deposition, demonstrated by Picro Sirius Red staining, was observed mostly in the periportal area, overlapping with pMLKL

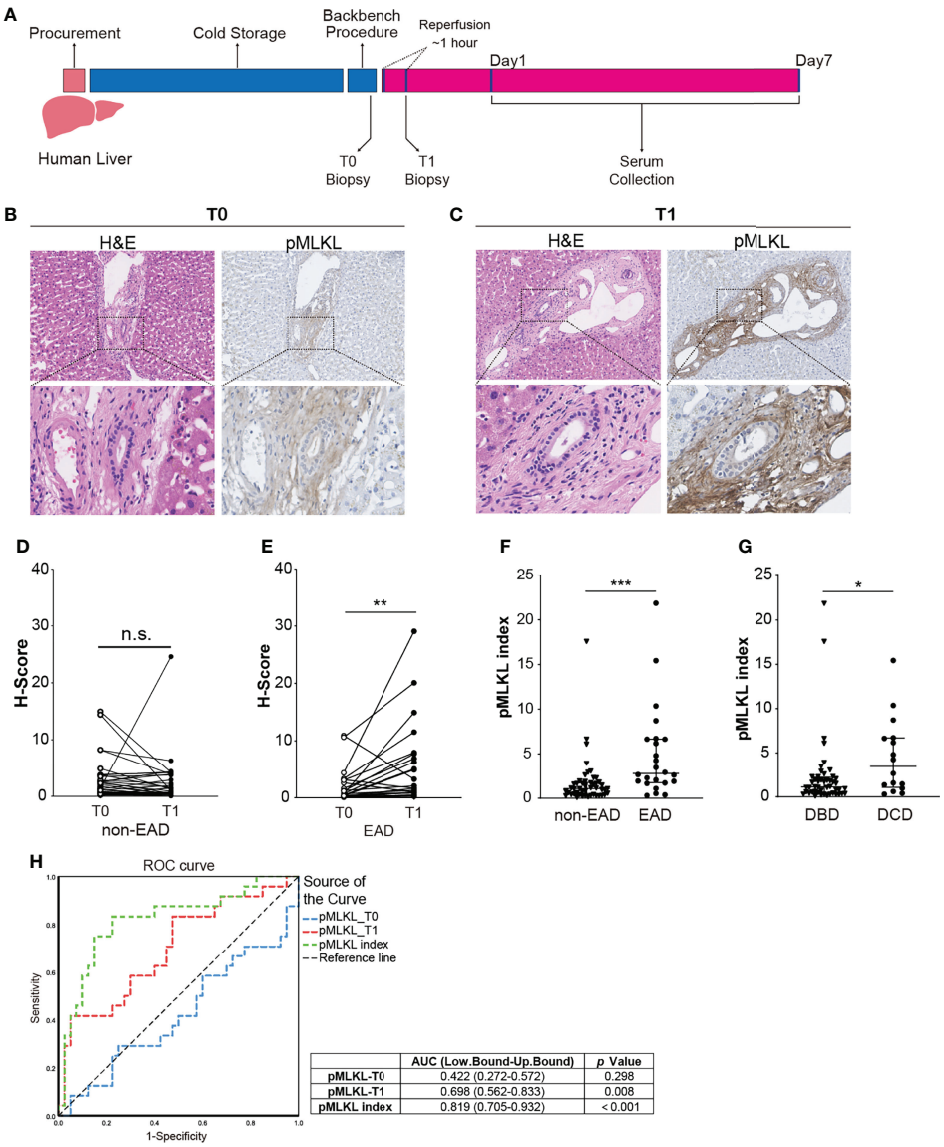

	AUC (Low.Bound-Up.Bound)	*p* Value
pMLKL-T0	0.422 (0.272-0.572)	0.298
pMLKL-T1	0.698 (0.562-0.833)	0.008
pMLKL index	0.819 (0.705-0.932)	< 0.001

FIGURE 2 | Periportal pMLKL expression in human LT biopsies. **(A)** Human graft livers were procured and stored in cold preservation solution following a conventional protocol. Liver biopsies were collected at the end of the backbench procedure (T0) and 1 hour after reperfusion (T1). Postoperative serums were collected in the first 7 post-LT days. **(B, C)** Representative microscopic images of HE and pMLKL staining on T0 and T1 graft livers that developed post-transplant EAD were shown (magnification, 100X). Enlarged images from the boxed area are shown in the bottom panel (magnification, 400X). The pMLKL positive cells were mainly localized at the periportal region, distributed within the stroma of the portal triad adjacent to the wall of the portal vein, hepatic artery, and biliary epithelium. **(D, E)** Paired comparison of pMLKL scores at T0 and T1 were performed separately in non-EAD and EAD groups (Wilcoxon matched-pairs signed-rank test). pMLKL-T1 was significantly higher than pMLKL-T0 in recipients that developed EAD compared to the non-EAD group. **(F)** pMLKL index were compared in non-EAD and EAD groups (Mann-Whitney test). The pMLKL index was significantly higher in the EAD group versus the non-EAD group. **(G)** pMLKL index were compared in DBD and DCD livers. (Mann-Whitney test). A significantly higher pMLKL index was observed in DCD liver grafts compared to the DBD livers **(H)** ROC curve showing the discriminative ability of pMLKL_T0, pMLKL_T1, and pMLKL index in the development of EAD. Data are presented as the median and interquartile range (IQR). n.s., not significant; *p < 0.05; **p < 0.01; ***p < 0.001.

positivity (**Figure 4A**). We reasoned that hepatic IRI might activate pMLKL predominantly in the myofibroblast after a short period of reperfusion. To this end, immunohistochemistry on serial sections for multiple markers was performed to identify the populations of periportal cells including cholangiocyte (KRT19), activated myofibroblast [α-smooth muscle actin (α-SMA)], hepatic stellate cells (HSCs) (Desmin), and macrophage (CD68) (**Figure 4B**). We found that area positive for pMLKL partially overlapped with α-SMA$^+$ cells, suggesting that myofibroblasts might be one of the cell types co-expressing pMLKL. The absence of Desmin$^+$ cells overlapping with pMLKL expression reveals that the myofibroblasts co-expressing pMLKL

TABLE 1 | Donors and recipients characteristics of liver grafts with low pMLKL index versus high pMLKL index.

	Low pMLKL index (n=35)	High pMLKL index (n=29)	p value
Donor characteristics			
Donor type (DCD)	7 (20%)	9 (31%)	0.234
Age (yr)	60 (26.0)	53 (13.0)	0.235
Sex (male)	18 (51%)	16 (55%)	0.274
BMI (kg/m2)	23.9 (4.3)	23.2 (4.0)	0.952
Last AST (U/l)	41.0 (30.0)	51.0 (35.5)	0.074
Last ALT (U/l)	25.0 (38.0)	34.0 (34.5)	0.395
Donor risk index	2.0 (0.8)	2.0 (3.88)	0.700
warm ischemia time (min)	27.0 (10.0)	26.0 (11.0)	0.787
cold ischemia time (min)	403.0 (118.0)	369 (109.0)	0.187
Recipient characteristics			
Age (yr)	46 (21.0)	53 (14.0)	0.040*
Sex (male)	16 (46%)	12 (41%)	0.146
Lab-Meld score	24.0 (7.0)	26.0 (15.0)	0.855
Transplantation indication			
-Autoimmune hepatitis	16 (46%)	12 (41%)	0.463
-Alcohol	2 (6%)	4 (14%)	0.250
-Hepatitis B/C	6 (17%)	7 (24%)	0.351
-Hepatocellular carcinoma	3 (9%)	9 (31%)	0.024*
-Other	9 (26%)	5 (17%)	0.306
Anastomosis ductus (Roux-Y)	5 (14%)	8 (28%)	0.140
Post-transplantation complication			
EAD	4 (11%)	20 (69%)	<0.001*
Hepatic artery thrombosis	4 (11%)	1 (3%)	0.242
Rejection	5 (14%)	6 (21%)	0.364
ITBL	7 (20%)	12 (41%)	0.056
AKI	6 (17%)	4 (14%)	0.454

Significance.

might be not derived from HSCs. Interestingly, part of biliary epithelial cells labeled with KRT19 also displays positive staining for pMLKL. CD68 staining further indicated that macrophages were not the predominant cells comprising the $pMLKL^+$ population.

To support our findings, we performed multiplex immunofluorescent staining on the biopsies collected from 3 human donor livers after perfusion to further determine the co-localization of $pMLKL^+$ cells with periportal cells. Likewise, we found $KRT19^+$ cholangiocytes constitute a small population of $pMLKL^+$ cells (5.92 ± 0.88%) (**Figures 5A, B**). It has been reported that CD90, CD34, and fibulin-2 represent the critical, but not exclusive, markers for liver myofibroblast residing near portal vein during chronic injury (30, 31). The periportal cells expressing CD90 (36.15 ± 28.4%), CD34 (36.9 ± 29.4%), and fibulin-2 (29 ± 23.79%) predominantly overlayed with $pMLKL^+$ cells in the portal triad (**Figure 5C**). Given that CD90 and CD34 could also be expressed on the surface of multiple cell types separately, such as lymphocytes and bone marrow-derived fibrocytes, we applied CD45, a leukocyte/hematopoietic marker, staining to further characterize the subpopulation of periportal $pMLKL^+$ cells. A large number of $pMLKL^+$ cells co-expressing CD90, CD34, and Fibulin-2 were accumulated in the portal triad and designated as PFs (**Figure 6A**) and exhibited a fibroblast-like spindle shape. On the other hand, a small number of $pMLKL^+$ $CD90^-$ cells co-expressed CD45 and CD34 were observed, indicating that these cells might be bone marrow-derived fibrocytes (30). Notably, we also found a few $pMLKL^+$ $CD90^+$ $CD45^+$ cells which could be separated into two distinct subpopulations including $CD34^+$ $fibulin\text{-}2^+$ cells (bone barrow-derived mesenchymal cells) and $CD34^-$ $fibulin\text{-}2^-$ cells (leukocytes) (42) (**Figure 6B**). Collectively, we concluded that necroptosis executor pMLKL could be activated by hepatic IRI predominantly in periportal non-parenchymal cells including PFs, fibrocytes, and a minority of cholangiocytes.

DISCUSSION

In this study, we demonstrated that the pMLKL expression increased significantly in the portal triads after reperfusion in both human and rat LT. The pMLKL index based on histological assessment correlates with early liver injury after LT and is predictive of post-transplant EAD. We further confirmed that activation of pMLKL occurs in multiple periportal non-parenchymal cells and cholangiocytes. To the best of our knowledge, our study is the first to investigate the clinical relevance of the necroptosis mediator in human liver transplantation.

Cell death is an eventual event in IRI during liver transplantation and is strongly linked to the short- and long-term outcomes of recipients. In the last decades, mitigating cell death represents one of the most investigated strategies to improve organ functionality and minimize post-transplant complications (43). In previous studies, apoptosis has been one of the key targets, but the translation into clinical practice has been merely lacking. Except for apoptosis, the emerging role of programmed cell death has been validated in hepatic IRI, expanding our knowledge of the different cell death programs during LT. We previously reported that most pMLKL

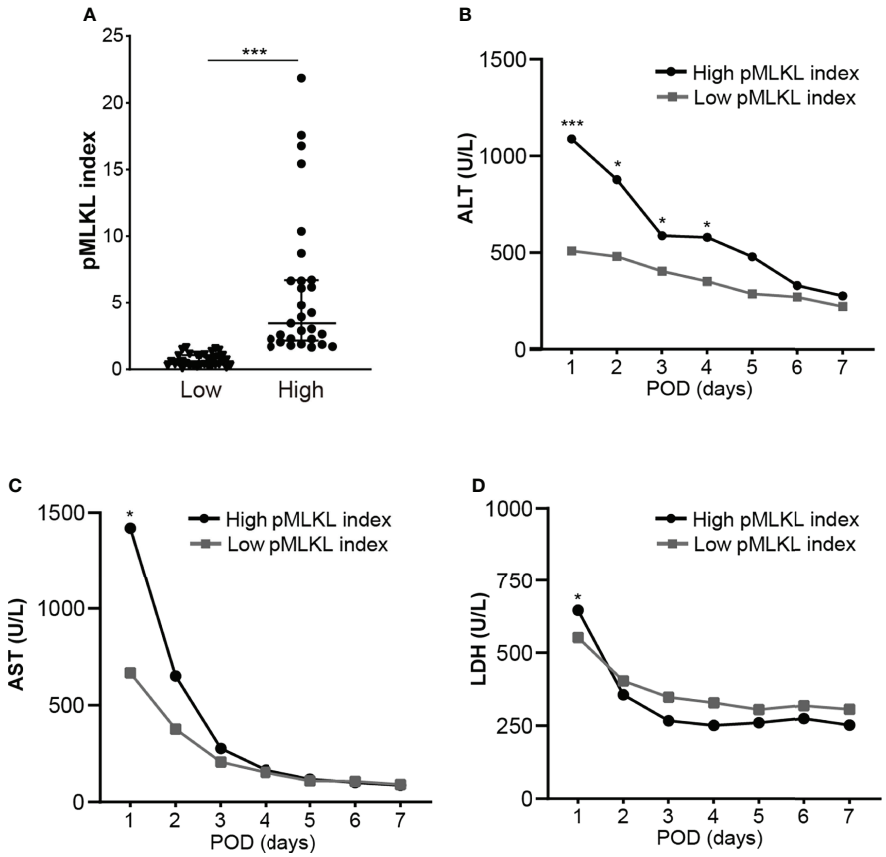

FIGURE 3 | The histological score of pMLKL correlates with early liver injury after reperfusion. **(A)** The dichotomy of graft pMLKL index is grouped as low and high. Recipients were classified into low (≤1.64) versus high (>1.64) pMLKL index. **(B, C, D)** Levels of serum ALT, AST, and LDH at POD1-7 were compared (median, two-way ANOVA test followed by Sidak's multiple comparisons test). The high pMLKL index group had significantly higher serum ALT/AST/LDH levels on POD1. Data are presented as the median and interquartile range (IQR). *p < 0.05; ***p < 0.001.

TABLE 2 | Univariate and multivariate analysis for risk factors for post-transplant EAD.

Factors	OR (95% CI)	Univariate		Multivariate	
		p value	OR (95% CI)	*p* value	C-statistics (low. limit-up. limit)
DCD graft	0.354 (0.111-1.129)	0.079	-	0.473	-
Male donor	0.409 (0.143-1.172)	0.096	-	0.064	-
pMLKL-T1	1.133 (0.995-1.290)	0.059	-	0.472	-
pMLKL index	1.347 (1.067-1.700)	0.012	1.348 (1.066-1.703)	0.013	0.819 (0.705-0.932)

OR, Odds ratio.

positive cells were found in the portal triads in LT biopsies, but were absent in ischemia-free liver biopsies collected from living donors grafts, suggesting the involvement of pMLKL-mediated cell death in hepatic IRI (27). Myofibroblasts are the main effectors of liver fibrosis (31) and we concluded in this study that myofibroblasts represent a major cell type with pMLKL activation. In fact, the periportal expression pattern of pMLKL and its activation in myofibroblast was barely found in liver biopsies obtained from patients with end-stage liver diseases, which were generally featured by severe liver fibrosis and extensively activated fibroblast (27). This discrepancy may imply that the activation of pMLKL during liver transplantation represents an event with a unique mechanism that is different from other chronic etiologies. Besides, in this study, immunostaining on both pre-and post-reperfusion biopsies further revealed an increase in pMLKL expression at T1 compared to T0. This suggests that during graft reperfusion extensive pMLKL-mediated cell death is possibly induced and therefore this might be the right time to mitigate cell death.

Considering that cells expressing pMLKL were mostly detected in the portal triad, we only selected the periportal

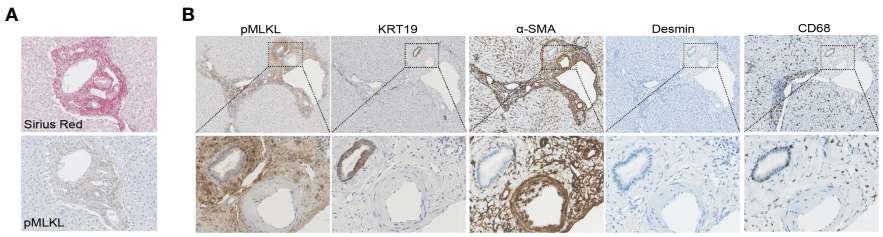

FIGURE 4 | Characterization of periportal cells expressed pMLKL. **(A, B)** Serial liver sections from T1 biopsies obtained from one donor liver were stained with Sirius Red, pMLKL, KRT19, α-SMA, Desmin, and CD68 (magnification 100X). Enlarged images from the boxed area are shown in the bottom panel (magnification 400X). ECM deposition was observed mostly in the periportal area and appeared to overlap with pMLKL positivity. Areas positive for pMLKL overlapped a lot with α-SMA$^+$, but not Desmin$^+$. Part of KRT19$^+$ cells also displayed positive staining for pMLKL, while few CD68$^+$ were observed to co-express pMLKL.

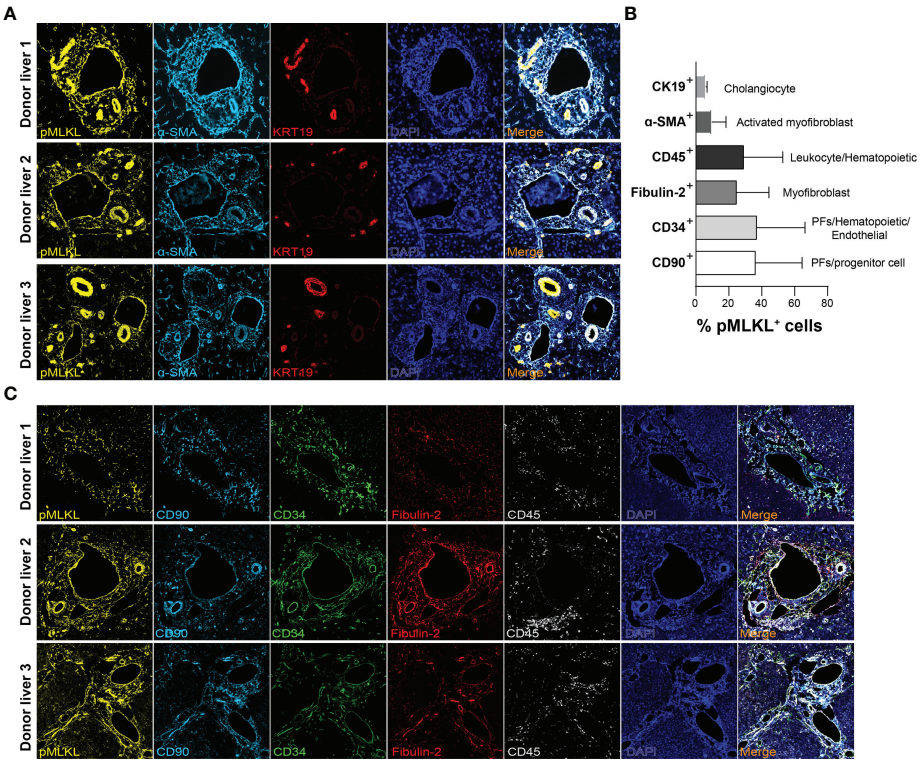

FIGURE 5 | Characterization of periportal cells expressed pMLKL. **(A, B)** Multiplex immunofluorescent staining was performed on T1 graft livers (n=3) for pMLKL, α-SMA, KRT19, CD90, CD34, Fibulin-2, and CD45 (magnification, 400X). **(C)** The composition of pMLKL+ cells (100%) was calculated as the percentage of cells co-expressed with multiple markers (mean ± SD). The periportal non-parenchymal cells and cholangiocytes predominantly constitute the population co-expressing pMLKL.

areas for the analysis. These areas account for a much smaller portion of the liver tissue compared to the parenchymal regions. We assume that this method provides a more precise score of periportal pMLKL expression. Interestingly, the pMLKL score appears to be associated not only with EAD but also with ITBL though the difference was not significant. It is well known that the liver cells, including hepatocytes and cholangiocytes, that are damaged during hepatic IRI, often direct the onset of EAD or ITBL. Our previous studies demonstrated that the release of cholangiocyte-derived microRNAs predicted the development of ITBL (34), while the hepatocyte-derived microRNAs predicted the occurrence of EAD (32). In this study, we found that during LT, pMLKL could be activated in cholangiocytes. This might be a potential cause of biliary injury during LT and possibly contributes to the high incidence of ITBL in our EAD cohort. In addition, the pMLKL index correlated with the serum levels of ALT and AST, often released from necrotic hepatocytes, on POD1, but not POD7 (data not shown). Given that low levels of

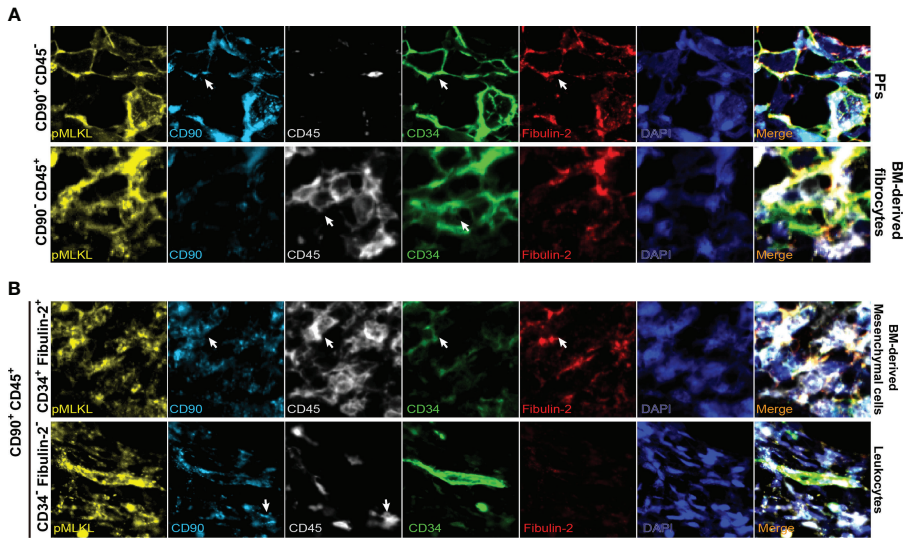

FIGURE 6 | Representative multiplex immunofluorescent images of distinct subpopulations of pMLKL expressed cells in portal triads (magnification, 2000X). Arrows indicate the cells with positive staining. The pMLKL$^+$ cells featured by CD90$^+$ CD45$^-$ (PFs), CD90$^-$ CD45$^+$ (BM-derived fibrocytes) **(A)**, CD90$^+$ CD45$^+$ CD34$^+$ fibulin-2$^+$ (BM-derived mesenchymal cells) and CD90$^+$ CD45$^+$ CD34$^-$ fibulin-2$^-$ (leukocytes) **(B)** were shown.

pMLKL expression were observed in the liver parenchyma, we speculate that the periportal necroptosis in nonparenchymal cells could have a detrimental effect on hepatocytes indirectly, though the exact mechanism is still unclear.

We further characterized the pMLKL-expressing cells and found that next to cholangiocytes, also non-parenchymal cells such as periportal mesenchymal cells, including PFs and fibrocytes, were mainly stained with pMLKL. In the adult liver, myofibroblasts represent the main effectors of fibrous stress during liver injury by regulating the wound healing response, including liver repair and regeneration (31). Upon this stress factor, liver mesenchymal cells, including HSCs, PFs, and fibrocytes can differentiate into myofibroblasts, depending on the mechanism of the insults. We speculate that myofibroblasts that expressed pMLKL, share similar signatures with PFs and fibrocytes, but not with HSCs. The pMLKL activation in myofibroblast and its relationship with hepatic IRI has been poorly investigated. In previous studies, activated PFs have been reported to contribute to fibrous scar production in chronic cholestatic fibrosis (30). Besides, a recent retrospective study revealed that histological scores of collagen deposition in donor livers at the time of procurement, correlated with an increased incidence of post-transplant EAD, suggesting an unexpected role of collagen-producing cells in hepatic IRI (44). Konishi et al. (45) also reported that fibrotic livers show accelerated recovery and repair after hepatic IRI compared to the normal liver in experimental models. Although the precise mechanisms of how pMLKL was activated in myofibroblasts during LT remain to be determined, we envision that the massive necroptosis of myofibroblasts residing in the fibrotic liver before LT, could be induced by short-time reperfusion, which might lead to an imbalance of hepatic damage and repair, finally resulting in "irreversible" IRI in graft liver. This could be led by impairment of liver regenerative capacity due to myofibroblast depletion or secondary necroinflammation mediated by necroptotic myofibroblasts. The interaction among hepatic IRI, myofibroblasts, and necroptosis is worth further investigation.

It is important to note that the necroptosis mediators, such as MLKL and RIPK3, could exert multifactorial functions which could be linked to other types of programmed cell death or even be independent of cell death (46, 47). For instance, we have previously reported that nuclear pMLKL was expressed in TNF-a-induced apoptosis in cholangiocyte organoids (27). Given that cytoplasmic and membrane translocation of pMLKL is widely regarded as the major functional form of MLKL for necroptosis execution, the nucleus-located pMLKL in apoptotic cholangiocyte organoids might suggest an event possibly serving a unique role independent of necroptosis. Cao et al. (18) demonstrated that nuclear MLKL represents a contributor to endoplasmic reticulum stress-related apoptosis, which might be a potential elucidation. In the present study, we observed distinct expression patterns of pMLKL in different liver cell types, in which both cytoplasmic/membrane and a minority of nuclear pMLKL were confirmed. This suggests that the increased expression of pMLKL during hepatic IRI might be invoked by multiple mechanisms and leads to distinct outcomes. We think it is important to reach a consensus on the definition of necroptosis, which is still lacking. Given that the interactions of MLKL with other cell death-dependent or -independent pathways are emerging, the cytoplasmic/membrane staining of pMLKL is not enough to define necroptotic cell death. In addition to pMLKL detection, ultrastructural examination using transmission electron microscopy analysis might be helpful to further determine the morphological change of dying cells and characterize the exact cell death type.

Our knowledge of the regulated necrosis network, such as necroptosis, ferroptosis, and pyroptosis is expanded in the last years. Notably, the expression of the mediators of multiple cell death programs differs among parenchymal and non-parenchymal liver cells at the transcriptional and protein levels, which potentially determines the cell death modalities in different types of cells upon certain stress factors (15, 48, 49). In our study, pMLKL was predominantly activated in cholangiocytes and nonparenchymal (stromal) cells. It has also been reported that pyroptosis induced in macrophages aggravates hepatic IRI by promoting an inflammatory response in experimental models (50, 51). Yamada N et al. demonstrated that an increase of ferroptosis markers in serum is a risk factor for human LT, and inhibition of ferroptosis prevents the infiltration of neutrophils and macrophages in the murine liver (52). Taken together, the multiple regulated necrosis modalities may contribute to hepatic IRI in a cell type-specific manner. Whether these regulated necrosis programs promote hepatic IRI independently or synergistically remains unclear. Future investigations should be performed based on human materials and animal models and using single-cell profiling methods including both transcriptomes and proteomes.

It is important to note that there are obvious limitations in our study, mostly because of the relatively small cohort and limited availability of multiple types of specimens. For instance, it remains a challenge to characterize the cells co-expressing pMLKL in clinical biopsies only in a histological manner. In this retrospective study, we were not able to obtain fresh biopsies to perform flow cytometry, which is supposed to be a better method for cellular populations identification. Based on an appropriate biopsy collection, future prospective studies should be performed including flow cytometry assessment. Besides, it would be interesting to further identify the distinct cellular populations using lineage tracing in experimental IRI models. Moreover, although we confirmed a significant increase in pMLKL scores after short-time reperfusion, we also observed strong pMLKL positivity in a few T0 biopsies, indicating that there might also be baseline injury or preservation damage in these donor's livers. Based on our study, we cannot conclude whether pMLKL has already been activated before procurement or could be induced or potentiated by cold preservation. This is obviously due to the lack of pre-preservation baseline biopsies. To address this, biopsies obtained at different time points during liver transplantation should be investigated in the future.

In conclusion, our study reveals that pMLKL expression increased significantly after reperfusion in both rodent and human LT. The histological score of pMLKL is predictive of post-transplant EAD and is associated with early liver injury after LT. Periportal non-parenchymal cells appear most susceptible to pMLKL-mediated cell death during hepatic IRI.

DATA AVAILABILITY STATEMENT

The raw data supporting the conclusions of this article will be made available by the authors, without undue reservation.

ETHICS STATEMENT

The studies involving human participants were reviewed and approved by Erasmus MC medical ethics council. The patients/participants provided their written informed consent to participate in this study. The animal study was reviewed and approved by Université catholique de Louvain.

AUTHOR CONTRIBUTIONS

SS, EB-R, IS, MV, and LL contributed to the conception and design of the study. SS, IS, and HR organized the database. SS, IS and KL performed the statistical analysis. SS wrote the first draft of the manuscript. EB-R, IS, and TB wrote sections of the manuscript. All authors contributed to manuscript revision, read, and approved the submitted version.

FUNDING

This study was partly funded by the Medical Delta program grant (Regenerative Medicine 4D) and TKI-LSH (Topconsortium Kennis en Innovatie-Life Sciences & Health) grant (RELOAD, EMC-LSH19002). SS is financially supported by the China Scholarship Council (No. 201706230252).

SUPPLEMENTARY MATERIAL

The Supplementary Material for this article can be found online at: https://www.frontiersin.org/articles/10.3389/fimmu.2022.890353/full#supplementary-material

Supplementary Table 1 | Donor and recipient characteristics.

Supplementary Table 2 | List of antibodies used in this study.

REFERENCES

1. Zarrinpar A, Busuttil RW. Liver Transplantation: Past, Present and Future. *Nat Rev Gastroenterol Hepatol* (2013) 10:434–40. doi: 10.1038/nrgastro.2013.88
2. Dar WA, Sullivan E, Bynon JS, Eltzschig H, Ju C. Ischaemia Reperfusion Injury in Liver Transplantation: Cellular and Molecular Mechanisms. *Liver Int* (2019) 39:788–801. doi: 10.1111/liv.14091
3. Hudcova J, Scopa C, Rashid J, Waqas A, Ruthazer R, Schumann R. Effect of Early Allograft Dysfunction on Outcomes Following Liver Transplantation. *Clin Transplant* (2017) 31:e12887. doi: 10.1111/ctr.12887
4. Kwon H, Moon Y, Jung K, Park Y, Jun I, Kim S, et al. Neutrophil-To-Lymphocyte Ratio Is a Predictor of Early Graft Dysfunction Following Living Donor Liver Transplantation. *Liver Int* (2019) 39:1545–56. doi: 10.1111/liv.14103
5. Agopian VG, Harlander-Locke MP, Markovic D, Dumronggittigule W, Xia V, Kaldas FM, et al. Evaluation of Early Allograft Function Using the Liver Graft

Assessment Following Transplantation Risk Score Model. *JAMA Surg* (2018) 153:436. doi: 10.1001/jamasurg.2017.5040
6. Lee DD, Croome KP, Shalev JA, Musto KR, Sharma M, Keaveny AP, et al. Early Allograft Dysfunction After Liver Transplantation: An Intermediate Outcome Measure for Targeted Improvements. *Ann Hepatol* (2016) 15:53–60. doi: 10.5604/16652681.1184212
7. Deschenes M. Early Allograft Dysfunction: Causes, Recognition, and Management. *Liver Transplant* (2013) 19:S6–8. doi: 10.1002/lt.23746
8. Golse N, Guglielmo N, El Metni A, Frosio F, Cosse C, Naili S, et al. Arterial Lactate Concentration at the End of Liver Transplantation Is an Early Predictor of Primary Graft Dysfunction. *Ann Surg* (2019) 270:131–8. doi: 10.1097/SLA.0000000000002726
9. Clavien P-A. Sinusoidal Endothelial Cell Injury During Hepatic Preservation and Reperfusion. *Hepatology* (1998) 28:281–5. doi: 10.1002/hep.510280201
10. Zhu Z, Tang Y, Huang S, Zhao Q, Schroder PM, Zhang Z, et al. Donor Liver Apoptosis Is Associated With Early Allograft Dysfunction and Decreased Short-Term Graft Survival After Liver Transplantation. *Clin Transplant* (2018) 32(12):e13438. doi: 10.1111/ctr.13438
11. Thomsen KL, Robertson FP, Holland-Fischer P, Davidson BR, Mookerjee RP, Møller HJ, et al. The Macrophage Activation Marker Soluble CD163 Is Associated With Early Allograft Dysfunction After Liver Transplantation. *J Clin Exp Hepatol* (2019) 9:302–11. doi: 10.1016/j.jceh.2018.09.006
12. Kurian SM, Fouraschen SMG, Langfelder P, Horvath S, Shaked A, Salomon DR, et al. Genomic Profiles and Predictors of Early Allograft Dysfunction After Human Liver Transplantation. *Am J Transplant* (2015) 15:1605–14. doi: 10.1111/ajt.13145
13. Klune JR, Tsung A. Molecular Biology of Liver Ischemia/Reperfusion Injury: Established Mechanisms and Recent Advancements. *Surg Clin North Am* (2010) 90:665–77. doi: 10.1016/j.suc.2010.04.003
14. Gujral J. Mechanism of Cell Death During Warm Hepatic Ischemia-Reperfusion in Rats: Apoptosis or Necrosis? *Hepatology* (2001) 33:397–405. doi: 10.1053/jhep.2001.22002
15. Shi S, Verstegen MMA, Mezzanotte L, Jonge J, Löwik CWGM, Laan LJW. Necroptotic Cell Death in Liver Transplantation and Underlying Diseases: Mechanisms and Clinical Perspective. *Liver Transplant* (2019) 25:1091–104. doi: 10.1002/lt.25488
16. Luedde T, Kaplowitz N, Schwabe RF. Cell Death and Cell Death Responses in Liver Disease: Mechanisms and Clinical Relevance. *Gastroenterology* (2014) 147:765–783.e4. doi: 10.1053/j.gastro.2014.07.018
17. Sun L, Wang H, Wang Z, He S, Chen S, Liao D, et al. Mixed Lineage Kinase Domain-Like Protein Mediates Necrosis Signaling Downstream of RIP3 Kinase. *Cell* (2012) 148:213–27. doi: 10.1016/j.cell.2011.11.031
18. Cao WX, Li T, Tang ZH, Zhang LL, Wang ZY, Guo X, Su MX, et al. MLKL Mediates Apoptosis *via* a Mutual Regulation With PERK/Eif2α Pathway in Response to Reactive Oxygen Species Generation. *Apoptosis* (2018) 23:521–31. doi: 10.1007/s10495-018-1475-6
19. Hong J-M, Kim S-J, Lee S-M. Role of Necroptosis in Autophagy Signaling During Hepatic Ischemia and Reperfusion. *Toxicol Appl Pharmacol* (2016) 308:1–10. doi: 10.1016/j.taap.2016.08.010
20. Li C, Sheng M, Lin Y, Xu D, Tian Y, Zhan Y, et al. Functional Crosstalk Between Myeloid Foxo1–β-Catenin Axis and Hedgehog/Gli1 Signaling in Oxidative Stress Response. *Cell Death Differ* (2021) 28:1705–19. doi: 10.1038/s41418-020-00695-7
21. Zhong W, Wang X, Rao Z, Pan X, Sun Y, Jiang T, et al. Aging Aggravated Liver Ischemia and Reperfusion Injury by Promoting Hepatocyte Necroptosis in an Endoplasmic Reticulum Stress-Dependent Manner. *Ann Transl Med* (2020) 8:869–9. doi: 10.21037/atm-20-2822
22. Yang F, Shang L, Wang S, Liu Y, Ren H, Zhu W, et al. TNF α -Mediated Necroptosis Aggravates Ischemia-Reperfusion Injury in the Fatty Liver by Regulating the Inflammatory Response. *Oxid Med Cell Longev* (2019) 2019:1–14. doi: 10.1155/2019/2301903
23. Baidya R, Gautheron J, Crawford DHG, Wang H, Bridle KR. Inhibition of MLKL Attenuates Necroptotic Cell Death in a Murine Cell Model of Hepatic Ischaemia Injury. *J Clin Med* (2021) 10:212. doi: 10.3390/jcm10020212
24. Saeed WK, Jun DW, Jang K, Chae YJ, Lee JS, Kang HT. Does Necroptosis Have a Crucial Role in Hepatic Ischemia-Reperfusion Injury? *PloS One* (2017) 12:e0184752. doi: 10.1371/journal.pone.0184752
25. Rosentreter D, Funken D, Reifart J, Mende K, Rentsch M, Khandoga A. RIP1-Dependent Programmed Necrosis Is Negatively Regulated by Caspases During Hepatic Ischemia-Reperfusion. *Shock* (2015) 44:72–6. doi: 10.1097/SHK.0000000000000371
26. Wang Z, Jiang H, Chen S, Du F, Wang X. The Mitochondrial Phosphatase PGAM5 Functions at the Convergence Point of Multiple Necrotic Death Pathways. *Cell* (2012) 148:228–43. doi: 10.1016/j.cell.2011.11.030
27. Shi S, Verstegen MMA, Roest HP, Ardisasmita AI, Cao W, Roos FJM, et al. Recapitulating Cholangiopathy-Associated Necroptotic Cell Death *In Vitro* Using Human Cholangiocyte Organoids. *Cell Mol Gastroenterol Hepatol* (2022) 13:541–64. doi: 10.1016/j.jcmgh.2021.10.009
28. Wu H, Chen C, Ziani S, Nelson LJ, Ávila MA, Nevzorova YA, et al. Fibrotic Events in the Progression of Cholestatic Liver Disease. *Cells* (2021) 10:1107. doi: 10.3390/cells10051107
29. Konishi T, Schuster RM, Lentsch AB. Liver Repair and Regeneration After Ischemia-Reperfusion Injury Is Associated With Prolonged Fibrosis. *Am J Physiol - Gastrointest Liver Physiol* (2019) 316:G323–31. doi: 10.1152/ajpgi.00154.2018
30. Nishio T, Hu R, Koyama Y, Liang S, Rosenthal SB, Yamamoto G, et al. Activated Hepatic Stellate Cells and Portal Fibroblasts Contribute to Cholestatic Liver Fibrosis in MDR2 Knockout Mice. *J Hepatol* (2019) 71:573–85. doi: 10.1016/j.jhep.2019.04.012
31. Lua I, Li Y, Zagory JA, Wang KS, French SW, Sévigny J, et al. Characterization of Hepatic Stellate Cells, Portal Fibroblasts, and Mesothelial Cells in Normal and Fibrotic Livers. *J Hepatol* (2016) 64:1137–46. doi: 10.1016/j.jhep.2016.01.010
32. Selten JW, Verhoeven CJ, Heedfeld V, Roest HP, de Jonge J, Pirenne J, et al. The Release of microRNA-122 During Liver Preservation Is Associated With Early Allograft Dysfunction and Graft Survival After Transplantation. *Liver Transplant* (2017) 23:946–56. doi: 10.1002/lt.24766
33. Olthoff KM, Kulik L, Samstein B, Kaminski M, Abecassis M, Emond J, et al. Validation of a Current Definition of Early Allograft Dysfunction in Liver Transplant Recipients and Analysis of Risk Factors. *Liver Transplant* (2010) 16:943–9. doi: 10.1002/lt.22091
34. Verhoeven CJ, Farid WRR, De Ruiter PE, Hansen BE, Roest HP, De Jonge J, et al. MicroRNA Profiles in Graft Preservation Solution Are Predictive of Ischemic-Type Biliary Lesions After Liver Transplantation. *J Hepatol* (2013) 59:1231–8. doi: 10.1016/j.jhep.2013.07.034
35. Ariyakhagorn V, Schmitz V, Olschewski P, Polenz D, Boas-Knoop S, Neumann U, et al. Improvement of Microsurgical Techniques in Orthotopic Rat Liver Transplantation. *J Surg Res* (2009) 153:332–9. doi: 10.1016/j.jss.2008.04.003
36. Wang Z, Liu Y, Liu J, Kong N, Jiang Y, Jiang R, et al. ATF3 Deficiency Impairs the Proliferative–Secretory Phase Transition and Decidualization in RIF Patients. *Cell Death Dis* (2021) 12(4):387. doi: 10.1038/s41419-021-03679-8
37. Argani P, Hicks J, De Marzo AM, Albadine R, Illei PB, Ladanyi M, et al. Xp11 Translocation Renal Cell Carcinoma (RCC): Extended Immunohistochemical Profile Emphasizing Novel RCC Markers. *Am J Surg Pathol* (2010) 34:1295–303. doi: 10.1097/PAS.0b013e3181e8ce5b
38. Varghese F, Bukhari AB, Malhotra R, De A. IHC Profiler: An Open Source Plugin for the Quantitative Evaluation and Automated Scoring of Immunohistochemistry Images of Human Tissue Samples. *PloS One* (2014) 9:e96801. doi: 10.1371/journal.pone.0096801
39. Howitt BE, Sun HH, Roemer MGM, Kelley A, Chapuy B, Aviki E, et al. Genetic Basis for PD-L1 Expression in Squamous Cell Carcinomas of the Cervix and Vulva. *JAMA Oncol* (2016) 2:518–22. doi: 10.1001/jamaoncol.2015.6326
40. Yang X, Li R, Xu L, Qian F, Sun L. Serum Amyloid A3 Is Required for Caerulein-Induced Acute Pancreatitis Through Induction of RIP3-Dependent Necroptosis. *Immunol Cell Biol* (2021) 99:34–48. doi: 10.1111/imcb.12382
41. Wang E, Hu T, Huang C, Chang Y, Yang S, Huang S, et al. Hepatoma-Derived Growth Factor Participates in Concanavalin A-Induced Hepatitis. *FASEB J* (2020) 34:16163–78. doi: 10.1096/fj.202000511RR
42. Katsumata LW, Miyajima A, Itoh T. Portal Fibroblasts Marked By The Surface Antigen Thy1 Contribute To Fibrosis In Mouse Models Of Cholestatic Liver Injury. *Hepatol Commun* (2017) 1(3):198–214. doi: 10.1002/hep4.1023
43. Cursio R. Caspase Inhibition in Liver Transplantation: From Basic Research to Clinical Studies. *HPB* (2010) 12:1–3. doi: 10.1111/j.1477-2574.2009.00123.x

44. Hirao H, Ito T, Kadono K, Kojima H, Naini BV, Nakamura K, et al. Donor Hepatic Occult Collagen Deposition Predisposes to Peritransplant Stress and Impacts Human Liver Transplantation. *Hepatology* (2021) 74:2759–73. doi: 10.1002/hep.32030
45. Konishi T, Schuster RM, Goetzman HS, Caldwell CC, Lentsch AB. Fibrotic Liver Has Prompt Recovery After Ischemia-Reperfusion Injury. *Am J Physiol Liver Physiol* (2020) 318:G390–400. doi: 10.1152/ajpgi.00137.2019
46. Moriwaki K, Chan FK-M. Necroptosis-Independent Signaling by the RIP Kinases in Inflammation. *Cell Mol Life Sci* (2016) 73:2325–34. doi: 10.1007/s00018-016-2203-4
47. Zhan C, Huang M, Yang X, Hou J. MLKL: Functions Beyond Serving as the Executioner of Necroptosis. *Theranostics* (2021) 11:4759–69. doi: 10.7150/thno.54072
48. Guicciardi ME, Malhi H, Mott JL, Gores GJ. Apoptosis and Necrosis in the Liver. *Compr Physiol* (2013) 3(2):977–1010. doi: 10.1002/cphy.c120020
49. Berghe TV, Linkermann A, Jouan-Lanhouet S, Walczak H, Vandenabeele P. Regulated Necrosis: The Expanding Network of Non-Apoptotic Cell Death Pathways. *Nat Rev Mol Cell Biol* (2014) 15:135–47. doi: 10.1038/nrm3737
50. Kadono K, Kageyama S, Nakamura K, Hirao H, Ito T, Kojima H, et al. Myeloid Ikaros–SIRT1 Signaling Axis Regulates Hepatic Inflammation and Pyroptosis in Ischemia-Stressed Mouse and Human Liver. *J Hepatol* (2022) 76(4):896–909. doi: 10.1016/j.jhep.2021.11.026
51. Li J, Zhao J, Xu M, Li M, Wang B, Qu X, et al. Blocking GSDMD Processing in Innate Immune Cells But Not in Hepatocytes Protects Hepatic Ischemia–Reperfusion Injury. *Cell Death Dis* (2020) 11:244. doi: 10.1038/s41419-020-2437-9
52. Yamada N, Karasawa T, Wakiya T, Sadatomo A, Ito H, Kamata R, et al. Iron Overload as a Risk Factor for Hepatic Ischemia-Reperfusion Injury in Liver Transplantation: Potential Role of Ferroptosis. *Am J Transplant* (2020) 20:1606–18. doi: 10.1111/ajt.15773

Conflict of Interest: The authors declare that the research was conducted in the absence of any commercial or financial relationships that could be construed as a potential conflict of interest.

Publisher's Note: All claims expressed in this article are solely those of the authors and do not necessarily represent those of their affiliated organizations, or those of the publisher, the editors and the reviewers. Any product that may be evaluated in this article, or claim that may be made by its manufacturer, is not guaranteed or endorsed by the publisher.

frontiers | Frontiers in Immunology

ORIGINAL RESEARCH
published: 25 May 2022
doi: 10.3389/fimmu.2022.891351

Prussian Blue Scavenger Ameliorates Hepatic Ischemia-Reperfusion Injury by Inhibiting Inflammation and Reducing Oxidative Stress

Yongxin Huang[1,2,3†], *Qinyuan Xu*[4†], *Jiang Zhang*[1,2,3], *Yanze Yin*[1,2,3], *Yixiao Pan*[1,2,3], *Yuanyi Zheng*[4], *Xiaojun Cai*[4*], *Qiang Xia*[1,2,3*] *and Kang He*[1,2,3*]

[1] Department of Liver Surgery, Renji Hospital, School of Medicine, Shanghai Jiao Tong University, Shanghai, China, [2] Shanghai Engineering Research Center of Transplantation and Immunology, Shanghai, China, [3] Shanghai Institute of Transplantation, Shanghai, China, [4] Department of Ultrasound in Medicine, Shanghai Jiao Tong University Affiliated Sixth People's Hospital, Shanghai, China

OPEN ACCESS

Edited by:
Helong Dai,
Central South University, China

Reviewed by:
Yansong Ge,
Heilongjiang Bayi Agricultural University, China
Pedro Elias Marques,
KU Leuven, Belgium

***Correspondence:**
Kang He
hekang929@163.com
Qiang Xia
xiaqiang@shsmu.edu.cn
Xiaojun Cai
c1x2j34@163.com

[†]*These authors have contributed equally to this work*

Specialty section:
This article was submitted to Molecular Innate Immunity, a section of the journal Frontiers in Immunology

Received: *07 March 2022*
Accepted: *28 April 2022*
Published: *25 May 2022*

Citation:
Huang Y, Xu Q, Zhang J, Yin Y, Pan Y, Zheng Y, Cai X, Xia Q and He K (2022) Prussian Blue Scavenger Ameliorates Hepatic Ischemia-Reperfusion Injury by Inhibiting Inflammation and Reducing Oxidative Stress. Front. Immunol. 13:891351. doi: 10.3389/fimmu.2022.891351

Oxidative stress and excessive inflammatory responses are the two critical mechanisms of hepatic ischemia-reperfusion injury (HIRI) encountered in many clinical settings, including following hepatectomy and liver transplantation. Effective anti-inflammatory and anti-oxidative pharmacological interventions are urgently needed to counter HIRI. The present study showed that a biocompatible Prussian blue (PB) scavenger with reactive oxygen species (ROS) scavenging and anti-inflammatory properties might be used a promising treatment for HIRI. Following intravenous administration, PB scavenger was mainly distributed in the liver, where it showed excellent ability to alleviate apoptosis, tissue injury and organ dysfunction after HIRI. PB scavenger was found to protect liver tissue by scavenging ROS, reducing neutrophil infiltration and promoting macrophage M2 polarization. In addition, PB scavenger significantly reduced oxidative stress in primary hepatocytes, restoring cell viability under oxidative stress condition. PB scavenger effectively reduced lipopolysaccharide-stimulated inflammation in RAW 264.7 cells. These findings indicate that PB scavenger may be a potential therapeutic agent for the treatment of HIRI, providing an alternative treatment for ROS-associated and inflammatory liver diseases.

Keywords: prussian blue, liver ischemia-reperfusion injury, inflammation, reactive oxygen species, macrophage polarization

1. INTRODUCTION

Ischemia-reperfusion injury (IRI) is a pathophysiological condition, in which organs and/or tissue experience hypoxia damage caused by the impairment of blood flow, followed by exacerbation of injury due to the restoration of blood circulation and oxygen delivery (1). Acute IRI can occur in various tissue and organs throughout the body, leading to tissue damage and dysfunction. The liver, being the largest solid organ in the human body, is likely to experience IRI in patients undergoing liver transplantation or hepatectomy, or in patients affected by hemorrhagic shock or liver injury

(2). The process of hepatic IRI involves a series of events, with inflammation and excessive reactive oxygen species (ROS) being the most critical factors contributing to apoptosis, tissue injury and organ dysfunction (3).

At present, the strategies for treatment of HIRI are limited to ischemic preconditioning (IPC), ischemic post-conditioning (IPostC) and machine perfusion, with no pharmacological interventions available to protect the liver from IRI (4–7). Because the pathophysiology of hepatic IRI involves various targets and mechanisms, many types of drugs are currently being tested for their ability to suppress IRI-associated damage and restore liver function (8).

Nanomaterials have unique properties, making their biological behaviors significantly different from those of conventional molecules, showing anti-cancer, anti-infection and antioxidation properties (9–11). Nanoscale drugs can enter capillaries, preferentially accumulating in mononuclear phagocyte systems (e.g., liver, spleen) and being taken up by Kupffer cells. This increases drug concentrations in injured liver tissue, enhancing their bioavailability and therapeutic efficacy. In addition, nanomaterials are more stable than conventional molecules in the circulatory system, with a longer half-life, allowing administered doses to be decreased and reducing side effects while maintaining efficacy. Aiming at the therapeutic targets of ROS and inflammation, bioactive nanomaterials including nanoceria (12), carnosic acid nanoparticles (13), and bilirubin nanoparticles have shown good therapeutic efficacy in the treatment of HIRI. Despite their efficacy, bioactive nanomaterials have several drawbacks that hinder their clinical translation. For example, nanoceria acting as a nano-antioxidant reduced HIRI injury by scavenging ROS, alleviating inflammation, and inhibiting activation of monocyte and macrophage cells (12). However, the biological activities of nanoceria are sensitive to their size, ratio of Ce^{3+}/Ce^{4+} and active crystal surface (14–16), which is still a great challenge under exploration. In addition, the biosafety and their ROS scavenging property of nanoceria need further exploration (17). It is of great significance to develop an alternative bioactive nanodrug for efficient treatment of HIRI.

Prussian blue (PB) is a bioactive nanomaterial that has shown good biosafety and been approved by the U.S. Food and Drug Administration to treat exposure to radioactive/non-radioactive cesium and/or thallium (18). PB has shown multienzyme-like activities, including peroxidase (POD), catalase (CAT), and superoxide dismutase (SOD) activities, and acts as a good ROS scavenger. The antioxidant properties of PB can be attributed to its rich variable valence states in the structure of PB (such as Fe^{3+}/Fe^{2+}, $[Fe(CN)_6]^{3-}/[Fe(CN)_6]^{4-}$) (19). Furthermore, PB has shown good preventive and therapeutic efficacy in various ROS-related diseases, including in the treatment of ischemic stroke (20, 21) and neurodegeneration (22), the prevention of vascular restenosis after endovascular interventions (23), in skin wound healing (24), and in the treatment of inflammatory bowel disease (25). A biocompatible PB scavenger with ROS-scavenging and anti-inflammatory properties may show potential in the treatment of HIRI.

The present study tested the ability of PB scavengers to protect livers from IRI based on their outstanding ROS scavenging and anti-inflammatory properties. PB scavengers were prophylactic administered to a mouse model of IRI. These scavengers mostly accumulated in the liver and effectively alleviated IRI-associated liver damage. These findings indicated that PB scavengers had excellent ability to manage oxidative stress, as well as having immunomodulatory activities.

2. MATERIAL AND METHODS

2.1 Materials

Analytical grade Potassium ferricyanide ($K_3[Fe(CN)_6]$), polyvinylpyrrolidone (PVP, K30), and hydrochloric acid (HCl, 36.0%) were purchased from Sinopharm Chemical Reagent Co., Ltd.

2.2 Synthesis of PB Scavengers

In a typical experiment, $K_3[Fe(CN)_6]$ (396 mg) and PVP (5 g) were dissolved and mixed in 1 M HCl (40 mL) at room temperature. After being stirred until clear, the solution was transferred to an oven and heated at 80°C for 24 h. The final product was collected by centrifugation and washed three times with deionized (DI) water, followed by dispersion in saline or lyophilization and storage at 4°C.

2.3 Characterization of PB Scavengers and Instruments

Sample morphology was assessed using a Zeiss Gemini 300 scanning electron microscope (SEM, Oberkochen, Germany). Transmission electron microscopy (TEM) and high-resolution TEM (HRTEM) images were obtained using a JEOL-2100F TEM (Tokyo, Japan). Hydrodynamic diameters and Zeta potentials were determined by dynamic light scattering (DLS, Malvern Zetasizer Nano-Z, Malvern, UK). X-ray diffraction (XRD) patterns were obtained on an X-ray diffractometer (Bruker D8 Advance, Karlsruhe, Germany). The surface valence of Fe was evaluated by X-ray photoelectron spectroscopy (XPS, Thermo Scientific K-Alpha, New York, NY, USA). Ultraviolet-visible (UV-vis) spectra were recorded using a PerkinElmer Lambda 750 spectrophotometer (Waltham, MA USA). Fourier transform infrared (FTIR) spectra were characterized using a Fourier Transform Infrared spectrometer (Nicolet iS20, Thermo Fisher Scientific). Raman spectroscopy was performed using a Renishaw Raman system (Renishaw inVia, London, UK). PB concentrations were determined by inductively coupled plasma atomic emission spectroscopy (ICP-AES) using a PerkinElmer Avio 200 system.

2.4 Catalase (CAT)-Like Activity of PB Scavengers

To assess the CAT-like activity of PB scavengers, 1.2 M hydrogen peroxide (H_2O_2) and 2.4 ug/mL PB were added to buffers at pH 5.5, 6.8 and 7.4, and the dissolved oxygen concentrations were

measured for 10 min using a portable dissolved oxygen meter (INESA JPBJ-609L, China).

2.5 Hydroxyl Radicals (•OH) Scavenging Capacity of PB Scavengers

The ability of PB scavengers to eliminate •OH was assessed by electron spin resonance (ESR, Bruker MS5000, Germany) spectroscopy. Briefly, •OH was generated by mixing $FeSO_4$ (50 mg/ml) and H_2O_2 (20 mM) and captured by the spin trap agent 5,5-dimethyl-1-pyrroline N-oxide (DMPO). Various concentrations of PB, DMPO and newly generated •OH were incubated for 8 min, and their ESR spectra were recorded at an X-ray microwave power of 10 mW, a modulation frequency of 100 kHz, a scan range of 3300–3450 G, and a modulation amplitude of 1 G.

2.6 Peroxidase (POD)-Like Activity of PB Scavengers

The POD-like activity of PB scavengers was tested using the chromogenic substrate 3,3′,5,5′-tetramethylbenzidine (TMB) in the presence of H_2O_2. Briefly, H_2O_2, TMB and PB scavengers at various concentrations were added to phosphate buffer saline (PBS) solutions of various pH. The POD-like behavior of PB was evaluated by recording the absorbance of oxidized TMB at 650 nm over time using a UV-vis spectrophotometer.

2.7 Animals

Male wild-type (WT) C57BL/6JGpt mice aged 8–10 weeks were purchased from Shanghai Model Organisms. All mice were housed under specific pathogen-free conditions in a temperature-controlled room (22–24°C) with normal light–dark cycle, and allowed food and water ad libitum. All animal protocols met the Guide for the Care and Use of Laboratory Animals (National Institutes of Health [NIH], Bethesda, MD, USA) and were approved by the Animal Use Board of the School of Medicine of Shanghai Jiao Tong University.

2.8 Establishment of a Mouse Hepatic Ischemia/Reperfusion Injury Model

Male WT C57BL/6JGpt mice aged 8–10 weeks were randomly divided into two groups, a sham treatment and a HIRI group, with each group subdivided into two groups and pretreated with PBS or 1 mg/kg PB scavenger 24 h before the procedure. To induce partial hepatic IRI, mice were first anesthetized by intraperitoneal injection of 1% pentobarbital. After a midline laparotomy, the arterial/portal vessels to the cephalad lobes were clamped with microvascular clamps for 90 min. The peritoneum was sealed and covered with warm saline-soaked sterile gauze to avoid dehydration. Clamps were removed after 90 min to initiate reperfusion. Mice were sacrificed at 6 hours after reperfusion, and liver and serum samples were collected for further analysis. Sham groups underwent the same surgical procedures but without obstruction of blood vessels.

2.9 Serum Analysis

Serum ALT and AST levels were measured by ALT/AST kit (ThermoFisher, Waltham, MA, USA) according to the manufacturer's instructions. Serum concentrations of TNF-α and IL-10 were measured using mouse TNF-α and IL-10 ELISA kits.

2.10 H&E Staining and TdT-Mediated dUTP Nick End Labelling Assay

Formalin-fixed liver tissue samples were dehydrated in graded alcohol, embedded in paraffin, and sectioned at 5-μm thickness. After deparaffinization, the sections were stained with hematoxylin and eosin (H&E) as routine protocols. Apoptotic cell death in liver tissue was analyzed by TUNEL staining.

2.11 Lipid Peroxidation Assay

Frozen liver tissue was homogenized in RIPA buffer and centrifuged. The MDA concentration in the homogenate was determined using a commercially available kit (Nanjing Jiancheng Bioengineering Institute, Nanjing, China), which measured thiobarbituric acid (TBA) reactivity. Briefly, the homogenate was mixed with trichloroacetic acid, the mixture was centrifuged and TBA was added to the supernatant. Lipid peroxidation was determined by measuring the red color of the solution at 532 nm with a spectrophotometer. Other procedures were performed according to the manufacturer's protocols.

2.12 Assay of ROS Levels *In Vivo*

Fresh liver tissue samples (50 mg) were homogenized in 1 mL buffer, followed by centrifugation of the homogenate at 4°C for 10 minutes. A 190-μL aliquot of each supernatant was incubated with 10 μL ROS probe (BestBio, China) in each well of a 96-well plate at 37°C in the dark for 30 minutes. ROS levels were analyzed using fluorescence microplate reader at an excitation wavelength of 488 nm and an emission wavelength of 530 nm.

2.13 Real-Time PCR

Total RNAs were isolated with Trizol reagent (Sigma), followed by synthesis of cDNA using a PrimeScript Reverse Transcription Reagent Kit (Takara, Otsu, Shiga, Japan). A Step One Plus Real-Time PCR System (Thermo Fisher Scientific) and Sybr Premix Ex Taq Kit (Takara) were used for qPCR, with the expression of each target gene normalized to that of GAPDH. Genes were amplified using primers for *Tnf-α* (5′-CCTGTAGCCCACGTCGTAG-3′ [forward] and 5′-GGGAGTAGACAAGGTACAACCC-3′ [reverse]); *Il-1β* (5′-CTCCATGAGCTTTGTACAAGG-3′ [forward] and 5′-TGCTGATGTACCAGTTGGGG-3′ [reverse]); *Arg-1* (5′-CTCCAAGCCAAAGTCCTTAGAG-3′ [forward] and 5′-GGAGCTGTCATTAGGGACATCA-3′ [reverse]); *IL-10* (5′-CTTACTGACTGGCATGAGGATCA-3′ [forward] and 5′-GCAGCTCTAGGAGCATGTGG-3′ [reverse]); and *GAPDH* (5′-GAAATCCCATCACCATCTTCCAGG-3′ [forward] and 5′-GAGCCCCAGCCTTCTCCATG-3′ [reverse]). The levels of expression (fold change) of *Tnf-α*, *Il-1β*, *Arg-1*, and IL-10 mRNAs relative to that of *GAPDH* mRNA in liver tissue samples and RAW 264.7 cells were determined by the Ct (ΔΔCt) method.

2.14 MPO Activity Determination

Liver MPO activity was determined using an MPO Detection Kit (Nanjing Jiancheng Bioengineering Institute,

China). Briefly, liver tissue was homogenized in 1 ml phosphate buffer (50 mM, pH 6.0) containing 0.5% hexadecyltrimethylammonium hydroxide and centrifuged at 12,000 r/min at 4°C for 20 min. A 10-μL aliquot of each supernatant was transferred to PBS (pH 6.0) containing 0.17 mg/mL 3,3′-dimethoxybenzidine and 0.0005% H_2O_2. The MPO activity of the supernatant was determined by measuring the H_2O_2-dependent oxidation of 3,3′-dimethoxybenzidine and normalized by measuring the total protein content in samples using a BCA protein assay kit.

2.15 Immunofluorescence Staining

Liver sections were deparaffinized, rehydrated, and blocked with 5% bovine serum albumin (BSA) for 1 hour at room temperature. After washing, the tissue slices were incubated overnight at 4°C with primary rabbit antibodies against F4/80 (1:5000, Servicebio), CD206 (1:400, Servicebio), and iNOS (1:200, Servicebio). After washing with PBS, the slices were incubated at room temperature for 1 h with goat anti-rabbit secondary antibodies labeled with HRP (1:500, Servicebio) or Cy3 (1:300, Servicebio). Nuclei were stained with DAPI (Sigma-Aldrich). Fluorescence images were obtained with a DM6B microscope (Leica Microsystems, Milan, Italy) and analyzed by ImageJ.

2.16 Isolation, Culture and Treatment of Primary Hepatocytes

Primary hepatocytes were isolated from livers as previously described (26). The isolated cells were cultured on dishes (3×10^6 cells/6-cm dish), 6-well plates (2×10^5 cells/well) or 96-well plates (1 x 10^4 cells/well) in high-glucose Dulbecco's modified Eagle's medium (DMEM), supplemented with 1% pen-strep and 10% FBS at 37°C in an atmosphere containing 5% CO_2. Cell viability was tested after treating primary hepatocytes with various concentrations of PB scavengers. The primary hepatocytes were also treated with various concentrations of H_2O_2 in the presence or absence of 50 μg/mL PB scavengers. Cell viability was analyzed by MTT assays (Sigma-Aldrich, St. Louis, MO, USA).

2.17 Assay of Intracellular Ferrous Iron Level

Intracellular levels of ferrous iron were determined using iron assay kits (#ab83366, Abcam). Briefly, primary hepatocytes were collected, washed with cold PBS, and homogenized in iron assay buffer, followed by the addition of iron reducer to the collected supernatant. An iron probe was added, and the samples were mixed and incubated for 1 hour. The optical density of each solution at 593 nm was immediately measured on a colorimetric microplate reader.

2.18 Intracellular ROS Measurements

Intracellular ROS generation was assessed using the ROS sensitive fluorescent probe DCFH-DA (Sigma-Aldrich). Briefly, primary hepatocytes were incubated with H_2O_2 (100 μM) for 16 h with or without PB scavengers. The cells were washed and incubated with 10 μM DCFH-DA for 30 min, with intracellular fluorescence visualized using a fluorescence microscope (TE2000, Nikon, Tokyo, Japan). To analyze the cellular ROS levels in RAW 264.7 cells, the cells were incubated with 10 μM of DCFH-DA at 37°C for 45 min in the dark, followed by washing, resuspension in HBSS and immediate analysis by flow cytometry.

2.19 *In Vivo* Biosafety of PB Scavengers

Male WT C57BL/6JGpt mice aged 8–10 weeks were randomly divided into two group, which were intravenously administered PBS (control group) or 1 mg/kg PB scavengers (PB nanozyme group) respectively through the tail vein. After 24 h, the mice were anesthetized and blood was collected from the venous sinus into an anticoagulant tube containing ethylenediaminetetraacetic acid (EDTA). The main organs of each mice were harvested, fixed and stained with hematoxylin and eosin (H&E). Routine blood tests were performed using standard procedures.

2.20 Statistical Analysis

Data were expressed as mean ± SEM. Results in two groups were compared by two-tailed t tests, whereas results in multiple groups were compared by one-way ANOVA. All statistical analyses were performed using GraphPad Prism software (version 8.0), with P values <0.05 considered statistically significant.

3. RESULTS AND DISCUSSION

3.1 Synthesis and Characterization of PB Scavengers

PB scavengers were prepared as described (27, 28), by heating mixtures of $K_3[Fe(CN)_6]$ and PVP dissolved in 1 M hydrochloric acid at 80°C for 24 h. In this synthesis process, PVP acted as a reducing agent under acidic conditions, as well as controlling and stabilizing size during lattice growth. The morphological features of PB scavengers were assessed by SEM and TEM, which showed that the constructed PB scavengers were approximately regular microspheres about 80.2 mm in diameter (**Figures 1A** and **S1**). Dynamic light scattering (DLS) showed that the mode hydrodynamic diameter of PB scavengers dispersed in various aqueous solutions was ~80 nm (**Figure 1B**). The crystallographic properties of PB were assessed by X-ray diffraction (XRD), which showed that the crystalline structure of PB perfectly matched the standard JCPDS card (73–0687) (**Figure 1C**) (29). X-ray photoelectron spectroscopy (XPS) substantiated the composition of PB The photoelectron spectroscopy of the Fe 2p orbit in PB. showed two split binding-energy peaks at 721.48 eV and 708.48 eV (**Figure 1D** and **S2**). PB scavengers showed a characteristic absorption peak at 700 nm due to the electron transition from Fe^{II} to Fe^{III} (**Figure 1E**). The chemical structure of PB was further evaluated by FTIR and Raman analysis. The FTIR spectrum showed a peak characteristic of a carbon-nitrogen triple bond (C≡N) at 2089 cm^{-1} (**Figure 1F**), whereas the remain spectrum showed a similar C≡N peak at 2155 cm^{-1} in the Raman spectrum (**Figure S3**). Zeta potentiometry showed

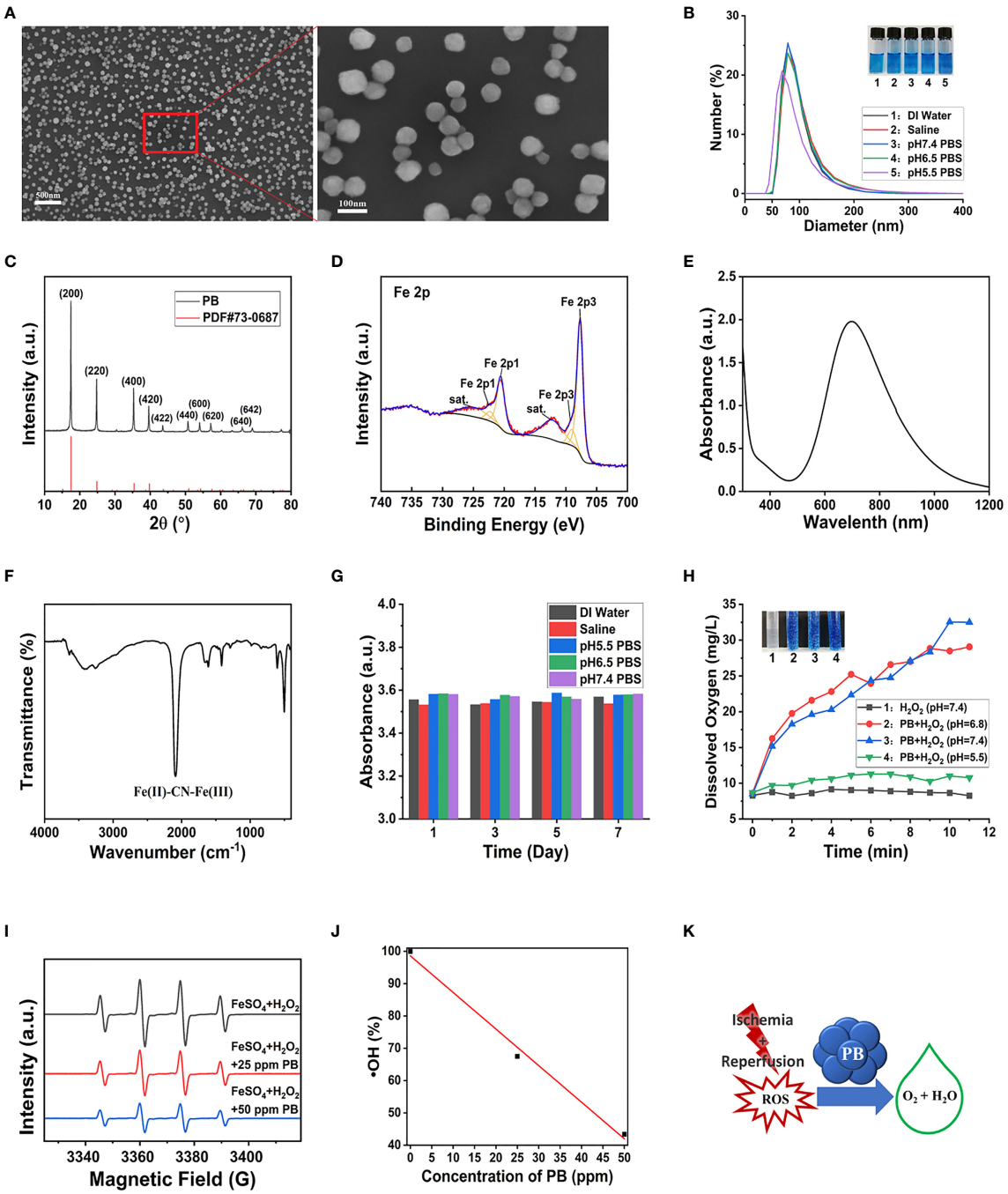

FIGURE 1 | Characterization and multi-enzyme-like activity of PB. **(A)** SEM image of PB. **(B)** DLS determination of hydrodynamic diameter distribution. **(C)** X-ray diffraction patterns. **(D)** Fe 2p XPS spectrum. **(E)** Characteristic UV-vis peak of PB by UV–vis. **(F)** FT-IR spectra of PB. **(G)** Effect of incubation in different media for 7 days on the UV–vis absorbance of PB. **(H)** Rate of generation of dissolved oxygen (Inset: Digital photo of O_2 bubbles generated from H_2O_2 15 min after mixing the reagents). **(I)** ESR signal of DMPO/($FeSO_4$+ H_2O_2)-generated •OH. **(J)** ESR analysis of the •OH scavenging effect of different concentrations of PB (R^2 = 0.99275). **(K)** Schematic representation of the mechanism by which PB scavenges ROS.

that the zeta potential of PB was ~-13.7 V (**Figure S4**), indicating that the surface of PB scavenger was is negatively charged. The stability of PB *in vitro* was also investigated. Both UV-vis and DLS analyses showed that good dispersion of PB in various aqueous solutions, with no changes over 7 days of incubation (**Figures 1G**, **S5**). Taken together, these results confirmed that PB scavengers had been successfully synthesized.

3.2 Ability of PB Scavengers to Scavenge Multiple ROS

3.2.1 CAT–Like Activity of PB Scavengers

CAT, which is synthesized in response to oxidative stimulation, is an important intracellular protective enzyme that catalyzes the decomposition of H_2O_2 to O_2 and H_2O (30). Thus, the rate of oxygen generation can reflect the catalase-like activity of PB scavengers. Measurements of the concentrations of dissolved oxygen produced over time by H_2O_2 and PB and recorded by the dissolved oxygen electrode showed that PB catalyzed the decomposition of H_2O_2 to generate abundant O_2 bubbles at pH 6.8 and pH 7.5, but generated fewer bubbles under acidic conditions (pH 5.5) (**Figure 1H**). By contrast, the control group without PB displayed no bubble generation. These findings indicated that PB scavengers exhibited CAT-like behavior through the decomposition of H_2O_2.

3.2.2 •OH Scavenging Capacity of PB Scavengers

•OH was produced through the classic Fenton reaction between $FeSO_4$ and H_2O_2 and examined by ESR. Because •OH is a powerful oxidizing agent, it has a short half-life, making it hard to detect. In this study, •OH was captured with the spin trap agent DMPO, forming DMPO/•OOH (31).

ESR spectra showed that the characteristic peak intensities of DMPO/•OH and DMPO/•OOH were markedly decreased with increasing concentrations of PB (**Figure 1I**). A linear correlation was observed between PB concentrations and •OH quenching, with 25 and 50 μg/mL PB concentrations having •OH quenching rates of 32.5% and 56.6%, respectively (**Figure 1J**). These findings showed that PB scavengers quenched •OH in a concentration-dependent manner regardless of Fe composition, showing the good •OH scavenging property. The ROS scavenging properties of PB scavenger may be ascribed to its variable valence state.

3.2.3 POD-Like Activity of PB Scavengers

POD is another type of antioxidant enzyme that can detoxify H_2O_2 to H_2O. H_2O_2 can oxidize the colorless compound TMB to the blue-colored oxidized TMB (TMBox) with a maximum absorbance at ~652 nm (32). The POD-like activity of PB scavengers was therefore assessed by measuring the absorbance of TMB. Because the blue color of PB was similar to that of TMBox (33), UV-vis absorbance was performed to ensure that the maximum absorption of oxidized TMB at 650 nm would not be masked by the 20-fold higher concentration of PB (**Figure S6A**). PB showed a concentration-dependent increase in catalytic activity (**Figure S6B**), with higher catalytic activity at slightly acidic pH (**Figure S6C**). To sum up, PB scavengers demonstrated a remarkable ability to scavenge multiple ROS (**Figure 1K**).

3.3 PB Scavengers Alleviated Hepatic Ischemia/Reperfusion Injury in Mice

The therapeutic efficacy of PB scavengers *in vivo* was assessed using a murine HIRI model, in which mice were exposed to ischemia for 90 minutes followed by reperfusion for 6 hours (**Figure 2A**). To determine the optimal timing of 1 mg/kg PB scavenger administrations, PB scavengers were administered at different time points, including 24 hours or 1 hour before the ischemia procedure and at the beginning of the reperfusion. Only prophylactic administration of PB scavengers 24 hours before I/R showed a significant protective effect against tissue damage caused by HIRI, as indicated by reduced serum ALT and AST levels (**Figures 2B, C**, **S7**). Thus, subsequent experiments were performed by prophylactically administrating PB scavengers 24 hours before the procedure.

Histopathological analysis of liver tissue by H&E staining was performed to evaluate damage to liver tissue. The control group of mice, treated with PBS prior to I/R, showed severe congestion, vacuolization and hepatic necrosis, whereas the mice treated with PB before I/R showed only mild or moderate congestion, vacuolization and hepatocyte necrosis (**Figures 2D, E**). Evaluation of hepatocyte apoptosis by TUNEL staining showed that TUNEL positive areas were mainly distributed around the large vessels, with much stronger TUNEL staining in the PBS group than in the PB group after I/R injury, suggesting that PB scavengers could effectively prevent tissue apoptosis (**Figure 2F**). In addition, quantitative analysis confirmed that the area of apoptotic hepatic tissue was larger in the PBS group than in the PB group (**Figure 2G**). Measurement of ROS levels in fresh liver tissue showed that PB scavengers had excellent ROS scavenging capacity *in vivo* (**Figure 2H**). Because lipid peroxidation is an indicator of excessive ROS generation resulting from I/R injury, the levels of MDA, a secondary product of lipid peroxidation, were measured in liver tissue. The level of MDA was markedly higher in the PBS group than in the sham group and the PB group (**Figure 2I**), indicating that PB scavengers could significantly alleviate HIRI injury through inhibition of lipid peroxidation.

3.4 PB Scavengers Promoted Macrophage Polarization to M2, Reduced Neutrophil Infiltration and Protected the Liver Against Inflammatory Damage After I/R

In addition to high ROS generation, inflammatory response is another strong hallmark of I/R injury. To evaluate the anti-inflammatory activity of PB scavengers in this mouse model of HIRI, the levels of expression of *TNF-α*, *IL-1β* and *IL-10* mRNAs were measured in the livers of PBS- and PB-treated mice. As expected, the levels of expression of the pro-inflammatory *TNF-α* and *IL-1β* were significantly higher in PBS- than in sham-treated mice, but were only slightly higher in PB- than in sham-treated mice (**Figures 3A, B**). The expression of the anti-inflammatory *IL-10* mRNA was significantly higher in PB-treated than in sham- and PBS-treated mice (**Figure 3C**). The anti-inflammatory activity of PB scavengers was further verified by measuring the serum concentrations of TNF-α and IL-10 in these mice (**Figures 3D, E**). MPO activity is often used as a biomarker of neutrophil recruitment in liver tissue after I/R injury (34). Although MPO was significantly higher in PBS-treated mice after I/R injury than in sham-treated mice, MPO activity after I/R injury was markedly decreased by treatment with PB scavengers (**Figure 3F**). Additionally, evaluation of macrophage activation and polarization in the livers of I/R groups

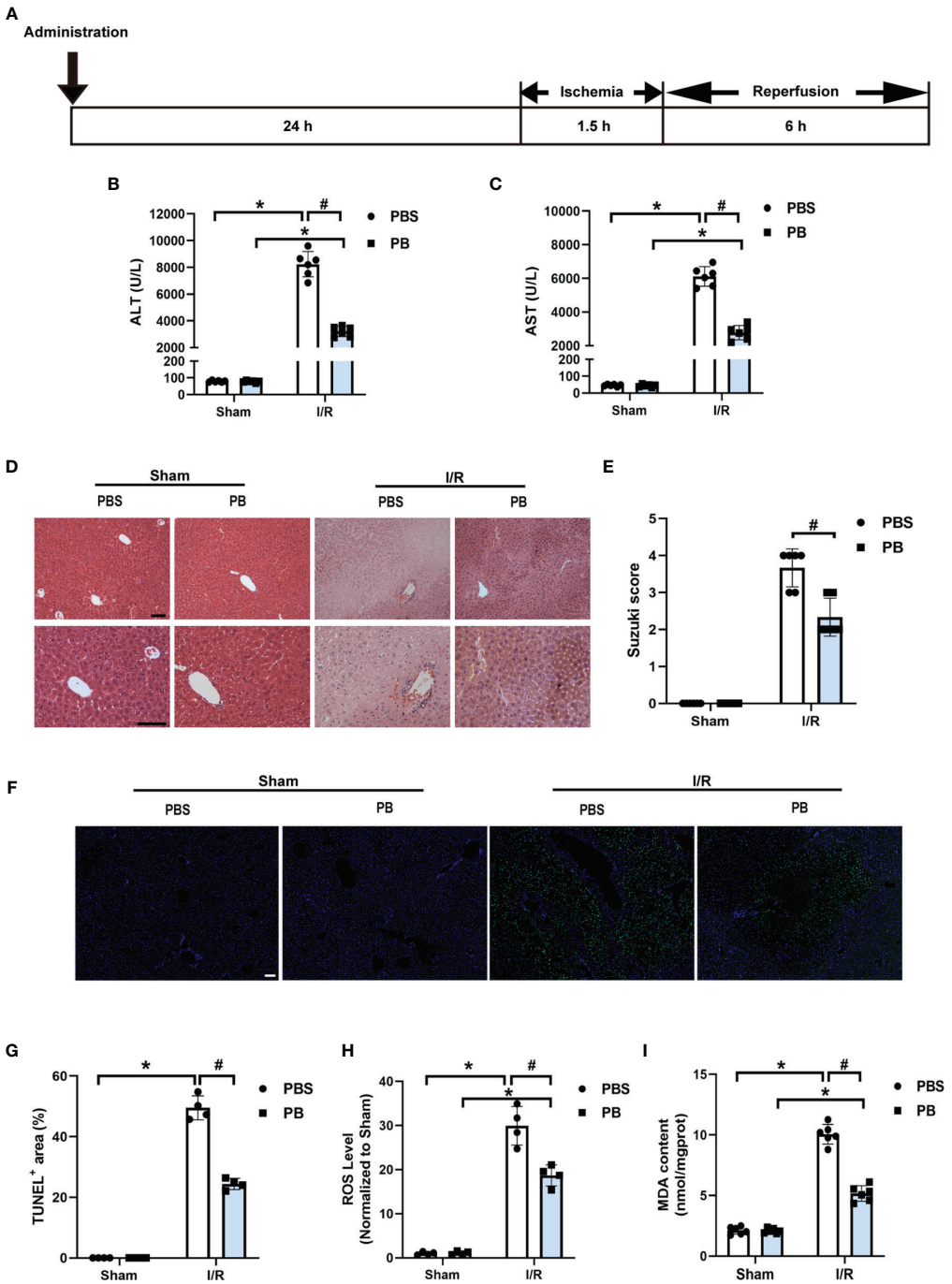

FIGURE 2 | PB scavengers significantly alleviated hepatic ischemia/reperfusion injury in mice. **(A)** Generation of an *in vivo* hepatic I/R injury model in mice. **(B, C)** Serum concentrations of **(B)** ALT and **(C)** AST in mice after 90 min of ischemia and 6 h of reperfusion (n = 6). **(D)** H&E staining of liver tissue harvested from mice administered different treatments. **(E)** Histological severity of hepatic IRI graded using Suzuki's score (n = 6). **(F)** TUNEL staining of liver sections. **(G)** Quantification of hepatic apoptotic areas in TUNEL-stained liver tissue (n = 4). **(H)** ROS levels of fresh liver tissue from various groups of mice (n = 4). **(I)** MDA levels of liver sections from various groups of mice (n = 6). *P < 0.05 versus the sham group; #P < 0.05 versus the PBS + I/R group. All scale bars = 100 μm.

by immunofluorescence staining with F4/80, a macrophage/Kupffer cell marker, CD206, an M2 polarization marker and iNOS, an M1 polarization marker, showed that, after the I/R procedure, most of the Kupffer cells in PBS-treated group were activated and had polarized to M1 type, as indicated by the increased number of F4/80$^+$iNOS$^+$ cells. In contrast, PB scavenger treatment increased the number of F4/80$^+$CD206$^+$ cells and reduced the number of F4/80$^+$iNOS$^+$ cells compared with the PBS-treated group

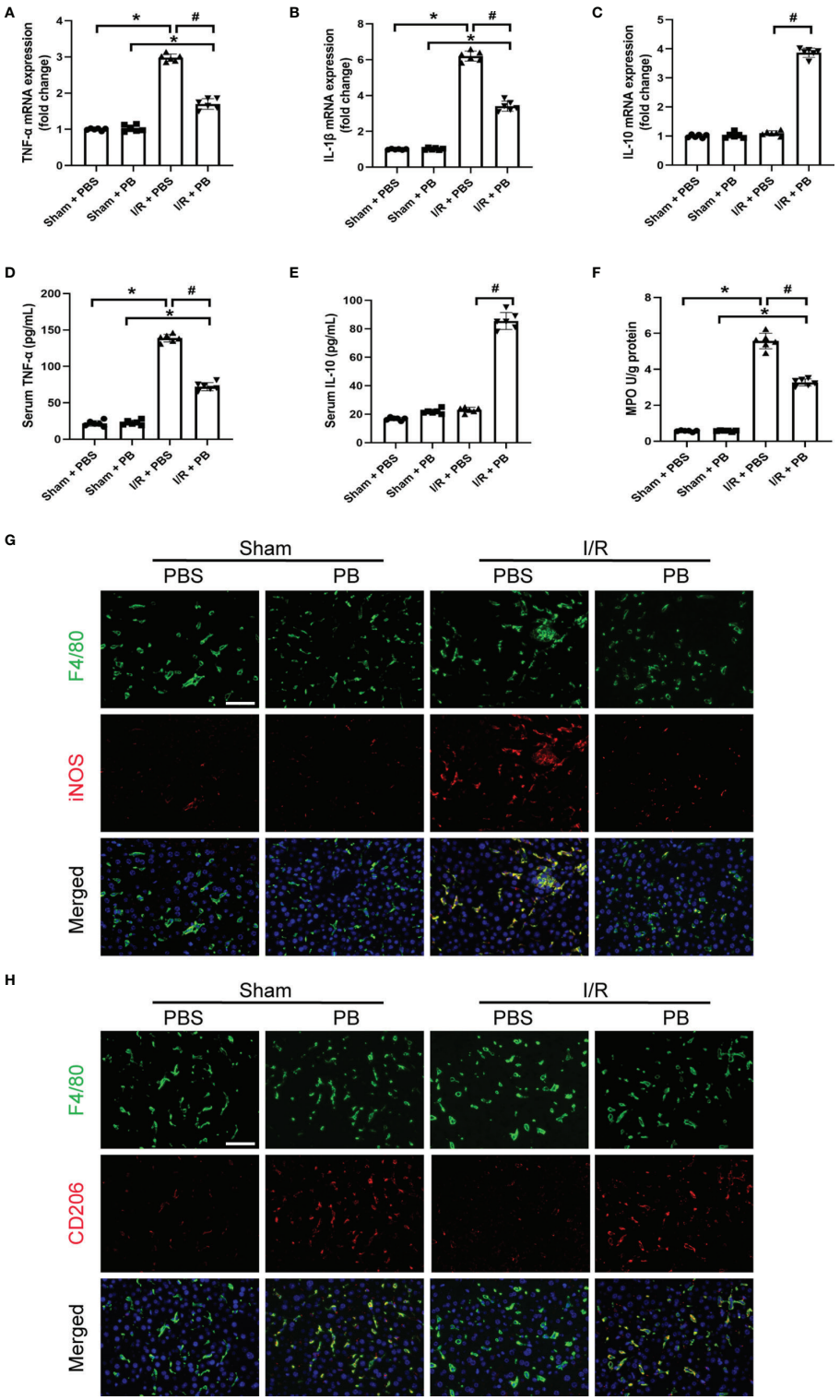

FIGURE 3 | PB scavengers promoted Kupffer cells polarization to M2, reduced neutrophil infiltration and protected liver against inflammatory damage after I/R. **(A–C)** Expression of mRNAs encoding pro-inflammatory (TNF-α, IL-1β) and anti-inflammatory (IL-10) cytokines in mouse liver (n = 6). **(D, E)** Serum concentration of **(D)** TNF-α and **(E)** IL-10 in mice after various treatments (n = 6). **(F)** MPO activity in liver sections of mice after various treatments (n = 6). **(G, H)** Immunofluorescence staining of liver tissue with F4/80 (green), iNOS/CD206 (red), markers of M1 and M2 macrophages, respectively, and the nucleus (blue) in various groups of mice. *P < 0.05 versus the sham group; #P < 0.05 versus the PBS + I/R group. All scale bars = 100 μm.

(**Figures 3G, H**). These results suggested that PB scavengers might reduce neutrophil recruitment and promote M2 polarization of macrophages, thereby protecting liver tissue against inflammatory damage during I/R.

3.5 PB Scavengers Showed Promising Cytoprotective Effect on Oxidative Stress Injury in Primary Hepatocytes

The cytoprotective effects of PB scavengers were also evaluated in primary hepatocytes. At concentrations <100 μg/mL, PB scavengers showed no significant cytotoxicity (**Figure 4A**). Because PB scavenger is an iron-based compound, intracellular iron levels were measured as an indicator of PB uptake by hepatocytes. Intracellular iron concentration increased as PB concentration increased, with intracellular iron peaking at 24 hours of incubation (**Figure 4B**). Primary hepatocytes with or without 50 μg/mL PB scavengers were subsequently treated with various concentrations of H_2O_2 to stimulate ROS generation. As expected, increasing H_2O_2 significantly reduced cell viability in the absence of PB scavengers, whereas treatment with PB scavengers restored hepatocyte viability (**Figure 4C**). To determine whether the cytoprotective effect of PB scavenger was due to its ROS scavenging ability, intracellular ROS generation in primary hepatocytes exposed to 100 μM of H_2O_2 with or without 50 μg/mL PB scavengers was evaluated using DCFH-DA, an ROS-sensitive fluorescent probe. The intracellular fluorescence signal, which was high in the H_2O_2 treated hepatocytes, was markedly reduced by PB scavengers, indicating that the latter were efficient scavengers of ROS (**Figure 4D**).

3.6 PB Scavengers Alleviated LPS-Induced Inflammation *In Vitro*

The *in vitro* anti-inflammatory properties of PB scavengers were tested using LPS-activated RAW 264.7 macrophage cells. Treatment of LPS-stimulated RAW 264.7 cells with PB scavengers increased the levels of expression of the anti-

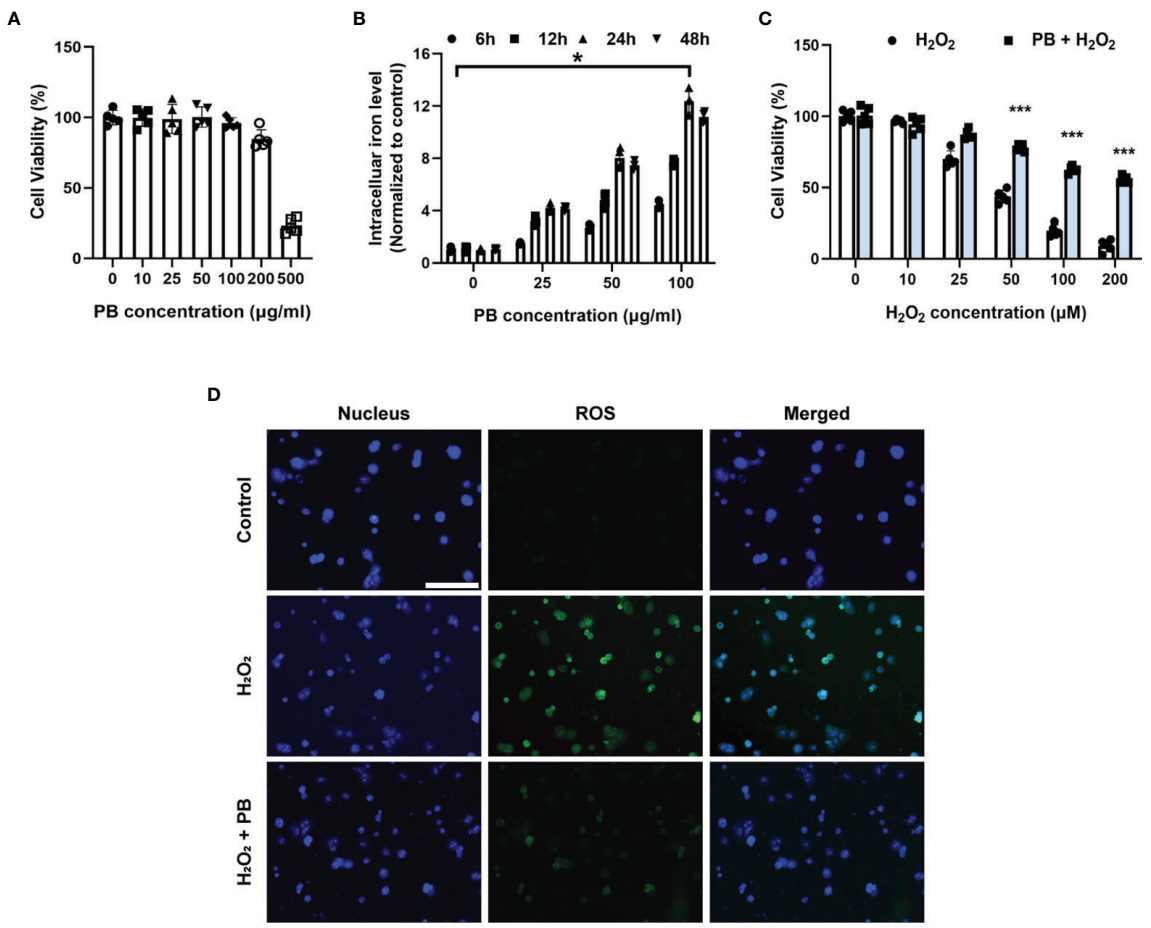

FIGURE 4 | Cytoprotective effect of PB scavengers against oxidative stress injury in primary hepatocytes. **(A)** Viability of primary hepatocytes after treating with different concentrations of PB scavengers for 24 hours (n = 5). **(B)** Intracellular iron levels in primary hepatocytes treated with various concentrations of PB scavengers (n = 4). **(C)** Effect of various concentrations of H_2O_2 on the viability of primary hepatocytes in the absence or presence of PB scavengers (50 μg/mL) (n = 5). **(D)** Fluorescence microscopy imaging of intracellular oxidative stress in primary hepatocytes after treatment with H_2O_2 (100 μM) for 16 h with or without PB scavengers (50 μg/mL). *P < 0.05 versus control group. ***P < 0.001 versus non-PB-protected groups. All scale bars = 100 μm.

inflammatory genes *IL-10* and *ARG-1*, but did not affect the expression of the pro-inflammatory genes *TNF-α* and *IL-1β*, compared with control cells, indicating that PB scavengers have anti-inflammatory effects on macrophages (**Figures 5A–D**). In addition, cells treated with LPS and PB scavengers showed significantly reduced levels of expression of *TNF-α* and *IL-1β* and increased levels of expression of *IL-10* and *ARG-1* compared with cells treated with LPS alone (**Figures 5A–D**). Evaluation of the secretion of TNF-α and IL-10 by ELISA showed that TNF-α concentrations were lower and IL-10 concentrations were higher in the supernatants of cells treated with PB scavengers plus LPS than in cells treated with LPS alone (**Figures 5E, F**). Because LPS stimulation of macrophages increased the generation of ROS, which contributed to inflammation, and the over-expression of pro-inflammatory genes may increase the further production of ROS (35), flow cytometry analysis was performed to assess LPS-induced ROS generation in RAW 264.7 cells. As expected, the level of intracellular ROS was higher in LPS-treated than in control cells, whereas PB scavengers reduced the level of LPS-induced ROS (**Figures 5G, H**).

3.7 Biosafety of PB Scavengers *In Vivo*

The *in vivo* biosafety of PB scavengers was assessed by H&E staining of various mouse organs. Evaluation of the heart, lungs, liver, spleen

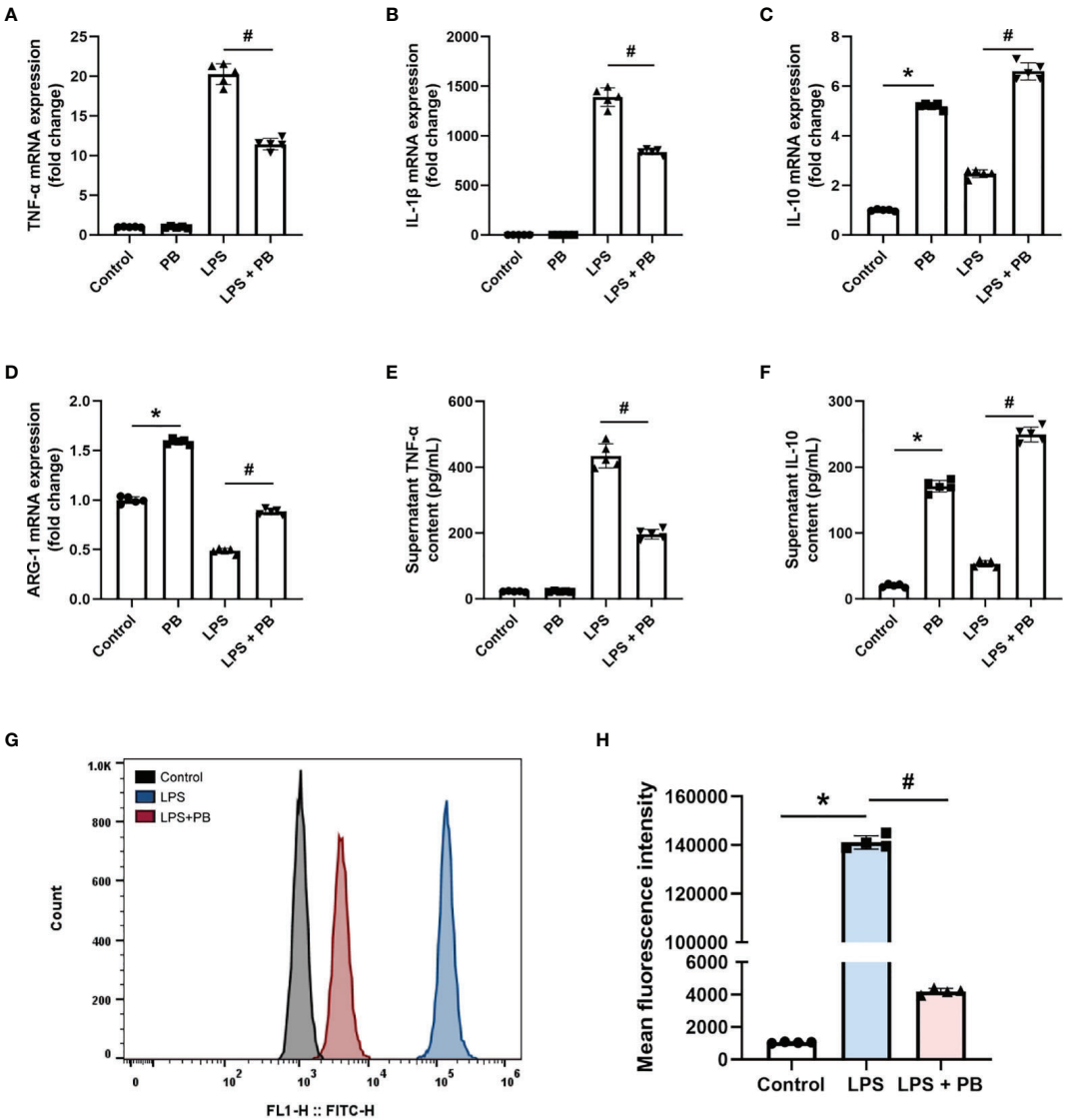

FIGURE 5 | PB scavengers alleviated LPS-induced inflammation in RAW 264.7 cells. **(A–D)** Effect of PB scavengers on the expression of mRNAs encoding the proinflammatory (TNF-α, IL-1β) and anti-inflammatory (IL-10, ARG-1) cytokines in LPS activated RAW 264.7 cells (n = 5). **(E, F)** Secretion of TNF-α and IL-10 by LPS activated RAW 264.7 cells treated with or without PB scavengers (n = 5). **(G)** Flow cytometry analysis of intracellular oxidative stress in the RAW 264.7 cells after LPS activation in the absence or presence of PB scavengers (50 μg/mL). **(H)** Quantitative representation of the flow cytometry results in G (n = 4). *P < 0.05 versus control group; #P < 0.05 versus the LPS-activated group.

and kidneys of PBS or PB-nanozyme treated mice showed no significant tissue abnormalities 24 hours after injection (**Figure 6A**). In addition, PB scavengers had no obvious effects on blood or biochemical indices in these mice (**Figure 6B**).

3.8 Discussion

The present study found that PB scavengers have promising therapeutic effects on hepatic ischemia reperfusion injury. HIRI injury model mice pretreated with PB scavengers experienced significantly less tissue damage than their positive controls. These nanoparticles with ROS scavenging and anti-inflammatory properties protected the liver of these mice by reducing oxidative stress in hepatocytes, by decreasing neutrophil infiltration, and by promoting macrophage M2 polarization (**Scheme 1**). To our knowledge, the present study is the first to report that systemic prophylactic administration of PB scavengers could protect the liver from acute injury and that systemic use of PB scavengers showed great biocompatibility.

The main strategies presently available to improve outcomes of IRI include reducing oxidative stress in the liver parenchyma and alleviating inflammatory damage (36). Although several drug delivery nanosystems have been designed to target HIRI (37), most are inapplicable clinically because of their poor liver targeting ability or their severe side effects (38, 39). PB scavengers, however, may be effective in the treatment of HIRI. PB itself is an FDA approved drug with high biosafety. Moreover, systemically administered PB scavengers were found to accumulate mostly in the liver and spleen, with little or no obvious tissue damage in the liver, heart, lungs, spleen and kidneys. PB scavenger is nonspecifically taken up by mononuclear phagocyte systems (e.g., liver, spleen), remove these particles from the circulation and resulting in the delivery of a sufficient dose of nano-antioxidants to the liver. In addition to protecting against acute liver injury, PB scavengers have been shown to have good therapeutic effects in ischemic stroke (21), wound healing (24) and inflammatory bowel disease (25), indicating its great potential for treating ROS-associated and inflammatory diseases. Evaluations of its mechanisms of action suggest that PB scavengers reduce intracellular ROS in hepatocytes and macrophages treated with various stimuli, suggesting that these may be critical mechanisms underlying the cytoprotective and anti-inflammatory properties or PB scavengers. ROS are important regulatory signal factors for the M1 polarization of macrophages *via* the downstream NF-κB signal. Suppressing ROS expression can switch polarization from M1 to M2 type (40, 41). PB scavengers were shown to switch macrophage polarization from the pro-inflammatory M1 type to the anti-inflammatory M2 type in the liver, as well as effectively reducing LPS-induced ROS generation in RAW 264.7 cells *in vitro*. These findings indicate that PB scavengers may scavenge intracellular ROS in activated macrophages and Kupffer cells, promoting their M2 polarization. This strategy also

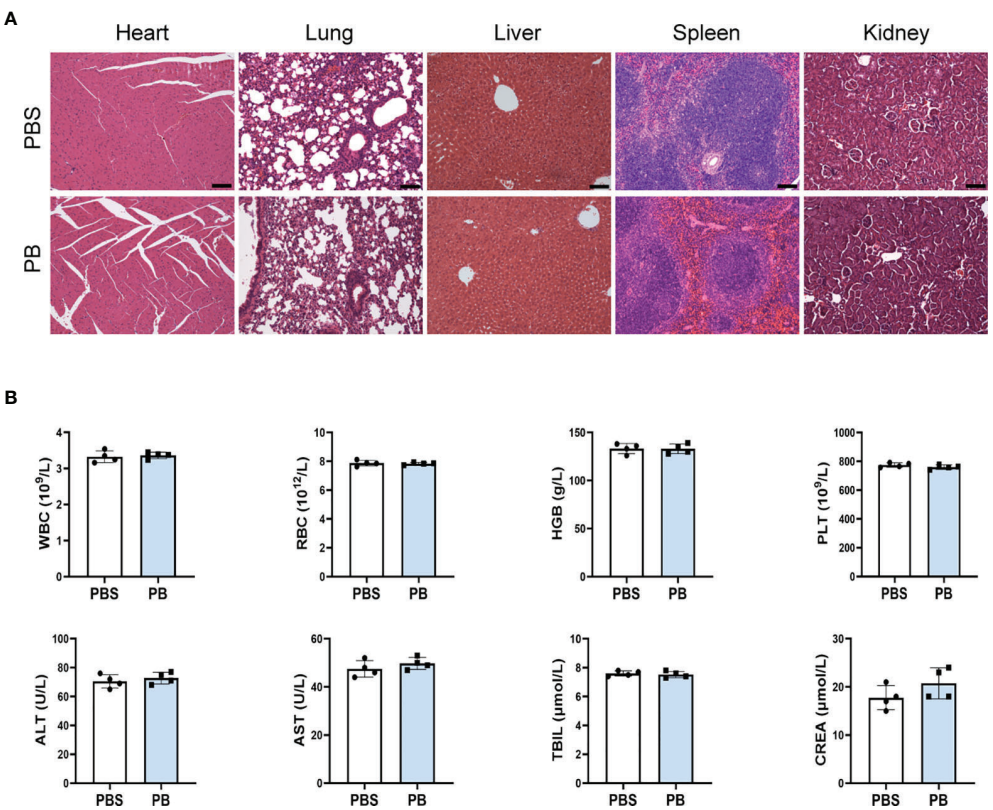

FIGURE 6 | *In vivo* biosafety of PB scavengers **(A)** H&E staining of the major organs of mice administered different treatments. **(B)** Hematological assays of mice 24 h after intravenous injection of PB scavengers (n = 4). All scale bars = 100 μm.

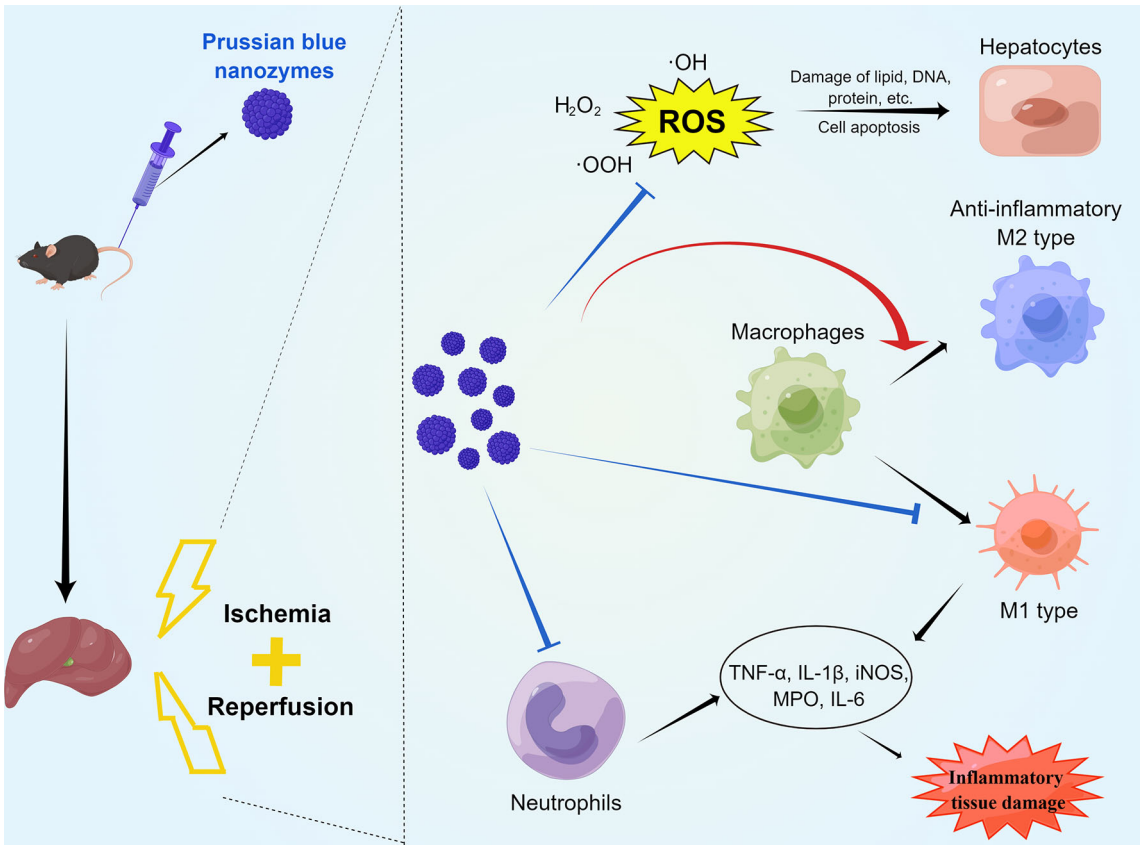

SCHEME 1 | Schematic diagram of the mechanisms by which PB scavengers protect against hepatic ischemia reperfusion injury. Prophylactically administered, PB scavengers can alleviate hepatic ischemia reperfusion injury by scavenging ROS in primary hepatocytes, reducing neutrophil infiltration and promoting macrophage polarization to the anti-inflammatory M2 type. Figure drawn by Figuredraw (www.Figuredraw.com).

offers clues to the application of nanozyme therapy to other liver diseases, such as fatty liver disease and drug-induced liver injury. PB scavengers have also shown other advantageous characteristics, including stability in blood, biocompatibility, biodegradability, and low cytotoxicity. In addition, they are easy to prepare and at low cost; have adjustable morphology and size and have high catalytic activity. These characteristics of PB scavenger can overcome some of the drawbacks of other clinically relevant antioxidants, such as poor solubility, insufficient target specificity, and systemic toxicity. Additional studies are needed to determine the optimum concentration for PB scavenger treatment and methods improving the targeting of PB scavengers to the liver. In addition, PB scavengers may act as drug carriers, combining with other drugs to achieve greater therapeutic effect in ROS-associated and inflammatory diseases.

4. CONCLUSION

This study described the synthesis of a biocompatible ROS scavenger using FDA-approved components. The synthesized PB scavengers effectively protected the liver from IRI by scavenging ROS in hepatocytes and macrophages, reducing apoptosis and alleviating inflammatory damage. Pretreatment with PB scavengers not only improved cell viability under high oxidative stress conditions but promoted macrophages polarization to M2 type and reduced the infiltration of neutrophils. PB scavengers may become a viable and effective treatment option for diseases associated with ROS stress and inflammation.

DATA AVAILABILITY STATEMENT

The original contributions presented in the study are included in the article/**Supplementary Material**. Further inquiries can be directed to the corresponding authors.

ETHICS STATEMENT

The animal study was reviewed and approved by School of Medicine, Shanghai Jiao Tong University.

AUTHOR CONTRIBUTIONS

YH and QXu had full access to all the data in the study and be responsible for the integrity of the data and the accuracy of the data analysis. Study design: KH, QXi and XC. Acquisition of data: YH, QXu, JZ, YY and YZ. Analysis and interpretation of data: YH, QXu and YP. Drafting of the manuscript: YH and QXu. Critical revision of the manuscript for important intellectual content: KH, QXi and XC. Statistical analysis: YH, QXu and JZ. Obtaining funding: KH, QXi and XC. Administrative, technical, or material support: YH, QXu, YY and YP. Supervision: KH, QXi and XC. All authors contributed to the article and approved the submitted version.

FUNDING

This study was supported by the Project of the Shanghai Municipal Health Commission (20204Y0012), the Innovative Research Team of High-Level Local Universities in Shanghai (SSMU-ZDCX20180802), the National Natural Science Foundation of China (81972205, 82172074), the Project of Shanghai Key Clinical Specialties (shslczdzk05801), the Seed Fund of Renji Hospital (RJZZ18-010), the Shenkang 3-year action plan (SHDC2020CR2003A, SHDC2020CR5012), Shanghai Rising-Star Program (21QA1407100), and the translational medicine national science and technology infrastructure (Shanghai) open project fund (TMSK-2020-004).

SUPPLEMENTARY MATERIAL

The Supplementary Material for this article can be found online at: https://www.frontiersin.org/articles/10.3389/fimmu.2022.891351/full#supplementary-material

REFERENCES

1. Peralta C, Jiménez-Castro MB, Gracia-Sancho J. Hepatic Ischemia and Reperfusion Injury: Effects on the Liver Sinusoidal Milieu. *J Hepatol* (2013) 59(5):1094–106. doi: 10.1016/j.jhep.2013.06.017
2. Saidi RF, Kenari SK. Liver Ischemia/Reperfusion Injury: An Overview. *J Invest Surg* (2014) 27(6):366–79. doi: 10.3109/08941939.2014.932473
3. Mao XL, Cai Y, Chen YH, Wang Y, Jiang XX, Ye LP, et al. Novel Targets and Therapeutic Strategies to Protect Against Hepatic Ischemia Reperfusion Injury. *Front Med* (2021) 8:757336. doi: 10.3389/fmed.2021.757336
4. Nemeth N, Peto K, Magyar Z, Klarik Z, Varga G, Oltean M, et al. Hemorheological and Microcirculatory Factors in Liver Ischemia-Reperfusion Injury-An Update on Pathophysiology, Molecular Mechanisms and Protective Strategies. *Int J Mol Sci* (2021) 22(4):1284. doi: 10.3390/ijms22041864
5. Pacher P, Haskó G. Endocannabinoids and Cannabinoid Receptors in Ischaemia-Reperfusion Injury and Preconditioning. *Br J Pharmacol* (2008) 153(2):252–62. doi: 10.1038/sj.bjp.0707582
6. Theodoraki K, Karmaniolou I, Tympa A, Tasoulis MK, Nastos C, Vassiliou I, et al. Beyond Preconditioning: Postconditioning as an Alternative Technique in the Prevention of Liver Ischemia-Reperfusion Injury. *Oxid Med Cell Longevity* (2016) 2016:8235921. doi: 10.1155/2016/8235921
7. Clarke G, Mergental H, Hann A, Perera M, Afford SC, Mirza DF. How Machine Perfusion Ameliorates Hepatic Ischaemia Reperfusion Injury. *Int J Mol Sci* (2021) 22(14):7523. doi: 10.3390/ijms22147523
8. Nakazato PCG, Victorino JP, Fina CF, Mendes KDS, Gomes MCJ, Evora PRB, et al. Liver Ischemia and Reperfusion Injury. Pathophysiology and New Horizons in Preconditioning and Therapy. *Acta Cirurgica Bras* (2018) 33 (8):723–35. doi: 10.1590/s0102-865020180080000008
9. Amreddy N, Babu A, Muralidharan R, Panneerselvam J, Srivastava A, Ahmed R, et al. Recent Advances in Nanoparticle-Based Cancer Drug and Gene Delivery. *Adv Cancer Res* (2018) 137:115–70. doi: 10.1016/bs.acr.2017.11.003
10. Thakur N, Manna P, Das J. Synthesis and Biomedical Applications of Nanoceria, a Redox Active Nanoparticle. *J Nanobiotechnol* (2019) 17(1):84. doi: 10.1186/s12951-019-0516-9
11. Gupta A, Mumtaz S, Li CH, Hussain I, Rotello VM. Combatting Antibiotic-Resistant Bacteria Using Nanomaterials. *Chem Soc Rev* (2019) 48(2):415–27. doi: 10.1039/c7cs00748e
12. Ni D, Wei H, Chen W, Bao Q, Rosenkrans ZT, Barnhart TE, et al. Ceria Nanoparticles Meet Hepatic Ischemia-Reperfusion Injury: The Perfect Imperfection. *Adv Materials* (2019) 31(40):e1902956. doi: 10.1002/adma.201902956
13. Li H, Sun JJ, Chen GY, Wang WW, Xie ZT, Tang GF, et al. Carnosic Acid Nanoparticles Suppress Liver Ischemia/Reperfusion Injury by Inhibition of Ros, Caspases and Nf-Kb Signaling Pathway in Mice. *Biomed Pharmacother* (2016) 82:237–46. doi: 10.1016/j.biopha.2016.04.064
14. Esposito V, Traversa E. Design of Electroceramics for Solid Oxides Fuel Cell Applications: Playing With Ceria. *J Am Ceram Soc* (2008) 91(4):1037–51. doi: 10.1111/j.1551-2916.2008.02347.x
15. Dunnick KM, Pillai R, Pisane KL, Stefaniak AB, Sabolsky EM, Leonard SS. The Effect of Cerium Oxide Nanoparticle Valence State on Reactive Oxygen Species and Toxicity. *Biol Trace Element Res* (2015) 166(1):96–107. doi: 10.1007/s12011-015-0297-4
16. Kwon HJ, Kim D, Seo K, Kim YG, Han SI, Kang T, et al. Ceria Nanoparticle Systems for Selective Scavenging of Mitochondrial, Intracellular, and Extracellular Reactive Oxygen Species in Parkinson's Disease. *Angewandte Chemie Int Edition* (2018) 57(30):9408–12. doi: 10.1002/anie.201805052
17. Soh M, Kang D-W, Jeong H-G, Kim D, Kim DY, Yang W, et al. Ceria–Zirconia Nanoparticles as an Enhanced Multi-Antioxidant for Sepsis Treatment. *Angewandte Chemie Int Edition* (2017) 56(38):11399–403. doi: 10.1002/anie.201704904
18. Busquets MA, Estelrich J. Prussian Blue Nanoparticles: Synthesis, Surface Modification, and Biomedical Applications. *Drug Discov Today* (2020) 25 (8):1431–43. doi: 10.1016/j.drudis.2020.05.014
19. Zhang W, Hu S, Yin JJ, He W, Lu W, Ma M, et al. Prussian Blue Nanoparticles as Multienzyme Mimetics and Reactive Oxygen Species Scavengers. *J Am Chem Soc* (2016) 138(18):5860–5. doi: 10.1021/jacs.5b12070
20. Zhang K, Tu M, Gao W, Cai X, Song F, Chen Z, et al. Hollow Prussian Blue Nanozymes Drive Neuroprotection Against Ischemic Stroke *Via* Attenuating Oxidative Stress, Counteracting Inflammation, and Suppressing Cell Apoptosis. *Nano Lett* (2019) 19(5):2812–23. doi: 10.1021/acs.nanolett.8b04729
21. Feng L, Dou C, Xia Y, Li B, Zhao M, Yu P, et al. Neutrophil-Like Cell-Membrane-Coated Nanozyme Therapy for Ischemic Brain Damage and Long-Term Neurological Functional Recovery. *ACS Nano* (2021) 15 (2):2263–80. doi: 10.1021/acsnano.0c07973
22. Ma X, Hao J, Wu J, Li Y, Cai X, Zheng Y. Prussian Blue Nanozyme as a Pyroptosis Inhibitor Alleviates Neurodegeneration. *Adv Mater* (2022) 34 (15):2106723. doi: 10.1002/adma.202106723
23. Feng L, Dou C, Xia Y, Li B, Zhao M, El-Toni AM, et al. Enhancement of Nanozyme Permeation by Endovascular Interventional Treatment to Prevent Vascular Restenosis *Via* Macrophage Polarization Modulation. *Adv Funct Mater* (2020) 30(52):2006581. doi: 10.1002/adfm.202006581
24. Sahu A, Jeon J, Lee MS, Yang HS, Tae G. Antioxidant and Anti-Inflammatory Activities of Prussian Blue Nanozyme Promotes Full-Thickness Skin Wound Healing. *Materials Sci Eng C Materials Biol Appl* (2021) 119:111596. doi: 10.1016/j.msec.2020.111596
25. Zhao J, Gao W, Cai X, Xu J, Zou D, Li Z, et al. Nanozyme-Mediated Catalytic Nanotherapy for Inflammatory Bowel Disease. *Theranostics* (2019) 9 (10):2843–55. doi: 10.7150/thno.33727
26. Wen Y, Feng D, Wu H, Liu W, Li H, Wang F, et al. Defective Initiation of Liver Regeneration in Osteopontin-Deficient Mice After Partial Hepatectomy

Due to Insufficient Activation of Il-6/Stat3 Pathway. *Int J Biol Sci* (2015) 11 (10):1236–47. doi: 10.7150/ijbs.12118
27. Xie X, Zhao J, Gao W, Chen J, Hu B, Cai X, et al. Prussian Blue Nanozyme-Mediated Nanoscavenger Ameliorates Acute Pancreatitis *Via* Inhibiting Tlrs/Nf-Kb Signaling Pathway. *Theranostics* (2021) 11(7):3213–28. doi: 10.7150/thno.52010
28. Zhao J, Cai X, Gao W, Zhang L, Zou D, Zheng Y, et al. Prussian Blue Nanozyme With Multienzyme Activity Reduces Colitis in Mice. *ACS Appl Materials Interf* (2018) 10(31):26108–17. doi: 10.1021/acsami.8b10345
29. Samain L, Grandjean F, Long GJ, Martinetto P, Bordet P, Strivay D. Relationship Between the Synthesis of Prussian Blue Pigments, Their Color, Physical Properties, and Their Behavior in Paint Layers. *J Phys Chem C* (2013) 117(19):9693–712. doi: 10.1021/jp3111327
30. Alfonso-Prieto M, Biarnés X, Vidossich P, Rovira C. The Molecular Mechanism of the Catalase Reaction. *J Am Chem Soc* (2009) 131 (33):11751–61. doi: 10.1021/ja9018572
31. Gligorovski S, Strekowski R, Barbati S, Vione D. Environmental Implications of Hydroxyl Radicals ((•)Oh). *Chem Rev* (2015) 115(24):13051–92. doi: 10.1021/cr500310b
32. Gao L, Zhuang J, Nie L, Zhang J, Zhang Y, Gu N, et al. Intrinsic Peroxidase-Like Activity of Ferromagnetic Nanoparticles. *Nat Nanotechnol* (2007) 2(9):577–83. doi: 10.1038/nnano.2007.260
33. Komkova MA, Karyakina EE, Karyakin AA. Catalytically Synthesized Prussian Blue Nanoparticles Defeating Natural Enzyme Peroxidase. *J Am Chem Soc* (2018) 140(36):11302–7. doi: 10.1021/jacs.8b05223
34. Yazdani HO, Chen HW, Tohme S, Tai S, van der Windt DJ, Loughran P, et al. Il-33 Exacerbates Liver Sterile Inflammation by Amplifying Neutrophil Extracellular Trap Formation. *J Hepatol* (2017) 68(1):130. doi: 10.1016/j.jhep.2017.09.010
35. Mills EL, O'Neill LA. Reprogramming Mitochondrial Metabolism in Macrophages as an Anti-Inflammatory Signal. *Eur J Immunol* (2016) 46 (1):13–21. doi: 10.1002/eji.201445427
36. Liu H, Man K. New Insights in Mechanisms and Therapeutics for Short- and Long-Term Impacts of Hepatic Ischemia Reperfusion Injury Post Liver Transplantation. *Int J Mol Sci* (2021) 22(15):8210. doi: 10.3390/ijms22158210
37. Ferreira-Silva M, Faria-Silva C, Baptista PV, Fernandes E, Fernandes AR, Corvo ML. Drug Delivery Nanosystems Targeted to Hepatic Ischemia and Reperfusion Injury. *Drug Deliv Trans Res* (2021) 11(2):397–410. doi: 10.1007/s13346-021-00915-8
38. Taha MS, Padmakumar S, Singh A, Amiji MM. Critical Quality Attributes in the Development of Therapeutic Nanomedicines Toward Clinical Translation. *Drug Deliv Trans Res* (2020) 10(3):766–90. doi: 10.1007/s13346-020-00744-1
39. Hua S, de Matos MBC, Metselaar JM, Storm G. Current Trends and Challenges in the Clinical Translation of Nanoparticulate Nanomedicines: Pathways for Translational Development and Commercialization. *Front Pharmacol* (2018) 9:790. doi: 10.3389/fphar.2018.00790
40. Moyano P, de Frias M, Lobo M, Anadon MJ, Sola E, Pelayo A, et al. Cadmium Induced Ros Alters M1 and M3 Receptors, Leading to Sn56 Cholinergic Neuronal Loss, Through Ache Variants Disruption. *Toxicology* (2018) 394:54–62. doi: 10.1016/j.tox.2017.12.006
41. Yuan Y, Chen Y, Peng T, Li L, Zhu W, Liu F, et al. Mitochondrial Ros-Induced Lysosomal Dysfunction Impairs Autophagic Flux and Contributes to M1 Macrophage Polarization in a Diabetic Condition. *Clin Sci (Lond)* (2019) 133 (15):1759–77. doi: 10.1042/cs20190672

Conflict of Interest: The authors declare that the research was conducted in the absence of any commercial or financial relationships that could be construed as a potential conflict of interest.

Publisher's Note: All claims expressed in this article are solely those of the authors and do not necessarily represent those of their affiliated organizations, or those of the publisher, the editors and the reviewers. Any product that may be evaluated in this article, or claim that may be made by its manufacturer, is not guaranteed or endorsed by the publisher.

frontiers | Frontiers in Immunology

REVIEW
published: 10 June 2022
doi: 10.3389/fimmu.2022.905423

The Role of NLRP3 Inflammasome Activation Pathway of Hepatic Macrophages in Liver Ischemia–Reperfusion Injury

Tong Wu[1], *Cheng Zhang*[2], *Tianfeng Shao*[3], *Jianzhong Chen*[4*] and *Diyu Chen*[2*]

[1] School of Medicine, Zhejiang University, Hangzhou, China, [2] Division of Hepatobiliary and Pancreatic Surgery, Department of Surgery, The First Affiliated Hospital, Zhejiang University School of Medicine, Hangzhou, China, [3] Department of General Practice, Shaoxing Yuecheng District Tashan Street Community Health Service Center, Shaoxing, China, [4] Institute of Immunology, School of Medicine, Zhejiang University, Hangzhou, China

Ischemia-reperfusion injury (IRI) is considered an inherent component involved in liver transplantation, which induce early organ dysfunction and failure. And the accumulating evidences indicate that the activation of host innate immune system, especially hepatic macrophages, play a pivotal role in the progression of LIRI. Inflammasomes is a kind of intracellular multimolecular complexes that actively participate in the innate immune responses and proinflammatory signaling pathways. Among them, NLRP3 inflammasome is the best characterized and correspond to regulate caspase-1 activation and the secretion of proinflammatory cytokines in response to various pathogen-derived as well as danger-associated signals. Additionally, NLRP3 is highly expressed in hepatic macrophages, and the assembly of NLRP3 inflammasome could lead to LIRI, which makes it a promising therapeutic target. However, detailed mechanisms about NLRP3 inflammasome involving in the hepatic macrophages-related LIRI is rarely summarized. Here, we review the potential role of the NLRP3 inflammasome pathway of hepatic macrophages in LIRI, with highlights on currently available therapeutic options.

Keywords: inflammasome, NLRP3, ischemia reperfusion injury, hepatic macrophage, liver transplantation

OPEN ACCESS

Edited by:
Qiang Wei,
Zhejiang University School of Medicine, China

Reviewed by:
Jinzhen Cai,
The Affiliated Hospital of Qingdao University, China
Jin Bin,
Shandong University, China

***Correspondence:**
Jianzhong Chen
chenjianzhong@zju.edu.cn
Diyu Chen
21618112@zju.edu.cn

Specialty section:
This article was submitted to Molecular Innate Immunity, a section of the journal Frontiers in Immunology

Received: *27 March 2022*
Accepted: *12 May 2022*
Published: *10 June 2022*

Citation:
Wu T, Zhang C, Shao T, Chen J and Chen D (2022) The Role of NLRP3 Inflammasome Activation Pathway of Hepatic Macrophages in Liver Ischemia–Reperfusion Injury. Front. Immunol. 13:905423. doi: 10.3389/fimmu.2022.905423

INTRODUCTION

The innate immunity acts as the first line of defense that recognizes and eradicates pathogens in human. It is implemented in the presence of pathogen-associated molecular patterns (PAMPs) (such as bacteria, viruses and parasites) or damage-associated molecular patterns (DAMPs) through pattern recognition receptors (PRRs) (1–4). In the past decades, various kinds of PRRs (inflammasomes) were discovered in succession, such as Nod-like receptor protein 1 (NLRP1), NLRP2, NLRP3, absent in melanoma 2 (AIM2) and NLR family CARD domain containing 4 (NLRC4) (5, 6). As the most well studied inflammasome, NLRP3 has been confirmed to be a critical component that mediates caspase-1 activation and cleavage of gasdermin D (GSDMD) in response to microbial infection and specific endogenous danger-related stimuli (7–11). Activated GSDMD

facilitate the formation of pore in the plasma membrane and trigger the pyroptotic cell death and enhance the secretion of inflammatory cytokines including IL-1β and IL-18 (12).

At present, liver transplantation (LT) is widely used as the most effective and definitive treatment for end-stage liver diseases, hepatic malignancies, acute fulminant hepatic failure, and metabolic disorders (13). During the LT surgery, the cell death in donor liver was exacerbated following the restoration of oxygen delivery. This special pathological disorder is concepted as liver ischemia reperfusion (I/R) injury (LIRI) (14). Due to the molecular characteristics, liver I/R could be categorized into two distinct stages. Followed by reopening of the spontaneous shunts, hepatocytes are deprived suddenly of oxygen and nutrient interruption. And this period is called ischemia stage. Then extended ischemia duration would lead to substantial parenchymal cell death. The other stage is reperfusion stage, in which the innate immunity and sterile inflammatory response are intensified. The macrophages in liver such as Kupffer cells (KCs) can be activated and play an important role in the context of LIRI (15). Recent studies have demonstrated that blocking the local inflammatory response in liver could effectively reduce LIRI. Thus, it is necessary to explore the potential strategies to prevent the innate immunity and inflammatory response activation during LIRI.

This review summarizes the recent advances in our understanding of the activation and regulation of the NLRP3 inflammasome activation, as well as its role in LIRI with highlights on the prevention of LIRI by inhibiting NLRP3 inflammasome aberrant activation.

THE NLRP3 INFLAMMASOME

The NLRP3 inflammasome complex consists of an amino-terminal pyrin domain (PYD), a central nucleotide-binding and oligomerization domain (NOD), and a C-terminal leucine-rich repeat (LRR) domain (7, 16, 17). The pyrin domain of NLRP3 frequently referred to apoptosis-associated speck-like protein (ASC), which initiates the assembly of inflammasome.

The NLRP3 inflammasome can be activated by a wide range of stimuli that include Candida albicans, bacteria that produce pore-forming toxins such as Staphylococcus aureus and Listeria monocytogenes, viruses (such as influenza virus) (5, 18). Moreover, it is identified that host-derived molecules (including extracellular ATP, hyaluronan, fibrillar amyloid-β peptide, extracellular glucose, monosodium urate (MSU) crystals, and uric acid *etc.)* are involved in the NLRP3 inflammasome activation (18). On the basis of structural and chemical differences between these stimuli, it is suggested that NLPR3 senses common cellular events induced by its stimuli, but does not directly bind to it. However, there is still no strong evidence to support this hypothesis. Currently, a two-signal model has been proposed for NLRP3 inflammasome activation. The first signal is responsible for initiating the NLRP3 inflammasome, which including microbial components or endogenous cytokines. The second signal from pore-forming toxins, extracellular ATP, or particulate matter activates the NLRP3 inflammasome.

The excessive molecular and cellular signaling events have been clearly recognized as the major consequences of NLRP3 stimuli, compromising reactive oxygen species (ROS), mitochondrial dysfunction, lysosomal damage, and ionic flux (10, 19). Proposed as the common signal for NLRP3 inflammasome activation, it is observed that the level of ROS increased after the NLRP3 stimuli treatment. Lysosomal NADPH oxidase is deemed to be the origin of ROS generation, and the accumulation process of ROS may be caused by respiratory function, which is closely related to the activation of inflammasome. Furthermore, it is illustrated that mitochondrial ROS (mtROS) is also a kind of production in dysfunctional mitochondria (20). As an essential element, mtROS can be continuously increased with the release of LPS and ATP and mitochondrial DNA (mtDNA) into the cytoplasm. This process is important for the mtROS-dependent manner of NLRP3 inflammasome activation. Furthermore, some kinds of particulate matter (such as MSU, alum, silica, asbestos, amyloid-β, cholesterol crystals, and calcium crystals) induces NLRP3 inflammasome activation in macrophages. Moreover, lysosomal damage after phagocytosis results in the leakage of lysosomal contents into the cytosol. However, the mechanism involves in lysosomal disruption to NLRP3 inflammasome activation remains unclear. Lysosomal acidification, leakage of active lysosomal enzymes such as Cathepsins B, L, C, S, and X may account for NLRP3 inflammasome activation. The ionic flux events, such as K^+ efflux, Ca^{2+} mobilization, Cl^- efflux, and Na^+ influx, could all be accelerated by NLRP3 stimuli, which are implicated in maintaining the NLRP3 inflammasome activity (**Figure 1**).

HEPATIC MACROPHAGE PARTICIPATING IN LIRI

Hepatic macrophages play an important role in the pathogenesis of LIRI and have been proposed as the primary cells for NLRP3 activation (15). Recent studies have revealed that hepatic macrophages are a heterogeneous population of innate immune cells. According to the molecular characteristics, hepatic macrophages can be categorized into liver-resident (KCs and liver capsular macrophages (LCMs)) and non-resident (monocyte-derived and peritoneal macrophages) cells (15).

KCs account for 20%~35% of all non-parenchymal cells in the liver and 80%~90% of tissue macrophages presented in the body. KCs are marked as $CD45^+F4/80^{high}CD11b^{low}CLEC4F^+$ cells in mice (21). Analyzing the single-cell RNA-sequencing data, the researchers identified two distinct subtypes of KCs in liver: the immunoregulatory KCs and the pro-inflammatory KCs (22).

Act as the microenvironment sensor, KCs resides at the luminal side of the hepatic sinusoidal endothelium. They are essential for maintaining local homeostasis, such as clearance of pathogens of systemic and gut origin, and regulation of iron

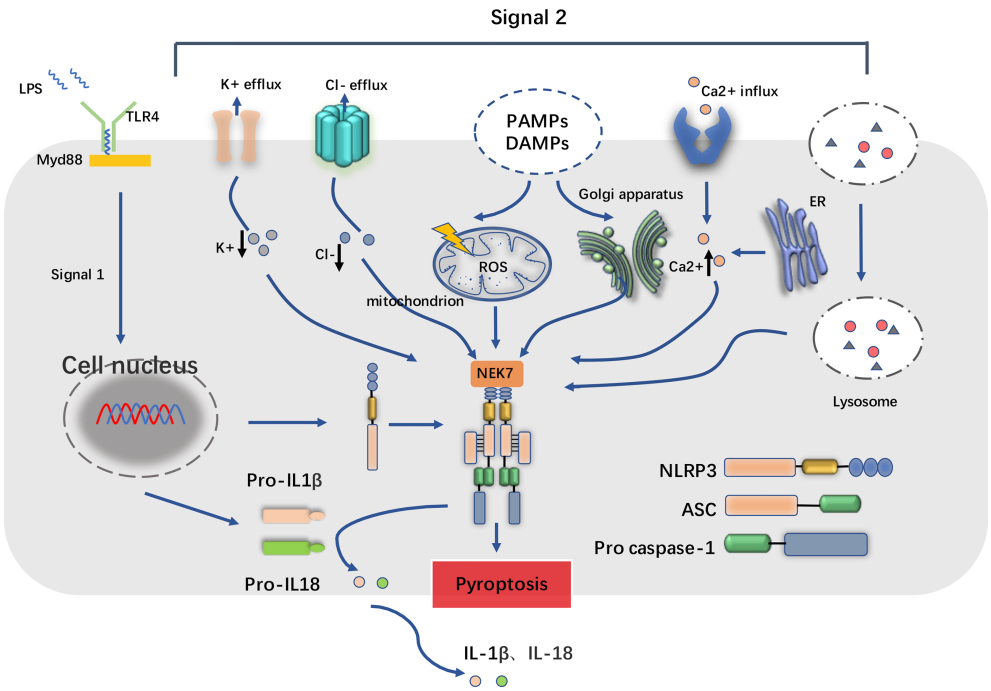

FIGURE 1 | Basic structure of NLRP3 inflammasome and its two-step process of priming and activation. The NOD-like receptor family pyrin domain containing 3 (NLRP3) inflammasome complex consists of NLRP3 monomers, apoptosis-associated speck-like protein containing a CARD (ASC) and the pro casepase-1. When inflammatory stimuli such as lipopolysaccharide (LPS) sensed by Toll-like receptors (TLRs) (e.g., TLR4) and cytokine receptors, the downstream singling adaptors such as MyD88 cooperatively contribute to the priming process, which upregulate the transcription of NLRP3 and IL1β/IL18, accumulate cytoplasmic pro-IL1β/pro-IL18. In addition, NEK7, one of the serine/threonine kinases, is also required for the activation of NLRP3 inflammasome. In the second step, pathogen-associated molecular patterns (PAMPs) and damage-associated molecular patterns (DAMPs) trigger cellular events including reactive oxygen species (ROS) release, endoplasmic reticulum stress, mitochondrial dysfunction, lysosomal damage, and ionic flux such as K+ efflux, Cl- efflux and Ca2+ influx. These facilitate the cleavage of pro casepase-1 into active form casepase-1, and in turn the maturation and release of IL1β/IL18, consequently leading to the inflammatory cell death known as pyroptosis.

metabolism. KCs play a vital role in the liver homeostasis by utilizing followed functions: (i) clearance of metabolic waste and cellular debris (22–24); (ii) preservation of iron homeostasis *via* engulf of red blood cells and the subsequent recycling of iron (25–28); (iii) regulation of cholesterol metabolism through the production of cholesteryl ester transfer proteins (29); (iv) mediation of antimicrobial defense (30, 31) and (v) promotion of immunological tolerance.

LCMs are newly identified murine liver-residents of the $CD11b^{+}F4/80^{+}CX3CR1^{+}MHC\ II^{+}$ phenotype. LCMs do not express classic Kupffer cell (TIM4 and CLEC4F) or monocyte-derived macrophage (Ly6C) markers and form a contiguous cellular network in the hepatic capsule (23). LCMs sense peritoneal bacteria and promote recruitment of neutrophil into the capsule. When LCMs populated in the hepatic sinusoids, they are responsible for monitoring the expand of intra-peritoneal bacteria. In order to avoid the exhaustion of LCMs, blood monocytes could supply and mature LCMs in the steady-state. Despite the growing recognition of the importance of LCMs in hepatic pathogen defense, whether LCMs play a role in LIRI-induced sterile inflammation in the liver remains unclear and needs to be further addressed.

Monocyte-derived macrophages (MoMϕs) are differentiated from bone marrow (BM) $CX3CR1^{+}CD117^{+}Lin^{-}$ progenitor cells-derived circulating monocytes. In mice, MoMϕs are $CD11b^{+}$, F4/80intermediate (int), $Ly6C^{+}$ and $CSF1R^{+}$ while KCs are $CD11b^{low}$, $F4/80^{high}$ and $Clec4F^{+}$ (21, 24). Hepatic MoMϕs could be classified into two main subpopulations on the basis of Ly6C expression: Ly6C high and Ly6C low MoMϕs in mouse models of liver diseases,

Based on the recent single-cell RNA-sequencing results, it is illustrated that $CD68^{+}MARCO^{+}$ KCs, $CD68^{+}MARCO^{-}$ macrophages, and $CD14^{+}$ monocytes are specifically enriched in the liver microenvironment (26). Through the further integrative analysis, it is also found that $CD68^{+}MARCO^{+}$ KCs could be recognized by immune tolerance (e.g., VSIG4) and inflammation inhibiting (e.g., CD163 and HMOX1) related genes. $CD68^{+}MARCO^{-}$ macrophages as recruited proinflammatory macrophages have a similar transcriptional profile (e.g., C1QC, IL-18, S100A8/9). However, peripheral $CD14^{+}$ monocytes show significantly proinflammatory responses than both $CD68^{+}MARCO^{-}$ macrophages and hepatic $CD14^{+}$ monocytes.

In the steady environment, KCs self-renew *via* homeostatic repopulation (27). Under cellular stress, the self-renewal of KCs

would be hampered, which results in the suppression of their homeostatic repopulation. Sterile inflammation (such as LIRI) decrease KC numbers, which would be replaced by bone marrow-derived monocytes replacing in a mouse LIRI model (28). Notably, infiltrating Ly6C^{high}-CCR2^{high}-CX3CR1^{low} monocyte-derived macrophages (MoMFs) show great plasticity maintaining phenotype and functions. In mouse models after depletion of Kupffer cell by diphtheria toxin receptor (DTR), MoMFs accumulate the hepatic macrophage differentiated towards functional and self-renewing KCs (21).

Since their depletion promotes liver inflammation, KCs undergoing cell death in response to LIRI may affect homeostasis and activate inflammatory macrophage in mice (28). Being in contact with DAMPs produced by dead or moribund LIRI-stressed cells, KCs are activated through sensing early organ damage *via* PRRs (**Figure 2**). Then these activated KCs secrete cytokines and chemokines that recruit circulating monocytes, neutrophils and T cells to promote liver injury (29). Liver sterile inflammation recruits new populations of extrahepatic macrophages (emergency repopulation) such as MoMFs and peritoneal macrophages. These monocytes consist of a bone marrow-derived pro-inflammatory Ly6C^{high}CCR2^{high}CX3CR1^{low} subset and an anti-inflammatory Ly6C^{low}CCR2^{low}CX3CR1^{high} subset in mice (27). Human monocytes are similarly defined as CX3CR1^{low} CD14^{+}CD11b^{high}CD11c^{+}CD62L^{+-}CD16^{low} or CX3CR1^{high} CD14^{low}CD16^{+}CD11b^{+}CD11c^{high} subsets. In summary, the above hepatic macrophages play a proinflammatory effect after sensing DAMPs and mediate pathogenesis in LIRI.

THE NLRP3 ACTIVATION OF LIVER MACROPHAGES IN LIRI

Constant monitoring for infection or non-infectious threats to tissue integrity is one of the major immune functions of liver-derived KCs (30). During hepatic injury, KCs can promote inflammasome formation while recognizing DAMPs or PAMPs that bind to PRRs such as NLRs. In the early stage of LIRI, ischemic injury leads to hypoxia in hepatocytes, which further causes pH changes and ATP depletion. These changes can increase the liver's dependence on glycogen for energy production. At the same time, these events mentioned above promote the release of ROS, increase the intracellular calcium concentration, and exacerbate organelle damage, ultimately leading to cell damage or death.

Reperfusion after liver transplantation can enhance the inflammatory cascade, thereby aggravating liver injury. Furthermore, the destruction and death of hepatocytes and sinusoidal endothelial cells can trigger the release of DAMPs such as ATP and HMGB1. These DAMPs potentially activate hepatic macrophages such as KCs to awaken innate inflammatory responses, which may assemble the NLRP3

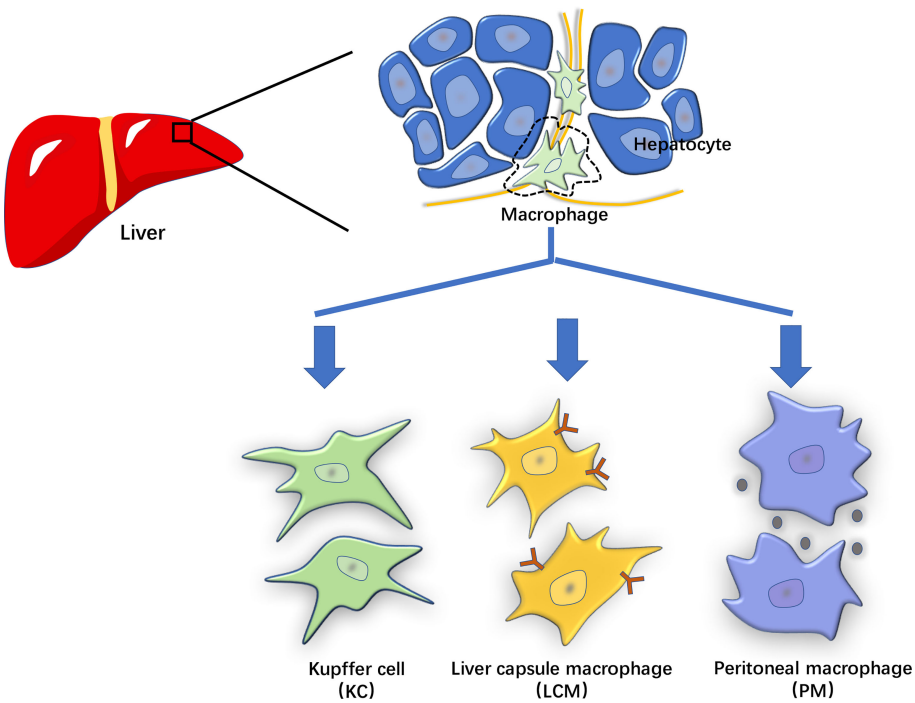

FIGURE 2 | The characterization of hepatic macrophages. The hepatic macrophages based on their origin and molecular features can be classified into liver-resident cells such as Kupffer cells (KCs) and liver capsular macrophages (LCMs), and non-resident cells such as monocyte-derived and peritoneal macrophages (PMs).

inflammasome and activate pyroptosis-regulated signaling pathways (31). These macrophages are critical in the mediation of LIRI, not only for recognizing damage-associated molecules to initiate inflammation and recruit immune cells, but also to help end inflammation and repair tissue damage.

The potential role of NLRP3 inflammasome activation pathway in LIRI has been investigated both *in vitro* and *in vivo* (32–34). Through the experiments, it was confirmed that the activation of NLRP3 inflammasome play a vital part in followed inflammatory response (33, 35). But utilizing the NLRP3 inflammasome inhibitors may mitigate hepatic inflammation through different signaling pathway.

Since both NLRP3 and caspase-1 knockout attenuated the inflammatory response in the LIRI mouse model, and these two genes are upregulated during injury. Thus, it is thought that NLRP3 activation is critical for LIRI progression (32, 33). The knockdown of NLRP3 in model mice decreased the serum alanine aminotransferase levels, lowered the secretion of proinflammatory cytokines (such as IL-1β, IL-18, TNF-α, and IL-6) and inhibited the release of HMGB1. Overall, NLRP3 knockdown decreased the infiltration of inflammatory cells and protected the liver from I/R injury. Furthermore, depletion of myeloid cell-specific GSDMD suppressed warm LIRI, suggesting that macrophage and neutrophil pyroptosis have a driving role during hepatic ischemic stress (36). In the further study, some studies discovered that NLRP3 is highly expressed in macrophages and monocytes while downregulated in hepatocytes and stellate cells, which also indicating that macrophages are the main effectors (37–39). Liver I/R stimuli upregulates NLRP3, but not ASC that containing a caspase recruitment domain. This suggests a feed-back pathway of NLRP3 inflammasome activation exists in LIRI, and it might be exploited for therapeutic purpose (35).

It is reported that aged liver receivers are sensitive to the liver I/R injury. Using integrative analysis, Zhong et al. showed that the STING-NLRP3 pathway is responsible for the proinflammatory response of aged macrophages in elderly patients (40). Additionally, aggravated liver I/R injury was found in db/db mice with increased ROS expression. N-Acetyl-L-cysteine (NAC) treatment significantly inhibited hepatocyte NLRP3 inflammasome activation and pyroptosis in db/db mice after I/R, suggesting that ROS plays an important role in mediating hepatocyte pyroptosis in the diabetic setting (41).

Studies have shown that both exosomes and pyroptosis play a role in LIRI and are essential in neuronal death. In the LIRI rat model, the NLRP3 inflammasome is activated and caspase-1-dependent pyroptosis occurs in the hippocampus and cortex. Serum-derived exosomes from LIRI-challenged rats not only penetrated the blood-brain barrier (BBB) but also caused neuronal cell pyroptosis. Furthermore, in the exosome challenge group, ROS and malondialdehyde (MDA) production were induced, while the NLRP3 inhibitor (MCC950) attenuated LIRI-mediated pyroptosis of hippocampal and cortical neurons (42).

Robust activation of the NLRP3 inflammasome was demonstrated in KCs during LIRI (33). Huang et al. showed that during liver I/R, endogenous extracellular histones activate the NLRP3 inflammasome in KCs through TLR9-dependent production of ROS. Activation of the NLRP3 inflammasome can also regulate neutrophils and inflammatory monocytes infiltrating the liver after I/R. However, loss of NLRP3 provides a stable innate immune environment. Also, the numbers of DCs, neutrophils and inflammatory monocytes remained unchanged compared to liver I/R. Sham KO mice. These data suggest that depletion of the NLRP3 inflammasome downregulates the innate immune response by reducing the influx of innate immune cells in the ischemic lobe after liver I/R (33). Inhibition of the NLRP3 inflammasome also attenuates I/R-mediated hepatocyte injury and prevents several pro-inflammatory cytokines such as IL-1β, IL-18, HMGB1 and IL-6 by preventing the stimulation of caspase-1, and the release of NF-κB pathway. Inoue et al. found that NLRP3(-/-) neutrophils reduced the concentration of keratinocyte-derived chemokine-induced intracellular calcium, ROS activation, and actin assembly formation, resulting in impaired migratory activity. NLRP3 can regulate chemokine-mediated functions and neutrophil recruitment, leading to liver I/R injury independent of the inflammasome. These discoveries reveal a novel role for NLRP3 in the pathophysiology of LIRI (35).

Activation of NLRP3 in LIRI is regulated by various signaling pathway. The heat shock factor 1 (HSF1)-β-catenin axis mediates the activation of NLRP3 by regulating the X-box binding protein 1 (XBP1) signaling axis. HSF1 activation promoted β-catenin expression, which in turn inhibited XBP1, resulting in NLRP3 inactivation and LIRI mitigation (43). Recently, dexmedetomidine was reported to show therapeutic potential by repressing the activation of NLRP3 inflammasome and alleviating LIRI *via* the miR- 494/JUND/PI3K/AKT/Nrf2 axis (44).

Thioredoxin-interacting protein(TXNIP) is an oxidative sensor that in homeostasisand is released after ROS stimulation (45)., TXNIP interacts with NLRP3 to promote its activation. Hypothermic oxygenated perfusion (HOPE) may modulate the TXNIP/NLRP3 inflammasome pathway from which liver injuries were reduced and liver function improved (46).

Autophagy, characterized by conserved autophagy, contributes to the degradation of intracellular components such as dysfunctional organelles, macromolecular complexes, long-lived cytoplasmic proteins, and foreign bodies. Recent studies have shown that autophagy negatively regulates the activation of the NLRP3 inflammasome during LIRI. Xue et al. reported that the antioxidant lycopene, elevated autophagosomes and increased protein levels of LC3B in KCs, and the autophagy inhibitor 3-methyladenine blocked the inhibitory effect of lycopene on the NLRP3 inflammasome in KCs (47). It is further demonstrated that lycopene promoted Nrf2/heme oxygenase 1 (HO-1) pathway activation and suppressed the NLRP3 inflammasome activation *via* enhancing KC autophagy (47). The expression of V-ATPase D2 subunit (ATP6V0D2) in liver macrophages was upregulated after LIRI which can promote the formation of autophagolysosomes to increase autophagy flux to limit the activation of liver inflammation

(48). Eva-1 homologous gene A (EVA1A) is a kind of lysosomal and endoplasmic reticulum-related protein that has been found to be involved in regulating autophagy and apoptosis (49). Knockdown of EVA1A in KCs inhibits the formation of autophagosomes through inhibiting formation of ATG5/ATG12 complex in I/R process. suppressed combined action with Atg16L1. Knockdown of transient receptor potential melastatin 2 (TRPM2) also prevents LIRI by inhibiting autophagy activation and NLRP3 inflammasome pathway, which is *via* the exogenous upregulation of LC3-II (50).

Abundant regulators inhibit NLRP3 inflammasomes activation to alleviate LIRI by regulating different pathways (51–62). Zarpou et al. found that Silibinin ameliorated inflammatory liver tissue injuries, including neutrophil and macrophage infiltration, hepatocyte degeneration, cytoplasmic vacuolation, vascular endothelial damages, and sinusoid dilation observed in the I/R group (51). Bruton's tyrosine kinase (BTK) is mainly expressed on KCs and sinusoidal endothelial cells, and BTK inhibitor ibrutinib effectively attenuates liver I/R injury by suppressing activation of the NLRP3 inflammasome in KCs (52). T3 and fisetin suppressed I/R liver injury-dependent AMPK pathway (63, 64). While the 12-hours fasting exerted beneficial effects on the prevention of LIRI by increasing serum β-hydroxybutyric acid (BHB), thus up regulated forkhead box transcription factor O1 (FOXO1) and HO-1, and by reducing the inflammatory responses and apoptotic cell death *via* the down-regulation of NF-κB and NLRP3 inflammasome (65). SET domain-containing protein 8 (SET8) negatively regulates liver I/R-mediated inflammatory response and ameliorates LIRI by suppressing microtubule affinity-regulating kinase 4 (MARK4)/NLRP3 inflammasome pathway (66). Docosahexaenoic acid (DHA) ameliorated I/R-induced injury by inhibiting pyroptosis of hepatocytes induced in liver I/R injury *in vivo* and *in vitro* through the PI3K/Akt pathway, providing a potential therapeutic option to prevent LIRI (67). The histone deacetylase Sirtuin-1 (SIRT1) inhibits the downstream XBP1/NLRP3 inflammatory pathway by activating miR-182, thus alleviating LIRI in mice (**Figure 3**) (68).

Isoflurane preconditioning significantly relieved liver IRI in mice and LPS-induced inflammation in liver macrophages by reduced intracellular Ca^{2+} levels, NF-κB translocation, and NLRP3 inflammasome activation in LPS-induced macrophages (69, 70). Iisoflurane pretreatment also inhibited caspase-11 expression and noncanonical pyroptosis-related production of cytokines (IL-1beta and IL-18). These findings suggest that isoflurane could be a pharmacological agent for liver IRI

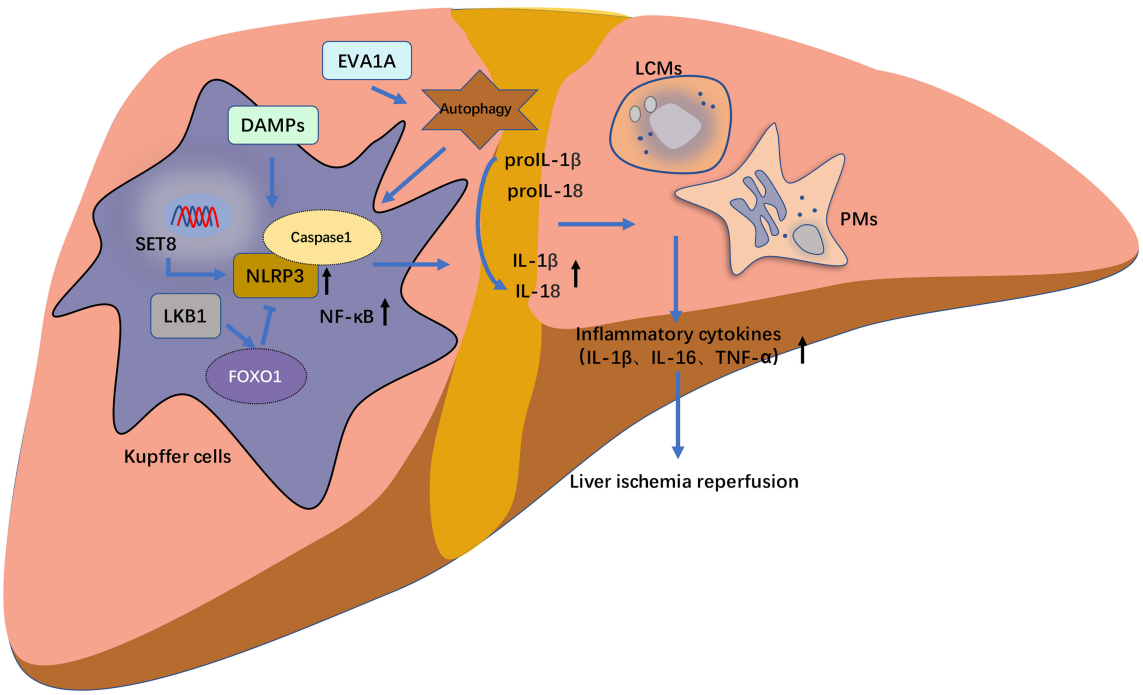

FIGURE 3 | The schematic diagram of NLRP3 inflammasome activation pathway of hepatic macrophages in liver ischemia–reperfusion injury (LIRI). The release of caspase-1 and following cell death of pyroptosis mediated by NLRP3 inflammasome activation pathway frequently occurs in hepatic macrophages including Kupffer cells (KCs), liver capsular macrophages (LCMs), monocyte-derived and peritoneal macrophages (PMs). These hepatic macrophages regulate on another and modulate the progression of LIRI-related NLRP3 inflammasome activation through the release of inflammatory cytokines such as IL1β, IL18 and TNF-α. In RAW 264.7 cells (mice macrophages), SET domain-containing protein 8 (SET8) negatively regulate LIRI inflammatory responses and ameliorate liver injury through the inhibition of MARK4/NLRP3 inflammasome activation pathway. Eva-1 homologous gene A (EVA1A) is upregulated in inflammatory responses of LIRI in Kupffer cells (KCs), in which its overexpression induces more formation of autophagosomes. Whereas EVA1A silencing can promote ASC activation and increase the cleavage of caspase 1 and IL1β by activating autophagy. Liver kinase B1 (LKB1) alleviates LIRI by inhibiting the activation of NLRP3 inflammasome and NF-κB. Additionally, this inhibitory effect could be mediated through the forkhead box protein O1 (FOXO1).

prevention and thus deserves more attention and further investigation (71).

CONCLUSION

Recent advances continue to improve our understanding of the mechanisms involved in activation of NLRP3 inflammasome in LIRI. The KCs play a main part in the process. However, the pathological sequences of other macrophages such as recently identified LCM and other macrophages need to be further investigated. The advance in the subject also will improve the development of clinical strategies against LIRI and prevention of liver transplantation failure.

AUTHOR CONTRIBUTIONS

TW: data analysis and writing. TS: statistics and data collection. CZ: statistics and program guidance. JC and DC: program guidance and supervision. All authors contributed to the article and approved the submitted version.

FUNDING

This study was supported by grants issued by the National Natural Science Foundation of China (82000618), Medical and Health Science and Technology Project of Zhejiang Province (2019KY290, 2021KY024).

REFERENCES

1. Gong T, Liu L, Jiang W, Zhou R. DAMP-Sensing Receptors in Sterile Inflammation and Inflammatory Diseases. *Nat Rev Immunol* (2020) 20:95–112. doi: 10.1038/s41577-019-0215-7
2. Zindel J, Kubes P. DAMPs, PAMPs, and LAMPs in Immunity and Sterile Inflammation. *Annu Rev Pathol* (2020) 15:493–518. doi: 10.1146/annurev-pathmechdis-012419-032847
3. Brubaker SW, Bonham KS, Zanoni I, Kagan JC. Innate Immune Pattern Recognition: A Cell Biological Perspective. *Annu Rev Immunol* (2015) 33:257–90. doi: 10.1146/annurev-immunol-032414-112240
4. Janeway CAJr., Medzhitov R. Innate Immune Recognition. *Annu Rev Immunol* (2002) 20:197–216. doi: 10.1146/annurev.immunol.20.083001.084359
5. Martinon F, Mayor A, Tschopp J. The Inflammasomes: Guardians of the Body. *Annu Rev Immunol* (2009) 27:229–65. doi: 10.1146/annurev.immunol.021908.132715
6. Ross C, Chan AH, von Pein JB, Maddugoda MP, Boucher D, Schroder K. Inflammatory Caspases: Toward a Unified Model for Caspase Activation by Inflammasomes. *Annu Rev Immunol* (2022) 40:249–69. doi: 10.1146/annurev-immunol-101220-030653
7. Huang Y, Xu W, Zhou R. NLRP3 Inflammasome Activation and Cell Death. *Cell Mol Immunol* (2021) 18:2114–27. doi: 10.1038/s41423-021-00740-6
8. Xu T, Du Y, Fang XB, Chen H, Zhou DD, Wang Y, et al. New Insights Into Nod-Like Receptors (NLRs) in Liver Diseases. *Int J Physiol Pathophysiol Pharmacol* (2018) 10:1–16.
9. Moretti J, Blander JM. Increasing Complexity of NLRP3 Inflammasome Regulation. *J Leukoc Biol* (2021) 109:561–71. doi: 10.1002/JLB.3MR0520-104RR
10. Swanson KV, Deng M, Ting JP. The NLRP3 Inflammasome: Molecular Activation and Regulation to Therapeutics. *Nat Rev Immunol* (2019) 19:477–89. doi: 10.1038/s41577-019-0165-0
11. Maiorino L, Dassler-Plenker J, Sun L, Egeblad M. Innate Immunity and Cancer Pathophysiology. *Annu Rev Pathol* (2022) 17:425–57. doi: 10.1146/annurev-pathmechdis-032221-115501
12. Liu X, Zhang Z, Ruan J, Pan Y, Magupalli VG, Wu H, et al. Inflammasome-Activated Gasdermin D Causes Pyroptosis by Forming Membrane Pores. *Nature* (2016) 535:153–8. doi: 10.1038/nature18629
13. Kumar R, Anand U, Priyadarshi RN. Liver Transplantation in Acute Liver Failure: Dilemmas and Challenges. *World J Transplant* (2021) 11:187–202. doi: 10.5500/wjt.v11.i6.187
14. Papadopoulos D, Siempis T, Theodorakou E, Tsoulfas G. Hepatic Ischemia and Reperfusion Injury and Trauma: Current Concepts. *Arch Trauma Res* (2013) 2:63–70. doi: 10.5812/atr.12501
15. Hirao H, Nakamura K, Kupiec-Weglinski JW. Liver Ischaemia-Reperfusion Injury: A New Understanding of the Role of Innate Immunity. *Nat Rev Gastroenterol Hepatol* (2021) 19:239–56. doi: 10.1038/s41575-021-00549-8
16. Ohto U, Kamitsukasa Y, Ishida H, Zhang Z, Murakami K, Hirama C, et al. Structural Basis for the Oligomerization-Mediated Regulation of NLRP3 Inflammasome Activation. *Proc Natl Acad Sci U.S.A.* (2022) 119:e2121353119. doi: 10.1073/pnas.2121353119
17. Rahman T, Nagar A, Duffy EB, Okuda K, Silverman N, Harton JA. NLRP3 Sensing of Diverse Inflammatory Stimuli Requires Distinct Structural Features. *Front Immunol* (2020) 11:1828. doi: 10.3389/fimmu.2020.01828
18. Schroder K, Tschopp J. The Inflammasomes. *Cell* (2010) 140:821–32. doi: 10.1016/j.cell.2010.01.040
19. Sharma BR, Kanneganti TD. NLRP3 Inflammasome in Cancer and Metabolic Diseases. *Nat Immunol* (2021) 22:550–9. doi: 10.1038/s41590-021-00886-5
20. Zhou R, Yazdi AS, Menu P, Tschopp J. A Role for Mitochondria in NLRP3 Inflammasome Activation. *Nature* (2011) 469:221–5. doi: 10.1038/nature09663
21. Scott CL, Zheng F, De Baetselier P, Martens L, Saeys Y, De Prijck S, et al. Bone Marrow-Derived Monocytes Give Rise to Self-Renewing and Fully Differentiated Kupffer Cells. *Nat Commun* (2016) 7:10321. doi: 10.1038/ncomms10321
22. MacParland SA, Liu JC, Ma XZ, Innes BT, Bartczak AM, Gage BK, et al. Single Cell RNA Sequencing of Human Liver Reveals Distinct Intrahepatic Macrophage Populations. *Nat Commun* (2018) 9:4383. doi: 10.1038/s41467-018-06318-7
23. Sierro F, Evrard M, Rizzetto S, Melino M, Mitchell AJ, Florido M, et al. A Liver Capsular Network of Monocyte-Derived Macrophages Restricts Hepatic Dissemination of Intraperitoneal Bacteria by Neutrophil Recruitment. *Immunity* (2017) 47:374–388.e376. doi: 10.1016/j.immuni.2017.07.018
24. Krenkel O, Tacke F. Liver Macrophages in Tissue Homeostasis and Disease. *Nat Rev Immunol* (2017) 17:306–21. doi: 10.1038/nri.2017.11
25. Takenaka E, Van Vo A, Yamashita-Kanemaru Y, Shibuya A, Shibuya K. Selective DNAM-1 Expression on Small Peritoneal Macrophages Contributes to CD4(+) T Cell Costimulation. *Sci Rep* (2018) 8:15180. doi: 10.1038/s41598-018-33437-4
26. Zhao J, Zhang S, Liu Y, He X, Qu M, Xu G, et al. Single-Cell RNA Sequencing Reveals the Heterogeneity of Liver-Resident Immune Cells in Human. *Cell Discovery* (2020) 6:22. doi: 10.1038/s41421-020-0157-z
27. McDonald B, Kubes P. Innate Immune Cell Trafficking and Function During Sterile Inflammation of the Liver. *Gastroenterology* (2016) 151:1087–95. doi: 10.1053/j.gastro.2016.09.048
28. Yue S, Zhou H, Wang X, Busuttil RW, Kupiec-Weglinski JW, Zhai Y. Prolonged Ischemia Triggers Necrotic Depletion of Tissue-Resident Macrophages To Facilitate Inflammatory Immune Activation in Liver Ischemia Reperfusion Injury. *J Immunol* (2017) 198:3588–95. doi: 10.4049/jimmunol.1601428
29. Li P, He K, Li J, Liu Z, Gong J. The Role of Kupffer Cells in Hepatic Diseases. *Mol Immunol* (2017) 85:222–9. doi: 10.1016/j.molimm.2017.02.018
30. Zannetti C, Roblot G, Charrier E, Ainouze M, Tout I, Briat F, et al. Characterization of the Inflammasome in Human Kupffer Cells in Response to Synthetic Agonists and Pathogens. *J Immunol* (2016) 197:356–67. doi: 10.4049/jimmunol.1502301

31. Du Y, Zhong F, Cheng H, Li T, Chen Y, Tan P, et al. The Dietary Supplement Gamma-Oryzanol Attenuates Hepatic Ischemia Reperfusion Injury *via* Inhibiting Endoplasmic Reticulum Stress and HMGB1/NLRP3 Inflammasome. *Oxid Med Cell Longev* (2021) 2021:4628050. doi: 10.1155/2021/4628050
32. Zhu P, Duan L, Chen J, Xiong A, Xu Q, Zhang H, et al. Gene Silencing of NALP3 Protects Against Liver Ischemia-Reperfusion Injury in Mice. *Hum Gene Ther* (2011) 22:853–64. doi: 10.1089/hum.2010.145
33. Huang H, Chen HW, Evankovich J, Yan W, Rosborough BR, Nace GW, et al. Histones Activate the NLRP3 Inflammasome in Kupffer Cells During Sterile Inflammatory Liver Injury. *J Immunol* (2013) 191:2665–79. doi: 10.4049/jimmunol.1202733
34. Kim HY, Kim SJ, Lee SM. Activation of NLRP3 and AIM2 Inflammasomes in Kupffer Cells in Hepatic Ischemia/Reperfusion. *FEBS J* (2015) 282:259–70. doi: 10.1111/febs.13123
35. Inoue Y, Shirasuna K, Kimura H, Usui F, Kawashima A, Karasawa T, et al. NLRP3 Regulates Neutrophil Functions and Contributes to Hepatic Ischemia-Reperfusion Injury Independently of Inflammasomes. *J Immunol* (2014) 192:4342–51. doi: 10.4049/jimmunol.1302039
36. Li J, Zhao J, Xu M, Li M, Wang B, Qu X, et al. Blocking GSDMD Processing in Innate Immune Cells But Not in Hepatocytes Protects Hepatic Ischemia-Reperfusion Injury. *Cell Death Dis* (2020) 11:244. doi: 10.1038/s41419-020-2437-9
37. Csak T, Ganz M, Pespisa J, Kodys K, Dolganiuc A, Szabo G. Fatty Acid and Endotoxin Activate Inflammasomes in Mouse Hepatocytes That Release Danger Signals to Stimulate Immune Cells. *Hepatology* (2011) 54:133–44. doi: 10.1002/hep.24341
38. Petrasek J, Bala S, Csak T, Lippai D, Kodys K, Menashy V, et al. IL-1 Receptor Antagonist Ameliorates Inflammasome-Dependent Alcoholic Steatohepatitis in Mice. *J Clin Invest* (2012) 122:3476–89. doi: 10.1172/JCI60777
39. Boaru SG, Borkham-Kamphorst E, Tihaa L, Haas U, Weiskirchen R. Expression Analysis of Inflammasomes in Experimental Models of Inflammatory and Fibrotic Liver Disease. *J Inflammation (Lond)* (2012) 9:49. doi: 10.1186/1476-9255-9-49
40. Zhong W, Rao Z, Rao J, Han G, Wang P, Jiang T, et al. Aging Aggravated Liver Ischemia and Reperfusion Injury by Promoting STING-Mediated NLRP3 Activation in Macrophages. *Aging Cell* (2020) 19:e13186. doi: 10.1111/acel.13186
41. Shi C, Wang Q, Rao Z, Shi Y, Wei S, Wang H, et al. Diabetes Induces Hepatocyte Pyroptosis by Promoting Oxidative Stress-Mediated NLRP3 Inflammasome Activation During Liver Ischaemia and Reperfusion Injury. *Ann Transl Med* (2020) 8:739. doi: 10.21037/atm-20-1839
42. Zhang L, Liu H, Jia L, Lyu J, Sun Y, Yu H, et al. Exosomes Mediate Hippocampal and Cortical Neuronal Injury Induced by Hepatic Ischemia-Reperfusion Injury Through Activating Pyroptosis in Rats. *Oxid Med Cell Longev* (2019) 2019:3753485. doi: 10.1155/2019/3753485
43. Yue S, Zhu J, Zhang M, Li C, Zhou X, Zhou M, et al. The Myeloid Heat Shock Transcription Factor 1/Beta-Catenin Axis Regulates NLR Family, Pyrin Domain-Containing 3 Inflammasome Activation in Mouse Liver Ischemia/Reperfusion Injury. *Hepatology* (2016) 64:1683–98. doi: 10.1002/hep.28739
44. Wu Y, Qiu G, Zhang H, Zhu L, Cheng G, Wang Y, et al. Dexmedetomidine Alleviates Hepatic Ischaemia-Reperfusion Injury *via* the PI3K/AKT/Nrf2-NLRP3 Pathway. *J Cell Mol Med* (2021) 25:9983–94. doi: 10.1111/jcmm.16871
45. Yoshihara E. TXNIP/TBP-2: A Master Regulator for Glucose Homeostasis. *Antioxid (Basel)* (2020) 9:765. doi: 10.3390/antiox9080765
46. He W, Ye S, Zeng C, Xue S, Hu X, Zhang X, et al. Hypothermic Oxygenated Perfusion (HOPE) Attenuates Ischemia/Reperfusion Injury in the Liver Through Inhibition of the TXNIP/NLRP3 Inflammasome Pathway in a Rat Model of Donation After Cardiac Death. *FASEB J* (2018) 32:6212–27. doi: 10.1096/fj.201800028RR
47. Xue R, Qiu J, Wei S, Liu M, Wang Q, Wang P, et al. Lycopene Alleviates Hepatic Ischemia Reperfusion Injury *via* the Nrf2/HO-1 Pathway Mediated NLRP3 Inflammasome Inhibition in Kupffer Cells. *Ann Transl Med* (2021) 9:631. doi: 10.21037/atm-20-7084
48. Wang Z, Wang H, Chen X, Han S, Zhu Y, Wang H, et al. Inhibiting ATP6V0D2 Aggravates Liver Ischemia-Reperfusion Injury by Promoting NLRP3 Activation *via* Impairing Autophagic Flux Independent of Notch1/Hes1. *J Immunol Res* (2021) 2021:6670495. doi: 10.1155/2021/6670495
49. Wang Z, Han S, Chen X, Li X, Xia N, Pu L. Eva1a Inhibits NLRP3 Activation to Reduce Liver Ischemia-Reperfusion Injury *via* Inducing Autophagy in Kupffer Cells. *Mol Immunol* (2021) 132:82–92. doi: 10.1016/j.molimm.2021.01.028
50. Zhang T, Huang W, Ma Y. Down-Regulation of TRPM2 Attenuates Hepatic Ischemia/Reperfusion Injury Through Activation of Autophagy and Inhibition of NLRP3 Inflammasome Pathway. *Int Immunopharmacol* (2022) 104:108443. doi: 10.1016/j.intimp.2021.108443
51. Zarpou S, Mosavi H, Bagheri A, Malekzadeh Shafaroudi M, Khonakdar-Tarsi A. NF-kappaB and NLRP3 Gene Expression Changes During Warm Hepatic Ischemia-Reperfusion in Rats With and Without Silibinin. *Gastroenterol Hepatol Bed Bench* (2021) 14:267–75.
52. Song SH, Liu F, Zhao YY, Sun KY, Guo M, Li PL, et al. Bruton's Tyrosine Kinase Inhibitor Attenuates Warm Hepatic Ischemia/Reperfusion Injury *via* Modulation of the NLR Family Pyrin Domain Containing 3 Inflammasome. *Transplant Proc* (2020) 52:2947–54. doi: 10.1016/j.transproceed.2019.10.024
53. El-Sisi AEE, Sokar SS, Shebl AM, Mohamed DZ, Abu-Risha SE. Octreotide and Melatonin Alleviate Inflammasome-Induced Pyroptosis Through Inhibition of TLR4-NF-kappaB-NLRP3 Pathway in Hepatic Ischemia/Reperfusion Injury. *Toxicol Appl Pharmacol* (2021) 410:115340. doi: 10.1016/j.taap.2020.115340
54. Cao Q, Luo J, Xiong Y, Liu Z, Ye Q. 25-Hydroxycholesterol Mitigates Hepatic Ischemia Reperfusion Injury *via* Mediating Mitophagy. *Int Immunopharmacol* (2021) 96:107643. doi: 10.1016/j.intimp.2021.107643
55. Cai J, Zhang X, Chen P, Li Y, Liu S, Liu Q, et al. The ER Stress Sensor Inositol-Requiring Enzyme 1alpha in Kupffer Cells Promotes Hepatic Ischemia-Reperfusion Injury. *J Biol Chem* (2022) 298:101532. doi: 10.1016/j.jbc.2021.101532
56. Qin Y, Wang C, Xu S, Wu C, Wang S, Pan D, et al. G Protein-Coupled Receptor 30 Activation Protects Hepatic Ischemia-Reperfusion Injury of Liver Tissue Through Inhibiting NLRP3 in the Rat Model. *J Histotechnol* (2021) 44:27–36. doi: 10.1080/01478885.2020.1826175
57. Lin Y, Lin L, Gao L, Wang S, Wu B. Rev-Erbalpha Regulates Hepatic Ischemia-Reperfusion Injury in Mice. *Biochem Biophys Res Commun* (2020) 529:916–21. doi: 10.1016/j.bbrc.2020.06.152
58. Li X, Wu Y, Zhang W, Gong J, Cheng Y. Pre-Conditioning With Tanshinone IIA Attenuates the Ischemia/Reperfusion Injury Caused by Liver Grafts *via* Regulation of HMGB1 in Rat Kupffer Cells. *BioMed Pharmacother* (2017) 89:1392–400. doi: 10.1016/j.biopha.2017.03.022
59. Huang R, Zhao Z, Jiang X, Li W, Zhang L, Wang B, et al. Liposomal Chrysin Attenuates Hepatic Ischaemia-Reperfusion Injury: Possible Mechanism *via* Inhibiting NLRP3 Inflammasome. *J Pharm Pharmacol* (2022) 74:216–26. doi: 10.1093/jpp/rgab153
60. Gendy A, Elnagar MR, Soubh A, Al-Mokaddem A, El-Haddad A, El-Sayed MK. Morin Alleviates Hepatic Ischemia/Reperfusion-Induced Mischief: *In Vivo* and *in Silico* Contribution of Nrf2, TLR4, and NLRP3. *BioMed Pharmacother* (2021) 138:111539. doi: 10.1016/j.biopha.2021.111539
61. Dai J, Chen Q, Huang W, Shi K, Zhang Y, Li T, et al. Liver Kinase B1 Attenuates Liver Ischemia/Reperfusion Injury *via* Inhibiting the NLRP3 Inflammasome. *Acta Biochim Biophys Sin (Shanghai)* (2021) 53:601–11. doi: 10.1093/abbs/gmab030
62. Ghoneim ME, Abdallah DM, Shebl AM, El-Abhar HS. The Interrupted Cross-Talk of Inflammatory and Oxidative Stress Trajectories Signifies the Effect of Artesunate Against Hepatic Ischemia/Reperfusion-Induced Inflammasomopathy. *Toxicol Appl Pharmacol* (2020) 409:115309. doi: 10.1016/j.taap.2020.115309
63. Vargas R, Videla LA. Thyroid Hormone Suppresses Ischemia-Reperfusion-Induced Liver NLRP3 Inflammasome Activation: Role of AMP-Activated Protein Kinase. *Immunol Lett* (2017) 184:92–7. doi: 10.1016/j.imlet.2017.01.007
64. Pu JL, Huang ZT, Luo YH, Mou T, Li TT, Li ZT, et al. Fisetin Mitigates Hepatic Ischemia-Reperfusion Injury by Regulating GSK3beta/AMPK/NLRP3 Inflammasome Pathway. *Hepatobiliary Pancreat Dis Int* (2021) 20:352–60. doi: 10.1016/j.hbpd.2021.04.013
65. Miyauchi T, Uchida Y, Kadono K, Hirao H, Kawasoe J, Watanabe T, et al. Up-Regulation of FOXO1 and Reduced Inflammation by Beta-Hydroxybutyric Acid are Essential Diet Restriction Benefits Against Liver Injury. *Proc Natl Acad Sci U.S.A.* (2019) 116:13533–42. doi: 10.1073/pnas.1820282116

66. Luo Y, Huang Z, Mou T, Pu J, Li T, Li Z, et al. SET8 Mitigates Hepatic Ischemia/Reperfusion Injury in Mice by Suppressing MARK4/NLRP3 Inflammasome Pathway. *Life Sci* (2021) 273:119286. doi: 10.1016/j.lfs.2021.119286
67. Ferro R, Adamska A, Lattanzio R, Mavrommati I, Edling CE, Arifin SA, et al. GPR55 Signalling Promotes Proliferation of Pancreatic Cancer Cells and Tumour Growth in Mice, and its Inhibition Increases Effects of Gemcitabine. *Oncogene* (2018) 37:6368–82. doi: 10.1038/s41388-018-0390-1
68. Li F, Zhang L, Xue H, Xuan J, Rong S, Wang K. SIRT1 Alleviates Hepatic Ischemia-Reperfusion Injury *via* the miR-182-Mediated XBP1/NLRP3 Pathway. *Mol Ther Nucleic Acids* (2021) 23:1066–77. doi: 10.1016/j.omtn.2020.11.015
69. Sinha A, Clatch RJ, Stuck G, Blumenthal SA, Patel SA. Isoflurane Hepatotoxicity: A Case Report and Review of the Literature. *Am J Gastroenterol* (1996) 91:2406–9.
70. Rao Z, Pan X, Zhang H, Sun J, Li J, Lu T, et al. Isoflurane Preconditioning Alleviated Murine Liver Ischemia and Reperfusion Injury by Restoring AMPK/mTOR-Mediated Autophagy. *Anesth Analg* (2017) 125:1355–63. doi: 10.1213/ANE.0000000000002385
71. Lu J, Wang X, Feng Z, Chen Y, Wen D, Liu Z. The Protective Effect of Isoflurane Pretreatment on Liver IRI by Suppressing Noncanonical Pyroptosis of Liver Macrophages. *Int Immunopharmacol* (2021) 99:107977. doi: 10.1016/j.intimp.2021.107977

Conflict of Interest: The authors declare that the research was conducted in the absence of any commercial or financial relationships that could be construed as a potential conflict of interest.

Publisher's Note: All claims expressed in this article are solely those of the authors and do not necessarily represent those of their affiliated organizations, or those of the publisher, the editors and the reviewers. Any product that may be evaluated in this article, or claim that may be made by its manufacturer, is not guaranteed or endorsed by the publisher.

frontiers | Frontiers in Immunology

ORIGINAL RESEARCH
published: 27 June 2022
doi: 10.3389/fimmu.2022.899525

Type 1 Innate Lymphoid Cells Are Proinflammatory Effector Cells in Ischemia-Reperfusion Injury of Steatotic Livers

*Jiman Kang[1,2], Jedson R. Liggett[1,3], Digvijay Patil[1], Suman Ranjit[2], Katrina Loh[1], Anju Duttargi[4], Yuki Cui[1], Kesha Oza[1], Brett S. Frank[1], DongHyang Kwon[5], Bhaskar Kallakury[5], Simon C. Robson[6], Thomas M. Fishbein[1], Wanxing Cui[1,2], Khalid Khan[1] and Alexander Kroemer[1]**

[1] MedStar Georgetown Transplant Institute, MedStar Georgetown University Hospital and the Center for Translational Transplant Medicine, Georgetown University Medical Center, Washington, DC, United States, [2] Department of Biochemistry and Molecular & Cellular Biology, Georgetown University, Washington, DC, United States, [3] Naval Medical Center Portsmouth, Portsmouth, VA, United States, [4] Department of Oncology, Lombardi Comprehensive Cancer Center, Georgetown University Medical Center, Washington, DC, United States, [5] Department of Pathology, MedStar Georgetown University Hospital, Washington, DC, United States, [6] Departments of Anesthesiology and Medicine, Beth Israel Deaconess Medical Center, Harvard Medical School, Boston, MA, United States

OPEN ACCESS

Edited by:
Bibo Ke,
University of California, Los Angeles, United States

Reviewed by:
Akira Shibuya,
University of Tsukuba, Japan
Geoffrey Camirand,
University of Pittsburgh, United States

***Correspondence:**
Alexander Kroemer
alexander.kroemer@gunet.georgetown.edu;
akroemer@me.com

Specialty section:
This article was submitted to Molecular Innate Immunity, a section of the journal Frontiers in Immunology

Received: 24 March 2022
Accepted: 24 May 2022
Published: 27 June 2022

Citation:
Kang J, Liggett JR, Patil D, Ranjit S, Loh K, Duttargi A, Cui Y, Oza K, Frank BS, Kwon D, Kallakury B, Robson SC, Fishbein TM, Cui W, Khan K and Kroemer A (2022) Type 1 Innate Lymphoid Cells Are Proinflammatory Effector Cells in Ischemia-Reperfusion Injury of Steatotic Livers. Front. Immunol. 13:899525. doi: 10.3389/fimmu.2022.899525

Innate lymphoid cells (ILCs), the most recently described family of lymphoid cells, play fundamental roles in tissue homeostasis through the production of key cytokine. Group 1 ILCs, comprised of conventional natural killer cells (cNKs) and type 1 ILCs (ILC1s), have been implicated in regulating immune-mediated inflammatory diseases. However, the role of ILC1s in nonalcoholic fatty liver disease (NAFLD) and ischemia-reperfusion injury (IRI) is unclear. Here, we investigated the role of ILC1 and cNK cells in a high-fat diet (HFD) murine model of partial warm IRI. We demonstrated that hepatic steatosis results in more severe IRI compared to non-steatotic livers. We further elicited that HFD-IRI mice show a significant increase in the ILC1 population, whereas the cNK population was unchanged. Since ILC1 and cNK are major sources of IFN-γ and TNF-α, we measured the level of *ex vivo* cytokine expression in normal diet (ND)-IRI and HFD-IRI conditions. We found that ILC1s in HFD-IRI mice produce significantly more IFN-γ and TNF-α when compared to ND-IRI. To further assess whether ILC1s are key proinflammatory effector cells in hepatic IRI of fatty livers, we studied both *Rag1*$^{-/-}$ mice, which possess cNK cells, and a substantial population of ILC1s versus the newly generated *Rag1*$^{-/-}$ *Tbx21*$^{-/-}$ double knockout (Rag1-Tbet DKO) mice, which lack type 1 ILCs, under HFD IRI conditions. Importantly, HFD Rag1-Tbet DKO mice showed significant protection from hepatic injury upon IRI when compared to *Rag1*$^{-/-}$ mice, suggesting that T-bet-expressing ILC1s play a role, at least in part, as proinflammatory effector cells in hepatic IRI under steatotic conditions.

Keywords: Type 1 innate lymphoid cells, T-bet, ischemia-reperfusion injury, fatty liver disease, liver transplantation, phasor fluorescence lifetime imaging, innate lymphoid cells, natural killer cells

INTRODUCTION

Ischemia-reperfusion injury (IRI) is an unavoidable consequence of organ transplantation that can contribute to early allograft failure and increases the risk for subsequent allograft rejection (1). Hepatic steatosis has been identified as an independent risk factor for greater severity in ischemia-reperfusion injury (2). Unfortunately, given the increasing demand for liver transplantation and relative lack of available organs, marginal allografts, including those with hepatic steatosis, are being considered for use, given careful donor to recipient matching. This has led to significant research efforts to identify modifiable immune mediators to minimize IRI within these marginal organs.

Innate lymphoid cells (ILCs) are the most recently described family of lymphoid cells and are known to play fundamental roles in the first-line defense of epithelial barriers (3, 4), tissue homeostasis, and immune regulation through the activation of host-derived cytokine expression (5, 6). Specifically, Group 1 ILCs are a subset of ILCs that include Type 1 ILC (ILC1s) and conventional natural killer (cNK). Both ILC1s and cNK cells potently secrete TNF-α and IFN-γ (7) in a T-bet transcription factor-dependent manner; Eomesodermin (Eomes) is required only for the maturation of cNK, not ILC1 (8, 9). Moreover, T-bet expression is required for cNK cell maturation in stages, which are elicited by changes in the expression of CD27 and CD11b (8, 9). In this regard, $CD11b^{-}$ $CD27^{+}$ NK cells are the most immature NK cells, whereas mature $CD11b^{+}CD27^{+}$ (double positive, DP) NK cells differentiate into terminally mature NK ($CD11b^{+}CD27^{-}$) cells. Further, while cNK cells are known to circulate throughout the body to eradicate deformed cells in a cytotoxic manner, ILC1s reside predominately within liver tissue (3, 6, 10) and elicit a variety of functions. It has previously been noted that ILC1s can serve a protective function through the production of IFN- γ, and upregulation of Bcl-xL, however, it is also known that these immune cells are prone to overactivation and dysregulation, contributing to autoimmune disorders (11). Additionally, recent work in hepatocellular carcinoma (HCC) using human tissue has associated ILC composition with HCC outcome, specifically denoting plasticity of cNK cells into tumor ILC1 (12).

While the activation of cNK cells has been associated with hepatic IRI (13), the role of ILC1s remains largely understudied. Given the resident and innate nature of ILC1s, the contribution to autoimmune disease, and plasticity of cNK cells to ILC1, we hypothesized that ILC1s are contributors to hepatic IRI, specifically in the setting of hepatic steatosis. In this present work, we utilized a high-fat diet (HFD) murine model of partial warm ischemia-reperfusion injury to elicit the presence of ILC1s in hepatic IRI. We then classified the function of ILC1 in comparison to cNK cells in IRI using *Rag1*$^{-/-}$ single knockout mice, which lack T and B cells but retain full ILC1 and cNK function versus *Rag1*$^{-/-}$ *Tbx21*$^{-/-}$ double knockout (Rag1-Tbet DKO) mice, which lack T and B cells as well as T-bet-dependent ILC1 cells but have retained $Eomes^{+}$ cNK cells. Taken together, we report that ILC1s are a proinflammatory effector subset, driving IRI through the release of IFN-γ and TNF-α.

MATERIALS AND METHODS

Mice

C57BL/6, *Rag1*$^{-/-}$ and *Tbx21*$^{-/-}$ (formal gene name *Tbx21*) mice were purchased from The Jackson Laboratory (Bar Harbor, ME). Rag1-Tbet DKO mice were obtained through crossbreeding of *Rag1*$^{-/-}$ mice with *Tbx21*$^{-/-}$ mice. Genotyping for Rag1-Tbet DKO was performed by Transnetyx. Mice were fed either standard chow (normal diet, ND) or a lard-based high fat diet (HFD). The ND, consisting of 4.09 kcal/gram,13.4% kJ/fat, was purchased from Lab Diet (St. Louis, MO). The HFD, consisting of 5.10 kcal/gram, 60% kJ/fat, was purchased from TestDiet (St. Louis, MO). ND was started at week four of life and maintained for 12-15 weeks for the ND group. For the HFD group experiment, HFD feeding was started between weeks five and seven of life. HFD continued for 12 weeks. All mice were bred and maintained within a pathogen-free facility in the Division of Comparative Medicine at Georgetown University Medical Center, with a standard 12-hour light-dark cycle. All procedures on animal subjects were fully approved by the Georgetown University Institutional Animal Care and Use Committee (protocol #2016-1351).

Partial Warm Ischemia-Reperfusion Injury Model

Mice were anesthetized using 2% isoflurane and oxygen inhalation. After a midline laparotomy, an atraumatic micro clip was applied to the hepatic hilus. Mice were subjected to 45 min of partial warm hepatic ischemia, which closely corresponds to the average warm ischemia time during human liver transplantation at our institution and others. After 45 min of hepatic ischemia, the clip was removed to initiate liver reperfusion, and the peritoneum was reapproximated with sutures and skin closed with staples. After completion of the operation, the mice were returned to their cage. All analysis was performed after 24 hours of reperfusion. Whole blood was collected by direct cardiac puncture as a terminal procedure. The left lobe of the liver and the whole spleen were collected. Control mice were subjected to anesthesia with 2% isoflurane and oxygen inhalation and subjected to midline laparotomy, whole blood collection *via* cardiac puncture, and collection of the entire liver.

Histology and Immunohistochemistry

Hematoxylin and eosin (H&E) staining was performed on five-micron sections from formalin-fixed paraffin-embedded liver tissues that were de-paraffinized with xylenes and rehydrated through a graded alcohol series. H&E staining was completed, followed by rehydration through a graded alcohol series using Autostainer XL (Leica Biosystems). Gr1 staining was performed using an ImmPRESS Goat anti-rat (Mouse absorbed IgG) Polymer Detection Kit (peroxidase) from Vector laboratories (MP-7444) according to the manufacturer's instructions. Additional slides were subsequently stained for CD68 using a horseradish peroxidase-labeled polymer from Dako (K4003)

according to the manufacturer's instructions. Both Gr1 and CD68 staining were quantified by viewing slides on an Olympus BX41 light microscope. The cells stained for the antibody were counted manually in five high-power field sections at 20x magnification in a blinded manner.

Measurement of Serum Alanine Aminotranferase and Aspartate Aminotransferase

ALT and AST levels were measured using a multichannel analyzer, Alfa Wassermann Vet Axcel, from the clinical diagnostics laboratory of VRL Maryland, LLC.

Cell Preparation and Flow Cytometry

The specified liver tissues were collected into RPMI-1640 culture medium (Gibco). Liver tissues were passed through a 70-μm cell strainer (Fisher Scientific), and leukocyte fractions were isolated *via* Percoll (Cytiva) density gradient. After Percoll gradient centrifugation at 1000xg (25°C), without brake for 20 min, the upper layer, including cell debris, was carefully discarded. Leukocyte layer was washed and resuspended in 1X PBS (Gibco). Liver leukocytes were stained with the following antibodies for flow cytometry analysis: PE-conjugated anti-CD49b (BioLegend), APC-conjugated anti-CD49a (BD Biosciences), Brilliant Violet 605™-conjugated anti-NK-1.1 (BioLegend), Alexa Fluor® 700-conjugated CD45 (BioLegend), PerCP-eFluor 710-conjugated anti-EOMES (eBioscience), PE/Dazzle™ 594-conjugated anti-T-bet (BioLegend), Brilliant Violet 510™-conjugated anti-CD11b (BioLegend), Brilliant Violet 711™-conjugated anit-CD107a (BioLegend), Brilliant Violet 650™-conjugated anti-CD27 (BioLegend), APC-conjugated anti-Perforin (BioLegend) and PE/Cyanine7-conjugated anti-Granzyme B (BioLegend). The lineage cocktail for mouse cells consisted of FITC-conjugated anti-CD3, CD5, CD19, Ly-6C, and CD11c (BioLegend). For ILC3, PE/Dazzle™ 594-conjuated anti-CD-127 (BioLegend), PE-Cyanine7-conjuated anti-NKp46 (eBioscience) and Alexa Fluor® 647-conjuated anti-RORγt (BD Biosciences). Data were acquired using a BD FACSAria III Cytometer (BD Biosciences) at our Flow Cytometry & Cell Sorting Shared Resource (FCSR). Any samples with the viability of 60% or lower (as determined by staining with live dead marker Zombie NIR™, BioLegend) were excluded from all analyses. Fluorescence minus one (FMO) controls were used for analysis of cell surface staining, isotype controls were used for T-bet and Eomes transcription factor staining, and unstimulated controls (absence of PMA/ionomycin restimulation) were used for all intracellular cytokine staining (**Supplementary Figure 1A**).

Cytokine Stimulation and Intracellular Cytokine Staining

Intracellular staining for the detection of cytokines was carried out from liver leukocytes. Approximately $1x10^6$ cells/ml RPMI supplemented with 10% FBS, 1% Penicillin Streptomycin, and 0.5% Gentamycin were cultured for 20 hours at 37°C in a cell culture flask. Recombinant mouse cytokine concentrations used were 10 ng/ml IL-12, 50 ng/ml IL-18, and 50 ng/ml IL-15 (R&D Systems). Cells were stimulated for 4 hours with Cell Activation Cocktail containing phorbol-12-myristate-13-acetate (PMA, 50ng/ml) and ionomycin (BioLegend) in the presence of 5 μg/ml brefeldin A (BioLegend). Following stimulation, the cells were stained with the following antibodies to detect cytokines: Brilliant Violet 650™-conjugated anti-IFN-γ (BD Biosciences) and Brilliant Violet 605™-conjugated anti-TNF-α (BioLegend). Cells were fixed (IC Fixation buffer, Invitrogen) and permeabilized (Permeabilization buffer, Invitrogen) according to manufacturer's instructions.

Real-Time PCR Array

Mouse liver specimens were stored in Allprotect Tissue Reagent (Qiagen). Total RNA was extracted using the RNeasy Mini kit with RNase-free DNase set (Qiagen). cDNA was synthesized utilizing RT² First Strand kit (Qiagen) followed by polymerase chain reaction (PCR) amplification and quantification using RT² Profiler™ PCR array for Mouse Cytokines & Chemokines (PAMM-150ZC-12, Qiagen). A total of 1.25μg RNA was pooled from at least three separate mice livers in an equal proportion to PCR profiler array. For the StepOnePlus (Applied Biosystems) thermocycler, the qPCR cycling conditions were 95°C for 10 minutes for 1 cycle, followed by 40 cycles of 95°C for 15 seconds and 60°C for 1 minute. Raw Ct values were analyzed to determine fold change and fold regulation using the GeneGlobe web tool (https://geneglobe.qiagen.com/us/). Non-IRI and IRI groups were tested separately for clustering analysis, considering IRI surgery-based changes in the Ct values for the housekeeping genes. Unsupervised hierarchical clustering for the $2^{-\Delta Ct}$ values was performed using the ClustVis (14) (https://biit.cs.ut.ee/clustvis) web tool to identify gene clusters specifically in non-IRI and IRI groups under two different diet regimens in *Rag1*$^{-/-}$ and Rag1-Tbet DKO mice and normalized using Actb and Hsp90ab1 as housekeeping genes. IRI-mediated genotype- and diet-specific fold regulation in gene expression was computed using respective ND (non-IRI) as a baseline and normalized using a housekeeping gene panel (Actb, Hsp90ab1, Gapdh) for *Rag1*$^{-/-}$ mice and automatically selected reference genes from the entire cataloged array (Nodal, IL-9, and Csf1) for Rag1-Tbet-DKO mice.

Phasor-FLIM Imaging for Steatosis Calculation

Autofluorescence from 5 μm thick liver sections was imaged using the homebuilt DIVER (Deep Imaging *via* Enhanced Recovery) microscope (15, 16). The details of this microscope have been described elsewhere (16–19), and it is a homebuilt modified detector based on an upright configuration. DIVER is connected to a FastFLIM (ISS, Champaign, IL) acquisition card that calculates the fluorescence decay from each pixel of decay and transforms them to the phasor plot (20–22). Signals in the blue part of the fluorescence spectra were collected using a custom filter (400 – 500 nm) in combination with two BG39 filters that constitute the incoming and outgoing window of the filter. The phasor plot is calibrated using Rhodamine 110 in water with a mono-exponential lifetime of 4.0 ns.

Steatosis calculation is based on identifying lipid droplets and then plotting the sizes. The position of long lifetime species (LLS) in the phasor plot was selected using the red circle (19, 21, 23) (**Figure 2B**), and the FLIM images were colored accordingly. LLS is a signature that can only be found in lipid droplets. Very small LLS areas can be caused by a lower signal-to-noise ratio of the acquired fluorescence photons, increasing the spread of the phasor plot. A lower threshold value of connected pixels of size 40 pixels were used to eliminate this misidentification. The individual droplet size distribution from each sample were calculated, and the average size of the droplets were plotted to see changes between sample groups.

Statistical Analysis

Mann–Whitney U test statistics and Multiple t-tests were performed using Prism Software (GraphPad, Inc. San Diego). All graphs show mean ± SEM unless stated otherwise. All p values presented were two-sided, and $p<0.05$ was considered statistically significant. The statistical difference between the samples in steatosis calculation using phasor-FLIM was calculated using student's t-test and Origin software (OriginLab Corporation, Northampton, MA).

RESULTS

HFD-IRI Mice Have Significant Increases in ILC1 Frequencies and Produce More IFN-γ and TNF-α When Compared to ND-IRI Mice

C57BL/6 wild-type high fat diet (HFD) mice gained significantly more body weight (averaging 47.7g versus 26.8g at age 20 weeks; $p<0.0001$) than normal diet (ND) mice. In the first set of experiments, circulating alanine transaminase (ALT) activities were used as indicators of hepatocellular injury. The serum ALT levels of HFD mice were higher ($p<0.05$) than those of mice fed a ND (**Figure 1A**). Compared to normal diet IRI (ND-IRI) mice, the ALT levels of high-fat diet IRI (HFD-IRI) mice were significantly increased ($p<0.01$), as shown in **Figure 1A**. IRI-mediated hepatocellular inflammation was then determined using CD68 and Gr1 immunohistochemistry staining (**Supplementary Figure 1B**). The numbers of infiltrating $CD68^+$ macrophages and $Gr1^+$ neutrophils in HFD-IRI mice were significantly increased when compared to ND-IRI mice (**Figure 1B**), indicating that HFD mice exhibited exacerbated liver injury under IRI conditions.

Given the critical role of group 1 ILCs in regulating hepatic immune responses in liver inflammation, we then investigated the role of ILC1 and cNK cells in naïve non-IRI and IRI livers of HFD mice compared to ND mice *via* polychromatic flow cytometry (**Figure 1C**). We did not observe any significant difference in frequencies of ILC1s (defined as $Lin^-NK1.1^+CD49a^+CD49b^-Tbet^+Eomes^-$) or cNKs (defined as $Lin^-NK1.1^+CD49a^-CD49b^+Tbet^+Eomes^+$) in naïve non-IRI livers of HFD mice compared to ND mice (**Figures 1D, E**). However, HFD-IRI mice showed a significant increase in frequencies of ILC1s (**Figure 1D**) but not of cNKs (**Figure 1E**). In line with this, the absolute cell numbers of ILC1s were significantly increased in the HFD-IRI mice when compared to ND-IRI mice (**Supplementary Figure 2A**), while the absolute cell numbers of cNKs were not different (**Supplementary Figure 2B**).

Having demonstrated that ILC1s are a dominant innate cell population in the livers of HFD-IRI wild-type mice, we speculated that they are also a major source of proinflammatory IFN-γ and TNF-α. To validate this, we restimulated hepatic lymphocytes *ex vivo* with IL-12, IL-15, and IL-18 and found that ILC1s from HFD-IRI mice produced significantly more IFN-γ ($p=0.01$) and TNF-α ($p=0.03$) when compared to cells isolated from ND-IRI mice (**Figures 1F, G**), indicating that ILC1s play a potentially important role as proinflammatory effector cells in fatty liver IRI. We did not observe a significant difference in the cytokine production from cNKs (**Figures 1F, H**).

HFD *Rag1*$^{-/-}$ and Rag1-Tbet DKO Mice Develop Comparable Levels of Hepatic Steatosis and Are a Novel Model for Studies of Group ILC1s

To assess whether ILC1s are truly key proinflammatory effector cells in hepatic IRI of fatty livers, *Rag1*$^{-/-}$ mice were utilized, which are known to lack T cells and B cells and have functional ILC and NK cell compartments. We further established a HFD murine model within these mice by subjecting them to HFD for 12-15 weeks (HFD *Rag1*$^{-/-}$) and compared them to *Rag1*$^{-/-}$ on ND (ND *Rag1*$^{-/-}$) for 12-15 weeks. Importantly, HFD *Rag1*$^{-/-}$ mice demonstrated significantly more weight gain than ND *Rag1*$^{-/-}$ mice at 15 weeks (33.30g vs. 23.69g, $p=0.0002$).

Moreover, to validate that ILC1s are true effector cells in hepatic IRI of fatty livers, Rag1-Tbet DKO mice were generated through crossbreeding of *Rag1*$^{-/-}$ mice with *Tbx21*$^{-/-}$ mice, which in addition to T and B cells also lack T-bet dependent ILC1s but still possess $Eomes^+$ cNKs. A HFD murine model was again created by subjecting Rag1-Tbet DKO mice to HFD for 12-15 weeks (HFD Rag1-Tbet DKO) and compared to Rag1-Tbet DKO mice, which received ND (ND Rag1-Tbet DKO). Importantly, HFD Rag1-Tbet DKO also showed significantly more weight gain than ND Rag1-Tbet DKO at 15 weeks (30.53g vs. 23.45g, $p=0.0015$). There was no statistically significant difference in body weights between Rag1-Tbet DKO and *Rag1*$^{-/-}$ mice under both ND and HFD conditions (averaging 23.5g and 23.7g for ND groups, $p=0.853$; and averaging 30.53g and 32.36g for HFD groups, $p=0.346$, respectively; **Supplementary Figure 3A**), confirming that ILC1-deficient Rag1-Tbet DKO mice possess a comparable HFD-phenotype to *Rag1*$^{-/-}$ mice.

To corroborate this at a microscopic level, we next utilized Phasor-FLIM (Fluorescence lifetime imaging microscopy) to characterize hepatic steatosis in both *Rag1*$^{-/-}$ and Rag1-Tbet DKO mice undergoing IRI. For this, we subjected all mice to our 45-minute partial warm IRI model and evaluated snap-frozen liver tissue from the affected left lobe. Selection of the phasor signature of LLS (red circles, **Figure 2B**, as mentioned in Method 2.8) was then utilized to identify lipid droplets (**Figure 2A**) and calculate lipid

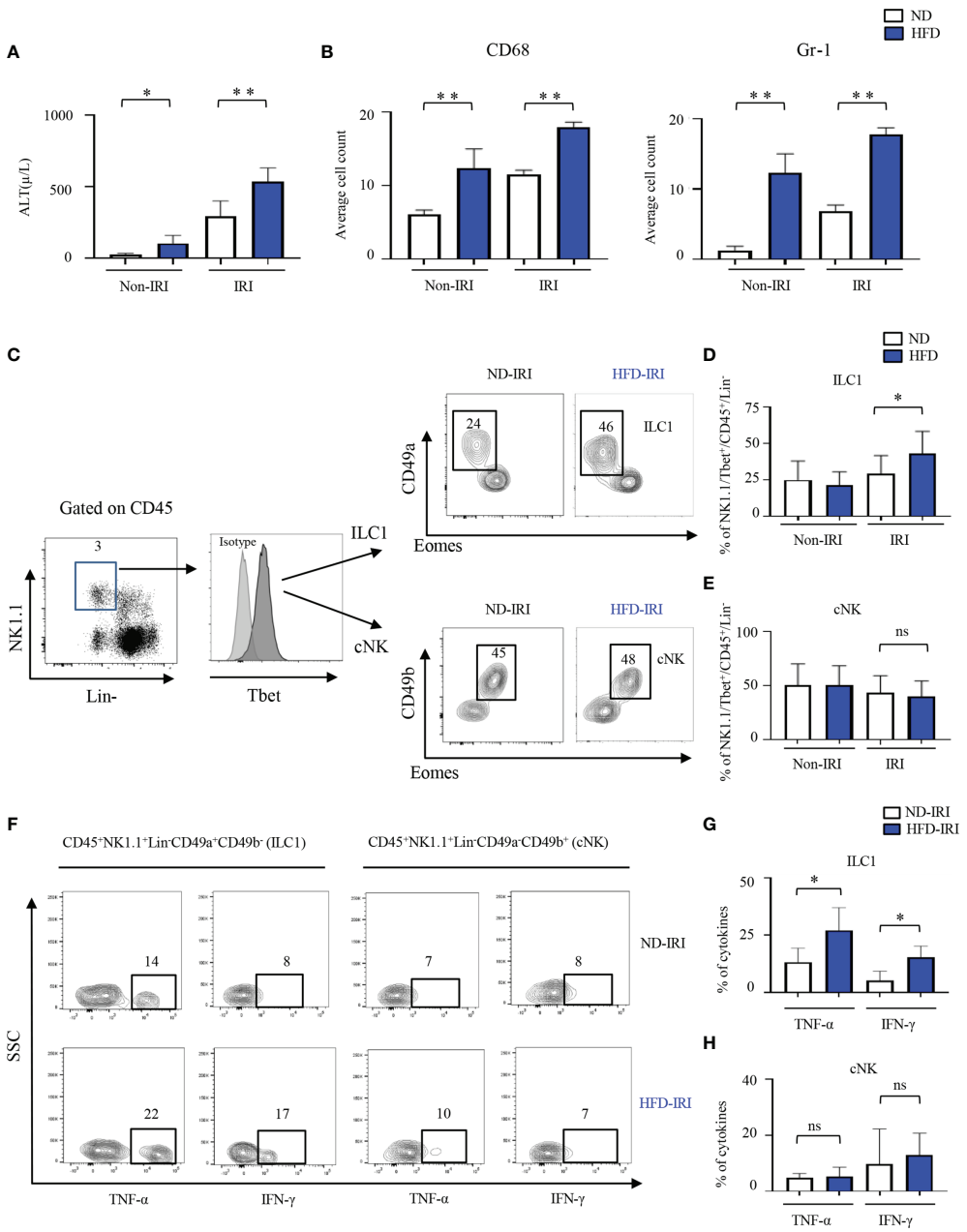

FIGURE 1 | ILC1s are elevated in the liver of C57B/6 wild-type HFD-IRI mice and produce IFN-γ and TNF-α. C57B/6 wild-type mice were fed either standard chow (normal diet, ND) or a lard-based high fat diet (HFD). HFD was started at five-to-seven weeks of age and maintained for 12 weeks. All mice were 17-23 weeks of age at the time of experimentation. A 45-minute partial warm ischemia time was used for IRI experiments. All analysis was performed following 24 hours of reperfusion. **(A)** Serum alanine aminotransferase (ALT), the indicator of liver damage, was measured (n=3-7 mice). **(B)** Numbers of the infiltration of inflammatory cells (i.e., $CD68^+$ and $Gr1^+$) in the ND and HFD mice after IRI were quantified (n=9-10). **(C)** Gating strategy of ILC1s and cNKs from the hepatic lymphocytes: lineage- negative (Lin^-) $NK1.1^+$ cells expressing CD45 were identified as ILC1s and cNKs by expression of CD49a, CD49b, T-bet, and Eomes. Representative flow plots showing ILC1 and cNK subsets in ND-IRI and HFD-IRI. The percentages of ILC1s **(D)** and NKs **(E)** in ND and HFD mice after non-IRI or IRI (n=7-16 mice). **(F)** Representative flow plots showing intracellular cytokine production ($IFN\text{-}\gamma^+$ and $TNF\text{-}\alpha^+$ cells) in ND-IRI and HFD-IRI. Fresh hepatic lymphocytes were stimulated with PMA/ionomycin for 4 hours in the presence of IL-12, IL-15, and IL-18. FACS plots gated on live, $CD45^+$, Lin^-, $NK1.1^+$, $CD49a^+$ and $CD49b^-$ for ILC1s and $CD45^+$, Lin^-, $NK1.1^+$, $CD45a^+$ and $CD45b^+$ for cNKs. The percentage of cytokines from ILC1 gated **(G)** and NK gated **(H)** cells in ND-IRI and HFD-IRI mice (n=5 mice per group). Significance was determined using Mann Whitney Test. *p<0.05; **p<0.01; ns, not significant.

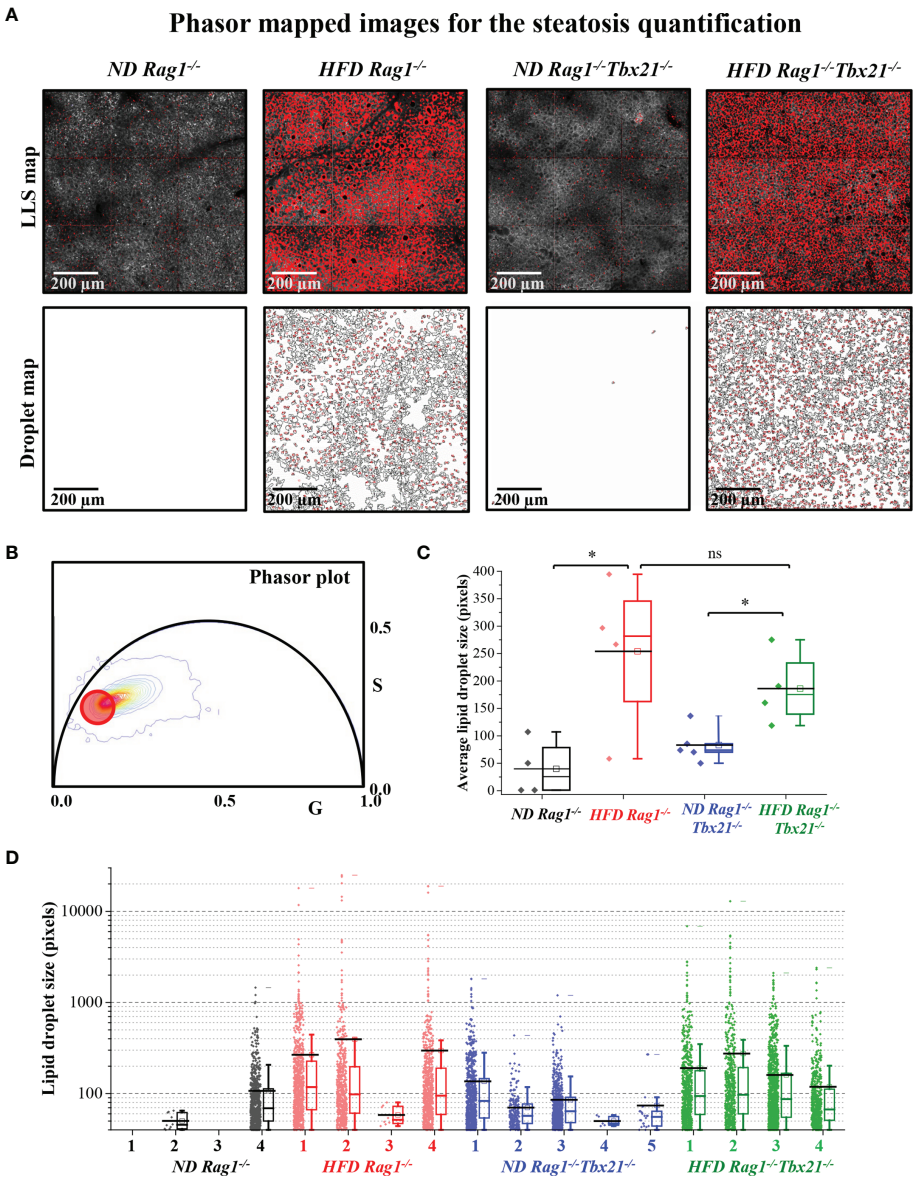

FIGURE 2 | Steatosis quantification using long lifetime species of phasor-in Rag1$^{-/-}$ and Rag1-Tbet DKO hepatic IRI mouse model. HFD was started at five-to-seven weeks of age and maintained for 12 weeks. All mice were 17-19 weeks at time of evaluation. **(A)** Fluorescence lifetime images were color mapped for long lifetime species (LLS) present in lipid droplets, and their size distribution was calculated using a custom ImageJ script (droplet map is shown in **Figure 2A**, bottom). **(B)** The LLS signal was selected based on the phasor-FLIM map (red circle). The calculated average lipid droplet sizes **(C)** and the individual droplet size distributions are plotted **(D)**. The excitation wavelengths used were 740 nm. Significance was determined using Mann Whitney Test. *p<0.05; ns, not significant. Each dot represents the value for a single mouse.

droplet size (**Figure 2A**, bottom) based on a 40-pixel lower limit to avoid the appearance of this signature in low signal-to-noise (S/N) ratio areas of the image. As expected, our data demonstrated that HFD *Rag1*$^{-/-}$ mice IRI and HFD Rag1-Tbet mice DKO IRI mice both had significantly larger lipid droplets and distributions than their ND IRI counterparts. Moreover, lipid droplet morphologies were similar between ND *Rag1*$^{-/-}$ IRI and ND Rag1-Tbet DKO mice (p= not significant; ns) as well as between HFD *Rag1*$^{-/-}$ IRI and HFD Rag1-Tbet DKO mice (p=ns), confirming comparable levels of hepatic steatosis between both mouse strains under HFD-IRI conditions at a microscopic level (**Figures 2C, D**).

HFD Rag1-Tbet DKO but Not *Rag1*$^{-/-}$ Mice Lack ILC1s and Are Protected From IRI in the Setting of Hepatic Steatosis

Next, we evaluated the severity of IRI between both ND and HFD *Rag1*$^{-/-}$ and Rag1-Tbet DKO mice. HFD *Rag1*$^{-/-}$ mice had significantly higher ALT levels than ND *Rag1*$^{-/-}$ mice upon

IRI (p=0.03, **Figure 3A**). Importantly, we did appreciate significantly higher ALT levels in HFD *Rag1*$^{-/-}$ mice than in HFD Rag1-Tbet DKO mice (p=0.002, **Figure 3A**). We also observed that HFD *Rag1*$^{-/-}$ mice had significantly higher AST levels than HFD Rag1-Tbet DKO mice (**Supplementary Figure 3C**). However, there was no statistical difference in ALT levels between ND and HFD Rag1-Tbet DKO mice, suggesting a relative protective IRI phenotype in HFD Rag1-Tbet DKO mice when compared to their HFD *Rag1*$^{-/-}$ counterparts.

We next utilized Gr1 and CD68 tissue staining to evaluate the influx of neutrophils and macrophages following IRI, respectively. Interestingly, the overall macrophage influx was similar between all mouse groups as indicated by CD68 immunostaining (**Figure 3B**). Critically, while there were no significant differences in frequencies of Gr1^{+} neutrophils as determined by Gr1 immunostaining between ND and HFD *Rag1*$^{-/-}$ mice or ND and Rag1-Tbet DKO mice, respectively, there was a significantly higher influx of neutrophils in *Rag1*$^{-/-}$ mice when compared to Rag1-Tbet DKO mice under both ND and HFD conditions, (**Figure 3C**, **Supplementary Figure 3B**). These findings further corroborate the increased protection against IRI afforded to Rag1-Tbet DKO mice, particularly, under hepatic steatosis conditions.

Given the greater degree of IRI demonstrated in HFD *Rag1*$^{-/-}$ mice, we next examined the existence of ILC1 and cNK cells in both ND and HFD *Rag1*$^{-/-}$ and Rag1-Tbet DKO mice following IRI (**Figure 3D**). Notably, the frequencies and absolute numbers of ILC1s were nearly absent in Rag1-Tbet DKO mice of both ND-IRI and HFD-IRI groups (**Figures 3E, F**), confirming a previous report (24). Interestingly, the frequencies of cNKs in Rag1-Tbet DKO mice were significantly higher compared to *Rag1*$^{-/-}$ mice (**Figure 3E**), whereas their absolute cell numbers were not significantly altered (**Figure 3F**). Finally, we studied T-bet-dependent ILC3 phenotype to characterize the ILC3 populations (defined as Lin^{-}CD127^{+}CD117^{+}NK46^{+}) present in our model. However, we did not observe any differences in the frequencies and absolute cell numbers of ILC3 between *Rag1*$^{-/-}$ and Rag1-Tbet DKO mice (**Supplementary Figures 4B, C**). Combined, these data confirm the presence of a substantial population of ILC1s in *Rag1*$^{-/-}$ mice, which may exacerbate IRI under HFD conditions.

ILC1s Are Producers of IFN-γ in *Rag1*$^{-/-}$ Mice With Hepatic Steatosis Undergoing IRI

Thus, we then assessed the distinct contributions of ILC1s vs cNKs to IRI-induced inflammation in our HFD model by comparing their respective cytokine production in *Rag1*$^{-/-}$ and Rag1-Tbet DKO mice upon IRI. First, we determined the production of IFN-γ and TNF-α by ILC1s from *Rag1*$^{-/-}$ mice after IRI. Importantly, IFN-γ levels in ILC1s from HFD-IRI *Rag1*$^{-/-}$ mice were significantly higher than from ND-IRI *Rag1*$^{-/-}$mice, while TNF-α levels were similar between both groups (**Figures 4A, B**). We also analyzed the IFN-γ and TNF-α production by cNKs from both *Rag1*$^{-/-}$ and Rag1-Tbet DKO mice after IRI and did not observe significant differences in cytokine production between groups (**Figure 4C**). Notably, we found that, in HFD-IRI *Rag1*$^{-/-}$ mice, ILC1s produced higher levels of IFN-γ than cNK cells indicating that hepatic ILC1s are a critical source of IFN-γ in HFD *Rag1*$^{-/-}$ mice, thereby contributing to exacerbated hepatic IRI of steatotic livers.

Rag1$^{-/-}$ ND and HFD Mice Have Similar cNK Cells Maturation Characteristics, Whereas cNK Maturation and Perforin Frequencies Are Significantly Altered in Rag1-Tbet DKO Mice

Given that the T-bet transcription factor is required for cNK cell maturation (25) and our observation that the cNK frequencies and absolute cell numbers were similar in both *Rag1*$^{-/-}$ and Rag1-Tbet DKO mice, we next investigated the maturation phenotype and cytotoxic function present within our model contingent on HFD status and IRI. We utilized a CD11b and CD27 gating strategy to further differentiate NK1.1^{+}/Lin^{-}/CD49b^{+} cNK for immature CD11b^{-}CD27^{+} (iNK), mature double positive CD11b^{+}CD27^{+} (DP) cells, and terminally mature CD11b^{+}CD27^{-} (mNK) cells (**Figure 5A**).

When comparing the ND and HFD *Rag1*$^{-/-}$ and Rag1-Tbet DKO, we demonstrated that these mice lack mNK cells in comparison to *Rag1*$^{-/-}$mice, while they have significantly higher frequencies of iNK and DP positive cells. However, there were no significant differences in iNK, DP, or mNK cell populations between *Rag1*$^{-/-}$ ND and HFD groups or the Rag1-Tbet DKO ND and HFD groups, respectively (**Figure 5B**).

We then studied the expression of degranulation and cytotoxic markers in NK cells under IRI and HFD conditions in our model, given that T-bet has been shown to promote the transcription of genes including perforin and granzyme B to activate NK cell cytotoxicity (9). We found that there were no significant differences in degranulation, as indicated by CD107a staining, and there were no differences in intracellular granzyme B staining (**Figures 5C, D**). However, we did find a significantly lower expression of perforin by cNK cells in the livers of Rag1-Tbet DKO mice when compared to *Rag1*$^{-/-}$ mice (**Figure 5E**) under IRI conditions in both the ND and HFD model. Interestingly, there was no difference in perforin expression between ND and HFD *Rag1*$^{-/-}$ mice under IRI conditions.

Rag1-Tbet DKO Mice Show Altered Expression of ILC1-Associated Genes Following IRI

Having established higher levels of ILC1-derived IFN-γ in HFD-IRI *Rag1*$^{-/-}$ mice, we validated ILC1 function within *Rag1*$^{-/-}$mice and defined the relative contributions to immune signaling following IRI using the RT^{2} Profiler qPCR cytokine/chemokine array. To identify diet-specific gene clusters in *Rag1*$^{-/-}$and Rag1-Tbet DKO mice, we performed the unsupervised hierarchical clustering approach for IRI (**Figure 6**) and non-IRI (**Supplementary Figure 5**) groups. We observed a pronounced ILC1-specific gene cluster in HFD *Rag1*$^{-/-}$ mice liver involving *IFNG*, tumor necrosis factor ligand superfamily member 10 (*TNFSF10*, also known as TNF-related apoptosis-inducing ligand *TRAIL*) and Fas ligand (*FasL*) and genes encoding ILC1-stimulatory cytokines such as *IL12B* and *IL15* in both non-IRI and IRI *Rag1*$^{-/-}$ mice but not in Rag1-Tbet DKO mice.

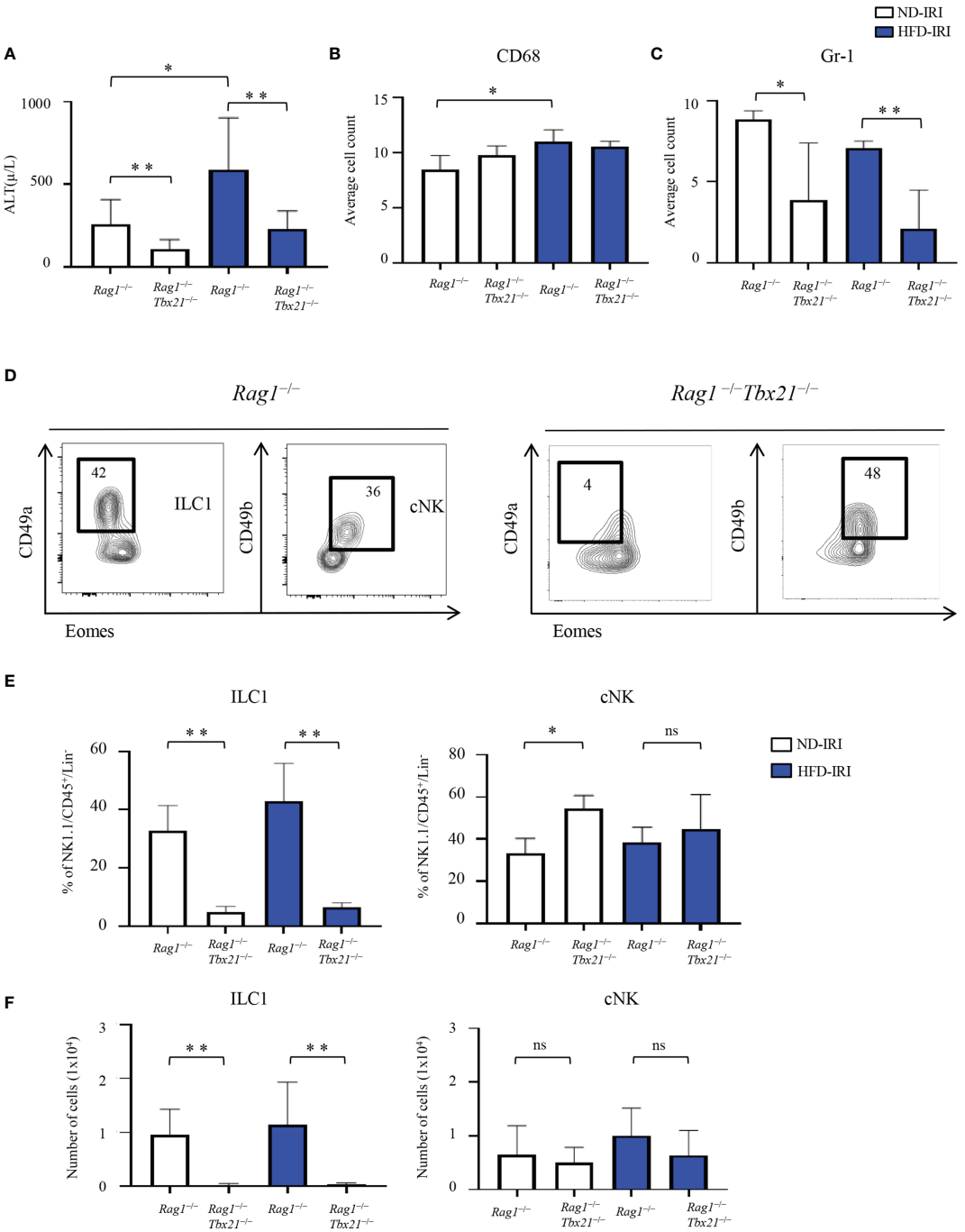

FIGURE 3 | Absence of ILCs lead to increased liver protection to IRI. HFD was started at five-to-seven weeks of age and maintained for 12 weeks. All mice were 17-19 weeks at time of evaluation. A 45-minute partial warm ischemia time was used for IRI experiments. All analysis was performed following 24 hours of reperfusion. **(A)** Serum alanine aminotransferase (ALT) was measured in ND-IRI and HFD-IRI between *Rag1*$^{-/-}$ and Rag1-Tbet DKO mice (n=5-7). The numbers of CD68^{+} **(B)** and Gr1^{+} **(C)** in the ND-IRI and HFD-IRI mice were quantified (n=9-10). **(D)** Representative flow plots show that the frequencies of ILC1s were nearly absent in Rag1-Tbet DKO. Data in Figure **(D)** are representative of ND IRI *Rag1*$^{-/-}$ or Rag1-Tbet DKO mice. **(E)** Percentage **(F)** and the absolute number of ILC1s and cNKs in *Rag1*$^{-/-}$ or Rag1-Tbet DKO mice following ND-IRI and HFD-IRI (n=5-7). Significance was determined using Mann Whitney Test. *p<0.05; **p<0.01; ns; not significant.

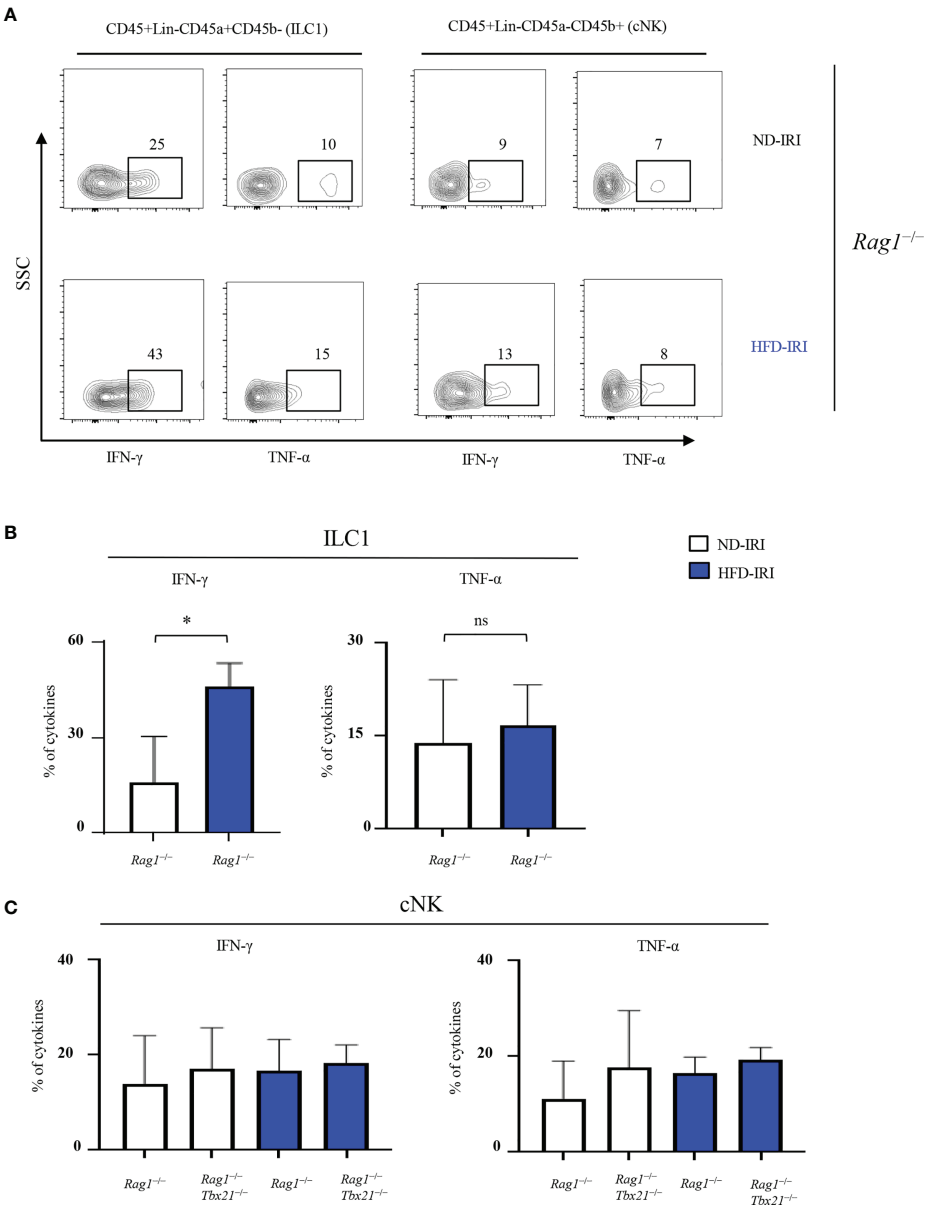

FIGURE 4 | ILC1s produce higher IFN-γ in HFD-IRI. **(A)** Representative flow plots showing intracellular cytokine production (IFN-g$^+$ and TNF-α$^+$ cells) in ND-IRI and HFD-IRI *Rag1*$^{-/-}$ mice. FACS plots gated on live, CD45$^+$, Lin$^-$, NK1.1$^+$, CD49a$^+$ and CD49b$^-$ for ILC1s and CD45$^+$, Lin$^-$, NK1.1$^+$, CD45a$^-$ and CD45b$^+$ for cNKs. **(B)** Percentage of cytokines from ILC1 gated cells in ND-IRI and HFD-IRI *Rag1*$^{-/-}$ mice. **(C)** Percentage of cytokines from cNK gated cells in *Rag1*$^{-/-}$ and Rag1-Tbet DKO mice (n=3-5 mice per group). Significance was determined using Mann Whitney Test. *p<0.05; ns, not significant.

We then analyzed the fold-change differences between ND-IRI and HFD-IRI liver tissues in *Rag1*$^{-/-}$ (**Figure 6B**) and Rag1-Tbet DKO (**Figure 6C**) mice compared to respective non-IRI groups. Upon IRI, we observed higher expression of proinflammatory cytokines encoding genes including *IFNG*, *TNF*, and *CSF2* (GM-CSF) in both ND and HFD *Rag1*$^{-/-}$mice (**Figure 6B**) compared to ND and HFD Rag1-Tbet DKO mice (**Figure 6C**), except IL-2, suggesting loss of Tbet-expressing ILC1s led to reduction in ILC1-derived effector cytokines. In a diet-independent manner, we also observed upregulation of the gene encoding *TRAIL* in *Rag1*$^{-/-}$mice as opposed to in Rag1-Tbet DKO mice. ILC1 cells can produce IFN-γ under the stimulation of IL-12, IL-15, and IL-18 (26). In IRI liver tissues, we observed an upregulation of *IL12b*, *IL15*, and *IL18* genes in *Rag1*$^{-/-}$mice while there was downregulation of the same genes in HFD Rag1-Tbet DKO mice (**Figure 6B**).

DISCUSSION

Recent studies have shown the intricate interplay between ILC1s and their environment in regulating immune-mediated liver

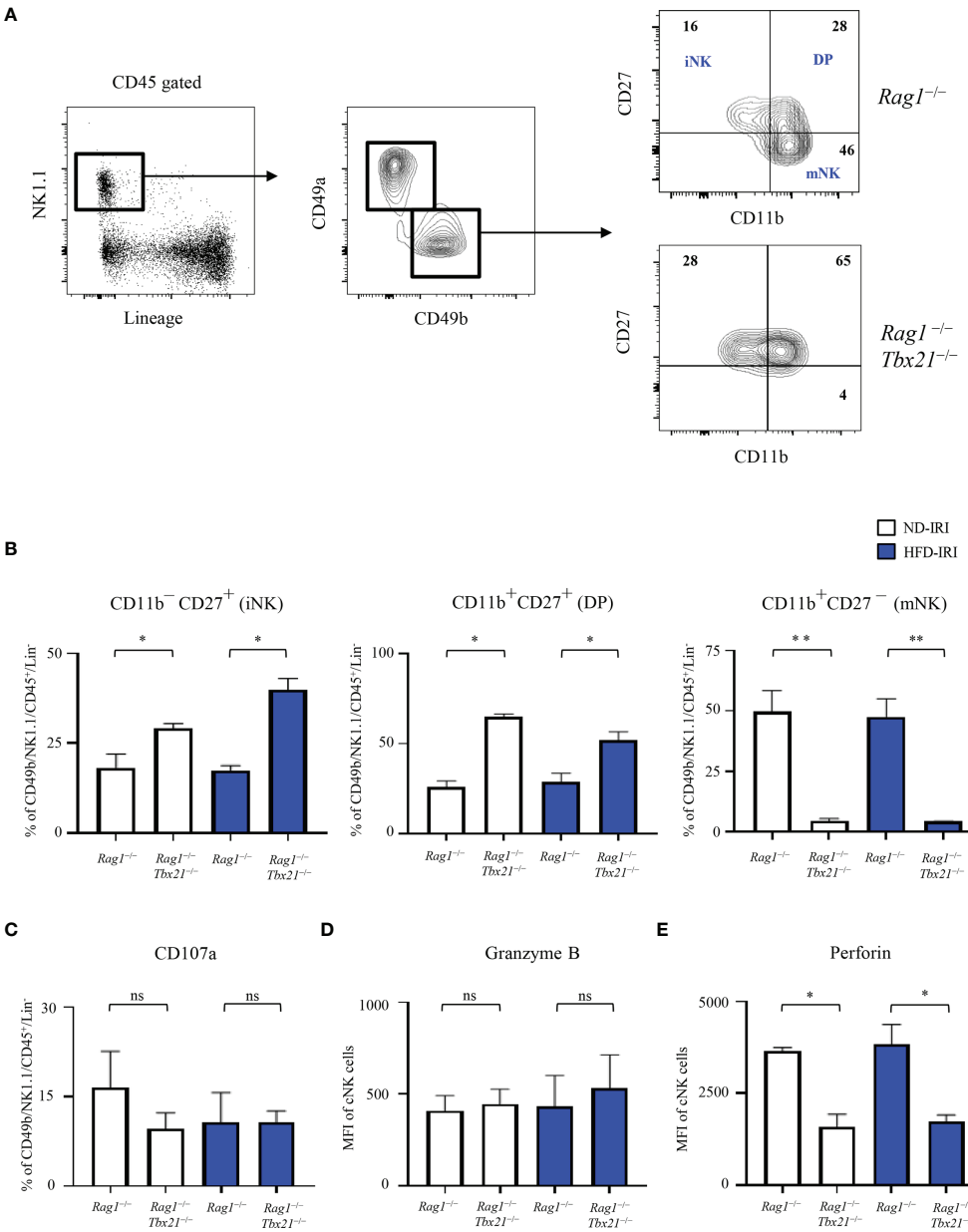

FIGURE 5 | Lack of T-bet leads to a decrease in mNK cells and lower expression of perforin. **(A)** Gating strategy of cNKs from the hepatic lymphocytes: lineage-negative (Lin$^-$) NK1.1$^+$ cells expressing CD45 were identified as cNKs by expression of CD49a and CD49b. Immature NK (CD11b$^-$ CD27$^+$), Double Positive (CD11b$^+$CD27$^+$, DP) and mature NK (CD11b$^+$CD27$^-$) were identified by CD11b and CD27 expression, as shown. Representative flow plots **(A)** from ND-IRI *Rag1*$^{-/-}$ compared with ND-IRI Rag1-Tbet DKO mice and bar graph **(B)** showing NK cell developmental stages in IRI *Rag1*$^{-/-}$ compared with IRI Rag1-Tbet DKO mice. n=4 mice per group. **(C)** The frequency of CD107a staining of cNK cells from ND-IRI and HFD-IRI mice. Fresh hepatic lymphocytes were cultured for 4 h in the presence of anti-CD107a and Brefeldin **(A)** MFI of granzyme B **(D)** and perforin **(E)** staining in cNK cells from ND-IRI and HFD-IRI mice. n=4 mice per group. Significance was determined using Mann Whitney Test. *p<0.05. **p<0.01; ns, not significant.

disease through the secretion of IFN-γ. However, little is known about the phenotype and function of ILC1s in the setting of hepatic ischemia-reperfusion injury, specifically in liver transplantation using "marginal" allografts. In this study, we utilized a HFD murine model in wild-type and genetically modified mice to help investigate the role of ILC1 in a partial warm ischemia-reperfusion injury model.

We first analyzed the ILC1 and cNK cell frequencies, and associated proinflammatory cytokine secretion, in wild-type mice following IRI. Our flow cytometric analysis distinguished significantly greater enrichment of IFN-γ and TNF-α producing ILC1s, compared to cNK cells, in HFD mice following IRI. This is consistent with our previous work in human intestinal transplantation, demonstrating increased ILC1 populations in

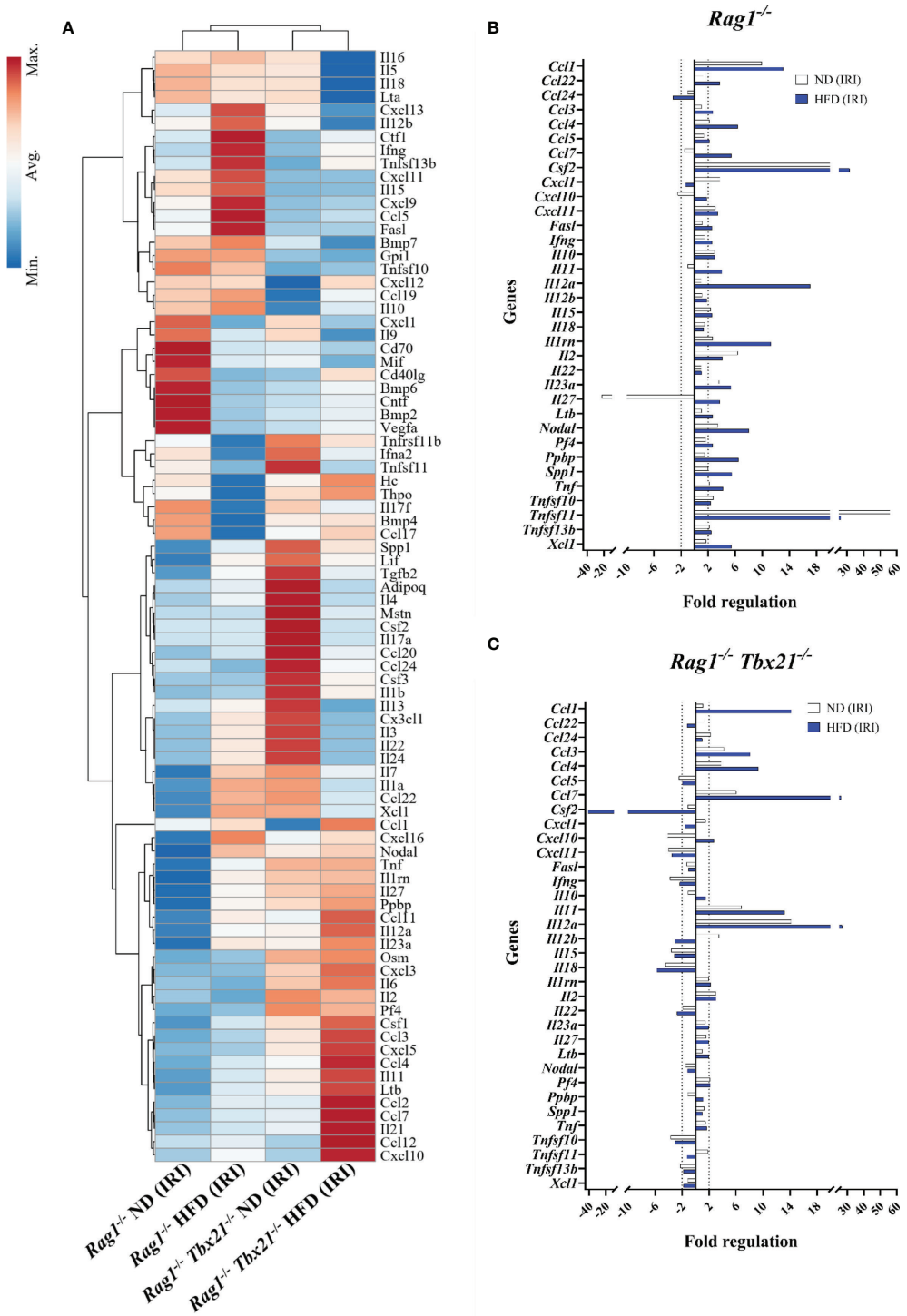

FIGURE 6 | Cytokine and chemokine gene expression array for mice liver IRI. **(A)** Clustergram represents unsupervised hierarchical clustering analysis of RT^2 qPCR profiler array for ND *Rag1*$^{-/-}$ HFD *Rag1*$^{-/-}$, ND Rag1-Tbet DKO, and HFD Rag1-Tbet DKO pooled, post-IRI mice liver tissues. Comparative fold regulation analysis of post-IRI cytokines and chemokines with at least 2-fold or more up-and down-regulation between **(B)** ND and HFD *Rag1*$^{-/-}$ and **(C)** ND and HFD Rag1-Tbet DKO mice liver tissues relative to the respective ND non-IRI control. Dotted vertical lines mark up-and down-regulation of the gene expression. All data are represented as a gene expression of at least three pooled bulk mouse liver tissues.

intestinal allografts 24 hours after reperfusion (27). Further studies in human samples have demonstrated that the proportion of ILC1s is increased in chronic hepatitis B patients compared to healthy controls, indicating a potential proinflammatory role of ILC1s (28) in liver diseases. This has also been alluded to using comparative studies of inflammation in both lung and kidney murine models. Specifically, the ILC1 population has been demonstrated to be higher in kidney specific IRI (29) and the overall ILC populations are higher in mice exposed to cigarette smoke than in control mice (30). Taken together, our initial data distinguishes the potential proinflammatory role of ILC1s in hepatic IRI under steatotic conditions.

While we hypothesized that ILC1s have a proinflammatory effect in our model, there have also been reports of a potential protective role of ILC1s in other models. Specifically, Nabekura et al. utilized a carbon tetrachloride (CCl4)-mediated liver injury model to show that activated ILC1s secrete IFN-γ, which subsequently promotes hepatocyte survival (11). This potentially alludes to the importance of ILC plasticity, as previously demonstrated (12). Cuff et al. demonstrated the plasticity of ILC1s showing a conversion of NK (defined as Lin-negative NK1.1$^+$CD49a$^-$CD49b$^+$) cells into ILC1-like cells (CD200r1$^+$ CD49a$^+$) in mice with non-alcoholic fatty liver disease (31), thus indicating that cNKs could also differentiate into proinflammatory ILC1s in our HFD IRI model thereby exacerbating hepatocellular injury *via* IFN-γ upon IRI in the setting of hepatic steatosis, where the same degree of injury may not be appreciated in non-steatotic livers.

To further investigate and characterize the role of ILC1s in IRI, we utilized *Rag1*$^{-/-}$ mice that have substantial frequencies of cNK cells and ILC1s but lack T and B cells, in comparison to Rag1-Tbet DKO mice which additionally also lack T-bet-dependent ILC1s but retain Eomes-expressing cNK cells. We first demonstrated that HFD *Rag1*$^{-/-}$ mice have a more severe IRI than ND *Rag1*$^{-/-}$ and all Rag1-Tbet DKO mice by ALT levels and Gr1 (neutrophil) cell counts. This is an important finding, as it is well known that neutrophils contribute to IRI by inducing hepatic apoptosis and fibrosis (32, 33). Conversely, the number of CD68 positive cells (macrophages) was not significantly altered (**Figure 3B**) between HFD *Rag1*$^{-/-}$ and HFD Rag1-Tbet DKO mice after IRI. This is not surprising, as macrophages have a dual proinflammatory and anti-inflammatory role characterized by intrinsic polarization into either type 1 or type 2 macrophages (34–37).

We then noted that the frequencies of Eomes$^+$ cNK-derived IFN-γ levels in *Rag1*$^{-/-}$ mice were comparable with Rag1-Tbet DKO mice. While the cytotoxic role of IFN-γ secreting liver resident cNK cells has been previously described (38, 39), and it is known that CD39 ablation is correlated with reduced IFN-γ-dependent responses by NK cells (13), our results did not correlate to clinical phenotype noted in our *Rag1*$^{-/-}$ HFD IRI model. Specifically, it is notable that there were no significant differences in absolute cell numbers of cNK cells or in the iNK, DP, and mNK cell populations between *Rag1*$^{-/-}$ ND and HFD groups, despite more severe IRI in the HFD *Rag1*$^{-/-}$ than in the ND *Rag1*$^{-/-}$ mice. This further supports that ILC1s have a contributory, proinflammatory role in IRI in the setting of hepatic steatosis. However, it is known that T-bet is a key transcription factor which results in the differentiation of iNK cells to mNK cells (9, 25), and it has been demonstrated that perforin-deficient mice develop less fibrosis in a model of non-alcoholic fatty liver disease, suggesting that reduction in cNK cell cytotoxicity is protective in the steatotic liver (31). To this regard, it remains possible that cNK cells and the apparent differences in perforin between the *Rag1*$^{-/-}$ and Rag1-Tbet DKO mice may contribute to the cytotoxicity of IRI in our model, as it has previously been demonstrated in a model of renal IRI (40). Moreover, given the emerging evidence supporting plasticity between cNK cells and ILC1, these cell types could be an intermediate phenotype in the differentiation from cNK to ILC1. More investigation is warranted to fully address whether this plasticity is present under HFD and IRI conditions.

We then evaluated the ILC1 frequency and associated ILC1 dependent IFN-γ production, which demonstrated significantly higher levels of ILC1s in *Rag1*$^{-/-}$mice, as compared to the cNKs. This ultimately indicates that ILC1 is a major source of IFN-γ. It has been described that IFN-γ-deficient mice are significantly protected against liver injury and hepatic fibrosis in a model of non-alcoholic steatohepatitis (41), and it has further been demonstrated that anti-IFN-γ treatment results in lower ALT levels and hepatocellular injury following 48 hours of reperfusion in a model of 60-minute partial warm ischemia (42). However, the exact role of IFN-γ as secreted by ILC1 remains unknown. While our results suggest a proinflammatory role, additional investigations are warranted to truly evaluate the proinflammatory function of IFN-γ from ILC1s, for instance, through the use of a *Rag1*$^{-/-}$ *IFN-γ*$^{-/-}$ deficient HFD mouse model.

We finally correlated this finding using our qPCR array to demonstrate the dynamic interplay of cytokines and chemokines in hepatic IRI. This highlighted the ILC1-specific elevated expression of TRAIL and CSF2 in *Rag1*$^{-/-}$ mice (**Figure 6B**) compared to Rag1-Tbet DKO mice (**Figure 6C**) independent of the diet regimens. Interestingly, our data also shows upregulation of FasL only in HFD *Rag1*$^{-/-}$ IRI but not in ND *Rag1*$^{-/-}$ IRI. FasL and TRAIL co-expression is more cytotoxic in hepatic ILC1 than the intestinal ILC1 (24). At the same time, independent studies in both mouse liver and kidney show that antibody-mediated inhibition of FasL is protective from liver failure (43) and ischemic acute kidney injury (44), respectively. Future investigation will be needed to identify the influence of hepatic steatosis on FasL-dependent immunomodulation and the exacerbation of liver injury.

Collectively, our findings indicate that hepatic ILC1s are, at least in part, an innate inflammatory effector subset, particularly in steatotic livers. Our findings provide deeper insights into the mechanisms of ILC1 and cNK cell function in IRI as well as identify further areas of interest in cNK cell to ILC1 plasticity and IFN-γ production in the setting of IRI and allow for additional translational studies in the use of "marginal allografts" in liver transplantation.

DATA AVAILABILITY STATEMENT

The original contributions presented in the study are publicly available. This data can be found in NCBI's Gene Expression Omnibus; GEO accession number: GSE205510.

ETHICS STATEMENT

The animal study was reviewed and approved by The Georgetown University Institutional Animal Care and Use Committee.

AUTHOR CONTRIBUTIONS

AK and SR designed the study and secured funding. JK, JL, DP, SR, KL, YC, AD, and WC carried out experiments. JK, JL, DP, SR, and AK acquired data and wrote the manuscript. JK, JL, DP, BF, AD, SR, and AK analyzed data. AK, SR, WC, BK, DK, KO, KK, SR, and TF provided a critical review of the manuscript. All authors read and approved the manuscript.

FUNDING

Funding was provided by NIH R21AI130800 (AK, SR) as well as by the Children's Rare Disease Organization Inc. (CRDO) (AK, JK, KK).

SUPPLEMENTARY MATERIAL

The Supplementary Material for this article can be found online at: https://www.frontiersin.org/articles/10.3389/fimmu.2022.899525/full#supplementary-material

REFERENCES

1. Fagenson AM, Xu K, Saaoud F, Nanayakkara G, Jhala NC, Liu L, et al. Liver Ischemia Reperfusion Injury, Enhanced by Trained Immunity, Is Attenuated in Caspase 1/Caspase 11 Double Gene Knockout Mice. *Pathogens* (2020) 9 (11):879. doi: 10.3390/pathogens9110879
2. Ito T, Naini BV, Markovic D, Aziz A, Younan S, Lu M, et al. Ischemia-Reperfusion Injury and Its Relationship With Early Allograft Dysfunction in Liver Transplant Patients. *Am J Transplant* (2021) 21(2):614–25. doi: 10.1111/ajt.16219
3. Huntington ND, Carpentier S, Vivier E, Belz GT. Innate Lymphoid Cells: Parallel Checkpoints and Coordinate Interactions With T Cells. *Curr Opin Immunol* (2016) 38:86–93. doi: 10.1016/j.coi.2015.11.008
4. Almeida FF, Jacquelot N, Belz GT. Deconstructing Deployment of the Innate Immune Lymphocyte Army for Barrier Homeostasis and Protection. *Immunol Rev* (2018) 286(1):6–22. doi: 10.1111/imr.12709
5. Sonnenberg GF, Artis D. Innate Lymphoid Cells in the Initiation, Regulation and Resolution of Inflammation. *Nat Med* (2015) 21(7):698–708. doi: 10.1038/nm.3892
6. Artis D, Spits H. The Biology of Innate Lymphoid Cells. *Nature* (2015) 517 (7534):293–301. doi: 10.1038/nature14189
7. Spits H, Bernink JH, Lanier L. Nk Cells and Type 1 Innate Lymphoid Cells: Partners in Host Defense. *Nat Immunol* (2016) 17(7):758–64. doi: 10.1038/ni.3482
8. Chiossone L, Chaix J, Fuseri N, Roth C, Vivier E, Walzer T. Maturation of Mouse Nk Cells Is a 4-Stage Developmental Program. *Blood* (2009) 113 (22):5488–96. doi: 10.1182/blood-2008-10-187179
9. Huang C, Bi J. Expression Regulation and Function of T-Bet in Nk Cells. *Front Immunol* (2021) 12:761920. doi: 10.3389/fimmu.2021.761920
10. Luci C, Vieira E, Perchet T, Gual P, Golub R. Natural Killer Cells and Type 1 Innate Lymphoid Cells Are New Actors in Non-Alcoholic Fatty Liver Disease. *Front Immunol* (2019) 10:1192. doi: 10.3389/fimmu.2019.01192
11. Nabekura T, Riggan L, Hildreth AD, O'Sullivan TE, Shibuya A. Type 1 Innate Lymphoid Cells Protect Mice From Acute Liver Injury *Via* Interferon-γ Secretion for Upregulating Bcl-Xl Expression in Hepatocytes. *Immunity* (2020) 52(1):96–108.e9. doi: 10.1016/j.immuni.2019.11.004
12. Heinrich B, Gertz EM, Schäffer AA, Craig A, Ruf B, Subramanyam V, et al. The Tumour Microenvironment Shapes Innate Lymphoid Cells in Patients With Hepatocellular Carcinoma. *Gut* (2021) 71(6):1161–75. doi: 10.1136/gutjnl-2021-325288
13. Beldi G, Banz Y, Kroemer A, Sun X, Wu Y, Graubardt N, et al. Deletion of Cd39 on Natural Killer Cells Attenuates Hepatic Ischemia/Reperfusion Injury in Mice. *Hepatology* (2010) 51(5):1702–11. doi: 10.1002/hep.23510
14. Metsalu T, Vilo J. Clustvis: A Web Tool for Visualizing Clustering of Multivariate Data Using Principal Component Analysis and Heatmap. *Nucleic Acids Res* (2015) 43(W1):W566–70. doi: 10.1093/nar/gkv468
15. Crosignani V, Dvornikov A, Aguilar JS, Stringari C, Edwards R, Mantulin WW, et al. Deep Tissue Fluorescence Imaging and *in Vivo* Biological Applications. *J BioMed Opt* (2012) 17(11):116023. doi: 10.1117/1.jbo.17.11.116023
16. Crosignani V, Jahid S, Dvornikov AS, Gratton E. A Deep Tissue Fluorescence Imaging System With Enhanced Shg Detection Capabilities. *Microsc Res Tech* (2014) 77(5):368–73. doi: 10.1002/jemt.22354
17. Ranjit S, Lanzanò L, Libby AE, Gratton E, Levi M. Advances in Fluorescence Microscopy Techniques to Study Kidney Function. *Nat Rev Nephrol* (2021) 17 (2):128–44. doi: 10.1038/s41581-020-00337-8
18. Ranjit S, Lanzano L, Gratton E. Mapping Diffusion in a Living Cell *Via* the Phasor Approach. *Biophys J* (2014) 107(12):2775–85. doi: 10.1016/j.bpj.2014.08.041
19. Ranjit S, Dvornikov A, Dobrinskikh E, Wang X, Luo Y, Levi M, et al. Measuring the Effect of a Western Diet on Liver Tissue Architecture by Flim Autofluorescence and Harmonic Generation Microscopy. *BioMed Opt Express* (2017) 8(7):3143–54. doi: 10.1364/boe.8.003143
20. Malacrida L, Ranjit S, Jameson DM, Gratton E. The Phasor Plot: A Universal Circle to Advance Fluorescence Lifetime Analysis and Interpretation. *Annu Rev Biophys* (2021) 50:575–93. doi: 10.1146/annurev-biophys-062920-063631
21. Ranjit S, Malacrida L, Jameson DM, Gratton E. Fit-Free Analysis of Fluorescence Lifetime Imaging Data Using the Phasor Approach. *Nat Protoc* (2018) 13(9):1979–2004. doi: 10.1038/s41596-018-0026-5
22. Digman MA, Caiolfa VR, Zamai M, Gratton E. The Phasor Approach to Fluorescence Lifetime Imaging Analysis. *Biophys J* (2008) 94(2):L14–6. doi: 10.1529/biophysj.107.120154
23. Datta R, Alfonso-García A, Cinco R, Gratton E. Fluorescence Lifetime Imaging of Endogenous Biomarker of Oxidative Stress. *Sci Rep* (2015) 5:9848. doi: 10.1038/srep09848
24. Tang L, Peng H, Zhou J, Chen Y, Wei H, Sun R, et al. Differential Phenotypic and Functional Properties of Liver-Resident Nk Cells and Mucosal Ilc1s. *J Autoimmun* (2016) 67:29–35. doi: 10.1016/j.jaut.2015.09.004
25. Townsend MJ, Weinmann AS, Matsuda JL, Salomon R, Farnham PJ, Biron CA, et al. T-Bet Regulates the Terminal Maturation and Homeostasis of Nk and Valpha14i Nkt Cells. *Immunity* (2004) 20(4):477–94. doi: 10.1016/s1074-7613(04)00076-7
26. Fuchs A, Vermi W, Lee JS, Lonardi S, Gilfillan S, Newberry RD, et al. Intraepithelial Type 1 Innate Lymphoid Cells Are a Unique Subset of Il-12- and Il-15-Responsive Ifn-γ-Producing Cells. *Immunity* (2013) 38(4):769–81. doi: 10.1016/j.immuni.2013.02.010
27. Kang J, Loh K, Belyayev L, Cha P, Sadat M, Khan K, et al. Type 3 Innate Lymphoid Cells Are Associated With a Successful Intestinal Transplant. *Am J Transplant* (2021) 21(2):787–97. doi: 10.1111/ajt.16163
28. Yang Z, Tang T, Wei X, Yang S, Tian Z. Type 1 Innate Lymphoid Cells Contribute to the Pathogenesis of Chronic Hepatitis B. *Innate Immun* (2015) 21(6):665–73. doi: 10.1177/1753425915586074

29. Baban B, Khodadadi H, Vaibhav K, Marchetti C, Riccardi C, Mozaffari MS. Regulation of Innate Lymphoid Cells in Acute Kidney Injury: Crosstalk Between Cannabidiol and Gilz. *J Immunol Res* (2020) 2020:6056373. doi: 10.1155/2020/6056373
30. Blomme EE, Provoost S, De Smet EG, De Grove KC, Van Eeckhoutte HP, De Volder J, et al. Quantification and Role of Innate Lymphoid Cell Subsets in Chronic Obstructive Pulmonary Disease. *Clin Transl Immunol* (2021) 10(6): e1287. doi: 10.1002/cti2.1287
31. Cuff AO, Sillito F, Dertschnig S, Hall A, Luong TV, Chakraverty R, et al. The Obese Liver Environment Mediates Conversion of Nk Cells to a Less Cytotoxic Ilc1-Like Phenotype. *Front Immunol* (2019) 10:2180. doi: 10.3389/fimmu.2019.02180
32. Klune JR, Tsung A. Molecular Biology of Liver Ischemia/Reperfusion Injury: Established Mechanisms and Recent Advancements. *Surg Clin North Am* (2010) 90(4):665–77. doi: 10.1016/j.suc.2010.04.003
33. Miyauchi T, Uchida Y, Kadono K, Hirao H, Kawasoe J, Watanabe T, et al. Up-Regulation of Foxo1 and Reduced Inflammation by B-Hydroxybutyric Acid Are Essential Diet Restriction Benefits Against Liver Injury. *Proc Natl Acad Sci U S A* (2019) 116(27):13533–42. doi: 10.1073/pnas.1820282116
34. Verreck FA, de Boer T, Langenberg DM, Hoeve MA, Kramer M, Vaisberg E, et al. Human Il-23-Producing Type 1 Macrophages Promote But Il-10-Producing Type 2 Macrophages Subvert Immunity to (Myco)Bacteria. *Proc Natl Acad Sci U S A* (2004) 101(13):4560–5. doi: 10.1073/pnas.0400983101
35. Murray PJ, Wynn TA. Protective and Pathogenic Functions of Macrophage Subsets. *Nat Rev Immunol* (2011) 11(11):723–37. doi: 10.1038/nri3073
36. Ma Q. Polarization of Immune Cells in the Pathologic Response to Inhaled Particulates. *Front Immunol* (2020) 11:1060. doi: 10.3389/fimmu.2020.01060
37. Atri C, Guerfali FZ, Laouini D. Role of Human Macrophage Polarization in Inflammation During Infectious Diseases. *Int J Mol Sci* (2018) 19(6):1801. doi: 10.3390/ijms19061801
38. Fasbender F, Obholzer M, Metzler S, Stöber R, Hengstler JG, Watzl C. Enhanced Activation of Human Nk Cells by Drug-Exposed Hepatocytes. *Arch Toxicol* (2020) 94(2):439–48. doi: 10.1007/s00204-020-02668-8
39. Martínez-Chantar ML, Delgado TC, Beraza N. Revisiting the Role of Natural Killer Cells in Non-Alcoholic Fatty Liver Disease. *Front Immunol* (2021) 12:640869. doi: 10.3389/fimmu.2021.640869
40. Zhang ZX, Wang S, Huang X, Min WP, Sun H, Liu W, et al. Nk Cells Induce Apoptosis in Tubular Epithelial Cells and Contribute to Renal Ischemia-Reperfusion Injury. *J Immunol* (2008) 181(11):7489–98. doi: 10.4049/jimmunol.181.11.7489
41. Luo XY, Takahara T, Kawai K, Fujino M, Sugiyama T, Tsuneyama K, et al. Ifn-γ Deficiency Attenuates Hepatic Inflammation and Fibrosis in a Steatohepatitis Model Induced by a Methionine- and Choline-Deficient High-Fat Diet. *Am J Physiol Gastrointest Liver Physiol* (2013) 305(12): G891–9. doi: 10.1152/ajpgi.00193.2013
42. Goto T, Ito Y, Satoh M, Nakamoto S, Nishizawa N, Hosono K, et al. Activation of Inkt Cells Facilitates Liver Repair After Hepatic Ischemia Reperfusion Injury Through Acceleration of Macrophage Polarization. *Front Immunol* (2021) 12:754106. doi: 10.3389/fimmu.2021.754106
43. Al-Saeedi M, Steinebrunner N, Kudsi H, Halama N, Mogler C, Büchler MW, et al. Neutralization of Cd95 Ligand Protects the Liver Against Ischemia-Reperfusion Injury and Prevents Acute Liver Failure. *Cell Death Dis* (2018) 9 (2):132. doi: 10.1038/s41419-017-0150-0
44. Ko GJ, Jang HR, Huang Y, Womer KL, Liu M, Higbee E, et al. Blocking Fas Ligand on Leukocytes Attenuates Kidney Ischemia-Reperfusion Injury. *J Am Soc Nephrol* (2011) 22(4):732–42. doi: 10.1681/asn.2010010121

Author Disclaimer: The views expressed in this manuscript reflect the results of research conducted by the authors and do not necessarily reflect the official policy or position of the Department of the Navy, Department of Defense, or the United States Government.

JL is a military service member. This work was prepared as part of official duties. Title 17, USC, Section 105 provides that Copyright protection under this title is not available for any work of the U.S. Government and defines a U.S. Government work as a work prepared by a military service member or employee of the U.S. Government as part of that person's official duties.

Conflict of Interest: The authors declare that the research was conducted in the absence of any commercial or financial relationships that could be construed as a potential conflict of interest.

Publisher's Note: All claims expressed in this article are solely those of the authors and do not necessarily represent those of their affiliated organizations, or those of the publisher, the editors and the reviewers. Any product that may be evaluated in this article, or claim that may be made by its manufacturer, is not guaranteed or endorsed by the publisher.

frontiers | Frontiers in Immunology

REVIEW
published: 01 July 2022
doi: 10.3389/fimmu.2022.887565

The Role of Neutrophils as a Driver in Hepatic Ischemia-Reperfusion Injury and Cancer Growth

Christof Kaltenmeier[1†], *Hamza O. Yazdani*[1†], *Sanah Handu*[1], *Brandon Popp*[2], *David Geller*[1] *and Samer Tohme*[1*]

[1] Department of Surgery, University of Pittsburgh Medical Center, Pittsburgh, PA, United States, [2] Lake Erie College of Osteopathic Medicine, Erie, PA, United States

The innate immune system plays an essential role in the response to sterile inflammation and its association with liver ischemia and reperfusion injury (IRI). Liver IRI often manifests during times of surgical stress such as cancer surgery or liver transplantation. Following the initiation of liver IRI, stressed hepatocytes release damage-associated molecular patterns (DAMPs) which promote the infiltration of innate immune cells which then initiate an inflammatory cascade and cytokine storm. Upon reperfusion, neutrophils are among the first cells that infiltrate the liver. Within the liver, neutrophils play an important role in fueling tissue damage and tumor progression by promoting the metastatic cascade through the formation of Neutrophil Extracellular Traps (NETs). NETs are composed of web-like DNA structures containing proteins that are released in response to inflammatory stimuli in the environment. Additionally, NETs can aid in mediating liver IRI, promoting tumor progression, and most recently, in mediating early graft rejection in liver transplantation. In this review we aim to summarize the current knowledge of innate immune cells, with a focus on neutrophils, and their role in mediating IRI in mouse and human diseases, including cancer and transplantation. Moreover, we will investigate the interaction of Neutrophils with varying subtypes of other cells. Furthermore, we will discuss the role and different treatment modalities in targeting Neutrophils and NETs to prevent IRI.

Keywords: neutrophil, ischemia reperfusion (I/R) injury, neutrophil extracelluar traps, cancer liver, liver transplantation

OPEN ACCESS

Edited by:
Qiang Wei,
Zhejiang University School of Medicine, China

Reviewed by:
Kojiro Nakamura,
Kyoto University, Japan
Paul Thompson,
The Scripps Research Institute, United States

***Correspondence:**
Samer Tohme
tohmest@upmc.edu

[†]These authors have contributed equally to this work

Specialty section:
This article was submitted to Molecular Innate Immunity, a section of the journal Frontiers in Immunology

Received: *01 March 2022*
Accepted: *02 June 2022*
Published: *01 July 2022*

Citation:
Kaltenmeier C, Yazdani HO, Handu S, Popp B, Geller D and Tohme S (2022) The Role of Neutrophils as a Driver in Hepatic Ischemia-Reperfusion Injury and Cancer Growth. Front. Immunol. 13:887565. doi: 10.3389/fimmu.2022.887565

INTRODUCTION

Liver ischemia and reperfusion injury (IRI) often presents in various surgical procedures such as cancer surgery or liver transplantation (1, 2). Orthotopic liver transplantation (OLT) is the current standard of care for patients with end-stage liver disease and selected hepatic malignancies. Early graft failure is common with an incidence of approximately 25% and a major contributor to morbidity and mortality (3). IRI is one of the leading causes of early graft dysfunction and a major factor for acute and chronic rejection (4). IRI also plays an important role in the setting of liver cancer surgery (2). Here, studies have shown that prolonged IRI promotes the growth of micro metastatic disease within the liver from primary or metastatic cancer (5). Prolonged IRI is strongly associated with early disease recurrence and decreased survival.

Prolonged IRI leads to a lack of oxygen and nutrient supply for cells within the liver parenchyma. During this time hepatocytes and Kupffer cells undergo anaerobic metabolism, reactive oxygen production, and subsequent cell death along with the release of damage associated patterns (DAMPs). Upon reperfusion, DAMPs are flushed into the circulation and a complex cascade of inflammatory mediators that promote tissue damage is initiated.

Although the reperfusion phase of the liver is the principal driver of tissue injury, the pretransplant cold storage itself can trigger organ damage (1, 6, 7). Studies have shown that several apoptosis inducing kinases are activated in parenchymal liver cells following cold-induced tissue injury, which subsequently promote cell death upon reperfusion 1. Reducing the cold ischemia time and limiting the damage of reperfusion are important targets in order to reduce graft dysfunction and rejection.

Liver damage is mostly caused during reperfusion when host cells are in metabolic anaerobic distress and excess infiltration of innate immune cells occurs. Neutrophils are among the first cells to arrive within the liver following IRI (5, 8, 9). There is overwhelming evidence that excessive neutrophil infiltration contributes to the pathogenesis of IRI. Neutrophil-induced liver injury is a multistep process that starts with neutrophil activation, recruitment of these cells to site of injury *via* transmigration, interaction with hepatic host and other immune cells (10).

In this review, we will discuss the current advances in understanding the role of neutrophils in cold and warm liver IRI, with a specific focus on the role and function of activated neutrophils and their interaction with liver parenchymal host and infiltrating immune cells. We will furthermore discuss non-pharmacological and pharmacological treatment options to limit IRI and/or decrease NET formation in the liver (**Figure 1**).

THE ROLE OF LIVER RESIDENT CELLS IN LIVER I/R AND THEIR ROLE IN NEUTROPHIL RECRUITMENT

IRI results in tissue and cellular necrosis which are the main contributors to liver damage following transplantation or cancer surgery (11). Even in the absence of microbial pathogens, excessive activation of a sterile inflammatory response following the restoration of blood flow can result in further dysfunction. The signaling events contributing to local hepatocellular damage are diverse and complex, and involve the interaction between hepatocytes, liver sinusoidal endothelial cells (LSEC), Kupffer cells (KC), and hepatic stellate cells (HSC), all leading to neutrophil activation and formation of neutrophil extracellular traps (NETs) (10, 12). During organ procurement and transplantation, the liver undergoes two insults classified as cold storage and warm IRI. During cold storage, organs are

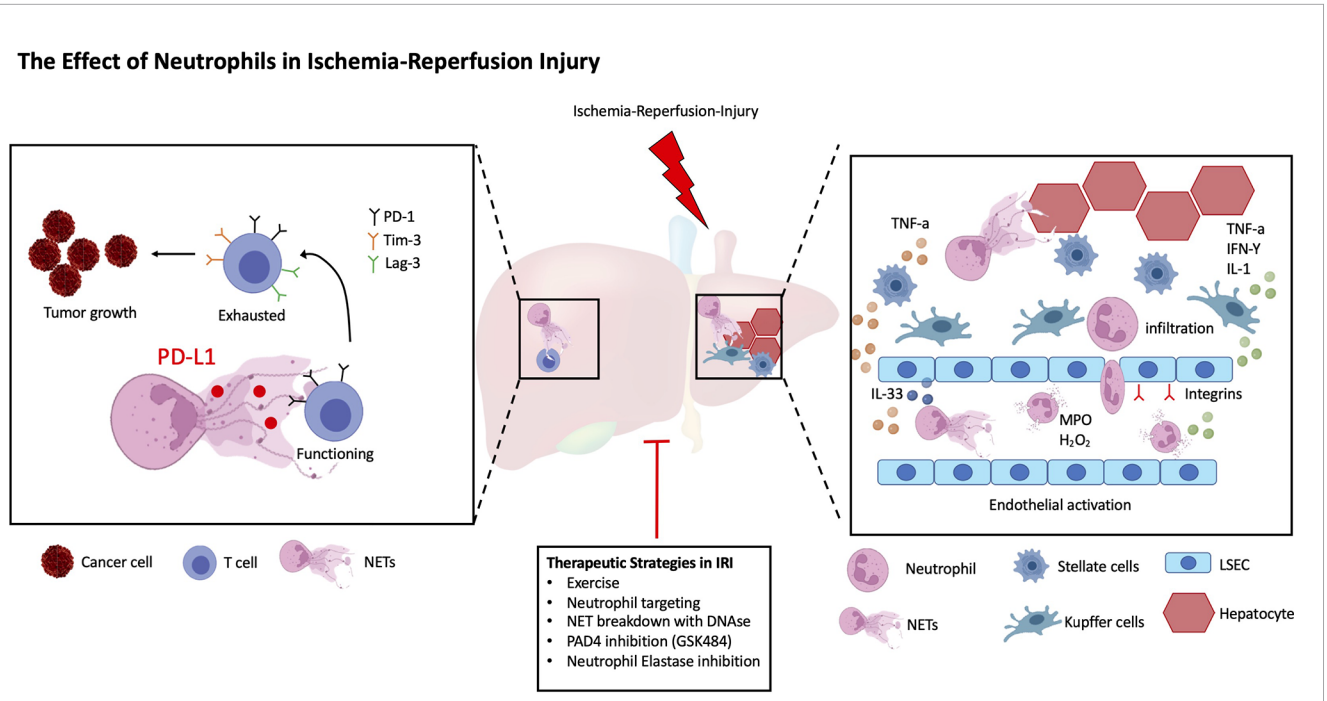

FIGURE 1 | The Role of Neutrophils in Ischemia-Reperfusion Injury. A simplified schematic representation of the roles of Neutrophils in liver IRI. Following IRI liver parenchymal cells promote the recruitment, activation, and phenotypic differentiation of neutrophils. LSECs increase the production of NETs *via* IL-33 signaling, in addition they upregulate adhesion markers to facilitate Neutrophil transmigration, extravasation and NET formation. Similarly, both HSCs and Kupffer cells secrete cytokines to increase Neutrophil homing. Within the tumor microenvironment (TME), NETs promote the exhaustion of T cells leading to increased tumor burden. Several, both non-pharmacological and pharmacological therapies have been described to decrease liver IRI.

deprived of blood flow and placed on ice to preserve their function and limit cellular metabolism. This is followed by warm IRI upon reperfusion of the liver. During cold and warm IRI, LSECs undergo varying alterations including nuclear membrane vacuolization and structural shifting towards a rounded shape. In addition, LSEC exhibit marked increased levels of reactive oxygen species (ROS) that decrease LSECs viability (12). The role of LSECs in liver injury has been reported in many experimental studies including: 1. Upregulation of surface adhesion molecules 2. Deregulation and disassembly of cell structure due to an increment in calcium-derived calpain activity 3. Apoptosis of LSEC to elastase-mediated paracrine interactions with leucocytes (13, 14).

Our group has previously reported that in a murine surgical model of *in situ* warm IRI (1h ischemia followed by 6h reperfusion time), increased activation of endothelial cell prompts the release of Interleukin 33 (IL-33) resulting in increased neutrophil cell activation and NET formation. The response to IL-33 signaling is determined by the expression of its surface receptor ST2 on the target cell which in humans are located on chromosome 11p14.3-p12. We were among the first group to show that mouse bone marrow-derived neutrophils express ST2 and that its expression is markedly increased by IL-33 stimulation. In addition, human data reveals that increased IL-33 serum levels are strongly associated with post-operative NET formation in individuals undergoing liver resection for hepatic malignancies (15).

In tandem with LSEC, activated Kupffer cells (KCs), resident macrophages in the liver, play an important role in the homeostatic response to IRI. Jaeschke et al. have shown that rat KCs when treated with high dose of retinol or propionibacterium acnes-activated KCs significantly upregulated plasma glutathione disulfide and ROS production (GSSG, an index for oxidative stress), while treatment with methyl palmitate or gadolinium chloride lead to formation of inactivated KCs leading to significant decrease in plasma GSSG levels. Inactivated KCs significantly protected the liver from IRI (16). Similarly, a study published by Dai et al. showed significant increase in the production and release of ROS and proinflammatory cytokines following IRI (17). Of the cytokines released by KCs, TNF-α has been shown to induce intraluminal expression of adhesion molecules such as ICAM-1 and P-selectin that facilitates adhesion of circulating neutrophils through a rolling and binding motion and further facilitates cell extravasation (18, 19). Since activated KCs also play a role in neutrophil chemotaxis, both TNF-α and IL-1 that are released from KCs upregulate MAC-1 adhesion protein on the neutrophil surface and promote the synthesis of IL-8 (20). In addition, Su et al. reported that KCs derived TNF-α promotes hepatocyte chemokine CXCL1 induction through the NF-κB pathway to mobilize neutrophils towards injured areas (21).

HSCs have been well studied in their role of IR. HSCs are quiescent, however during liver injury they release retinoids and can undergo differentiation into a myofibroblast-like phenotype. This activation is associated with loss of GFAP and the expression of alpha-smooth muscle actin (α-sma). A recent publication by Hwang et al. has shown that activated HSCs promote liver fibrosis *via* transfer of retinol form HSCs to hepatocytes *via* STRA6 (Stimulated by retinoic acid 6). This finding was confirmed in the liver of cirrhotic patients showing high expression of STRA6 compared to normal liver controls (22). While HSCs have been noted to directly communicate with immune cells inside sinusoids following endothelial cell damage, there is still much to investigate regarding their capacity in their ability to recruit immune cells along with regulation of sinusoidal inflammation, especially in the context of I/R injury (23). Puche et al. developed a model for depleting HSCs to investigate its properties in liver I/R injury. They utilized transgenic mice that expressed herpes simplex virus Thymidine Kinase gene (HSV-Tk) and treated them with carbon tetrachloride for 10 days to promote proliferation and subsequent making them susceptible to cell killing by treating them with ganciclovir. Approximately, 70% of HSCs were depleted and intrahepatic neutrophil infiltration was significantly decreased. Furthermore, they reported that expression of TNF-α, CXCL1, and endothelin-A receptor were also attenuated. According to these findings, HSCs are implicated in hepatic CXCL1 synthesis and contribute to neutrophil recruitment and microcirculatory failure caused by endothelin-A receptor stimulation (24, 25).

THE ROLE OF NEUTROPHILS IN I/R INDUCED INFLAMMATION

Neutrophils, an essential component of IRI, are one of the first cell types to be recruited from the bloodstream to sites of injury. Neutrophils are recruited to ischemic sites *via* DAMPs, which are produced by intracellular organelles and the extracellular matrix of damaged cells (26). DAMPs, such as HMGB1, S100 proteins, heat shock proteins, circulating RNA/DNA all trigger a broad variety of inflammatory responses that promote the secretion of pro-inflammatory cytokines and chemokines. These circulating mediators promote the upregulation of adhesion molecules on the endothelium, acute inflammation and the recruitment of neutrophils to the site of injury (27). Within the liver, Neutrophil induced inflammation is further maintained *via* CXC chemokines, generated by hepatocytes. Within the ischemic tissue, neutrophils form hydrogen peroxide and myeloperoxidase (MPO) (28). Hydrogen peroxide induces intracellular oxidant stress by direct diffusion into hepatocytes. MPO uses hydrogen peroxide to create hypochlorous acid, which enters target cells and causes damage. Neutrophil elastase secreted by activated neutrophils has been shown to inhibit PGI2 production. PGI2 is a vasodilator that is released from endothelial cells and is protective during hepatic IRI by maintaining proper hepatic circulation. When activated neutrophils release neutrophil elastase, the protective effect of PGI2 is inhibited, and hepatic injury ensues (29, 30).

Complement induced recruitment of neutrophils plays an important role in liver IRI. The complement system is part of the innate immune system and can be activated by one of three pathways. These pathways include the classical pathway, which is

antibody dependent, the alternative pathway and the mannose-binding lectin pathway. In IRI, the complement cascade is activated by detecting cellular contents that were released into the extracellular space as a result of ischemia. Complement activation leads to the formation of the soluble bioactive peptides, C3a and C5a, and the membrane attack complex, which results in the recruitment of inflammatory cells. C5a, from the complement system, stimulates Kupffer cell activation, which produces TNF-alpha, IL-1 and ROS. This ultimately leads to neutrophil recruitment and influx into liver sinusoids to promote further inflammation (31).

Another major contributing factor of neutrophil-induced inflammation is the formation of neutrophil extracellular traps (NETs). NETs are net-like structures, composed of a meshwork of chromatin fibers that contain enzymes such as MPO, neutrophil elastase, and cathepsin G. NET release from neutrophils is believed to happen *via* two different mechanisms. The first method, termed NETosis, is through the release of chromatin and granular contents into the extracellular space as the plasma membrane dissolves. Although similar to apoptosis, neutrophils appear to not be cleared by phagocytic cells after undergoing NETosis because they do not display apoptotic signals and therefore remain alive. The second method of NET release is *via* DNA/serine protease released from intact neutrophils (32). NETs have also been shown to activate the complement system and thereby further contribute to inflammation. NETs stimulate components necessary for the formation of C3bBb, which is eventually necessary for membrane attack complex formation (33).

In vitro studies have shown that Neutrophils increase the death of hepatocytes and KCs and thereby promote the release of more proinflammatory cytokines and DAMPs such as HMGB1 and histones. These DAMPs then further promote the stimulation of NETs through Toll-like receptor (TLR4)- and TLR9-MyD88 signaling pathways (34, 35).

Neutrophils tend to have relatively short lifespans, surviving for less than 24 hours in the bloodstream before undergoing apoptosis and clearance by macrophages. During periods of inflammation, numerous factors have been shown to inhibit neutrophil apoptosis and prolong their survival. It has been shown that hepatic IRI upregulates OX40, a costimulatory molecule that is constitutively expressed in human peripheral neutrophils. Increased OX40 levels promote neutrophil survival, prolonging the neutrophil release of proinflammatory factor (36). Myeloid cell leukemia-1 (MCL-1), an anti-apoptotic member of the Bcl-2 family, has been shown to downregulate neutrophil apoptosis, and promote its survival. MCL-1 has been shown to be upregulated in in models of cerebral IRI, which promote neutrophil survival (37). Other factors including DAMPs, lipid mediators, hormones, chemokines, and cytokines have been described as neutrophil survival factors (38, 39).

NETs play an important role in hepatic IRI in the context of acute rejection. Liu et al. have shown in their study that HMGB1 upon liver transplantation contributes to the development of acute liver rejection. It has been very well characterized that HMGB1 through TLR4 and RAGE receptor can activate neutrophils and promote NET formation. The authors observed increased NET levels in the serum of transplanted patients which negatively corelated with immediate postoperative liver function. In addition, both HMGB1 and NET levels correlated positive in the serum following transplantation. They further show that hepatic Kupffer cells where the main source of HMGB1 production and were polarized to M1 phenotype through NETs. Furthermore, a combination of TAK-242 (a TLR-4 inhibitor) as well as rapamycin reduced the damaging effects of acute rejection after liver transplantation more efficiently than either of them alone (40).

NEUTROPHIL EXTRACELLULAR TRAP AND ITS INTERACTION WITH PLATELETS

Accumulating evidence shows that patients that underwent liver surgery are hypercoagulable in the immediate post-operative setting (41). The mechanism of this pro-coagulation state in the postoperative period is still under investigation. We have previously shown within a murine model of liver IRI, induction of NETs can activate platelets resulting in systemic immune-thrombosis and distant organ injury (42, 43). Our data showed that 1-hour of ischemia followed by 6 hours of reperfusion significantly activated platelet and increased platelet-neutrophil aggregation. This led to increased NET-platelet rich micro-thrombi in the microvasculature after liver IRI. When NETs were blocked by DNase-1 therapy, immunological thrombi and organ damage were significantly reduced. In addition, we observed a significant decrease in the NET induced platelet activation in a TLR4 depleted platelets. Furthermore, when compared to control mice, platelet-specific TLR4 KO animals showed much less distant organ damage, with lower circulating platelet activation and platelet-neutrophil aggregates following liver I/R.

NEUTROPHILS CROSSTALK WITH ADAPTIVE IMMUNE CELLS IN THE TUMOR MICROENVIRONMENT

Recent studies have shown that Neutrophils have bidirectional interactions with B- and T-lymphocytes subsets. *In vitro*, human Neutrophils have been shown to secrete cytokines that are crucial in the survival and maturation of B-lymphocytes. These cytokines include B-cell-activating factor of the tumor necrosis factor family (BAFF) and A Proliferation-Inducing Ligand (APRIL). These findings have been substantiated by the discovery of pro-helper Neutrophils in the perifollicular area of the spleen in humans, these Neutrophils were therefore named B-cell helper neutrophils. These Neutrophils secrete higher amounts B cell stimulating and attracting factors such as CD40L, interleukin-21 and CXCL12. Interestingly, human splenic Neutrophils have been shown to lose their selective perifollicular topography and start to infiltrate the germinal centers of splenic follicles under systemic inflammatory stress (44). Tumor associated Neutrophils (TANs) have been shown to promote B cell chemotaxis to the tumor by secretion of TNFα thereby playing a role in tumor progression (45).

During liver IRI, Neutrophils can stimulate the recruitment and activation of CD8+ T cells through varying cytokines and chemokines expressed within the chromatin of activated Neutrophils (46). In addition, Neutrophils can serve as antigen-presenting cells to CD4+ T cells and cross-presenting cell to CD8+ T cells (44, 47). Several studies have shown important crosstalk between neutrophils and liver-resident lymphocytes (48). Recent studies by our laboratory have shown that NETs can directly promote the exhaustion of T cells that are found within the liver following IRI. NETs harbor the immunomodulating protein program-death ligand 1 (PD-L1) which binds PD-1 on activated T cells to render them non-functioning and exhausted. This discovery represents a novel finding with possible clinical implications to overcome T cell exhaustion and tumor growth by targeting neutrophils and NETs (9, 49).

NON-PHARMACOLOGICAL METHODS TO TARGET NEUTROPHIL MEDIATED LIVER ISCHEMIA-REPERFUSION INJURY

There is broad epidemiologic and observational evidence that regular physical exercise reduces the risk of cancer, slows tumor progression, and improves outcomes when combined with other oncologic treatment strategies. A variety of trials have shown that regular exercise can improve cancer prognosis and therefore should be seen as an important adjunct to conventional treatments. Over the last decade, a lot of emphasis has been placed on preoperative rehabilitation of frail patients who have any impairment in activities of daily living. The role of pre-habilitation is to optimize functional status in frail patients undergoing major surgery. Pre-operative exercise in the non-frail patients can have several effects that are postulated to be secondary to changes in the immune system resulting in changes in immune cell subsets, infiltration of immune cells to the site of injury, as well as secretion of inflammatory mediators (50).

We have shown that 1 hour of daily exercise for 4 weeks confers sustainable protection against IRI in a murine model. Exercise-trained mice (ExT) that underwent IRI showed a decrease in liver necrosis, significantly diminished hepatic chemokine levels, and fewer infiltrating innate immune cells. Interestingly, we observed that ExT conditioned neutrophils (isolated from circulation or bone marrow) showed decreased in NET formation when stimulated with phorbol myristate acetate (PMA). We also found that exercise reduced the inflammatory cytokine storm and decreased neutrophil adhesion and migration by downregulating endothelial adhesion molecules and increased the infiltration of M2 phenotypic anti-inflammatory macrophages. Furthermore, ExT suppressed tumor metastatic growth when injected through splenic vein 4 weeks after training and enhanced NK cell infiltration to the tumor. This is of interest, since M2 phenotypic macrophages generally known to be anti-inflammatory but pro-tumorigenic in nature. In our model of preconditioning mice with ExT, the anti-inflammatory state that developed over a 4-week period lead to increased infiltration of NK cells into the liver which attenuated the growth of micrometastatic disease. We believe that the ratio of M1/M2 macrophages in the liver of ExT mice is important to determine the actual effect on the tumor, however the presence of NK and other adaptive immune cells dictates the anti-tumor immunity within the TME. Further single-cell experience will need to be carried out in ExT vs. sedentary mice to fully delineate the type of immune cells infiltrating the liver.

However, the mechanism of ExT in preventing IRI and thereby reducing the effect on cancer growth is an important and novel observation. This finding of aerobic ExT as a nonpharmacological therapy before liver surgery might provide a rationale to extend these studies to other clinical scenarios of liver IRI such as transplantation (19).

TARGETING OF NEUTROPHIL EXTRACELLULAR TRAPS TO PREVENT LIVER ISCHEMIA-REPERFUSION INJURY

Oxidative stress is the inevitable feature of liver IRI. Excessive levels of superoxide (O2-) generated through hypoxanthine and xanthine oxidase can promotes proinflammatory milieu. Several studies, by utilizing antioxidant therapy, has shown to reduce liver IR injury in animal models (51). We have previously shown that superoxide stimulates neutrophils to release NETs through the TLR4/NOX signaling pathways. Our findings have shown that treating mice with allopurinol (superoxide inhibitor) in combination with diphenyleneiodonium (NOX inhibitor) attenuated NET formation and significantly decreased liver injury (52).

Similarly, using a mathematical model of Dynamic Network Analysis (DyNA) in a mouse model of warm *in situ* liver IRI we have previously shown that the inflammatory cytokine IL-17 plays a central role in mediating and sustaining a pro-inflammatory environment promoting I/R induced injury (53). The injury was reversed when an IL-17 neutralizing antibody was administered prior to IR injury. In addition, increase in the serum levels of IL-17 directly corresponded with the increase of intrahepatic neutrophil infiltration and NET formation suggesting IL-17 as a potent NET inducer. Similarly, in a mouse model of renal IRI, it was observed that infiltrating neutrophils were the major source of IL-17 production which further facilitated neutrophil transmigration. Furthermore, Lin et al. has shown that IL-17 positive neutrophils that are abundantly present in the human psoriasis lesions can release IL-17 through the induction of NETs. Hence targeting IL-17 using IL-17 neutralizing antibody can decrease IR induced injury *via* decreasing NET formation (54).

More recently, in a liver transplantation model, use of recombinant thrombomodulin (TM) has been shown to target NET formation and subsequently decreased liver injury in rat models. TM is a glycoprotein that is highly expressed by endothelial cells and has shown to play a protective role against liver IRI in both mouse and rat models. A study published by Yanyao et al. observed a significant decrease in neutrophil infiltration and NET formation by pretreating rats with recombinant TM (5mg/kg) intravenously 1h before the

transplantation. They further show that recombinant TM suppressed TLR-4 activity and its downstream extracellular signal (kinase/c-Jun NH2 terminal kinase and NADPH/reactive oxygen species/PAD4) signaling pathways, mostly regulated by stressed released DAMPs (55).

NETs harbor a wide variety of proinflammatory cytokines and chemokines within the NET chromatin. Protein arginine deiminase 4 (PAD4) is a key mediator of NET formation. PAD4 facilitates histone citrullination to promote chromatin decondensation and the expulsion of chromosomal DNA. Studies have shown that global PAD4 knockout mice have diminished NET production and decreased primary and metastatic cancer growth compared to wild-type mice. Similar effects have been shown by targeting neutrophil elastase (NE) or using specific MPO-inhibitors in murine models. These studies were carried out by injecting a colorectal cancer cell line (MC-38) in subcutaneous or intra-splenic fashion into wildtype or PAD4 KO animals. Wildtype animals were further treated with a NE inhibitor (56-58). PAD4KO or wildtype animals treated with NE inhibitor showed significant smaller tumors with less neutrophil infiltration and NETs compared to wildtype animals.

Another important target is the destruction of NET chromatin within the tumor. DNA, the backbone of NETs can be targeted using DNase-I. In fact, DNase-I treatment has shown promising results in preclinical murine cancer models as well as clinical trials in patients with lupus nephritis, rheumatoid arthritis or cystic fibrosis. DNAse-I has a very short half-life within the circulation and therefore requires multiple injections to achieve effective concentrations. Several inhibitors of NE and PAD4 showed decreased tumor growth when tested in the tumor burdened animal models. Several pre-clinical trials in non-cancer patients using these targets have been performed, it is therefore reasonable that these inhibitors could be beneficial and improve clinical outcomes in cancer patients alike (59-62).

In addition, blocking the direct crosstalk of NETs with adjacent cancer cells in the tumor microenvironment has shown promising results in reducing the NET effect on cancer cells. As previously described, NETs have many effects on cancer cells including enhancing their ability to invade into tissue, in addition they can alter their metabolism and subsequently increase their metastatic potential and growth. Several mediators of cancer-NET interaction have been identified including TLR4-NE, tumor-specific integrins, and most recently a surface protein called CCDC25 (35, 56, 63). Targeting these receptors using specific antagonist or knockouts have shown promising results in decreasing tumor cell migration, metastatic niche formation, and growth in murine models (35, 56).

CONCLUSION

Liver ischemia and reperfusion injury (IRI) is an important inducer of inflammation. This review discusses the importance of IRI and Neutrophils in mediating tissue damage and transplant rejection. IRI promotes the recruitment of Neutrophils to the liver which can in turn promote transplant rejection and tumor progression of micro metastatic disease. Within the liver Neutrophils/NETs can directly interact with Kupffer cells, macrophages and T cells in the transplanted liver and the TME. Taken together, this review provides an overview of the many roles of Neutrophils and NETs following liver damage *via* IRI.

AUTHOR CONTRIBUTIONS

Manuscript preparation: CK, HY, SH, and BP; Manuscript revision: DG and ST; Figure creation CK and HY. All authors contributed to the article and approved the submitted version.

REFERENCES

1. Nakamura K, Kageyama S, Kaldas FM, Hirao H, Ito T, Kadono K, et al. Hepatic CEACAM1 Expression Indicates Donor Liver Quality and Prevents Early Transplantation Injury. *J Clin Invest* (2020) 130:2689–704. doi: 10.1172/JCI133142
2. Tohme S, Simmons RL, Tsung A. Surgery for cancer: A trigger for metastases. *Cancer Res* (2017) 77:1548–52. doi: 10.1158/0008-5472.CAN-16-1536
3. Hudcova J, Scopa C, Rashid J, Waqas A, Ruthazer R, Schumann R. Effect of early allograft dysfunction on outcomes following liver transplantation. *Clin Transplant.* (2017) 31. doi: 10.1111/ctr.12887
4. Rampes S, Ma D. Hepatic ischemia-reperfusion injury in liver transplant setting: mechanisms and protective strategies. *J BioMed Res* (2019) 33:221–34. doi: 10.7555/JBR.32.20180087
5. van der Windt DJ, Sud V, Zhang H, Varley PR, Goswami J, Yazdani HO, et al. Neutrophil extracellular traps promote inflammation and development of hepatocellular carcinoma in nonalcoholic steatohepatitis. *Hepatology* (2018) 68:1347–60. doi: 10.1002/hep.29914
6. Liu X, Cao H, Li J, Wang B, Zhang P, Dong Zhang X, et al. Autophagy induced by DAMPs facilitates the inflammation response in lungs undergoing ischemia-reperfusion injury through promoting TRAF6 ubiquitination. *Cell Death Differ* (2017) 24:683–93. doi: 10.1038/cdd.2017.1
7. Nakamura K, Kageyama S, Kupiec-Weglinski JW. The Evolving Role of Neutrophils in Liver Transplant Ischemia-Reperfusion Injury. *Curr Transplant Rep* (2019) 6:78–89. doi: 10.1007/s40472-019-0230-4
8. Yang F, Zhang Y, Ren H, Wang J, Shang L, Liu Y, et al. Ischemia reperfusion injury promotes recurrence of hepatocellular carcinoma in fatty liver *via* ALOX12-12HETE-GPR31 signaling axis. *J Exp Clin Cancer Res* (2019) 38:489. doi: 10.1186/s13046-019-1480-9
9. Kaltenmeier C, Yazdani HO, Morder K, Geller DA, Simmons RL, Tohme S. Neutrophil extracellular traps promote T cell exhaustion in the tumor microenvironment. *Front Immunol* (2021) 12:785222. doi: 10.3389/fimmu.2021.785222
10. Oliveira THC, de, Marques PE, Proost P, Teixeira MMM. Neutrophils: a cornerstone of liver ischemia and reperfusion injury. *Lab Invest* (2018) 98:51–62. doi: 10.1038/labinvest.2017.90
11. Kalogeris T, Baines CP, Krenz M, Korthuis RJ. Cell biology of ischemia/reperfusion injury. *Int Rev Cell Mol Biol* (2012) 298:229–317. doi: 10.1016/B978-0-12-394309-5.00006-7
12. Dar WA, Sullivan E, Bynon JS, Eltzschig H, Ju C. Ischaemia reperfusion injury in liver transplantation: Cellular and molecular mechanisms. *Liver Int* (2019) 39:788–801. doi: 10.1111/liv.14091
13. Saviano A, Baumert TF. Unraveling the role of liver sinusoidal endothelial cells in COVID-19 liver injury. *J Hepatol* (2021) 75:503–5. doi: 10.1016/j.jhep.2021.07.008
14. Wang X-K, Peng Z-G. Targeting liver sinusoidal endothelial cells: an attractive therapeutic strategy to control inflammation in nonalcoholic fatty liver disease. *Front Pharmacol* (2021) 12:655557. doi: 10.3389/fphar.2021.655557

15. Yazdani HO, Chen H-W, Tohme S, Tai S, van der Windt DJ, Loughran P, et al. IL-33 exacerbates liver sterile inflammation by amplifying neutrophil extracellular trap formation. *J Hepatol* (2017). doi: 10.1016/j.jhep.2017.09.010
16. Jaeschke H, Farhood A. Neutrophil and Kupffer cell-induced oxidant stress and ischemia-reperfusion injury in rat liver. *Am J Physiol* (1991) 260:G355–62. doi: 10.1152/ajpgi.1991.260.3.G355
17. Dai Q, Jiang W, Liu H, Qing X, Wang G, Huang F, et al. Kupffer cell-targeting strategy for the protection of hepatic ischemia/reperfusion injury. *Nanotechnology* (2021) 32. doi: 10.1088/1361-6528/abde02
18. Yang H, Li N, Du Y, Tong C, Lü S, Hu J, et al. Neutrophil adhesion and crawling dynamics on liver sinusoidal endothelial cells under shear flow. *Exp Cell Res* (2017) 351:91–9. doi: 10.1016/j.yexcr.2017.01.002
19. Yazdani HO, Kaltenmeier C, Morder K, Moon J, Traczek M, Loughran P, et al. Exercise training decreases hepatic injury and metastases through changes in immune response to liver ischemia/reperfusion in mice. *Hepatology* (2021) 73:2494–509. doi: 10.1002/hep.31552
20. Sumagin R, Prizant H, Lomakina E, Waugh RE, Sarelius IH. LFA-1 and Mac-1 define characteristically different intralumenal crawling and emigration patterns for monocytes and neutrophils in situ. *J Immunol* (2010) 185:7057–66. doi: 10.4049/jimmunol.1001638
21. Su L, Li N, Tang H, Lou Z, Chong X, Zhang C, et al. Kupffer cell-derived TNF-α promotes hepatocytes to produce CXCL1 and mobilize neutrophils in response to necrotic cells. *Cell Death Dis* (2018) 9:323. doi: 10.1038/s41419-018-0377-4
22. Hwang I, Lee EJ, Park H, Moon D, Kim H-S. Retinol from hepatic stellate cells *via* STRA6 induces lipogenesis on hepatocytes during fibrosis. *Cell Biosci* (2021) 11:3. doi: 10.1186/s13578-020-00509-w
23. Hou X-J, Ye F, Li X-Y, Liu W-T, Jing Y-Y, Han Z-P, et al. Immune response involved in liver damage and the activation of hepatic progenitor cells during liver tumorigenesis. *Cell Immunol* (2018) 326:52–9. doi: 10.1016/j.cellimm.2017.08.004
24. Stewart RK, Dangi A, Huang C, Murase N, Kimura S, Stolz DB, et al. A novel mouse model of depletion of stellate cells clarifies their role in ischemia/reperfusion- and endotoxin-induced acute liver injury. *J Hepatol* (2014) 60:298–305. doi: 10.1016/j.jhep.2013.09.013
25. Puche JE, Lee YA, Jiao J, Aloman C, Fiel MI, Muñoz U, et al. A novel murine model to deplete hepatic stellate cells uncovers their role in amplifying liver damage in mice. *Hepatology* (2013) 57:339–50. doi: 10.1002/hep.26053
26. Roh JS, Sohn DH. Damage-Associated Molecular Patterns in Inflammatory Diseases. *Immune Netw* (2018) 18:e27. doi: 10.4110/in.2018.18.e27
27. Pittman K, Kubes P. Damage-associated molecular patterns control neutrophil recruitment. *J Innate Immun* (2013) 5:315–23. doi: 10.1159/000347132
28. Adams DH, Ju C, Ramaiah SK, Uetrecht J, Jaeschke H. Mechanisms of immune-mediated liver injury. *Toxicol Sci* (2010) 115:307–21. doi: 10.1093/toxsci/kfq009
29. Okajima K, Harada N, Uchiba M, Mori M. Neutrophil elastase contributes to the development of ischemia-reperfusion-induced liver injury by decreasing endothelial production of prostacyclin in rats. *Am J Physiol Gastrointest Liver Physiol* (2004) 287:G1116–23. doi: 10.1152/ajpgi.00061.2004
30. Kawai M, Harada N, Takeyama H, Okajima K. Neutrophil elastase contributes to the development of ischemia/reperfusion-induced liver injury by decreasing the production of insulin-like growth factor-I in rats. *Transl Res* (2010) 155:294–304. doi: 10.1016/j.trsl.2010.02.003
31. Hu Z-G, Zhou Y, Lin C-J, Yuan G-D, He S-Q. Emerging recognition of the complement system in hepatic ischemia/reperfusion injury, liver regeneration and recovery (Review). *Exp Ther Med* (2021) 21:223. doi: 10.3892/etm.2021.9654
32. Kaplan MJ, Radic M. Neutrophil extracellular traps: double-edged swords of innate immunity. *J Immunol* (2012) 189:2689–95. doi: 10.4049/jimmunol.1201719
33. Ravindran M, Khan MA, Palaniyar N. Neutrophil extracellular trap formation: physiology, pathology, and pharmacology. *Biomolecules.* (2019) 9. doi: 10.3390/biom9080365
34. McCracken JM, Allen L-AH. Regulation of human neutrophil apoptosis and lifespan in health and disease. *J Cell Death* (2014) 7:15–23. doi: 10.4137/JCD.S11038
35. Huang H, Tohme S, Al-Khafaji AB, Tai S, Loughran P, Chen L, et al. Damage-associated molecular pattern-activated neutrophil extracellular trap exacerbates sterile inflammatory liver injury. *Hepatology* (2015) 62:600–14. doi: 10.1002/hep.27841
36. Jin H, Zhang C, Sun C, Zhao X, Tian D, Shi W, et al. OX40 expression in neutrophils promotes hepatic ischemia/reperfusion injury. *JCI Insight* (2019) 4. doi: 10.1172/jci.insight.129736
37. Huang Z, Lu L, Jiang T, Zhang S, Shen Y, Zheng Z, et al. miR-29b affects neurocyte apoptosis by targeting MCL-1 during cerebral ischemia/reperfusion injury. *Exp Ther Med* (2018) 16:3399–404. doi: 10.3892/etm.2018.6622
38. Tan C, Aziz M, Wang P. The vitals of NETs. *J Leukoc Biol* (2021) 110:797–808. doi: 10.1002/JLB.3RU0620-375R
39. Brostjan C, Oehler R. The role of neutrophil death in chronic inflammation and cancer. *Cell Death Discovery* (2020) 6:26. doi: 10.1038/s41420-020-0255-6
40. Liu A, Fang H, Dirsch O, Jin H, Dahmen U. Oxidation of HMGB1 causes attenuation of its pro-inflammatory activity and occurs during liver ischemia and reperfusion. *PloS One* (2012) 7:e35379. doi: 10.1371/journal.pone.0035379
41. Gordon N, Riha G, Billingsley K, Schreiber M. Malignancy does not dictate the hypercoagulable state following liver resection. *Am J Surg* (2015) 209:870–4. doi: 10.1016/j.amjsurg.2014.12.022
42. Potze W, Alkozai EM, Adelmeijer J, Porte RJ, Lisman T. Hypercoagulability following major partial liver resection - detected by thrombomodulin-modified thrombin generation testing. *Aliment Pharmacol Ther* (2015) 41:189–98. doi: 10.1111/apt.13022
43. Zhang H, Goswami J, Varley P, van der Windt DJ, Ren J, Loughran P, et al. Hepatic surgical stress promotes systemic immunothrombosis that results in distant organ injury. *Front Immunol* (2020) 11:987. doi: 10.3389/fimmu.2020.00987
44. Costa S, Bevilacqua D, Cassatella MA, Scapini P. Recent advances on the crosstalk between neutrophils and B or T lymphocytes. *Immunology* (2019) 156:23–32. doi: 10.1111/imm.13005
45. Shaul ME, Zlotnik A, Tidhar E, Schwartz A, Arpinati L, Kaisar-Iluz N, et al. Tumor-Associated Neutrophils Drive B-cell Recruitment and Their Differentiation to Plasma Cells. *Cancer Immunol Res* (2021) 9:811–24. doi: 10.1158/2326-6066.CIR-20-0839
46. Minton K. Chemokines: Neutrophils leave a trail for T cells. *Nat Rev Immunol* (2015) 15:597. doi: 10.1038/nri3917
47. Marini O, Costa S, Bevilacqua D, Calzetti F, Tamassia N, Spina C, et al. Mature CD10+ and immature CD10- neutrophils present in G-CSF-treated donors display opposite effects on T cells. *Blood* (2017) 129:1343–56. doi: 10.1182/blood-2016-04-713206
48. Zhai Y, Busuttil RW, Kupiec-Weglinski JW. Liver ischemia and reperfusion injury: new insights into mechanisms of innate-adaptive immune-mediated tissue inflammation. *Am J Transplant* (2011) 11:1563–9. doi: 10.1111/j.1600-6143.2011.03579.x
49. Kaltenmeier C, Simmons RL, Tohme S, Yazdani HO. Neutrophil extracellular traps (nets) in cancer metastasis. *Cancers (Basel).* (2021) 13. doi: 10.3390/cancers13236131
50. Hanna K, Ditillo M, Joseph B. The role of frailty and prehabilitation in surgery. *Curr Opin Crit Care* (2019) 25:717–22. doi: 10.1097/MCC.0000000000000669
51. Fernández L, Heredia N, Grande L, Gómez G, Rimola A, Marco A, et al. Preconditioning protects liver and lung damage in rat liver transplantation: role of xanthine/xanthine oxidase. *Hepatology* (2002) 36:562–72. doi: 10.1053/jhep.2002.34616
52. Sener G, Tosun O, Sehirli AO, Kaçmaz A, Arbak S, Ersoy Y, et al. Melatonin and N-acetylcysteine have beneficial effects during hepatic ischemia and reperfusion. *Life Sci* (2003) 72:2707–18. doi: 10.1016/s0024-3205(03)00187-5
53. Tohme S, Yazdani HO, Sud V, Loughran P, Huang H, Zamora R, et al. Computational Analysis Supports IL-17A as a Central Driver of Neutrophil Extracellular Trap-Mediated Injury in Liver Ischemia Reperfusion. *J Immunol* (2019) 202:268–77. doi: 10.4049/jimmunol.1800454
54. Lin AM, Rubin CJ, Khandpur R, Wang JY, Riblett M, Yalavarthi S, et al. Mast cells and neutrophils release IL-17 through extracellular trap formation in psoriasis. *J Immunol* (2011) 187:490–500. doi: 10.4049/jimmunol.1100123
55. Liu Y, Lei Z, Chai H, Xiang S, Wang Y, Yan P, et al. Thrombomodulin-mediated Inhibition of Neutrophil Extracellular Trap Formation Alleviates Hepatic Ischemia-reperfusion Injury by Blocking TLR4 in Rats Subjected to Liver Transplantation. *Transplantation* (2022) 106:e126–40. doi: 10.1097/TP.0000000000003954

56. Yazdani HO, Roy E, Comerci AJ, van der Windt DJ, Zhang H, Huang H, et al. Neutrophil extracellular traps drive mitochondrial homeostasis in tumors to augment growth. *Cancer Res* (2019) 79:5626–39. doi: 10.1158/0008-5472.CAN-19-0800
57. Tohme S, Yazdani HO, Liu Y, Loughran P, van der Windt DJ, Huang H, et al. Hypoxia mediates mitochondrial biogenesis in hepatocellular carcinoma to promote tumor growth through HMGB1 and TLR9 interaction. *Hepatology* (2017) 66:182–97. doi: 10.1002/hep.29184
58. Tohme S, Yazdani HO, Al-Khafaji AB, Chidi AP, Loughran P, Mowen K, et al. Neutrophil Extracellular Traps Promote the Development and Progression of Liver Metastases after Surgical Stress. *Cancer Res* (2016) 76:1367–80. doi: 10.1158/0008-5472.CAN-15-1591
59. Davis JC, Manzi S, Yarboro C, Rairie J, Mcinnes I, Averthelyi D, et al. Recombinant human Dnase I (rhDNase) in patients with lupus nephritis. *Lupus* (1999) 8:68–76. doi: 10.1191/096120399678847380
60. Aliko A, Kamińska M, Falkowski K, Bielecka E, Benedyk-Machaczka M, Malicki S, et al. Discovery of novel potential reversible peptidyl arginine deiminase inhibitor. *Int J Mol Sci* (2019) 20. doi: 10.3390/ijms20092174
61. Martín Monreal MT, Rebak AS, Massarenti L, Mondal S, Šenolt L, Ødum N, et al. Applicability of Small-Molecule Inhibitors in the Study of Peptidyl Arginine Deiminase 2 (PAD2) and PAD4. *Front Immunol* (2021) 12:716250. doi: 10.3389/fimmu.2021.716250
62. Perdomo J, Leung HHL, Ahmadi Z, Yan F, Chong JJH, Passam FH, et al. Neutrophil activation and NETosis are the major drivers of thrombosis in heparin-induced thrombocytopenia. *Nat Commun* (2019) 10:1322. doi: 10.1038/s41467-019-09160-7
63. Yang L, Liu Q, Zhang X, Liu X, Zhou B, Chen J, et al. DNA of neutrophil extracellular traps promotes cancer metastasis via CCDC25. *Nature* (2020) 583:133. doi: 10.1038/s41586-020-2394-6

Conflict of Interest: The authors declare that the research was conducted in the absence of any commercial or financial relationships that could be construed as a potential conflict of interest.

Publisher's Note: All claims expressed in this article are solely those of the authors and do not necessarily represent those of their affiliated organizations, or those of the publisher, the editors and the reviewers. Any product that may be evaluated in this article, or claim that may be made by its manufacturer, is not guaranteed or endorsed by the publisher.

frontiers | Frontiers in Immunology

TYPE Review
PUBLISHED 28 July 2022
DOI 10.3389/fimmu.2022.891868

OPEN ACCESS

EDITED BY
Tao Qiu,
Renmin Hospital of Wuhan University, China

REVIEWED BY
Edward N Harris,
University of Nebraska System, United States
Shao-wei Li,
Taizhou Hospital of Zhejiang Province Affiliated to Wenzhou Medical University, China

*CORRESPONDENCE
Yuming Peng
41216250@qq.com
Qiang Yin
qiangyin@hotmail.com

SPECIALTY SECTION
This article was submitted to Molecular Innate Immunity, a section of the journal Frontiers in Immunology

RECEIVED 08 March 2022
ACCEPTED 27 June 2022
PUBLISHED 28 July 2022

CITATION
Peng Y, Yin Q, Yuan M, Chen L, Shen X, Xie W and Liu J (2022) Role of hepatic stellate cells in liver ischemia-reperfusion injury.
Front. Immunol. 13:891868.
doi: 10.3389/fimmu.2022.891868

Role of hepatic stellate cells in liver ischemia-reperfusion injury

Yuming Peng[1,2]*, Qiang Yin[1,2]*, Miaoxian Yuan[1,2], Lijian Chen[1,2], Xinyi Shen[1,2], Weixin Xie[1,2] and Jinqiao Liu[3]

[1]First Department of General Surgery, Hunan Children's Hospital, Changsha, China, [2]Zhaolong Chen Academician Workstation, Changsha, China, [3]Department of Ultrasound, Hunan Children's Hospital, Changsha, China

Liver ischemia-reperfusion injury (IRI) is a major complication of liver trauma, resection, and transplantation. IRI may lead to liver dysfunction and failure, but effective approach to address it is still lacking. To better understand the cellular and molecular mechanisms of liver IRI, functional roles of numerous cell types, including hepatocytes, Kupffer cells, neutrophils, and sinusoidal endothelial cells, have been intensively studied. In contrast, hepatic stellate cells (HSCs), which are well recognized by their essential functions in facilitating liver protection and repair, have gained less attention in their role in IRI. This review provides a comprehensive summary of the effects of HSCs on the injury stage of liver IRI and their associated molecular mechanisms. In addition, we discuss the regulation of liver repair and regeneration after IRI by HSCs. Finally, we highlight unanswered questions and future avenues of research regarding contributions of HSCs to IRI in the liver.

KEYWORDS

ischemia-reperfusion injury, hepatic stellate cells, hepatocytes, Kupffer cells, neutrophils, sinusoidal endothelial cells, liver transplantation, liver

Introduction

Liver diseases have become one of the leading causes of death worldwide in the past few decades. It was estimated that over two million deaths were attributed to major liver diseases, such as cirrhosis and liver cancer (1), highlighting the demand for liver transplantation, which is currently the optimal treatment for end-stage liver diseases. Upon restoration of blood supply after interruption, the liver subjects to further injury that aggravates the initial injury caused by ischemia. This pathophysiological process is called liver ischemia-reperfusion injury (IRI) (2). Liver IRI can be classified into warm and cold IRI, which share similar mechanisms with differences mainly in the clinical settings (3). Warm IRI, initiated by hepatocellular damage, develops *in situ* during liver trauma and transplantation where hepatic blood flow falls transiently. Cold IRI, initiated by liver sinusoidal endothelial cells (LSECs) damage and microcirculatory disruption, occurs ex vivo during cold storage of the liver before transplantation surgery (4). Liver IRI is a critical complication in several clinical settings including liver trauma, resection,

and transplantation (5–7). The degree of liver IRI depends on the period, methods of ischemia, and baseline liver condition (8). Continuous occlusion as short as 5 min can still lead to liver damage 1 d postoperatively in rat model of liver IRI, and IRI is much exacerbated in steatotic liver (9). IRI is an important cause of liver dysfunction (10), yet no reliable treatment option has been discovered. A better understanding of the cellular and molecular mechanisms of liver IRI may lead to improvements to clinical outcomes of liver disease patients, particularly those undergoing liver transplantation.

Substantial knowledge has been accumulated in regard to mechanisms underlying hepatic ischemic injury due to success of animal models. It is proposed that liver IRI consists of initial and late phases with distinct pathophysiological characteristics. Initial phase of liver IRI occurs 1-3 h after reperfusion (11–13), and manifests as rapid Kupffer cell activation after reperfusion (11, 14). Reactive oxygen species (ROS) is released by Kupffer cells, leading to oxidative stress and liver injury. Subsequently, the early liver injury triggers the release of a series of pro-inflammatory cytokines, such as TNF-α and IL-1β, inducing immune cell recruitment and more severe liver injury (15). The late phase of liver IRI, which occurs at 6-24 h after reperfusion (11, 12), is characterized by the recruitment of neutrophils to the liver and subsequent damage to hepatocytes (14).

Multiple cell types, including hepatocytes, liver sinusoidal endothelial cells (LSECs), Kupffer cells, hepatic stellate cells (HSCs) extrahepatic macrophages, neutrophils, and platelets, are involved in the progression of liver IRI (14, 16). Hepatocytes and LSECs are the main cell types subject to IRI induced cell death (17). Extensive studies indicate that Kupffer cells play a critical role in regulating IRI by promoting inflammatory injury mediated by cytokines and chemokines (2, 17). Neutrophils act as the main actor of cell injury during liver IRI following their recruitment to the liver regulated by Kupffer cells releasing of chemokines. Upon migration and infiltration to the liver, neutrophils respond to signals released by injured hepatocytes, inducing release of ROS and degranulation to cause further injury (17, 18). HSCs, which reside in the perisinusoidal space of liver and are known for their essential function of regulating hepatic fibrosis (19), has not been long investigated in liver IRI. As more recent studies shed light in the role of HSCs in liver IRI, we aimed to summarize the effects of HSCs on regulation of liver IRI in both injury and repair/regeneration stages, their intercellular communications with other cell types during IRI, and the associated molecular mechanisms.

Quiescence and activation of HSCs in liver IRI

HSCs are localized in the subendothelial space of Disse between hepatocytes and LSECs and comprise approximately 15% of total cells in human liver (20). Due to anatomic features, intercellular crosstalk can occur between adjacent cell types including hepatocytes, Kupffer cells, bone marrow-derived macrophages, LSECs, infiltrating leukocytes, and nerve cells (20, 21). HSCs are identified by expression of both mesenchymal and neuronal markers including desmin, vimentin, nestin, and glial fibrillary acidic protein (GFAP) (22). Under physiological circumstance, HSCs sustain a non-proliferative and quiescent phenotype with angular, rounded cell bodies, extended cytoplasmic processes, and unique vitamin A storage in lipid droplets (23). In normal liver, HSCs contribute to liver regeneration, regulation of sinusoidal circulation, and vitamin A storage and release (24–26). HSCs are important sources of myofibroblasts during liver damage (27). When liver injury occurs, however, HSCs become activated and transdifferentiate into proliferative, contractile, and inflammatory myofibroblasts, which are characterized by secretion of extracellular matrix (ECM) molecules (28, 29). In this condition, HSCs are marked by expression of α-smooth muscle actin (α-SMA) (30). Activated HSCs secrete endothelin-1 (ET-1), which is a molecule with potent vesoconstricting effect, promoting proliferation and fibrogenesis, and thus is supposed to contribute to portal hypertension (31, 32). HSCs have been identified as a critical driver of fibrosis in liver injury (19, 33). It is postulated that during liver IRI, HSCs are activated by TNF-α, IL-6, and nitric oxide (NO), followed by transdifferentiation into myofibroblast phenotype (17). Activation of HSCs results in secretion of matrix metalloproteinases (MMPs), cytokines, and chemokines, leading to ECM destruction, further activation of HSC, and infiltration of neutrophils and platelets (17). These effects imply HSCs can play an important role in regulating hepatic inflammation during IRI.

Effects of HSCs on liver IRI

Functional roles of HSCs in injury stage of hepatic IRI has received much less attention than Kupffer cells, partly because functional inhibitor of Kupffer cells, gadolinium chloride, has enabled direct manipulation of these cells in experimental models (34). HSCs as a whole promote liver damage in the early phase of IRI, but they may mediate protective effect upon some pharmacological interventions or external stimuli as well. Thus HSCs may be regulated by specific signaling to combat IRI in the liver. **Figure 1** summarizes the molecular mechanisms of liver IRI mediated by HSCs, which are discussed below.

The involvement of HSCs in liver IRI was proposed based on preliminary observational studies. For instance, Takeda et al. found that heparin diminished serum levels of ET-1, aspartate transaminase (AST) and recovered hepatic IRI induced disturbance of oxidized and deoxidized hemoglobin after 1 h of IRI in rabbit model. Interestingly, electron microscopy

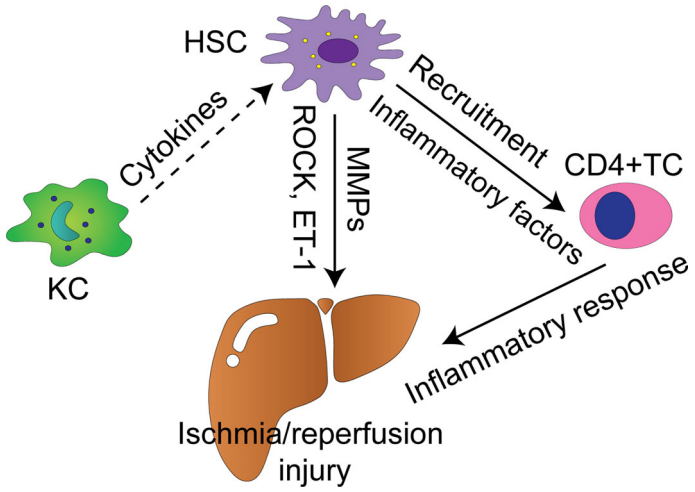

FIGURE 1
Cellular and molecular mechanisms by which HSCs modulate liver IRI. Solid arrows indicate positively regulatory effect with supporting experiment data, whereas dash arrows indicate putative positively regulatory effect. KC, Kupffer cell; TC, T cell; HSC, hepatic stellate cell; MMPs, matrix metalloproteinases; ROCK, Rho-associated coiled-coil forming protein serine/threonine kinase; ET-1, endothelin-1.

revealed that IRI induced structural alteration of HSCs, which were target cells for ET-1, was normalized upon administration of heparin (35). These results suggested that HSCs mediated liver protective effect of heparin *via* microcirculation regulatory molecule ET-1. Further studies supported HSC's role in hepatic IRI was partly mediated by regulation of microcirculation. HSCs play a key role in regulating hepatic microcirculation. In response to some stimuli, HSCs can contract or relax themselves, thus enlarging or shrinking the diameter of the sinusoidal lumen (36). Rho family of small GTPases regulates cell structure and motility mainly *via* rearrangement of actin cytoskeletons (37, 38). Rho-associated coiled-coil forming protein serine/threonine kinase (ROCK) was identified as one of the critical regulators of HSCs motility (39). In contrast to the scenario where HSCs appear to protect hepatocytes against IRI, HSCs drive liver injury mediated partly by ROCK. Administration of a specific inhibitor of ROCK named Y-27632 in rat attenuated IRI induced liver dysfunction manifested as increased deoxidized hemoglobin, decreased cytochrome oxidase, and elevated transaminase 1 h after reperfusion (40, 41). Consistently, Y-27632 resulted in relaxation of HSCs even in the presence of ET-1 *in vitro* (41). Liver protective effect of ROCK inhibition on IRI was also confirmed by another study in rat with steatotic liver. Kuroda et al. demonstrated that suppressing ROCK with specific inhibitor fasudil ameliorated IRI induced increase in portal perfusion pressure and liver damage at early stage of IRI in steatotic liver (42). In particular, Rho/ROCK signaling in HSCs from steatotic livers was activated and the activation was related to increased contractility and ET-1, making it more vulnerable to IRI (42). Specificity of the effect of ROCK regulator on HSCs was further supported by the findings that HSCs targeting inhibition of ROCK by vitamin A-coupled liposomes suppressed HSC activation, hepatic blood supply, portal perfusion pressure during early hepatic IRI, and improved survival rate after the damage in rat steatotic liver (43).

A more clear landscape of functions of HSC in liver IRI is delineated by specific manipulating approaches for HSCs *in vivo*. Functional experiments in rodent model suggest that HSCs exacerbate injury during hepatic IRI mediated by TNF-α and ET-1. Exploiting genetically engineered mice expressing HSV-thymidine kinase under the GFAP promoter coupled with ganciclovir and CCL_4 to eliminate actively proliferating HSCs, a seminal research by Stewart et al. showed that hepatic injury in both IRI and endotoxemia scenarios was attenuated in HSCs depleted mice (approximately 70%) (44, 45). The decreased injury was accompanied by significantly reduced hepatocyte pro-inflammatory cytokine TNF-α, neutrophil expression of chemoattractant CXCL1 and endothelin-A receptor (45). Of note, liver IRI and endotixin-induced acute injury might share similar cellular pathogenesis *via* HSC regulated inflammation. However, the time to evaluate the liver damage, mRNA and protein expression was not mentioned in this study, making it not feasible to infer whether HSCs regulate early or late liver IRI. Pharmacological approach alone has also been found to deplete HSCs *in vivo*. Gliotoxin induces apoptosis in both human and rat HSCs *in vitro*, and rat HSCs *in vivo* leading to resolution of fibrosis (46–48). Liver IRI in early phase was significantly reduced and sinusoidal perfusion was recovered by pretreatment with gliotoxin in HSCs decreased rat, suggesting

HSCs exerted exacerbating effect on the magnitude of early liver ischemic injury (49).

Matrix metalloproteinases (MMPs) are a family of zinc-dependent proteases which are essential in the degradation of ECM to enable cellular movement and tissue reorganization (50). MMP activation and release are involved in liver IRI due to their profound effects on tissue integrity (51). It has been asserted that prolonged or over expression of MMP exerts harmful effects on the liver (52). Kupffer cells and HSCs are main sources of MMPs in the liver, although LSECs and leukocytes can also secrete MMPs (50, 53, 54). The involvement of MMPs in liver IRI is demonstrated by their concomitant expression and functional effects. HSCs contribute to MMP-9 production in the liver (55, 56). MMP-9 is increased 6 h after hepatic IRI in the steatotic rat orthotopic liver transplantation (OLT) model, and serum MMP-9 is elevated significantly 7 d post IRI in human OLT (57, 58). Furthermore, several MMPs, including MMP-9, are induced during early phase of liver IRI, and blocking MMPs with specific inhibitors reduces liver IRI and the release of proinflammatory cytokines (12, 59). MMP-9 deficiency and anti-MMP-9 neutralizing monoclonal antibodies also result in protection against damage during early phase of liver IRI in mice (60).

Despite the *in-vivo* data indicating HSCs exacerbate damage during IRI collectively, they may aid in or mediate liver protection *via* distinct signals. ROS have been proposed as key initiators of IRI response in the liver by causing direct cellular damage and inducing inflammatory response *via* high mobility group box-1 (HMGB1) and NF-κB (61–63). An *in-vitro* study suggested that HSCs protected hepatocytes against ROS injury (64). In addition, pretreating mice with HSCs ameliorated liver IRI at 12 h after reperfusion in a regulatory T cells (Tregs)-dependent manner (65). It should be noted that, however, the HSCs administered were primary cell lines not subject to activation following hypoxia/reoxygenation (H/R) stress, which could largely explain the differences with HSC depletion results *in-vivo*. Post-conditioning with the volatile anesthetic drug sevoflurane protected the liver from IRI 1 d post reperfusion in a randomized controlled trial, and *in-vitro* study suggested that HSC might be the effector of the protection by reducing apoptosis of hepatocytes (66, 67). More specifically, supernatants of HSCs previously exposed to H/R induced apoptosis of hepatocytes, but this effect was attenuated with sevoflurane postconditioning (67). Fibroblast growth factor 10 (FGF10) belongs to the fibroblast growth factor (FGF) family, whose members play crucial roles in organ development, homeostasis, and repair (68). FGF10 binds to fibroblast growth factor receptor 2b (FGFR2b) and this signaling controls hepatoblast survival and liver size (69, 70). Li et al. demonstrated that HSCs secreted fibroblast growth factor 10 (FGF10) *in vitro*, which ameliorated inflammation and necrosis, and protected hepatocytes from apoptosis during early phase of liver IRI *in vivo* (71). These results elucidated the protective effects of FGF10 in early liver IRI, and strongly implied these effects were modulated by HSCs.

HSCs in liver repair and regeneration after IRI

The liver has a large regenerative capacity following physical or functional loss, with the potential of hepatocyte proliferation to sustain liver function. Necrotic tissue in the postischemic liver is cleared and remodeled by phagocytes, HSCs, and other cells, followed by hepatocyte regeneration and reconstruction of functional liver architecture (14). Far less is elucidated about the mechanisms of these processes compared with the mechanisms of hepatic IRI. Particularly, the role of HSCs in the process of liver repair after IRI is not clear (72).

MMPs derived from HSCs may promote liver repair after IRI in the liver, although they have been shown to promote damage by destruction of ECM and recruitment of leukocytes (73). Specifically, reduction in liver damage at 24 h after reperfusion and significant delay of liver repair after 72 h of reperfusion were observed in MMP-9 knockout mice, compared with wild type mice (74). MMP-9 was found to increase TGF-β activation after IRI. *In-vitro* study showed that MMP-9 activated TGF-β secreted by HSCs, indicating involvement of HSC in liver repair (74). A recent study exquisitely examined pathology of liver fibrosis during the repair process after IRI and highlighted involvement of HSC and MMPs. Konishi et al. found that the number of activated HSCs increased along the damaged areas 1 wk after IRI (72). Liver fibrosis took place at the interface between necrotic site and regenerating liver associated with HSCs during the reparative process after IRI, and noticeably, the number of HSCs decreased shortly after resolution of injury and restoration of disrupted liver structure. They also investigated the expression of several MMPs related to degradation of extracellular matrix components and reported that the expression of MMP-2 and MMP-9 increased at 1 wk after liver IRI and diminished thereafter. In contrast, MMP-13 expression remained at low level 1 wk after IRI but significantly elevated after 2 wk and the trend was stable up to 8 wk post IRI. The trends of MMP-2 and MMP-9 expression were associated with resolution of liver fibrosis and concomitant increase and decrease thereafter in the number of activated HSCs (72). Akin to MMP-9, MMP-13 is expressed in and produced by HSCs (75, 76). In relation to the injury stage, MMP-9 plays both deleterious and protective roles in hepatic IRI, which is dependent on the timing (74). It can be inferred from the pathological findings and source of MMPs that HSCs participate in the reparative process after liver IRI.

Recent innovative works involving Yes-associated protein (YAP) also underline the critical role of HSC in liver repair and regeneration after IRI. YAP and transcriptional coactivator with

PDZ-binding motif (TAZ) are downstream effectors of the Hippo signalling pathway, which have been identified as essential regulators controlling cellular proliferation and organ size (77). Marked activation and proliferation of HSCs was observed at both injury and repair/regeneration phases after liver IRI in mice, with concurrent selective activation of YAP and TAZ and expression of their target genes. Inhibiting YAP and TAZ after injury phase significantly diminished HSC and hepatocyte proliferation, suggesting the dependence of liver repair and regeneration after IRI on HSC (78). Liu et al. demonstrated that YAP inhibition prior to ischemia and reperfusion operation delayed liver repair and increased hepatic fibrosis at 7 days after IRI. These changes were associated with enhanced HSC stimulation manifested as fibrogenic and contractile characteristics *in-vitro* (79). This study indicated HSC might serve as a regulator of liver repair and fibrogenesis in an YAP dependent manner.

HSCs contribute to liver fibrosis during reparative process after IRI. ECM accumulation generated by HSCs potentiates at the boundary between necrotic and hepatocyte regenerating region. Resolution of liver fibrosis is associated with decreased activation of HSC (72). In fibrotic liver, HSCs may also promote liver repair after IRI. Fibrotic liver shows more severe injury but more rapid repair and regeneration compared with nonfibrotic liver in mice, which are accompanied by prominent accumulation of HSCs in fibrotic liver in early reparative phase (80).

Intercellular communications involving HSCs in liver IRI

The signaling cascades leading to hepatic damage are various and complex, involving interactions between hepatocytes, Kupffer cells, HSCs, LSECs, recruited neutrophils, macrophages, and platelets (81). HSCs are highly versatile cells with complex crosstalk with residential hepatic cells and circulating immune cells, including hepatocytes, Kupffer cells, LSECs, natural killer cells (NK cells), T cells, and B cells (26, 27, 82, 83). This notion is demonstrated with enormous evidence mainly in the context of chronic hepatic injury leading to hepatic fibrosis, such as viral infection and alcoholic liver disease, but only a few works elucidate the crosstalk involving HSCs in liver IRI. As mentioned above, Kupffer cells are fundamental drivers of the early hepatic IRI. The crosstalk between Kupffer cells and HSCs were validated by *in-vitro* model (84, 85). This crosstalk was mediated by H_2O_2 and IL-6 (84). Furthermore, Kupffer cells can activate HSCs *in vitro* and *in vivo* mediated by IL-1 and TNF during fibrogenesis (86). It is believed that TNF-α and IL-6 released by Kupffer cells activate HSCs in the early phase of liver IRI (17). As liver fibrosis is a component of liver repair after IRI (72), Kupffer cells may induce activation and proliferation of HSCs in the recovery of IRI. In the scenario of liver fibrosis following chronic liver injury, activation and proliferation of HSCs are induced by TNF-α, IL-6, TGF-β, platelet-derived growth factor (PDGF), and ROS secreted by Kupffer cells (87, 88). CD4+ T cells are essential in promoting pro-inflammatory immune response in the liver and play an important role in hepatic IRI (89–91). Reifart et al. reported that CD4+ T cells interacted with HSCs along their migration to the liver *in vivo*. Depletion of HSCs diminished CD4+ T cell recruitment to the postischemic tissue and protected the liver from IRI (92). LSECs form the vascular wall of the liver sinusoid and play crucial protective roles in vascular homeostasis, and inflammation. LSECs are prominently vulverable to IRI, making them one of a key factors leading to hepatic IRI (81). LSECs suffering from ischemic challenge decrease production of NO, and together with elevated ET-1 production, contribute to contraction of HSCs. These events lead to narrowing of the sinusoidal lumen and microcirculatory dysfunction (81, 93). Cellular and molecular mechanisms by which HSCs regulate hepatic IRI are shown in **Figure 1**.

Conclusion and future direction

Despite decades of research into the development of liver IRI and its intervention, liver IRI is still a major cause of mortality and morbidity after hepatic surgery and transplantation. Much less attention has been focused on the roles of HSCs in liver IRI compared to other cell types involved. HSCs become activated and proliferate in response to IRI, likely through signals from Kupffer cells. HSCs promote early phase hepatic IRI by constraining hepatic microcirculation mediated by ROCK, effects of ET-1 signalling, and pro-inflammatory cascades initiated by TNF-α. MMPs derived from HSCs may also increase damage by destruction of ECM and recruitment of leukocytes. HSCs can mediate hepatic protective effect *via* external stimuli such as sevoflurane, and FGF10. During the repair and regeneration stage, HSCs play an fundamental role in potentiating liver recovery. Molecular mechanisms involve activation of TGF-β signalling pathway by MMP-9, activation of YAP and TAZ. During the reparative stage of liver IRI, HSCs also regulate fibrogenesis, the extent of which may be critical to functional recovery of the liver.

Future research regarding involvement of HSCs in liver IRI can be aimed at three directions to aid in better understanding of the pathophysiology of IRI and development of novel therapeutic interventions. Intercellular communications between HSCs and other cell types should be studied using *in vivo* visualization techniques and cell-type specific genetic animal models. Furthermore, it is clinically useful to identify HSCs derived biomarkers predictive of transplantation outcomes with less expensive modern multi-omics technologies. It is of paramount

TABLE 1 Clinical trials of drugs targeting HSC activation.

Drug	Target	Main findings	Phase of Trial	Status	NCT number	Reference
Pioglitazone	PPARγ agonist	Reduces serum aminotransferase levels, hepatic steatosis, lobular inflammation for NASH without diabetes	III	completed	NCT00063622	(94)
Obeticholic acid	Farnesoid X receptor agonist	Increases insulin sensitivity, reduces biomarkers of liver inflammation and fibrosis for NFAD with T2DM	II	completed	NCT00501592	(95)
		Improves liver fibrosis and NASH disease activity for NASH	III	active	NCT02548351	(96)
Elafibranor	Dual PPARα–PPARδ ligand	Induces resolution of NASH without worsening fibrosis in patients with NASH without cirrhosis	III	completed	NCT01694849	(97)
Cenicriviroc	Dual CCR2–CCR5 receptor antagonist	Improves liver fibrosis without impacting steatohepatitis for NASH with liver fibrosis	II	completed	NCT02217475	(98)
Belapectin (GR-MD-02)	Galectin-3 antagonist	Does not improve liver fibrosis for NASH with liver fibrosis evaluated by imaging methods	II	completed	NCT02421094	N/A
		Does not improve portal hypertension in patients with NASH, cirrhosis, and portal hypertension, but reduces portal pressure in patients without esophageal varices and varices development	II	completed	NCT02462967	(99)
ND-L02-s0201	HSP47	N/A	I	completed	NCT02227459	N/A

NASH, nonalcoholic steatohepatitis; NFAD, nonalcoholic fatty liver disease; T2DM, type 2 diabetes mellitus; N/A, not applicable.

importance to screen and identify novel agents to ameliorate hepatic IRI, given that clinical trials of many drugs targeting HSCs for anti-fibrosis are completed or under way (26). An update of the clinical trials and drugs is shown in **Table 1** (94–99). Because HSCs contribute to damage and repair of liver IRI, it is likely that anti-fibrotic drug has an effect on combating IRI.

Author contributions

YP, MY, LC, XS, WX, JL, and QY contributed to the writing and editing of the manuscript. All authors contributed to the article and approved the submitted version.

Funding

This study was supported by Technical Innovation Project of Hunan Provincial Health Commission (No.: Memo [2018]187 of Xiangwei Medical Administration Office), International Talent Project of Hunan Children's Hospital.

Conflict of interest

The authors declare that the research was conducted in the absence of any commercial or financial relationships that could be construed as a potential conflict of interest.

Publisher's note

References

1. Byass P. The global burden of liver disease: A challenge for methods and for public health. *BMC Med* (2014), 12:159. doi: 10.1186/s12916-014-0159-5

2. Saidi RF, Kenari SKH. Liver ischemia/reperfusion injury: an overview. *J Invest Surg* (2014) 27(6):366–79. doi: 10.3109/08941939.2014.932473

3. Rampes S, Ma D. Hepatic ischemia-reperfusion injury in liver transplant setting: mechanisms and protective strategies. *J BioMed Res* (2019) 33(4):221–34. doi: 10.7555/JBR.32.20180087

4. Zhai Y, Petrowsky H, Hong JC, Busuttil RW, Kupiec-Weglinski JW. Ischaemia–reperfusion injury in liver transplantation–from bench to bedside. *Nat Rev Gastroenterol Hepatol* (2013) 10(2):79–89. doi: 10.1038/nrgastro.2012.225

5. Kim YI. Ischemia-reperfusion injury of the human liver during hepatic resection. *J Hepatobil Pancreat Surg* (2003) 10(3):195–9. doi: 10.1007/s00534-002-0730-x

6. Huguet C, Gavelli A, Bona S. Hepatic resection with ischemia of the liver exceeding one hour. *J Am Coll Surg* (1994) 178(5):454–8.

7. Lemasters JJ, Thurman RG. Reperfusion injury after liver preservation for transplantation. *Annu Rev Pharmacol Toxicol* (1997) 37:327–38. doi: 10.1146/annurev.pharmtox.37.1.327

8. Abu-Amara M, Yang SY, Tapuria N, Fuller B, Davidson B, Seifalian A. Liver ischemia/reperfusion injury: processes in inflammatory networks–a review. *Liver Transpl* (2010) 16(9):1016–32. doi: 10.1002/lt.22117

9. Kostakis ID, Sikalias N, Alexiou K, Mountzalia L, Papalois A, Karatzas T. How much ischemia can the severely steatotic rat liver tolerate? *In Vivo* (2018) 32 (6):1381–6. doi: 10.21873/invivo.11390

10. Casillas-Ramírez A, Mosbah IB, Ramalho F, Roselló-Catafau J, Peralta C. Past and future approaches to ischemia-reperfusion lesion associated with liver transplantation. *Life Sci* (2006) 79(20):1881–94. doi: 10.1016/j.lfs.2006.06.024

11. Jaeschke H, Farhood A. Neutrophil and kupffer cell-induced oxidant stress and ischemia-reperfusion injury in rat liver. *Am J Physiol* (1991) 260(3 Pt 1):G355–362. doi: 10.1152/ajpgi.1991.260.3.G355

12. Cursio R, Mari B, Louis K, Rostagno P, Saint-Paul MC, Giudicelli J, et al. Rat liver injury after normothermic ischemia is prevented by a phosphinic matrix metalloproteinase inhibitor. *FASEB J* (2002) 16(1):93–5. doi: 10.1096/fj.01-0279fje

13. Crockett ET, Galligan JJ, Uhal BD, Harkema J, Roth R, Pandya K. Protection of early phase hepatic ischemia-reperfusion injury by cholinergic agonists. *BMC Clin Pathol* (2006) 6:3. doi: 10.1186/1472-6890-6-3

14. Konishi T, Lentsch AB. Hepatic Ischemia/Reperfusion: Mechanisms of tissue injury, repair, and regeneration. *Gene Expr* (2017) 17(4):277–87. doi: 10.3727/105221617X15042750874156

15. Granger DN, Kvietys PR. Reperfusion injury and reactive oxygen species: The evolution of a concept. *Redox Biol* (2015) 6:524–51. doi: 10.1016/j.redox.2015.08.020

16. Hirao H, Nakamura K, Kupiec-Weglinski JW. Liver ischaemia-reperfusion injury: a new understanding of the role of innate immunity. *Nat Rev Gastroenterol Hepatol* (2022) 19(4):239–56. doi: 10.1038/s41575-021-00549-8

17. Dar WA, Sullivan E, Bynon JS, Eltzschig H, Ju C. Ischaemia reperfusion injury in liver transplantation: Cellular and molecular mechanisms. *Liver Int* (2019) 39(5):788–801. doi: 10.1111/liv.14091

18. Huang H, Tohme S, Al-Khafaji AB, Tai S, Loughran P, Chen L, et al. Damage-associated molecular pattern-activated neutrophil extracellular trap exacerbates sterile inflammatory liver injury. *Hepatology* (2015) 62(2):600–14. doi: 10.1002/hep.27841

19. Friedman SL. Molecular regulation of hepatic fibrosis, an integrated cellular response to tissue injury. *J Biol Chem* (2000) 275(4):2247–50. doi: 10.1074/jbc.275.4.2247

20. Friedman SL. Hepatic stellate cells: protean, multifunctional, and enigmatic cells of the liver. *Physiol Rev* (2008) 88(1):125–72. doi: 10.1152/physrev.00013.2007

21. Heymann F, Tacke F. Immunology in the liver–from homeostasis to disease. *Nat Rev Gastroenterol Hepatol* (2016) 13(2):88–110. doi: 10.1038/nrgastro.2015.200

22. Asahina K. Hepatic stellate cell progenitor cells. *J Gastroenterol Hepatol* (2012) 27(s2):80–4. doi: 10.1111/j.1440-1746.2011.07001.x

23. Schachtrup C, Le Moan N, Passino MA, Akassoglou K. Hepatic stellate cells and astrocytes. *Cell Cycle* (2011) 10(11):1764–71. doi: 10.4161/cc.10.11.15828

24. Yin C, Evason KJ, Asahina K, Stainier DYR. Hepatic stellate cells in liver development, regeneration, and cancer. *J Clin Invest* (2013) 123(5):1902–10. doi: 10.1172/JCI66369

25. Zhang F, Wang F, He J, Lian N, Wang Z, Shao J, et al. Regulation of hepatic stellate cell contraction and cirrhotic portal hypertension by wnt/β-catenin signalling *via* interaction with Gli1. *Br J Pharmacol* (2021) 178(11):2246–65. doi: 10.1111/bph.15289

26. Tsuchida T, Friedman SL. Mechanisms of hepatic stellate cell activation. *Nat Rev Gastroenterol Hepatol* (2017) 14(7):397–411. doi: 10.1038/nrgastro.2017.38

27. Ezhilarasan D. Hepatic stellate cells in the injured liver: Perspectives beyond hepatic fibrosis. *J Cell Physiol* (2022) 237(1):436–49. doi: 10.1002/jcp.30582

28. Kisseleva T, Brenner DA. Hepatic stellate cells and the reversal of fibrosis. *J Gastroenterol Hepatol* (2006) 21 Suppl 3:S84–87. doi: 10.1111/j.1440-1746.2006.04584.x

29. Puche JE, Saiman Y, Friedman SL. Hepatic stellate cells and liver fibrosis. *Compr Physiol* (2013) 3(4):1473–92. doi: 10.1002/cphy.c120035

30. Cheng F, Li Y, Feng L, Li S. Hepatic stellate cell activation and hepatic fibrosis induced by ischemia/reperfusion injury. *Transplant Proc* (2008) 40 (7):2167–70. doi: 10.1016/j.transproceed.2008.06.052

31. Li T, Shi Z, Rockey DC. Preproendothelin-1 expression is negatively regulated by IFNγ during hepatic stellate cell activation. *Am J Physiol Gastrointest Liver Physiol* (2012) 302(9):G948–957. doi: 10.1152/ajpgi.00359.2011

32. Rockey DC. Hepatic blood flow regulation by stellate cells in normal and injured liver. *Semin Liver Dis* (2001) 21(3):337–49. doi: 10.1055/s-2001-17551

33. Higashi T, Friedman SL, Hoshida Y. Hepatic stellate cells as key target in liver fibrosis. *Adv Drug Deliv Rev* (2017) 121:27–42. doi: 10.1016/j.addr.2017.05.007

34. Suzuki S, Toledo-Pereyra LH, Rodriguez F, Lopez F. Role of kupffer cells in neutrophil activation and infiltration following total hepatic ischemia and reperfusion. *Circ Shock* (1994) 42(4):204–9.

35. Matsumoto T, Yamaguchi M, Kikuchi H, Nakano H, Midorikawa T, Kumada K, et al. Heparin reduces serum levels of endothelin-1 and hepatic ischemia reperfusion injury in rabbits. *Surg Today* (2000) 30(6):523–5. doi: 10.1007/s005950070119

36. Zhang JX, Bauer M, Clemens MG. Vessel- and target cell-specific actions of endothelin-1 and endothelin-3 in rat liver. *Am J Physiol* (1995) 269(2 Pt 1):G269–277. doi: 10.1152/ajpgi.1995.269.2.G269

37. Hall A. Rho GTPases and the actin cytoskeleton. *Science* (1998) 279 (5350):509–14. doi: 10.1126/science.279.5350.509

38. Schaks M, Giannone G, Rottner K. Actin dynamics in cell migration. *Essays Biochem* (2019) 63(5):483–95. doi: 10.1042/EBC20190015

39. Kawada N, Seki S, Kuroki T, Kaneda K. ROCK inhibitor y-27632 attenuates stellate cell contraction and portal pressure increase induced by endothelin-1. *Biochem Biophys Res Commun* (1999) 266(2):296–300. doi: 10.1006/bbrc.1999.1823

40. Ishizaki T, Uehata M, Tamechika I, Keel J, Nonomura K, Maekawa M, et al. Pharmacological properties of y-27632, a specific inhibitor of rho-associated kinases. *Mol Pharmacol* (2000) 57(5):976–83.

41. Mizunuma K, Ohdan H, Tashiro H, Fudaba Y, Ito H, Asahara T. Prevention of ischemia-reperfusion-induced hepatic microcirculatory disruption by inhibiting stellate cell contraction using rock inhibitor. *Transplantation* (2003) 75(5):579–86. doi: 10.1097/01.TP.0000052593.16876.AF

42. Kuroda S, Tashiro H, Igarashi Y, Tanimoto Y, Nambu J, Oshita A, et al. Rho inhibitor prevents ischemia-reperfusion injury in rat steatotic liver. *J Hepatol* (2012) 56(1):146–52. doi: 10.1016/j.jhep.2011.04.029

43. Kuroda S, Tashiro H, Kimura Y, Hirata K, Tsutada M, Mikuriya Y, et al. Rho-kinase inhibitor targeting the liver prevents ischemia/reperfusion injury in the steatotic liver without major systemic adversity in rats. *Liver Transpl* (2015) 21 (1):123–31. doi: 10.1002/lt.24020

44. Geerts A. History, heterogeneity, developmental biology, and functions of quiescent hepatic stellate cells. *Semin Liver Dis* (2001) 21(3):311–35. doi: 10.1055/s-2001-17550

45. Stewart RK, Dangi A, Huang C, Murase N, Kimura S, Stolz DB, et al. A novel mouse model of depletion of stellate cells clarifies their role in ischemia/reperfusion- and endotoxin-induced acute liver injury. *J Hepatol* (2014) 60 (2):298–305. doi: 10.1016/j.jhep.2013.09.013

46. Wright MC, Issa R, Smart DE, Trim N, Murray GI, Primrose JN, et al. Gliotoxin stimulates the apoptosis of human and rat hepatic stellate cells and enhances the resolution of liver fibrosis in rats. *Gastroenterology* (2001) 121 (3):685–98. doi: 10.1053/gast.2001.27188

47. Orr JG, Leel V, Cameron GA, Marek CJ, Haughton EL, Elrick LJ, et al. Mechanism of action of the antifibrogenic compound gliotoxin in rat liver cells. *Hepatology* (2004) 40(1):232–42. doi: 10.1002/hep.20254

48. Dekel R, Zvibel I, Brill S, Brazovsky E, Halpern Z, Oren R. Gliotoxin ameliorates development of fibrosis and cirrhosis in a thioacetamide rat model. *Dig Dis Sci* (2003) 48(8):1642–7. doi: 10.1023/A:1024792529601

49. Takahashi T, Yoshioka M, Uchinami H, Nakagawa Y, Otsuka N, Motoyama S, et al. Hepatic stellate cells play a functional role in exacerbating ischemia-reperfusion injury in rat liver. *Eur Surg Res* (2019) 60(1–2):74–85. doi: 10.1159/000499750

50. Wang X, Khalil RA. Matrix metalloproteinases, vascular remodeling, and vascular disease. *Adv Pharmacol* (2018) 81:241–330. doi: 10.1016/bs.apha.2017.08.002

51. Viappiani S, Sariahmetoglu M, Schulz R. The role of matrix metalloproteinase inhibitors in ischemia-reperfusion injury in the liver. *Curr Pharm Des* (2006) 12(23):2923–34. doi: 10.2174/138161206777947560

52. Palladini G, Ferrigno A, Richelmi P, Perlini S, Vairetti M. Role of matrix metalloproteinases in cholestasis and hepatic ischemia/reperfusion injury: A review. *World J Gastroenterol* (2015) 21(42):12114–24. doi: 10.3748/wjg.v21.i42.12114

53. Mormone E, George J, Nieto N. Molecular pathogenesis of hepatic fibrosis and current therapeutic approaches. *Chem Biol Interact* (2011) 193(3):225–31. doi: 10.1016/j.cbi.2011.07.001

54. Deleve LD, Wang X, Tsai J, Kanel G, Strasberg S, Tokes ZA. Sinusoidal obstruction syndrome (veno-occlusive disease) in the rat is prevented by matrix metalloproteinase inhibition. *Gastroenterology* (2003) 125(3):882–90. doi: 10.1016/S0016-5085(03)01056-4

55. Yp H. Matrix metalloproteinases, the pros and cons, in liver fibrosis. *J Gastroenterol Hepatol* (2006) 21 Suppl 3(Suppl 3):88–91. doi: 10.1111/j.1440-1746.2006.04586.x

56. Han YP, Yan C, Zhou L, Qin L, Tsukamoto H. A matrix metalloproteinase-9 activation cascade by hepatic stellate cells in trans-differentiation in the three-dimensional extracellular matrix. *J Biol Chem* (2007) 282(17):12928–39. doi: 10.1074/jbc.M700554200

57. Moore C, Shen XD, Gao F, Busuttil RW, Coito AJ. Fibronectin-alpha4beta1 integrin interactions regulate metalloproteinase-9 expression in steatotic liver ischemia and reperfusion injury. *Am J Pathol* (2007) 170(2):567–77. doi: 10.2353/ajpath.2007.060456

58. Kuyvenhoven JP, Ringers J, Verspaget HW, Lamers CBHW, van Hoek B. Serum matrix metalloproteinase MMP-2 and MMP-9 in the late phase of ischemia and reperfusion injury in human orthotopic liver transplantation. *Transplant Proc* (2003) 35(8):2967–9. doi: 10.1016/j.transproceed.2003.10.049

59. Shirahane K, Yamaguchi K, Koga K, Watanabe M, Kuroki S, Tanaka M. Hepatic ischemia/reperfusion injury is prevented by a novel matrix metalloproteinase inhibitor, ONO-4817. *Surgery* (2006) 139(5):653–64. doi: 10.1016/j.surg.2005.10.002

60. Hamada T, Fondevila C, Busuttil RW, Coito AJ. Metalloproteinase-9 deficiency protects against hepatic ischemia/reperfusion injury. *Hepatology* (2008) 47(1):186–98. doi: 10.1002/hep.21922

61. van Golen RF, van Gulik TM, Heger M. The sterile immune response during hepatic ischemia/reperfusion. *Cytokine Growth Factor Rev* (2012) 23(3):69–84. doi: 10.1016/j.cytogfr.2012.04.006

62. Reiniers MJ, van Golen RF, van Gulik TM, Heger M. Reactive oxygen and nitrogen species in steatotic hepatocytes: a molecular perspective on the pathophysiology of ischemia-reperfusion injury in the fatty liver. *Antioxid Redox Signal* (2014) 21(7):1119–42. doi: 10.1089/ars.2013.5486

63. Csak T, Ganz M, Pespisa J, Kodys K, Dolganiuc A, Szabo G. Fatty acid and endotoxin activate inflammasomes in mouse hepatocytes that release danger signals to stimulate immune cells. *Hepatology* (2011) 54(1):133–44. doi: 10.1002/hep.24341

64. Jameel NM, Thirunavukkarasu C, Murase N, Cascio M, Prelich J, Yang S, et al. Constitutive release of powerful antioxidant-scavenging activity by hepatic stellate cells: protection of hepatocytes from ischemia/reperfusion injury. *Liver Transpl* (2010) 16(12):1400–9. doi: 10.1002/lt.22172

65. Feng M, Wang Q, Wang H, Wang M, Guan W, Lu L. Adoptive transfer of hepatic stellate cells ameliorates liver ischemia reperfusion injury through enriching regulatory T cells. *Int Immunopharmacol* (2014) 19(2):267–74. doi: 10.1016/j.intimp.2014.01.006

66. Beck-Schimmer B, Breitenstein S, Bonvini JM, Lesurtel M, Ganter M, Weber A, et al. Protection of pharmacological postconditioning in liver surgery: results of a prospective randomized controlled trial. *Ann Surg* (2012) 256(5):837–44; discission 844-845. doi: 10.1097/SLA.0b013e318272df7c

67. Beck-Schimmer B, Roth Z'graggen B, Booy C, Köppel S, Spahn DR, Schläpfer M, et al. Sevoflurane protects hepatocytes from ischemic injury by reducing reactive oxygen species signaling of hepatic stellate cells: translational findings based on a clinical trial. *Anesth Analg* (2018) 127(4):1058–65. doi: 10.1213/ANE.0000000000003692

68. Itoh N, Ornitz DM. Fibroblast growth factors: from molecular evolution to roles in development, metabolism and disease. *J Biochem* (2011) 149(2):121–30. doi: 10.1093/jb/mvq121

69. Watson J, Francavilla C. Regulation of FGF10 signaling in development and disease. *Front Genet* (2018) 9:500. doi: 10.3389/fgene.2018.00500

70. Berg T, Rountree CB, Lee L, Estrada J, Sala FG, Choe A, et al. Fibroblast growth factor 10 is critical for liver growth during embryogenesis and controls hepatoblast survival *via* β-catenin activation. *Hepatology* (2007) 46(4):1187–97. doi: 10.1002/hep.21814

71. Li S, Zhu Z, Xue M, Pan X, Tong G, Yi X, et al. The protective effects of fibroblast growth factor 10 against hepatic ischemia-reperfusion injury in mice. *Redox Biol* (2021) 40:101859. doi: 10.1016/j.redox.2021.101859

72. Konishi T, Schuster RM, Lentsch AB. Liver repair and regeneration after ischemia-reperfusion injury is associated with prolonged fibrosis. *Am J Physiol Gastrointest Liver Physiol* (2019) 316(3):G323–31. doi: 10.1152/ajpgi.00154.2018

73. Ji J. Dual role of matrix metalloprotease 9 in liver ischemia and reperfusion injury. *J Surg Res* (2013) 185(2):545–6. doi: 10.1016/j.jss.2012.12.028

74. Feng M, Wang H, Wang Q, Guan W. Matrix metalloprotease 9 promotes liver recovery from ischemia and reperfusion injury. *J Surg Res* (2013) 180(1):156–61. doi: 10.1016/j.jss.2012.09.042

75. Díaz-Sanjuán T, García-Ruiz I, Rodríguez-Juan C, Muñoz-Yagüe T, Solís-Muñoz P, Solís-Herruzo JA. Interferon alpha increases metalloproteinase-13 gene expression through a polyomavirus enhancer activator 3-dependent pathway in hepatic stellate cells. *J Hepatol* (2009) 50(1):128–39. doi: 10.1016/j.jhep.2008.07.034

76. George J, Tsutsumi M, Tsuchishima M. MMP-13 deletion decreases profibrogenic molecules and attenuates n-nitrosodimethylamine-induced liver injury and fibrosis in mice. *J Cell Mol Med* (2017) 21(12):3821–35. doi: 10.1111/jcmm.13304

77. Zhao B, Tumaneng K, Guan KL. The hippo pathway in organ size control, tissue regeneration and stem cell self-renewal. *Nat Cell Biol* (2011) 13(8):877–83. doi: 10.1038/ncb2303

78. Konishi T, Schuster RM, Lentsch AB. Proliferation of hepatic stellate cells, mediated by YAP and TAZ, contributes to liver repair and regeneration after liver ischemia-reperfusion injury. *Am J Physiol Gastrointest Liver Physiol* (2018) 314(4): G471–82. doi: 10.1152/ajpgi.00153.2017

79. Liu Y, Lu T, Zhang C, Xu J, Xue Z, Busuttil RW, et al. Activation of YAP attenuates hepatic damage and fibrosis in liver ischemia-reperfusion injury. *J Hepatol* (2019) 71(4):719–30. doi: 10.1016/j.jhep.2019.05.029

80. Konishi T, Schuster RM, Goetzman HS, Caldwell CC, Lentsch AB. Fibrotic liver has prompt recovery after ischemia-reperfusion injury. *Am J Physiol Gastrointest Liver Physiol* (2020) 318(3):G390–400. doi: 10.1152/ajpgi.00137.2019

81. Peralta C, Jiménez-Castro MB, Gracia-Sancho J. Hepatic ischemia and reperfusion injury: effects on the liver sinusoidal milieu. *J Hepatol* (2013) 59 (5):1094–106. doi: 10.1016/j.jhep.2013.06.017

82. Fasbender F, Widera A, Hengstler JG, Watzl C. Natural killer cells and liver fibrosis. *Front Immunol* (2016) 7:19. doi: 10.3389/fimmu.2016.00019

83. Koda Y, Teratani T, Chu PS, Hagihara Y, Mikami Y, Harada Y, et al. CD8+ tissue-resident memory T cells promote liver fibrosis resolution by inducing apoptosis of hepatic stellate cells. *Nat Commun* (2021) 12(1):4474. doi: 10.1038/s41467-021-24734-0

84. Nieto N. Oxidative-stress and IL-6 mediate the fibrogenic effects of [corrected] kupffer cells on stellate cells. *Hepatology* (2006) 44(6):1487–501. doi: 10.1002/hep.21427

85. Cubero FJ, Nieto N. Ethanol and arachidonic acid synergize to activate kupffer cells and modulate the fibrogenic response *via* tumor necrosis factor alpha, reduced glutathione, and transforming growth factor beta-dependent mechanisms. *Hepatology* (2008) 48(6):2027–39. doi: 10.1002/hep.22592

86. Pradere JP, Kluwe J, De Minicis S, Jiao JJ, Gwak GY, Dapito DH, et al. Hepatic macrophages but not dendritic cells contribute to liver fibrosis by promoting the survival of activated hepatic stellate cells in mice. *Hepatology* (2013) 58(4):1461–73. doi: 10.1002/hep.26429

87. Prosser CC, Yen RD, Wu J. Molecular therapy for hepatic injury and fibrosis: where are we? *World J Gastroenterol* (2006) 12(4):509–15. doi: 10.3748/wjg.v12.i4.509

88. Marrone G, Shah VH, Gracia-Sancho J. Sinusoidal communication in liver fibrosis and regeneration. *J Hepatol* (2016) 65(3):608–17. doi: 10.1016/j.jhep.2016.04.018

89. Zhai Y, Busuttil RW, Kupiec-Weglinski JW. Liver ischemia and reperfusion injury: new insights into mechanisms of innate-adaptive immune-mediated tissue inflammation. *Am J Transplant* (2011) 11(8):1563–9. doi: 10.1111/j.1600-6143.2011.03579.x

90. Shen X, Wang Y, Gao F, Ren F, Busuttil RW, Kupiec-Weglinski JW, et al. CD4 T cells promote tissue inflammation *via* CD40 signaling without *de novo* activation in a murine model of liver ischemia/reperfusion injury. *Hepatology* (2009) 50(5):1537–46. doi: 10.1002/hep.23153

91. Zhang Y, Ji H, Shen X, Cai J, Gao F, Koenig KM, et al. Targeting TIM-1 on CD4 T cells depresses macrophage activation and overcomes ischemia-reperfusion injury in mouse orthotopic liver transplantation. *Am J Transplant* (2013) 13(1):56–66. doi: 10.1111/j.1600-6143.2012.04316.x

92. Reifart J, Rentsch M, Mende K, Coletti R, Sobocan M, Thasler WE, et al. Modulating CD4+ T cell migration in the postischemic liver: hepatic stellate cells as new therapeutic target? *Transplantation* (2015) 99(1):41–7. doi: 10.1097/TP.0000000000000461

93. Serracino-Inglott F, Habib NA, Mathie RT. Hepatic ischemia-reperfusion injury. *Am J Surg* (2001) 181(2):160–6. doi: 10.1016/S0002-9610(00)00573-0

94. Sanyal AJ, Chalasani N, Kowdley KV, McCullough A, Diehl AM, Bass NM, et al. Or placebo for nonalcoholic steatohepatitis. *N Engl J Med* (2010) 362 (18):1675–85. doi: 10.1056/NEJMoa0907929

95. Mudaliar S, Henry RR, Sanyal AJ, Morrow L, Marschall HU, Kipnes M, et al. Efficacy and safety of the farnesoid X receptor agonist obeticholic acid in patients with type 2 diabetes and nonalcoholic fatty liver disease. *Gastroenterology* (2013) 145(3):574–82. doi: 10.1053/j.gastro.2013.05.042

96. Younossi ZM, Ratziu V, Loomba R, Rinella M, Anstee QM, Goodman Z, et al. Obeticholic acid for the treatment of non-alcoholic steatohepatitis: interim analysis from a multicentre, randomised, placebo-controlled phase 3 trial. *Lancet* (2019) 394(10215):2184–96. doi: 10.1016/S0140-6736(19)33041-7

97. Ratziu V, Harrison SA, Francque S, Bedossa P, Lehert P, Serfaty L, et al. Elafibranor, an agonist of the peroxisome proliferator-activated receptor-α and -δ, induces resolution of nonalcoholic steatohepatitis without fibrosis worsening. *Gastroenterology* (2016) 150(5):1147–1159.e5. doi: 10.1053/j.gastro.2016.01.038

98. Ratziu V, Sanyal A, Harrison SA, Wong VWS, Francque S, Goodman Z, et al. Cenicriviroc treatment for adults with nonalcoholic steatohepatitis and fibrosis: final analysis of the phase 2b CENTAUR study. *Hepatology* (2020) 72 (3):892–905. doi: 10.1002/hep.31108

99. Chalasani N, Abdelmalek MF, Garcia-Tsao G, Vuppalanchi R, Alkhouri N, Rinella M, et al. Effects of belapectin, an inhibitor of galectin-3, in patients with nonalcoholic steatohepatitis with cirrhosis and portal hypertension. *Gastroenterology* (2020) 158(5):1334–1345.e5. doi: 10.1053/j.gastro.2019.11.296

frontiers | Frontiers in Immunology

TYPE Original Research
PUBLISHED 29 July 2022
DOI 10.3389/fimmu.2022.869365

OPEN ACCESS

EDITED BY
Helong Dai,
Second Xiangya Hospital, Central South University (CSU), Changsha, China

REVIEWED BY
Andre Herbelin,
Institut National de la Santéet de la Recherche Médicale (INSERM), France
Shuyu Fu,
Wistar Institute, United States

*CORRESPONDENCE
Li-Ying Sun
sunxlx@outlook.com
Zhi-Jun Zhu
zhu-zhijun@outlook.com

†These authors contributed equally and share first authorship

SPECIALTY SECTION
This article was submitted to Molecular Innate Immunity, a section of the journal Frontiers in Immunology

RECEIVED 04 February 2022
ACCEPTED 06 July 2022
PUBLISHED 29 July 2022

CITATION
Zhang H-M, Chen X-J, Li S-P, Zhang J-M, Sun J, Zhou L-X, Zhou G-P, Cui B, Sun L-Y and Zhu Z-J (2022) ILC2s expanded by exogenous IL-33 regulate CD45+CD11b+F4/80high macrophage polarization to alleviate hepatic ischemia-reperfusion injury. *Front. Immunol.* 13:869365. doi: 10.3389/fimmu.2022.869365

ILC2s expanded by exogenous IL-33 regulate CD45+CD11b+F4/80high macrophage polarization to alleviate hepatic ischemia-reperfusion injury

Hai-Ming Zhang[1,2†], Xiao-Jie Chen[1,2†], Shi-Peng Li[1,2], Jin-Ming Zhang[1,2], Jie Sun[1,2], Liu-Xin Zhou[1,2], Guang-Peng Zhou[1,2], Bin Cui[1,2], Li-Ying Sun[1,2,3*] and Zhi-Jun Zhu[1,2*]

[1]Liver Transplantation Center, National Clinical Research Center for Digestive Diseases, Beijing Friendship Hospital, Capital Medical University, Beijing, China, [2]Clinical Research Center for Pediatric Liver Transplantation of Capital Medical University, Beijing, China, [3]Department of Critical Liver Disease, Liver Research Center, Beijing Friendship Hospital, Capital Medical University, Beijing, China

Hepatic ischemia-reperfusion injury (IRI) is an adverse consequence of hepatectomy or liver transplantation. Recently, immune mechanisms involved in hepatic IRI have attracted increased attention of investigators working in this area. In specific, group 2 innate lymphoid cells (ILC2s), have been strongly implicated in mediating type 2 inflammation. However, their immune mechanisms as involved with hepatic IRI remain unclear. Here, we reported that the population of ILC2s is increased with the development of hepatic IRI as shown in a mouse model in initial stage. Moreover, M2 type CD45+CD11b+F4/80high macrophages increased and reached maximal levels at 24 h followed by a significant elevation in IL-4 levels. We injected exogenous IL-33 into the tail vein of mice as a mean to stimulate ILC2s production. This stimulation of ILC2s resulted in a protective effect upon hepatic IRI along with an increase in M2 type CD45+CD11b+F4/80high macrophages. In contrast, depletion of ILC2s as achieved with use of an anti-CD90.2 antibody substantially abolished this protective effect of exogenous IL-33 and M2 type CD45+CD11b+F4/80high macrophage polarization in hepatic IRI. Therefore, this exogenous IL-33 induced potentiation of ILC2s appears to regulate the polarization of CD45+CD11b+F4/80high macrophages to alleviate IRI. Such findings provide the foundation for the development of new targets and strategies in the treatment of hepatic IRI.

KEYWORDS

ischemia-reperfusion injury (I/R), group 2 innate lymphoid cells (ILC2s), Kupffer cells (KCs), M2 polarization, IL-4

Introduction

Impairments in liver function resulting from ischemia-reperfusion injury (IRI) in liver transplantation or partial hepatectomy represent a significant adverse factor that not only affects the recovery, but may also contribute to the high morbidity and mortality rates associated with this procedure. With IRI, there exist numbers of possible sources of damage including that from oxidative stress, apoptosis, autophagy and pyroptosis, all of which can play important roles in occurrence and development of these adverse effects (1, 2). In addition, activities of immune cells can also affect hepatic IRI process. For example, tissue-resident macrophages in liver, play essential roles in hepatic IRI. As based on differences in their phenotypes and functions, activated macrophages can be divided into either M1 or M2 groups. During the initial stages of IRI, M1 macrophages produce reactive oxygen species (ROS) and proinflammatory factors (TNF-α, IL-1, IL-6) which can instigate this liver damage (3, 4). In contrast, in the later stages of IRI, polarized M2 macrophages secrete anti-inflammatory factors (Arg-1, IL-10, TGF-β, HO-1) to alleviate hepatic IRI (5, 6). However, these polarization mechanisms of M2 macrophages in hepatic IRI remain unclear.

Results from recent studies have shown that phenotypic changes in macrophages may be affected by group 2 innate lymphoid cells (ILC2s) (7). ILC2s, which are mainly found in lung, intestine, skin and liver, are tissue-resident cells derived from lymphoid progenitors (8). They can be activated by alarmins such as IL25, IL-33 after tissue damage (9, 10) and play crucial roles in metabolic homeostasis, parasite infection and tissue repair through inducing type 2 inflammation (11). In asthma, the number of ILC2s have been shown to be positively correlated with the number of M2 macrophages in induced sputum from asthmatic patients (12), and the expression of M2 macrophage related genes can be induced in co-cultures of ILC2s and Alveolar Macrophages (13). ILC2s can be found in various locations and exert a number of different roles depending on their current surroundings. For example, in bone marrow, ILC2s potentiate an IL-33 down-regulation of RANKL expression and transform bone marrow-derived monocytes/macrophages into M2 macrophage like cells through the production of granulocyte macrophage colony stimulating factor (GM-CSF) and IL-13 (14). As shown in studies related to inflammatory injuries, ILC2s also play a key role in tumor immunity and ILC2s proliferation can promote the pathogenesis of cancer by inducing M2 Macrophage polarization (15–17). Moreover, results from a recent report have indicated that ILC2s are involved in the repair process of damaged organs (18). Despite all this evidence regarding the immune mechanisms of ILC2s, such mechanisms as related to liver IRI have yet to be established.

Exogenous IL-33 is a potent stimulator of ILC2 proliferation (19), and a role for IL-33 in mouse models of hepatic IRI has been previously described. Li Shu et al. demonstrated that pretreatment with exogenous IL-33 reduced warm hepatic IRI in mice, and that this protective effect of IL-33 on hepatic IRI was mainly due to a Th1 to Th2 type shift (20). However, it remains unclear as to which group of cells are mainly involved in this effect. Further evidence for a protective effect of exogenous IL-33 on hepatic IRI was provided by Sakai et al (21). In contrast to these demonstrations of IL-33-induced protection, Yazdani reported that exogenous IL-33 exacerbated hepatic IRI by amplifying the neutrophil extracellular trap formation (22), and while Barbier (23) also reported a deleterious effect of endogenous IL-33 on liver IRI. Accordingly, this effect of IL-33 on hepatic IRI clearly warrants further study.

Work within our laboratory has indicated that levels of intrahepatic ILC2s vary as a function of the stage of IRI. Here, we reported that in the initial stages of IRI, as the time of reperfusion injury gradually progresses, ILC2s demonstrate a continuous upward trend, reaching peak levels at 12 h post-reperfusion. Interestingly, during this IRI period, there is a positive correlation between these changes in ILC2s and the proportion of M2 type CD45+CD11b+F4/80high macrophages. With a potentiation of ILC2s, as can be achieved with an exogenous administration of IL-33, intrahepatic IL-4 expression is also significantly increased followed by an increase in the proportion of M2 CD45+CD11b+F4/80high macrophages. Hepatocyte injury is dramatically mitigated in response to this IL-33 administration, while ILC2s depletion, as achieved with use of the anti-CD90.2 antibody, substantially abolished this protective effect of exogenous IL-33 and M2 CD45+CD11b+F4/80high macrophage polarization in hepatic IRI. When collating these findings, we found that ILC2s expanded by exogenous IL-33 alleviated hepatic IRI by promoting the M2 polarization of CD45+CD11b+F4/80high macrophages. Such findings provide the impetus for the development of new treatment strategies involving use of exogenous IL-33 and ILC2s in the treatment of IRI.

Results

Intrahepatic ILC2s vary as a function of hepatic IRI stage

As an approach to determine whether liver-resident ILC2s change as a function of IRI stage, we established a mouse hepatic IRI model. Compared with that observed in the sham group, the main manifestations of hepatic IRI included hepatocyte edema, hepatic vessel congestion and necrosis. Mild edema and congestion were the main lesions present at 6 h post-IRI. At 12 h post-IRI, there was a progression of this damage with the gradual presence of punctate necrosis and inflammatory cell infiltration, while at 24 h, flake coagulation necrosis can be seen, but edema and congestion were reduced (Figure 1A). Quantified

assessment of this hepatic IRI with use of Suzuki's Scores demonstrated that the liver injury induced by ischemia-reperfusion was clearly time-dependent, with scores showing a gradual increase as a function of reperfusion time, reaching maximal levels at 24 h post-reperfusion (Figure 1B, $P<0.001$ versus sham). Results of Western blotting of Caspase-3, BAX and Bcl-2 in liver tissue indicated that hepatocyte apoptosis gradually increased over the initial 12 h period, but decreased thereafter (Figures 1D, E). Moreover, results of this assay also showed a similar trend for serum ALT and AST, which increased immediately after reperfusion and peaked at 12 h (Figure 1C, $P<0.001$ versus sham).

Furthermore, the proportion of ILC2s on CD45+ cells in the liver were analyzed using multicolor flow cytometry. After pre-gating on single and live cells, CD45+cells were gated to exclude non-hematopoietic cells, such as hepatocytes. In this way, lineage-CD90.2+ST2+CD25+ cells could now be delineated as intrahepatic ILC2s (the Gating strategy is presented in Supplementary Figure 1A). We found that there was an increase in the ratio of ILC2s among CD45+ cells as hepatic IRI progressed, peaking at 12h post-IRI (Figures 1F, G P<0.05). Moreover, the number of ILC2s per gram of liver tissue gradually increased after reperfusion (Figure 1G). Based on these findings we propose that ILC2s may be critically involved in the regulation of hepatic IRI.

M2 CD45+CD11b+F4/80high macrophages vary as a function of IRI progression

During hepatic IRI, we not only observed changes in levels of liver intrahepatic ILC2s, but also in CD45+CD11b+F4/80high macrophages, especially in proportions of the M2 type. To further evaluate these findings, we first determined expressions of CD206 in response to hepatic IRI using immunohistochemistry. CD206 expression gradually increased, showing a slight increase at 12 h after reperfusion and then a significant increase at 24 h (Figures 2A, B). Results from flow cytometry analysis revealed that a similar trend was observed for M2 CD45+CD11b+F4/80high CD206+ macrophage ratios (increases in the proportion of CD206+ cells were assumed to represent a M2 polarization among

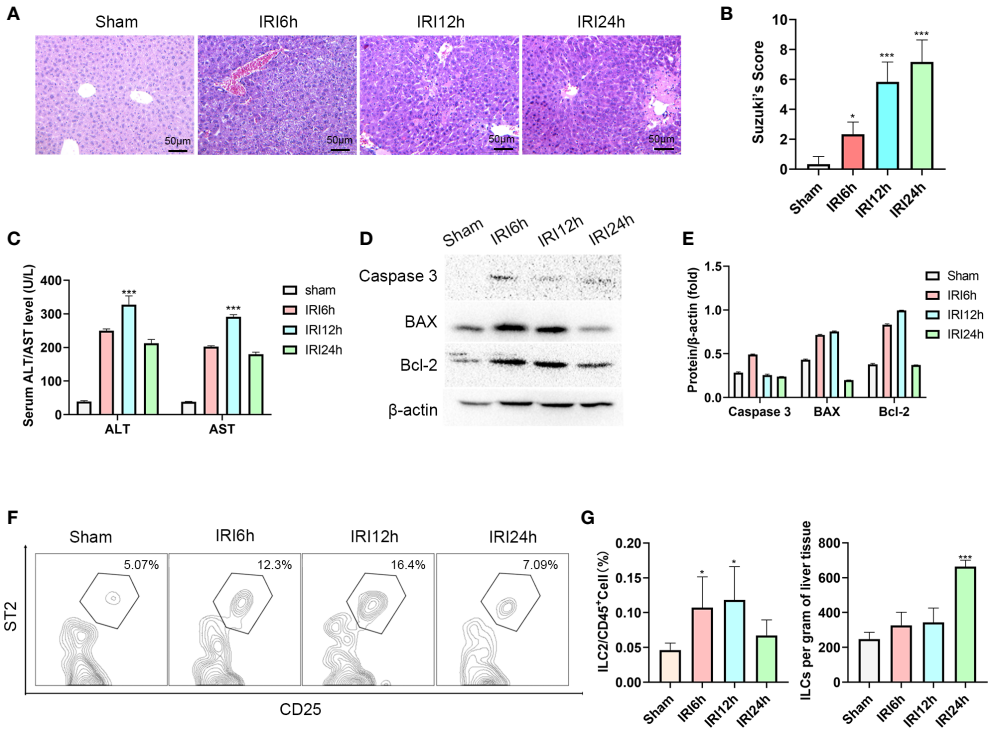

FIGURE 1
Intrahepatic ILC2s vary as a function of hepatic IRI stage. **(A)** HE staining of formalin fixed paraffin embedded liver tissue after ischemia followed by reperfusion at 6, 12 or 24 h and Sham controls (x200). **(B)** Suzuki's scores for IR-induced liver injury among the four groups (n = 6 per group). **(C)** Serum ALT and AST levels were assessed in Sham and IRI groups at different post-reperfusion time periods. **(D, E)** western blot and semi-quantification of BAX, Bcl-2 and Caspase3 from liver tissue of Sham and IRI groups at different post-reperfusion time periods. **(F)** Proportion of ILC2s within the different IRI Groups. **(G)** Histograms of percent of ILC2s in CD45+cells and ILC2s per gram of liver tissue (n = 5 per group). (ns $P>0.05$, *$P<0.05$, ***$P<0.001$ versus sham).

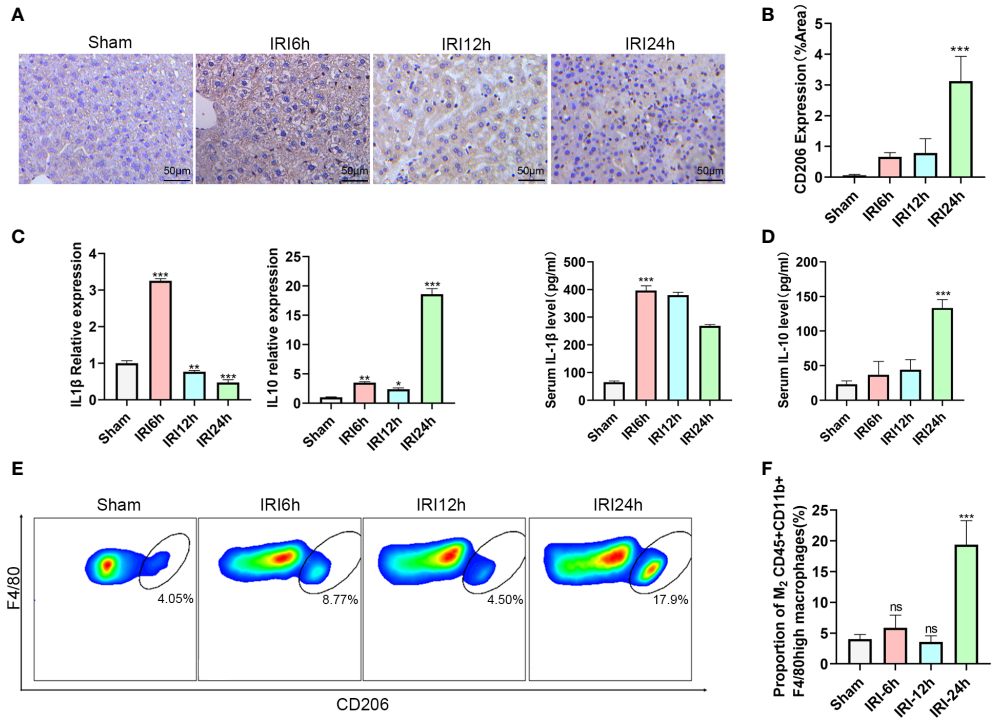

FIGURE 2
Proportion of M2 CD45+CD11b+F4/80high macrophages varies as a function of hepatic IRI stage. **(A)** Immunohistochemistry assay results demonstrating the changes in CD206 as a function of IRI time. **(B)** Semi-quantification of CD206 expression. **(C)** Relative gene expressions of IL-1β and IL-10 in macrophages purified from mice liver at 6,12 or 24 h post-IRI and sham controls. **(D)** Serum IL-1β and IL-10 levels in Sham and IRI groups at different post-reperfusion time periods. **(E)** Representative FACS analysis showing the percent of M2 CD45+ CD11b+ F4/80high macrophages in sham, IRI6h, IRI12h, IRI24h. (An CD206+ increase in proportion was assumed as a M2 polarization among CD45+CD11b + F4/80high cells) **(F)** Histograms of the percent of M2 CD45+CD11b+F4/80high macrophages (n = 5 per group). (ns $P>0.05$, *$P<0.05$,**$P<0.01$, ***$P<0.001$ versus sham).

CD45+CD11b+ F4/80high cells), increasing slightly at 6 h, then decreasing at 12 h and finally reaching maximal levels at 24 h (Figures 2E, F $P<0.001$ versus sham). Moreover, we also detected mRNA and serum protein levels of IL-1β and IL-10 in these macrophages, with IL-1β being significantly increased at 6 h after IRI, then gradually decreasing to minimal levels at 24 h. In contrast, the M2 CD45+CD11b+F4/80high macrophage related cytokine, IL-10, showed a slight increase at 6 h, followed by a marked rise at 24 h (Figures 2C, D; $P<0.001$ versus sham). Chronologically, M2 CD45+CD11b+F4/80high macrophage ratios increased after that of ILC2s, leading us to speculate that the polarization of M2 may be promoted by the increases in ILC2s.

ILC2s alleviate hepatic IRI by increasing the proportion of M2 CD45+CD11b+F4/80high macrophages

To determine whether ILC2s could alleviate hepatic IRI, we performed manipulations in which ILC2s levels were either increased or decreased in a mouse model (Recombinant mouse IL-33 for 5 consecutive days before IRI to stimulate ILC2s and anti-CD90.2 on day -4 and -1 before IRI to deplete ILC2s Figure 3B). In mice receiving recombinant mouse IL-33 there was a substantial increase in intrahepatic ILC2s, while these levels were markedly decreased in those receiving IL33 +anti-CD90.2 (Figure 3A). HE staining, as performed in the harvested liver of these IRI mice at 12 h after reperfusion, revealed little, if any, observation of liver necrosis in mice injected with IL-33, while a considerable amount of necrosis was observed in the PBS and IL33+antiCD90.2 group. However, mild hepatocyte edema and small vessel congestion were present in sections from the IL-33 injected group as compared with sham mice (Figure 3C). Results from Suzuki's Scores indicated that liver injuries within the IL-33 group were less than that observed in the PBS group after reperfusion and, there were more serious damage in IL33+antiCD90.2 groups than IL-33 Group (Figure 3D), suggesting that ILC2s had a protective effect on hepatic IRI. In order to further verify the protective effect of ILC2s upon hepatic IRI, the extent of hepatocyte apoptosis was determined in these mice at 12 h after reperfusion. As shown in

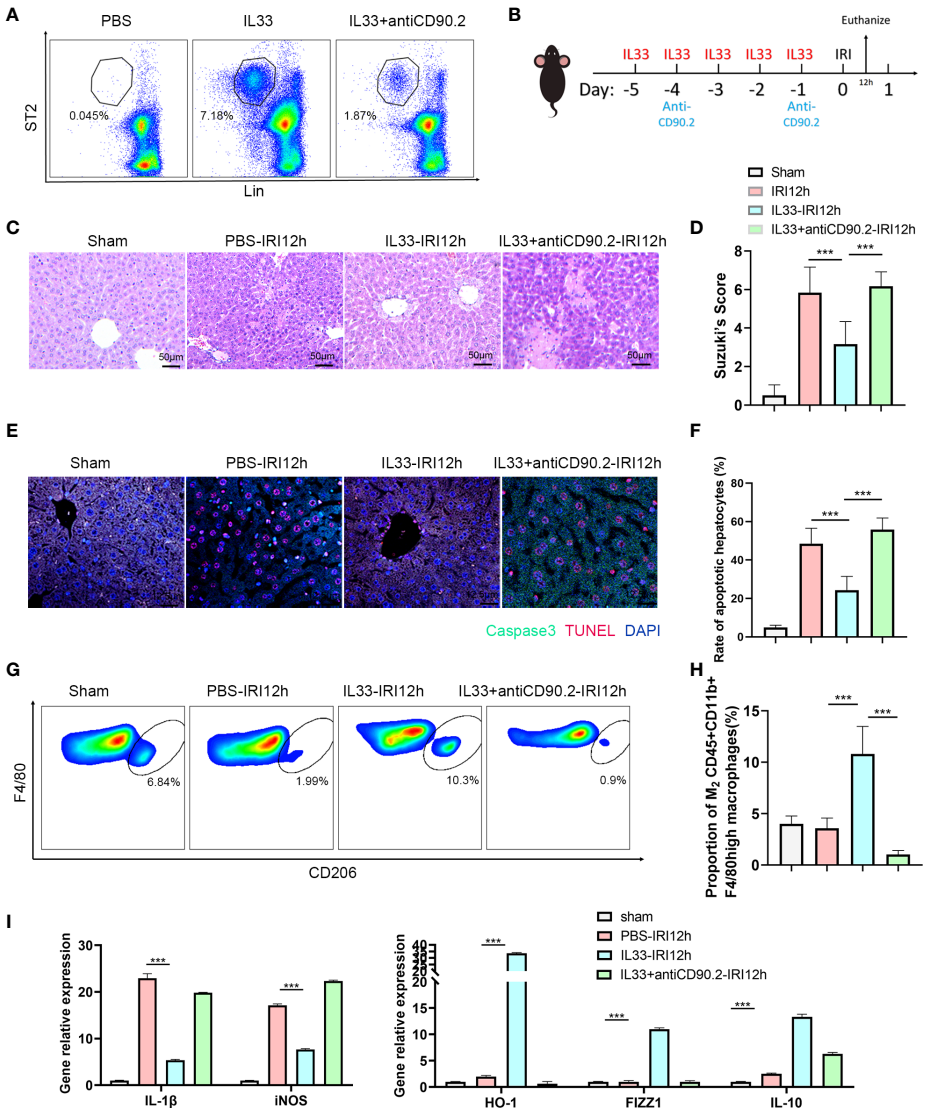

FIGURE 3
ILC2s protect liver from IRI by increasing the proportion of M2 CD45+CD11b+F4/80high macrophages **(A)** Representative FACS analysis showing that exogenous IL-33 administration significantly increased the proportion of ILC2s in liver as compared with PBS controls and IL-33 receiving anti-CD90.2 administration, which significantly depleted ILC2s. **(B)** Sketch map of medicine administration and IRI surgery. Mice were treated with exogenous IL-33 daily for 5 consecutive days as well as anti-CD90.2 antibody twice before IRI surgery. Mice were euthanized 12 h after reperfusion. **(C)** HE staining of Sham, PBS, IL-33 and IL33&anti-CD90.2 groups as determined at 12 h after reperfusion (×200). **(D)** Suzuki's Scores resulting from IR-induced liver injury in Sham, PBS, IL-33 and IL33&anti-CD90.2 groups (n=6 per group). **(E)** Representative cell apoptosis immunofluorescence of the 4 groups as determined at 12 h post-reperfusion. Cell apoptosis was measured using TUNEL (red) and Caspase3 (green). Apoptotic cells display a red nucleus (TUNEL) and green cytoplasm (Caspase-3) while normal cells show blue nuclei (DAPI) (×400). **(F)** Histograms of quantitative analysis of TUNEL-positive cells (n = 6 per group). **(G)** Representative FACS analysis showing the proportion change of M2 CD45+CD11b+F4/80high macrophages. (An CD206+ increase in proportion was assumed as a M2 polarization among CD45+CD11b+ F4/80high cells) **(H)** Quantitative analysis of percent of M2 CD45+CD11b+F4/80high macrophages (n = 5 per group). **(I)** Relative gene expressions of IL-1β, iNOS, HO-1, FIZZ1 and IL-10 in macrophages purified from mice liver in different groups. (***P<0.05, ***P<0.001).

Figure 3E, results from our immunofluorescent assay revealed that a large proportion of hepatocyte nuclei were stained red (TUNEL) and the cytoplasm green (Caspase-3) in mice injected with PBS or IL33+antiCD90.2, indicating that a substantial amount of hepatocyte apoptosis was present. In contrast, the percent of TUNEL and Caspase-3 positive cells were significantly decreased in the IL-33 injection group (Figure 3F; P<0.001). We also found that following ILC2s proliferation, as achieved with an exogenous injection of IL-33, a marked increase in M2 CD45+CD11b+F4/80high macrophages was

observed in these mice when compared with that in the PBS group, as based on FACS analysis (Figures 3G, H). In order to determine the relative proportion of M1 versus M2 CD45+CD11b+F4/80high macrophages, these were isolated from liver tissue and their cytokine contents were assessed. As shown in Figure 3I, the pro-inflammatory factor IL-1β and iNOS decreased significantly in the IL-33 treated group, while the anti-inflammatory factors HO-1, FIZZ1 and IL-10 were significantly increased. Such results suggest that exogenous IL-33 modulates CD45+CD11b+F4/80high macrophage polarization *in vivo*. However, with ILC2s depletion, as achieved with the administration of anti-CD90.2, these alterations in CD45+CD11b+F4/80high macrophages were substantially attenuated. Therefore, we hypothesized that the protective effect of ILC2s in IRI may, in part, result from the promotion of M2 polarization of CD45+CD11b+F4/80high macrophages.

Macrophage depletion attenuates the protective effects of exogenous IL-33 in hepatic IRI

In order to determine whether CD45+CD11b+F4/80high macrophages are essential for the protective effect of exogenous IL-33 in hepatic IRI, we assessed the effects of macrophages depletion in this mouse model. This was achieved with an administration of Clodronate Liposomes (CL). As shown in Figure 4A, there was a significant reduction in CD45+CD11b+F4/80high macrophages in response to this CL treatment. We euthanized mice 12 hours after hepatic IRI to detect hepatic structural and functional injury. With this depletion of macrophages, the protective effects of exogenous IL-33 on hepatic IRI were no longer present and serum ALT and AST levels of mice treated with IL-33+CL were significantly greater than that in mice treated with IL-33+Control (Figure 4B).

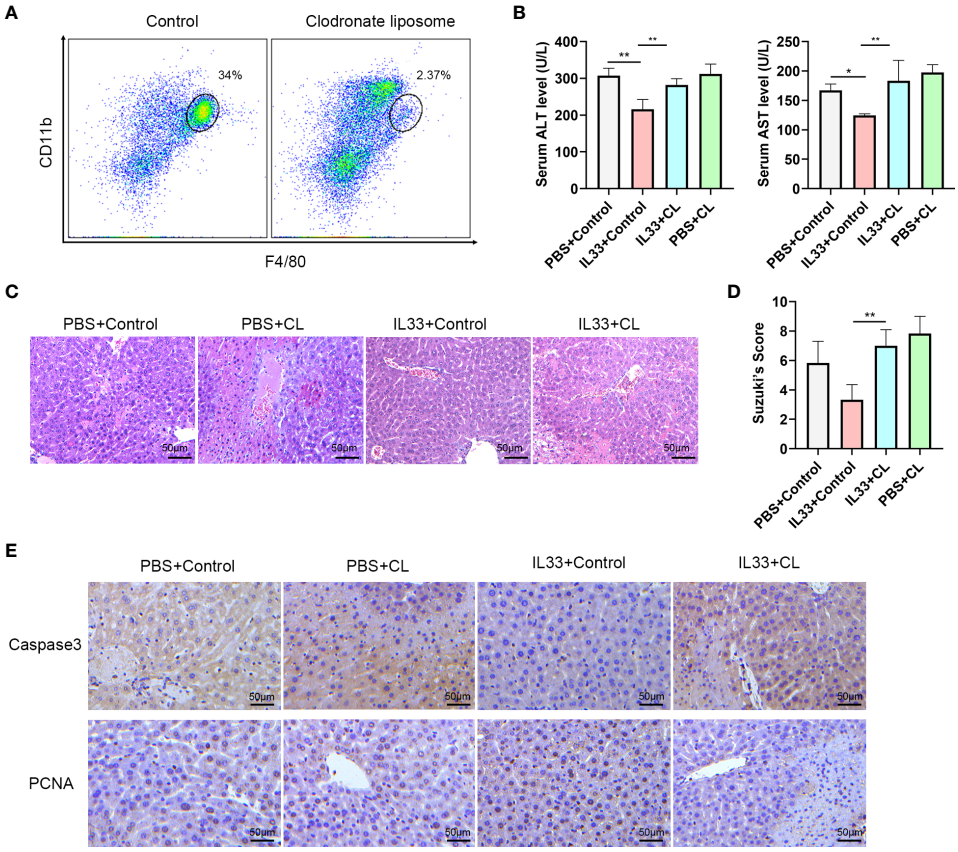

FIGURE 4
Macrophages depletion prevents protective effects of exogenous IL-33 on hepatic IRI **(A)** Representative FACS analysis showing depletion of macrophages following administration of Clodronate Liposomes (CL). **(B)** Serum ALT and AST levels of mice in PBS+control, PBS+CL, IL33+control and IL33+CL groups 12 h after IRI. **(C)** Histopathological changes in livers within the different treatment groups 12 h after IRI. **(D)** Suzuki's Scores quantifying the capacity for CL to attenuate the protective effects of exogenous IL-33 against hepatic IRI (n=6 per group) (mice were Euthanized 12h after IRI). **(E)** Histochemistry of caspase3 and PCNA in the four groups (mice were euthanized 12h after IRI). (*P<0.05, **P<0.01).

Results from our histological analysis corroborated these findings, as mice injected with IL-33 showed significantly less necrosis as compared with that of the other groups, while severe necrosis, hepatocyte edema and vessels congestion were observed in mice treated with IL-33+CL (Figure 4C). Suzuki's Scores of the IL33+CL group were significantly greater than that of the IL33+Control group, indicating that macrophages depletion weakened the protection of exogenous IL-33 against hepatic IRI (Figure 4D). Similarly, when assessing apoptosis, we found that IL-33 treatment significantly reduced the proportion of Caspase-3 positive cells while remarkably increasing PCNA positive cells, indicating that IL-33 administration reduced liver apoptosis and promoted liver regeneration in hepatic IRI. When compared with that of the IL-33 group, the number of Caspase-3 positive cells in the IL-33+CL group was significantly increased while PCNA positive cells remarkably decreased, implying that the depletion of macrophages severely attenuated the ability for ILC2s to resist apoptosis and promote regeneration in hepatic IRI (Figure 4E).

IL-4 polarizes CD45+CD11b+F4/80high macrophages to the M2 type *via* the JNK/Stat3 pathway

ILC2s mainly exert their effects by secreting Th2 cytokines such as, IL-4, IL-5 and IL-13 (24). To determine which cytokine may be critical for the M2 phenotype transformation mediated by ILC2s, we examined mRNA levels of these cytokines within the liver. As expected, IL-4 and IL-13 expression levels in liver tissue increased after IL-33 injections, and IL-4 was clearly greater than that of IL-13 (Figure 5A). Moreover, in IL-33 +antiCD90.2 group, the increase of IL-4 decreased significantly. Therefore, we considered that IL-4 may serve as the cytokine through which ILC2 regulates phenotypic changes in CD45+CD11b+F4/80high macrophages. To test this hypothesis, primary macrophages were extracted from C57BL/6 mice and treated with IL-4 or an IL-4+Stat3 inhibitor NSC74859 (abbreviated as NSC). When IL-4 was added to the culture medium for 24 h prior to hypoxia and reoxygenation (H/R), the proportion of M2 macrophages was significantly increased. However, this trend for M2 macrophage polarization was clearly reduced when NSC was combined with IL-4 (Figure 5B). In addition, cells treated with IL-4 had reduced expressions of M1 macrophage markers, including IL-1β, iNOS, and enhanced expressions of M2 macrophage markers, including IL-10, FIZZ1 and HO-1 (Figure 5C). From the level of protein assessment, as performed using western blot, IL-4 administration was shown to upregulate the expressions of p-Stat3 and p-JNK, while treatment with the IL4+Stat3 inhibitor downregulated these expressions (Figure 5D). Finally, we co-cultured hepatocyte AML12 cells with macrophages treated with IL4 or IL4+Stat3 inhibitor and then analyzed the degree of apoptosis within these AML12 cells using flow cytometry analysis. As shown in Figure 5E, after 1 h of hypoxia and 12 h of reoxygenation, AML12 cells showed a considerable degree of apoptosis, while those co-cultured with IL4-treated macrophages demonstrated a significant reduction in hepatocyte apoptosis. However, when co-cultured with macrophages treated with IL-4 +NSC, the apoptosis within these hepatocytes was significantly increased ($P<0.001$) (Figure 5F).

Taken together, the findings are consistent with the hypothesis that ILC2s alleviate hepatic IRI by promoting M2 polarization of CD45+CD11b+F4/80high macrophages through the IL-4/JNK/Stat3 pathway. Whether other cells are involved in the release of IL-4 awaits further research. Such findings provide the foundation for the development of novel strategies to alleviate hepatic IRI as achieved through modulation of ILC2.

Discussion

Hepatic IRI, represents a significant risk factor affecting the prognosis of hepatectomy or liver transplantation (25). The mechanisms of hepatic IRI are complex, involving oxidative stress, apoptosis, autophagy, pyroptosis and immune factors (26, 27), and it is also certain that resident liver macrophages, play an important role in this liver injury process (28–30). According to the different functions exerted by macrophages, they can be divided into M1 macrophages that promote or M2 macrophages that inhibit inflammation (31). A number of studies have focused on procedures involved with increasing the proportion of M2 macrophages as an approach to reduce IRI (6, 32, 33). Our current results show that with an exogenous administration of IL-33, ILC2s are increased along with a proportional increase in M2 CD45+CD11b+F4/80high macrophages, effects which are accompanied with a reduction in IRI. Such effects can be attenuated following ILC2s depletion, as achieved with anti-CD90.2. Accordingly, it appears that ILC2s proliferation can alleviate IRI through the promotion of M2 macrophage polarization

While the results of our present study provide the first evidence for a role of ILC2s in hepatic IRI, the role of exogenous IL-33 in hepatic IRI has been described previously by Li and his colleagues (20). They demonstrated that the effects of exogenous IL-33 in hepatic IRI were associated with a Th1 to Th2 cytokine type shift and, in this way, exogenous IL-33 may suppress inflammation of hepatic IRI by inducing IL-4, IL-5 and IL-13 release. Interestingly, ILC2s represent a heterogeneous group of immune cells which can be activated by IL-33 and IL-25 and mainly mediate type 2 inflammation by releasing IL-4, IL-5 and IL-13 (34–36). Such a cascade of events most likely serves as a medium for IL-33 to play its role in hepatic IRI.

Endogenous IL-33 is immediately released during liver IRI and contributes to early tissue injury as an alarmin (23). Discrepant effects of exogenous IL-33 on hepatic IRI have been reported. Yazdani demonstrated that exogenous IL-33

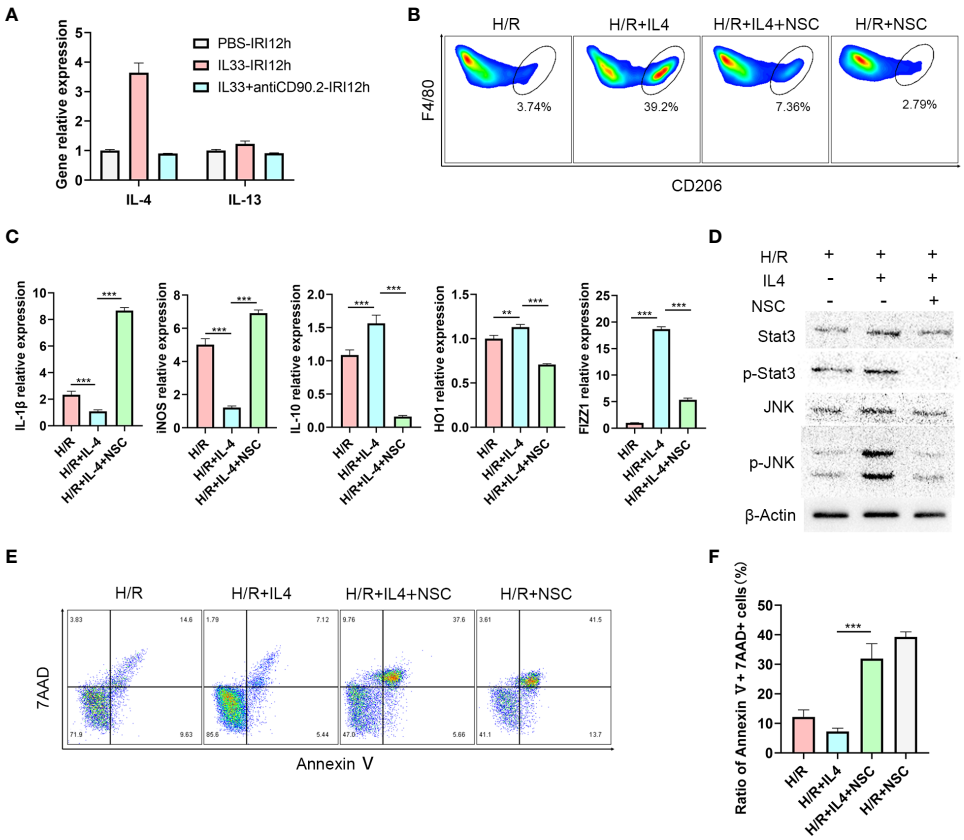

FIGURE 5
IL-4 polarizes CD45+CD11b+F4/80high macrophages to M2 type *via* the JNK/Stat3 pathway **(A)** Relative expression levels of IL-4 and IL13 mRNA in liver tissue of mice treated with IL-33 and IL-33+antiCD90.2 at 12 h following IRI. **(B)** Representative FACS analysis showing M2 CD45+CD11b+F4/80high macrophages proportion changes of treated with IL-4 or IL-4+Stat3 inhibitor NSC74859 (abbreviated as NSC) at 12 h following hypoxia and reoxygenation. (An increase CD206+ in proportion was assumed as a M2 polarization among CD45+CD11b+ F4/80high cells) **(C)** IL1β, iNOS, HO-1, IL-10 and FIZZ-1 mRNA expression levels in macrophages within the different groups were determined using quantitative PCR. **(D)** Stat3, p-Stat3, JNK and p-JNK protein levels were assessed using western blot in RAW264.7 cells at 12 h after hypoxia and reoxygenation in the presence or absence of IL-4 or Stat3 inhibitor. **(E)** Apoptosis of AML12 cells after co-culture with different macrophages. **(F)** Histograms of quantitative analysis of 7AAD and Annexin V double positive cells. (***P*<0.01, ****P*<0.001).

exacerbates liver IRI by amplifying a neutrophil extracellular trap formation causing excessive sterile inflammation (22), However, it has also been reported that exogenous IL-33 significantly reduces hepatocellular injury in IRI and liver neutrophil accumulation (21). Such variations in results may be attributable to differences in doses and/or the timing of exogenous IL-33 administration. Yazdani used a high dose (up to 10 ug) which was administered at 1 h before or immediately after ischemia, while in our study a low dose, long-course pretreatment of IL-33, consisting of a daily dose of 0.3 ug for 5 consecutive days, was administered prior to IRI surgery. With our protocol, a milder effect was achieved, enabling this pretreatment sufficient time for the immune system to alter the proportion and phenotype of ST2-expressing cells, particularly ILC2s, to prepare for the future injury. It is also possible that this exogenous IL-33 pretreatment may alter other cells expressing ST2 *in vivo*, such as, regulatory T (Treg) cells, TH1 cells, CD8+ T cells, natural killer (NK) cells (37) and iNKT cells (38). Notably, Ngo reported that an exogenous injection of IL-33 induced a remarkable increase of Th2 associated cytokines accompanied with an accumulation of Tregs and ILC2s in the colon, which could play a protective role in severe acute colitis (39). Our findings suggest a specific role for ILC2s, as depletion with the anti-CD90.2 antibody substantially reduced the protective effect of exogenous IL-33 on IRI. Such results strongly suggest that the IL-33 induction of ILC2s was the critical component for this protective role in hepatic IRI.

It appears that the *in vivo* regulation of liver resident macrophage polarization by IL-33 is critically dependent on ILC2s. Previously, we have directly treated liver resident macrophages with recombinant mouse IL-33 *in vitro* and failed to observe any of the production changes in inflammatory factors which could be observed when recombinant mouse IL-33 is administered *in vivo*. Similar

results were reported by Li and Sakai et al (20, 21), who found that ST2, the receptor for IL-33, was not expressed by liver resident macrophages, thereby demonstrating that endogenous IL-33 exerts a hepatoprotective effect as a result of increased NF-κB and Bcl-2 expression in hepatocyte and is independent of KCs. However, results from several studies have indicated that IL-33/ILC2s regulate M2 polarization of macrophages (40–42) and that IL-33 can stimulate ILC2 proliferation (19, 43, 44), leading to the conclusion that although IL-33 is capable of regulating the polarization of macrophages *in vivo*, this ability is reliant on ILC2s. Our findings, as described above, suggest that the protective effects of ILC2s in hepatic IRI may rely on exogenous IL-33. In the ILC2s depletion group, the pathological damage observed within liver tissue was essentially the same as that of the control group (Supplementary Figure 1B) and Suzuki's Score between the two groups were not significantly different (Supplementary Figure 1C). In this way, in the absence of exogenous IL-33, ILC2s may be redundant in the hepatic ischemia-reperfusion injury. Such a phenomenon has been observed in renal IRI (45).

In our hepatic IRI model, IL-4 increased significantly at 12 h after reperfusion, which represents an important stimulatory component for shifting of the macrophage phenotype to the M2 type. However, the major sources for IL-4 remain unclear. In addition to ILC2s (46), there exist several types of cells capable of producing IL-4, such as CD4+Th cells, Treg cells (39) and iNKT (38). Any of these cells may provide a source for IL-4 in the liver IRI model. Instead of individually screening IL-4 producing candidate cells, we eliminated the effects of ILC2s with use of a monoclonal antibody. The reduction in IL-4 after CD90.2 administration suggests that ILC2 could produce the IL-4 necessary for promoting this change to the M2 phenotype of macrophages. However, it should be noted that ILC2s are not the only source of IL-4, as iNKT cell-derived IL-4 could also be involved in promoting M2-like macrophages during hepatic IRI as reported by Goto et al (47). Accordingly, whether other cells are involved in this release of IL-4 will require further investigation.

Intravenous injection with Clodronate Liposomes depleted macrophages in organs where liposomes had an unhindered access to. When macrophages in the liver are depleted, those in the spleen are also cleared, thereby alleviating the potential for macrophage recruitment to the liver after IRI. However, with an administration of IL-33, the ratio of M2 type macrophages both in the liver and spleen are increased. These "protective" macrophages would then be available for recruitment from the spleen to the liver in response to hepatic IR. In this way, the existence of "protective" macrophages as induced by IL-33 may not only involve the liver but also the spleen as a very likely source.

In conclusion, we have demonstrated that the proliferation of ILC2s, as stimulated by exogenous IL-33, can alleviate hepatic IRI, primarily by inducing the polarization of CD45+CD11b +F4/80high macrophages to the M2 type. The possible molecular mechanisms for this process may, in part, involve the secretion of IL-4 by ILC2s *via* regulation of the JNK/Stat3 pathway in CD45+ CD11b+ F4/80high macrophages. These findings demonstrating the immune mechanisms of ILC2s in the alleviation of hepatic IRI can serve as the foundation for the development of new targets and strategies to prevent the injuries in liver function that accompany liver surgery.

Materials and methods

Animals

Male C57BL/6 mice (8-10 weeks old, 23 ± 2g) were purchased from the SiPeiFu (Beijing) Biotechnology Co., LTD [license SYXK (Beijing) 2017-0010] and were housed under specific pathogen-free condition with free access to water and food. The animal welfare and use protocol was approved by the Animal Ethics Committee of the Beijing Friendship Hospital of Capital Medical University.

Mouse model and treatment

The segmental (70%) hepatic ischemia model was employed in these experiments as described previously (48). Briefly, after a midline abdominal excision, the hepatic pedicle was carefully exposed and arterial and portal venous blood supplies to the cephalad lobes were clamped for 1 h using a nontraumatic sterile clamp. After this ischemic period, the clamps were released to induce reperfusion. Animals were euthanized at 6, 12 or 24 h post-reperfusion. Mice in the sham group were subjected to an identical procedure, except for the vascular occlusion.

For exogenous IL-33 administration, 0.2 ug of mouse recombinant IL-33 (Absin, abs04085) was injected through caudal vein daily for 5 consecutive days prior to the IRI treatment (43). Control animals received PBS only. Macrophages depletion was induced by administration of 10 mg/kg Clodronate Liposomes (LIPOSOMA C-005) *via* caudal vein injection as administered once at 24 h prior to IRI treatment. Anti-CD90.2 antibody (Biolegend, 105352) was injected into teil vein at -4 and -1 day before IRI surgery.

Intrahepatic lymphocytes and macrophages isolation

Intrahepatic lymphocytes and macrophage extraction was performed as described in previous studies (43, 49). Briefly, intrahepatic lymphocytes were obtained with use of *in vitro* collagenase type IV (Sigma, USA) digestion and discontinuous density gradient centrifugation by Ficoll (GE, 17-5442-02). Macrophages were isolated from the liver by *in situ*

collagenase type IV digestion and discontinuous density gradient centrifugation by 25%-50% Percoll. Then, anti-F4/80 MicroBeads UltraPure, (Miltenyi Biotec, Germany, 130-110-443) were used to sort macrophages for further culturing or RNA extraction.

Histology, immunohistochemistry and immunofluorescence

Formalin fixed and paraffin embedded liver tissue was cut into 4 μm-thick sections and stained with H+E to evaluate the degree of liver damage. Suzuki's Scores were calculated to quantify the damage. To identify apoptosis and regeneration of hepatocytes resulting from hepatic IRI, Caspase 3 (1:200, ab109201; Abcam), PCNA (1:200, ab92552; Abcam) and CD206 (1:200, ab252921; Abcam) rabbit antibodies were used for immunohistochemical staining. Image J was used to semi-quantitative analysis. Terminal deoxynucleotidyl transferase dUTP nick-end labeling (TUNEL) reaction was performed using an *In Situ* Cell Death Detection Kit, TMR red to assess apoptosis. The mean number of TUNEL-positive cells in five different fields (400×) were averaged for quantification.

Serology detection

Serum ALT, AST and cytokine levels of IL-4, and IL1β were assayed by ELISA according to instructions of the manufacturer (all ELISA kits were purchased from R&D Systems). All samples were measured in duplicate.

Cell culture and treatments

RAW264.7 and AML12 cell lines were purchased from the Procell Life Science and Technology Co., Ltd. (cat no.: CL-0190; Wuhan, China). Primary macrophages extracted from C57BL/6 mice were cultured with DMEM medium containing 10% FBS and 1% Penicillin+ Streptomycin mixture. AML12 cell lines were cultured with DMEM/F12 medium containing the same concentration of FBS and antibiotics as described above.

RAW 264.7 cells were plated in 6-well plates at a density of 4×10^5 cells/well and were divided into 3 groups: 1) Hypoxia and reoxygenation (H/R) - cells were immersed in paraffin oil for 1 h to produce an anoxic environment and then cultured in DMEM or DMEM/F12 for 12 h to induce hypoxia and reoxygenation injuries, 2) H/R+IL-4 - cells were treated with 20 ng/ml mouse recombinant IL-4 (CST, 5208SC) for 24 h before the H/R procedure and 3) H/R+IL-4+Stat3 inhibitor - cells were treated with 100 μM NSC 74859 (S3I-201) (MedChemExpress, HY-15146.) for 24 h following the H/R procedure. AML12 were co-cultured with RAW264.7 cells from the different groups during hypoxia and reoxygenation and then remained in these co-cultures for 12 h.

Flow cytometry analysis

ILC2s were defined as lineage negative (Lineage: TCRβ, TCRγ/δ, CD4, CD11c, CD5, CD8a, NK1.1, CD11b, ly-6G (Gr-1), TER-119, CD45R (B220), CD3e) and CD45, CD90.2 (Thy1), ST2, CD25 positive cells. Macrophages were suspended as single cells and stained with antibodies to CD45 (30-F11) Rat mAb (FITC Conjugate), CD11b/ITGAM (M1/70) Rat mAb (PE Conjugate), F4/80(BM8) Rat mAb (AF700 Conjugate) or CD206(C068C2) Rat mAb (BV711 Conjugate). (Supplementary Table 1) All antibodies were purchased from CST or BioLegend. Cells were analyzed on an Attune NxT flow cytometer (Thermo Fisher). CD206 was regarded as a marker for M2 macrophages. FlowJo software (Tree Star Inc., Ashland, OR, USA) was used to analyze the results. Annexin V (FITC Conjugated) and 7AAD (PE Conjugated) were used to test apoptosis conditions.

QRT-PCR

Total RNA was extract from liver tissue or RAW264.7 cells or purified macrophagess using TRIzol (absin, abs60154) according to operation steps of the instructions. Total RNA (1500ng) was then reversed with use of a TRUEscript 1st Strand cDNA Synthesis Kit (PC1802; Aidlab). Real-time PCR assays were performed on the ABI7500 Fast system (Applied Biosystems) using SYBR mastermix (Invitrogen) according to manufacturers' instructions.

Western blotting

Protein samples from liver tissue and RAW264.7 cells were extracted using RIPA buffer with a protease inhibitor (P0013B; Beyotime, Shanghai, China). Protein samples were separated *via* 8–12% SDS-PAGE (Bio-Rad, Redmond, WA, USA), electroblotted onto polyvinylidene difluoride membranes (Billerica, MA, USA), and then incubated with primary anti-Caspase-3 (1:2000, ab184787; Abcam), anti-BAX (1:2000, ab182733; Abcam), anti-Bcl2 (1:2000, ab182858; Abcam), anti-Stat3 (1:2000, #30835; CST), anti- phosph-JNK (1:2000, ab239886; Abcam) or anti-β-actin (1:2000, #4970; CST) rabbit antibodies at 4°C overnight. Horseradish-peroxidase-conjugated anti-rabbit IgG was used as the secondary antibody (1:3000; Cell Signaling Technology). Antibody binding was detected using a chemiluminescence system (Tanon-5200 Multi; Shanghai, China). Image J was used to semi-quantitative analysis.

Statistical analysis

Data are shown as Means ± SEMs. Differences among groups (≥3) were performed by one-way ANOVA with the *post-hoc* Tukey test used for pairwise comparisons of subgroups. A student's t-test was used to compare data between two groups. The SPSS 19.0 was used for conducting these analyses. $P < 0.05$ was required for results to be considered as statistically significant.

Data availability statement

The original contributions presented in the study are included in the article/supplementary material. Further inquiries can be directed to the corresponding author/s.

Ethics statement

The animal study was reviewed and approved by Animal Ethics Committee of Beijing Friendship Hospital, Capital Medical University.

Author contributions

Z-JZ, L-YS, X-JC and H-MZ participated in the research design. S-PL, J-MZ and L-XZ performed the molecular investigations; S-PL and X-JC participated in *in vivo* and *in vitro* experiment. JS, BC and G-PZ performed the data management and statistical analyses after discussion with all authors. S-Pi and X-JC wrote the manuscript. All authors contributed to the article and approved the submitted version.

Funding

This work was supported by the National Natural Science Foundation of China (No. 81970562).

Conflict of interest

The authors declare that the research was conducted in the absence of any commercial or financial relationships that could be construed as a potential conflict of interest.

Publisher's note

All claims expressed in this article are solely those of the authors and do not necessarily represent those of their affiliated organizations, or those of the publisher, the editors and the reviewers. Any product that may be evaluated in this article, or claim that may be made by its manufacturer, is not guaranteed or endorsed by the publisher.

Supplementary material

The Supplementary Material for this article can be found online at: https://www.frontiersin.org/articles/10.3389/fimmu.2022.869365/full#supplementary-material

References

1. Zhang T, Huang W, Ma Y. Down-regulation of TRPM2 attenuates hepatic ischemia/reperfusion injury through activation of autophagy and inhibition of NLRP3 inflammasome pathway. *Int IMMUNOPHARMACOL* (2022) 104:108443. doi: 10.1016/j.intimp.2021.108443

2. Rautou PE, Mansouri A, Lebrec D, Durand F, Valla D, Moreau R. Autophagy in liver diseases. *J Hepatol* (2010) 53:1123–34. doi: 10.1016/j.jhep.2010.07.006

3. Konishi T, Lentsch AB. Hepatic Ischemia/Reperfusion: Mechanisms of tissue injury, repair, and regeneration. *Gene Expr* (2017) 17:277–87. doi: 10.3727/105221617X15042750874156

4. Mosser DM, Edwards JP. Exploring the full spectrum of macrophage activation. *Nat Rev Immunol* (2008) 8:958–69. doi: 10.1038/nri2448

5. Devey L, Ferenbach D, Mohr E, Sangster K, Bellamy CO, Hughes J, et al. Tissue-resident macrophages protect the liver from ischemia reperfusion injury *via* a heme oxygenase-1-dependent mechanism. *Mol Ther* (2009) 17:65–72. doi: 10.1038/mt.2008.237

6. Lu TF, Yang TH, Zhong CP, Shen C, Lin WW, Gu GX, et al. Dual effect of hepatic macrophages on liver ischemia and reperfusion injury during liver transplantation. *Immune Netw* (2018) 18:e24. doi: 10.4110/in.2018.18.e24

7. You Y, Zhang X, Wang X, Yue D, Meng F, Zhu J, et al. ILC2 proliferated by IL-33 stimulation alleviates acute colitis in Rag1(-/-) mouse through promoting M2 macrophage polarization. *J Immunol Res* (2020) 2020:5018975. doi: 10.1155/2020/5018975

8. Olguin-Martinez E, Ruiz-Medina BE, Licona-Limon P. Tissue-specific molecular markers and heterogeneity in type 2 innate lymphoid cells. *Front Immunol* (2021) 12:757967. doi: 10.3389/fimmu.2021.757967

9. Huang Y, Guo L, Qiu J, Chen X, Hu-Li J, Siebenlist U, et al. IL-25-responsive, lineage-negative KLRG1(hi) cells are multipotential 'inflammatory' type 2 innate lymphoid cells. *Nat Immunol* (2015) 16:161–9. doi: 10.1038/ni.3078

10. Salimi M, Barlow JL, Saunders SP, Xue L, Gutowska-Owsiak D, Wang X, et al. A role for IL-25 and IL-33-driven type-2 innate lymphoid cells in atopic dermatitis. *J Exp Med* (2013) 210:2939–50. doi: 10.1084/jem.20130351

11. Kabata H, Moro K, Koyasu S. The group 2 innate lymphoid cell (ILC2) regulatory network and its underlying mechanisms. *Immunol Rev* (2018) 286:37–52. doi: 10.1111/imr.12706

12. Kang H, Bang JY, Mo Y, Shin JW, Bae B, Cho SH, et al. Effect of acinetobacter lwoffii on the modulation of macrophage activation and asthmatic inflammation. *Clin Exp Allergy* (2021) 52(4):518–529. doi: 10.1111/cea.14077

13. Kim J, Chang Y, Bae B, Sohn KH, Cho SH, Chung DH, et al. Innate immune crosstalk in asthmatic airways: Innate lymphoid cells coordinate polarization of lung macrophages. *J Allergy Clin Immunol* (2019) 143:1769–82. doi: 10.1016/j.jaci.2018.10.040

14. Momiuchi Y, Motomura Y, Suga E, Mizuno H, Kikuta J, Morimoto A, et al. Group 2 innate lymphoid cells in bone marrow regulate osteoclastogenesis in a

reciprocal manner *via* RANKL, GM-CSF and IL-13. *Int Immunol* (2021) 33:573–85. doi: 10.1093/intimm/dxab062

15. Cui W, Zhang W, Yuan X, Liu S, Li M, Niu J, et al. Vitamin a deficiency execrates Lewis lung carcinoma *via* induction of type 2 innate lymphoid cells and alternatively activates macrophages. *Food Sci Nutr* (2019) 7:1288–94. doi: 10.1002/fsn3.961

16. Afferni C, Buccione C, Andreone S, Galdiero MR, Varricchi G, Marone G, et al. The pleiotropic immunomodulatory functions of IL-33 and its implications in tumor immunity. *Front Immunol* (2018) 9:2601. doi: 10.3389/fimmu.2018.02601

17. Mi LL, Zhu Y, Lu HY. A crosstalk between type 2 innate lymphoid cells and alternative macrophages in lung development and lung diseases (Review). *Mol Med Rep* (2021) 23. doi: 10.3892/mmr.2021.12042

18. Zhang Y, Qi C, Li L, Hua S, Zheng F, Gong F, et al. CD8(+) T cell/IL-33/ILC2 axis exacerbates the liver injury in con a-induced hepatitis in T cell-transferred Rag2-deficient mice. *Inflammation Res* (2019) 68:75–91. doi: 10.1007/s00011-018-1197-9

19. Zhu G, Cai H, Ye L, Mo Y, Zhu M, Zeng Y, et al. Small proline-rich protein 3 regulates IL-33/ILC2 axis to promote allergic airway inflammation. *Front Immunol* (2021) 12:758829. doi: 10.3389/fimmu.2021.758829

20. Li S, Zhu FX, Zhang HB, Li H, An YZ. Pretreatment with interleukin-33 reduces warm hepatic ischemia/reperfusion injury in mice. *Chin Med J (Engl)* (2013) 126:1855–9. doi: 10.3760/cma.j.issn.0366-6999.20123530

21. Sakai N, Van Sweringen HL, Quillin RC, Schuster R, Blanchard J, Burns JM, et al. Interleukin-33 is hepatoprotective during liver ischemia/reperfusion in mice. *HEPATOLOGY* (2012) 56:1468–78. doi: 10.1002/hep.25768

22. Yazdani HO, Chen HW, Tohme S, Tai S, van der Windt DJ, Loughran P, et al. IL-33 exacerbates liver sterile inflammation by amplifying neutrophil extracellular trap formation. *J Hepatol* (2017) S0168–8278(17):32291–2. doi: 10.1016/j.jhep.2017.09.010

23. Barbier L, Robin A, Sindayigaya R, Ducousso H, Dujardin F, Thierry A, et al. Endogenous interleukin-33 acts as an alarmin in liver ischemia-reperfusion and is associated with injury after human liver transplantation. *Front Immunol* (2021) 12:744927. doi: 10.3389/fimmu.2021.744927

24. Maggi L, Mazzoni A, Capone M, Liotta F, Annunziato F, Cosmi L. The dual function of ILC2: From host protection to pathogenic players in type 2 asthma. *Mol ASPECTS Med* (2021) 80:100981. doi: 10.1016/j.mam.2021.100981

25. Li S, Zhang J, Wang Z, Wang T, Yu Y, He J, et al. MicroRNA-17 regulates autophagy to promote hepatic ischemia/reperfusion injury *via* suppression of signal transductions and activation of transcription-3 expression. *LIVER Transplant* (2016) 22:1697–709. doi: 10.1002/lt.24606

26. Li SP, He JD, Wang Z, Yu Y, Fu SY, Zhang HM, et al. miR-30b inhibits autophagy to alleviate hepatic ischemia-reperfusion injury *via* decreasing the Atg12-Atg5 conjugate. *World J Gastroenterol* (2016) 22:4501–14. doi: 10.3748/wjg.v22.i18.4501

27. Li S, He J, Xu H, Yang J, Luo Y, Song W, et al. Autophagic activation of IRF-1 aggravates hepatic ischemia-reperfusion injury *via* JNK signaling. *MedComm (2020)* (2021) 2:91–100. doi: 10.1002/mco2.58

28. Hirao H, Nakamura K, Kupiec-Weglinski JW. Liver ischaemia-reperfusion injury: A new understanding of the role of innate immunity. *Nat Rev Gastroenterol Hepatol* (2021) 19(4):239–256. doi: 10.1038/s41575-021-00549-8

29. Goikoetxea-Usandizaga N, Serrano-Macia M, Delgado TC, Simon J, Fernandez RD, Barriales D, et al. Mitochondrial bioenergetics boost macrophage activation, promoting liver regeneration in metabolically compromised animals. *HEPATOLOGY* (2022) 75:550–66. doi: 10.1002/hep.32149

30. Ni M, Zhang J, Sosa R, Zhang H, Wang H, Jin D, et al. T-Cell immunoglobulin and mucin domain-containing protein-4 is critical for kupffer cell homeostatic function in the activation and resolution of liver ischemia reperfusion injury. *HEPATOLOGY* (2021) 74:2118–32. doi: 10.1002/hep.31906

31. Nakata Y, Kono H, Akazawa Y, Hirayama K, Wakana H, Fukushima H, et al. Role of podoplanin and kupffer cells in liver injury after ischemia-reperfusion in mice. *Surg Today* (2022) 52:344–53. doi: 10.1007/s00595-021-02378-3

32. Xie Y, Zhao D, Dong P, Lai L. Macrophage-targeting fasudil treatment protects liver from the ischemia/reperfusion injury by promoting M2 macrophage polarization. *Biosci Rep* (2018). doi: 10.1042/BSR20171734

33. Yue S, Rao J, Zhu J, Busuttil RW, Kupiec-Weglinski JW, Lu L, et al. Myeloid PTEN deficiency protects livers from ischemia reperfusion injury by facilitating M2 macrophage differentiation. *J Immunol* (2014) 192:5343–53. doi: 10.4049/jimmunol.1400280

34. Clottu AS, Humbel M, Fluder N, Karampetsou MP, Comte D. Innate lymphoid cells in autoimmune diseases. *Front Immunol* (2021) 12:789788. doi: 10.3389/fimmu.2021.789788

35. Wang L, Netto KG, Zhou L, Liu X, Wang M, Zhang G, et al. Single-cell transcriptomic analysis reveals the immune landscape of lung in steroid-resistant asthma exacerbation. *Proc Natl Acad Sci USA* (2021) 118. doi: 10.1073/pnas.2005590118

36. Miller MM, Reinhardt RL. The heterogeneity, origins, and impact of migratory iILC2 cells in anti-helminth immunity. *Front Immunol* (2020) 11:1594. doi: 10.3389/fimmu.2020.01594

37. Liew FY, Girard JP, Turnquist HR. Interleukin-33 in health and disease. *Nat Rev Immunol* (2016) 16:676–89. doi: 10.1038/nri.2016.95

38. Bourgeois E, Van LP, Samson M, Diem S, Barra A, Roga S, et al. The pro-Th2 cytokine IL-33 directly interacts with invariant NKT and NK cells to induce IFN-gamma production. *Eur J Immunol* (2009) 39:1046–55. doi: 10.1002/eji.200838575

39. Ngo TPN, Palmieri V, Adamczyk A, Klopfleisch R, Langhorst J, Hansen W, et al. IL-33 drives expansion of type 2 innate lymphoid cells and regulatory T cells and protects mice from severe, acute colitis. *Front Immunol* (2021) 12:669787. doi: 10.3389/fimmu.2021.669787

40. Mindt BC, Krisna SS, Duerr CU, Mancini M, Richer L, Vidal SM, et al. The NF-kappaB transcription factor c-rel modulates group 2 innate lymphoid cell effector functions and drives allergic airway inflammation. *Front Immunol* (2021) 12:664218. doi: 10.3389/fimmu.2021.664218

41. Sasaki E, Asanuma H, Momose H, Furuhata K, Mizukami T, Hamaguchi I. Nasal alum-adjuvanted vaccine promotes IL-33 release from alveolar epithelial cells that elicits IgA production *via* type 2 immune responses. *PloS Pathog* (2021) 17: e1009890. doi: 10.1371/journal.ppat.1009890

42. Yin H, Li XY, Jin XB, Zhang BB, Gong Q, Yang H, et al. IL-33 prolongs murine cardiac allograft survival through induction of TH2-type immune deviation. *TRANSPLANTATION* (2010) 89:1189–97. doi: 10.1097/TP.0b013e3181d720af

43. Cao Q, Wang Y, Niu Z, Wang C, Wang R, Zhang Z, et al. Potentiating tissue-resident type 2 innate lymphoid cells by IL-33 to prevent renal ischemia-reperfusion injury. *J Am Soc Nephrol* (2018) 29:961–76. doi: 10.1681/ASN.2017070774

44. Hikichi Y, Motomura Y, Takeuchi O, Moro K. Posttranscriptional regulation of ILC2 homeostatic function *via* tristetraprolin. *J Exp Med* (2021) 218. doi: 10.1084/jem.20210181

45. Cameron G, Cautivo KM, Loering S, Jiang SH, Deshpande AV, Foster PS, et al. Group 2 innate lymphoid cells are redundant in experimental renal ischemia-reperfusion injury. *Front Immunol* (2019) 10:826. doi: 10.3389/fimmu.2019.00826

46. Noval RM, Burton OT, Oettgen HC, Chatila T. IL-4 production by group 2 innate lymphoid cells promotes food allergy by blocking regulatory T-cell function. *J Allergy Clin Immunol* (2016) 138:801–11. doi: 10.1016/j.jaci.2016.02.030

47. Goto T, Ito Y, Satoh M, Nakamoto S, Nishizawa N, Hosono K, et al. Activation of iNKT cells facilitates liver repair after hepatic ischemia reperfusion injury through acceleration of macrophage polarization. *Front Immunol* (2021) 12:754106. doi: 10.3389/fimmu.2021.754106

48. Ji H, Shen X, Gao F, Ke B, Freitas MC, Uchida Y, et al. Programmed death-1/B7-H1 negative costimulation protects mouse liver against ischemia and reperfusion injury. *HEPATOLOGY* (2010) 52:1380–9. doi: 10.1002/hep.23843

49. Romera-Hernandez M, Matha L, Steer CA, Ghaedi M, Takei F. Identification of group 2 innate lymphoid cells in mouse lung, liver, small intestine, bone marrow, and mediastinal and mesenteric lymph nodes. *Curr Protoc Immunol* (2019) 125:e73. doi: 10.1002/cpim.73

frontiers | Frontiers in Immunology

TYPE Original Research
PUBLISHED 05 September 2022
DOI 10.3389/fimmu.2022.898799

OPEN ACCESS

EDITED BY
Tao Qiu,
Renmin Hospital of Wuhan University, China

REVIEWED BY
JingHong Wan,
INSERM U1149 Centre de Recherche sur l'Inflammation, France
Lan Wu,
Vanderbilt University Medical Center, United States

*CORRESPONDENCE
Alexander Kroemer
alexander.kroemer@gunet.georgetown.edu;
akroemer@me.com
Suman Ranjit
suman.ranjit@georgetown.edu

†These authors have contributed equally to this work and share first authorship

SPECIALTY SECTION
This article was submitted to Molecular Innate Immunity, a section of the journal Frontiers in Immunology

RECEIVED 17 March 2022
ACCEPTED 11 July 2022
PUBLISHED 05 September 2022

CITATION
Liggett JR, Kang J, Ranjit S, Rodriguez O, Loh K, Patil D, Cui Y, Duttargi A, Nguyen S, He B, Lee Y, Oza K, Frank BS, Kwon D, Li HH, Kallakury B, Libby A, Levi M, Robson SC, Fishbein TM, Cui W, Albanese C, Khan K and Kroemer A (2022) Oral N-acetylcysteine decreases IFN-γ production and ameliorates ischemia-reperfusion injury in steatotic livers. *Front. Immunol.* 13:898799. doi: 10.3389/fimmu.2022.898799

Oral N-acetylcysteine decreases IFN-γ production and ameliorates ischemia-reperfusion injury in steatotic livers

Jedson R. Liggett[1,2†], Jiman Kang[1,3†], Suman Ranjit[3,4*†], Olga Rodriguez[5,6], Katrina Loh[1], Digvijay Patil[1], Yuki Cui[1], Anju Duttargi[6], Sang Nguyen[5], Britney He[5], Yichien Lee[5,6], Kesha Oza[1], Brett S. Frank[1], DongHyang Kwon[7], Heng-Hong Li[6], Bhaskar Kallakury[7], Andrew Libby[8], Moshe Levi[3], Simon C. Robson[9], Thomas M. Fishbein[1], Wanxing Cui[1,3], Chris Albanese[5,6,10], Khalid Khan[1] and Alexander Kroemer[1*]

[1]MedStar Georgetown Transplant Institute, MedStar Georgetown University Hospital and the Center for Translational Transplant Medicine, Georgetown University Medical Center, Washington, DC, United States, [2]Department of Surgery, Naval Medical Center Portsmouth, Portsmouth, VA, United States, [3]Department of Biochemistry and Molecular & Cellular Biology, Georgetown University, Washington, DC, United States, [4]Microscopy & Imaging Shared Resource, Georgetown University, Washington, DC, United States, [5]Center for Translational Imaging, Georgetown University Medical Center, Washington, DC, United States, [6]Department of Oncology, Lombardi Comprehensive Cancer Center, Georgetown University Medical Center, Washington, DC, United States, [7]Department of Pathology, MedStar Georgetown University Hospital, Washington, DC, United States, [8]Division of Endocrinology, Metabolism, & Diabetes, University of Colorado Anschutz Medical Campus, Aurora, CO, United States, [9]Departments of Anesthesiology and Medicine, Beth Israel Deaconess Medical Center, Harvard Medical School, Boston, MA, United States, [10]Department of Radiology, MedStar Georgetown University Hospital, Washington, DC, United States

Type 1 Natural Killer T-cells (NKT1 cells) play a critical role in mediating hepatic ischemia-reperfusion injury (IRI). Although hepatic steatosis is a major risk factor for preservation type injury, how NKT cells impact this is understudied. Given NKT1 cell activation by phospholipid ligands recognized presented by CD1d, we hypothesized that NKT1 cells are key modulators of hepatic IRI because of the increased frequency of activating ligands in the setting of hepatic steatosis. We first demonstrate that IRI is exacerbated by a high-fat diet (HFD) in experimental murine models of warm partial ischemia. This is evident in the evaluation of ALT levels and Phasor-Fluorescence Lifetime (Phasor-FLIM) Imaging for glycolytic stress. Polychromatic flow cytometry identified pronounced increases in CD45+CD3+NK1.1+NKT1 cells in HFD fed mice when compared to mice fed a normal diet (ND). This observation is further extended to IRI, measuring *ex vivo* cytokine expression in the HFD and ND. Much higher interferon-gamma (IFN-γ) expression is noted in the HFD mice after IRI. We further tested our hypothesis by performing a lipidomic analysis of hepatic tissue and compared this to Phasor-FLIM imaging using "long lifetime species", a byproduct of lipid oxidation. There are higher levels of

triacylglycerols and phospholipids in HFD mice. Since N-acetylcysteine (NAC) is able to limit hepatic steatosis, we tested how oral NAC supplementation in HFD mice impacted IRI. Interestingly, oral NAC supplementation in HFD mice results in improved hepatic enhancement using contrast-enhanced magnetic resonance imaging (MRI) compared to HFD control mice and normalization of glycolysis demonstrated by Phasor-FLIM imaging. This correlated with improved biochemical serum levels and a decrease in IFN-γ expression at a tissue level and from CD45+CD3+CD1d+ cells. Lipidomic evaluation of tissue in the HFD+NAC mice demonstrated a drastic decrease in triacylglycerol, suggesting downregulation of the PPAR-γ pathway.

KEYWORDS

NKT (natural killer T) cell, hepatic steatosis, IFN-gamma, ischemia-reperfusion injury (IRI), N-acetylcysteine (NAC), phasor-FLIM, gadoxetate disodium, liver transplantation

Introduction

Hepatic ischemia-reperfusion injury (IRI) remains a significant complication in both surgical liver resection and liver transplantation. IRI is a complex and incompletely understood process that leads to the disruption of cellular integrity with the release of damages-associated molecular patterns and subsequent innate immune system activation (1), though identification of key mediators remains the point of ongoing research. In liver transplantation, the degree of IRI is more profound in the setting of hepatic steatosis and has historically been shown to increase the risk of primary non-function, dysfunction, and reduce graft and patient survival (1). Unfortunately, due to the increasing demand for liver transplantation and a lack of transplantable livers, "marginal" allografts, including those with hepatic steatosis, are being considered despite an elevated risk of IRI.

Currently, there are few available therapeutic options in the prevention and treatment of IRI, and N-acetylcysteine (NAC), a thiol-containing synthetic compound, remains a mainstay in the treatment. While the efficacy of NAC has been established in the treatment of acetaminophen toxicity and has shown some efficacy against IRI and fulminant liver failure, its mechanisms, optimization of treatment, and impact on long-term survival remain understudied (2). Given the limited treatment options for IRI and the increasing demand for liver transplantation, significant research efforts are required to not only identify key mediators and therapeutic options for IRI, but also accurately evaluate donor allografts for high-risk stigmata in order to safely utilize these "marginal" organs while decreasing the associated risk.

While no standard exists, donor allograft biopsy is frequently performed to aid in allograft selection, and greater than 30% hepatic macro steatosis is often a deterrent for allograft use. However, a recent study by Patel et al. has shown that steatotic allografts can be successfully utilized with appropriate recipient selection (3). To aid in the selection process, advanced methods to investigate the integrity and function of the allograft may be essential for the use of marginal allografts. Both Magnetic Resonance Imaging (MRI) and Phasor Fluorescence Lifetime Imaging (FLIM) are promising modalities to evaluate liver function and injury. T2 mapping by MRI has previously been shown as a feasible, non-invasive technique in assessing acute liver injury (4), while FLIM has been demonstrated to assess for liver injury more accurately *via* the evaluation of steatosis, fibrosis (5), and glycolytic activity (6) in experimental models.

Invariant natural killer T (NKT) cells are a unique group of cells that can recognize both self and lipid antigens that are presented to them by MHC class I-like CD1d molecules (7). Type I invariant Natural Killer T-cells (NKT1 cells) not only express CD1d, but also express markers of both T-cells (CD3+) and conventional NK cells (NK1.1+) and can potently secrete IFN-γ and TNF-α (8–10). NKT1 cells have emerged as key mediators in hepatic IRI (10, 11) and have been shown to worsen this process in a NAFLD murine model, despite lower baseline populations (1). Interestingly, it is also known that NKT1 cells express a wide variety of activating antigens including endogenous lipid antigens such as phosphatidylcholine (12–15), which may lead to an enhanced response to IRI. Thus, preventing activation of NKT1 cells following IRI in NAFLD may aid in developing new therapeutic approaches that merit further investigation. In addition to the known benefits in IRI, NAC has also been demonstrated to alter metabolism and have benefits in the treatment of metabolic syndrome, in addition to the known benefit in IRI. However, the immunomodulatory capacity of NAC in liver injury remains understudied.

Given the activation of NKT1 cells by lipid antigens and potential roles of NKT1 cells in hepatic IRI, we hypothesized that NAC supplementation would ameliorate IRI in a high-fat diet (HFD) murine model *via* decreased activation of NKT1 cells. In our present work, we utilize advanced Phasor-FLIM imaging to interrogate tissue following IRI and further evaluate the innate immune response to IRI. This study successfully identifies NKT1 cells and IFN-γ as mediators in IRI in the setting of hepatic steatosis and shows an improved clinical phenotype following NAC supplementation at least in part secondary to reduced NKT1 cell activation.

Materials and methods

Diets

The normal diet (ND), #5001, was purchased from Lab Diet, St. Louis MO, (4.09 kcal/gram,13.4% kJ/fat). The high-fat diet (HFD), 58Y1 blue, was purchased from TestDiet, St. Louis, MO (5.10 kcal/gram, 60% kJ/fat). HFD was stored in refrigerated conditions at 4°C. NAC was purchased from Sigma, St. Louis, MO and was added to the treatment group drinking water in a concentration of 10 gram/liter.

Animals

All animal procedures in this study were fully approved by the Georgetown University Institutional Animal Care and Use Committee under protocol number 2016-1351. C57BL/6 mice were obtained at five to six weeks of age from Charles River Laboratories and The Jackson Laboratory, Bar Harbor, ME. The mice were maintained in the Division of Comparative Medicine at Georgetown University Medical Center, with a standard 12-hour light-dark cycle. Male mice were used for all experiments. Food and water were provided *ab libitum* in the four experimental groups: ND, ND + NAC, HFD, and HFD + NAC. The ND diets were administered at the beginning of the study and maintained for 19-23 weeks. The HFD was started at six to seven weeks of age and continued for 19-23 weeks. NAC drinking water was administered to the ND + NAC and HFD + NAC groups following three weeks of ND or HFD and maintained for 16-20 weeks. The NAC-supplemented drinking water was changed weekly. Consumption of the HFD and individual animal weights were measured weekly. Additional C57BL/6 mice were purchased at 25 weeks of age from The Jackson Laboratory, Bar Harbor, ME on a ND, #5K52 from Lab Diet (3.50 kcal/gram, 16.6% fat), for supplemental use in select groups.

Partial warm IRI model

All procedures performed on C57BL/6 mice were fully approved by the Georgetown University Institutional Animal Care and Use Committee under protocol number 2016-1351. Mice were anesthetized with 2% isoflurane and oxygen inhalation. A midline laparotomy was performed, and an atraumatic micro clip was placed across the hepatic hilus, which interrupted the blood supply to the left and median lobes of the liver. The abdomen was temporarily closed with skin staples, and the mice remained anesthetized. A 45-minute ischemic time was utilized to represent a clinically relevant model, more closely corresponding to the average warm ischemia time in human liver transplantation. This also prevented excess animal death under anesthesia, given the metabolic changes associated within the HFD model. Following 45 minutes of partial hepatic ischemia, the clip was removed to initiate hepatic reperfusion. The abdominal wall was closed with sutures, the skin was reapproximated with staples, and the animals were returned to their cage. All mice undergoing Magnetic Resonance Imaging following IRI, had their abdominal wall and skin reapproximated with sutures. After 24 hours of reperfusion, mice were anesthetized and underwent a second laparotomy. Whole blood was obtained *via* direct cardiac puncture as a terminal procedure. The left lobe of the liver and the whole spleen were collected. Sham controls underwent the same procedure but without vascular occlusion.

Magnetic resonance imaging

Magnetic resonance imaging (MRI) was performed in the Georgetown-Lombardi Preclinical Imaging Research Laboratory on either a 7T/20 Avance III/ParaVision 5 or a 7T/30 USR Avance NEO/ParaVision 360 (S10 OD025153) scanner. The mice were anesthetized (1.5% isoflurane in a gas mixture of 30% oxygen and 70% nitrous oxide) and placed on a custom-manufactured (ASI Instruments, Warren, MI) stereotaxic device, with built-in temperature and cardio-respiratory monitoring as described (B, C), and compatible with a 40 mm Bruker mouse body volume coil.

Adipose tissue. MRI of abdominal and liver fat was performed with a three-dimensional rapid acquisition with rapid enhancement (3D-RARE) sequence in the coronal orientation with the following parameters: TR: 2855 ms, TE: 12 ms, RARE Factor: 4, Matrix: 220 x 220, FOV: 50 mm x 40 mm, Averages: 4, Slice thickness: 0.75 mm, Slices: 50 and respiratory gating Quantification of visceral fat depots in the imaging datasets was performed by thresholding and voxel-counting with ImageJ software (NIH), as previously described (16–18). We used a maximum intensity projection algorithm of

the 3D-reconstructed image with an intensity threshold intended to segment fat only. The abdominal region analyzed was defined by superior and inferior anatomical landmarks, that is, the proximal border of the left kidney and the convergence of the left and right common iliac veins, respectively. The lateral landmark was the abdominal wall, avoiding subcutaneous fat. The percentage area corresponding to fat depots within the abdomen was calculated *via* the sum of the visceral fat voxels versus total abdominal voxels. Mouse liver fat was measured by quantifying the mean intensity of the region of interest (ROI) localized on the mouse liver placed in homogenous areas, avoiding structures such as large vessels and ducts. ROIs on three separate slices were selected and averaged for each mouse. For imaging of the nuchal fat, a 3-D T1-weighted RARE sequence in the sagittal orientation was run with TR: 2437 ms, TE: 15 ms, FA: 74.1, Matrix: 256 x 256, FOV: 40 mm x 40 mm, Slice thickness: 0.5 mm, Averages: 4, Slices: 35. The mean intensity of nuchal brown adipose tissue (BAT) and white adipose tissue (WAT) was measured by localizing ROIs on the BAT and the WAT. ROIs on three separate slices were selected and averaged for each mouse.

Dynamic Contrast-Enhanced MRI (DCE-MRI) using Gadoxetate Disodium (Eovist®, Bayer). DCE-MRI was performed with a T1-weighted RARE protocol in the coronal orientation, without respiratory gating, with TE: 8.2 ms, TR: 400 ms, slice thickness: 1 mm, matrix: 128 x128, FOV: 40 mm x 40 mm, rare factor: 2, fat suppression and a duration of 25 s. Ten baseline (pre-contrast) scans were run, followed by subcutaneous parenteral administration of 0.025 mmol/kg Eovist. Immediately after injection, 60 MRI scans were acquired repetitively over approximately 30 minutes, and the uptake and excretion of contrast was measured over time. Relative liver enhancement (RLE) was used to quantify hepatic function. Briefly, the mean intensity of regions of interest (ROI) localized in homogenous areas of the liver were quantified in baseline and post-injection images. Liver function was calculated using the formula $RLE = (SI_{Liver\ enh} - SI_{Liver\ unenh})/SI_{Liver\ unenh}\ x\ 100$. The area-under-the-curve (AUC) and the slope were derived from the corresponding RLE data. The slopes were measured for the first 20 minutes post-injection, where after this time point, the curves reached their plateau. Both the AUC and the slopes were calculated with a 95% confidence interval.

T2 mapping A two-dimensional multi-echo multi-slice sequence in the axial orientation was used for T2 mapping with TR: 2000 ms, Flip Angle: 180 deg, Averages: 2, and the following echo times, TE: 10, 20, 30, 40, 50, 60, 70 and 80 ms, with respiratory gating. In order to measure T2 relaxation times, we used the Paravision360 Image Sequence Analysis tool to generate T2-fit and T2-maps. ROI were localized on the left and right liver areas in four slices per mouse, excluding non-homogenous structures such as large hepatic vessels or ducts, after which T2 values were quantified and averaged.

Measurement of alanine aminotransferase (ALT)

Whole blood was obtained by direct cardiac puncture as a terminal procedure. ALT levels were measured using a multichannel analyzer, Alfa Wassermann Vet Axcel, from the clinical diagnostics laboratory of VRL Maryland, LLC.

Histology and immunohistochemistry

Hematoxylin and eosin (H&E) and immunohistochemical staining was performed on five-micron sections from formalin-fixed paraffin-embedded liver tissues. H&E staining was completed, and samples were then rehydration through a graded alcohol series using the Autostainer XL (Leica Biosystems). Gr-1 and CD68 staining was performed using the ImmPRESS Goat anti-rat Polymer Detection Kit (peroxidase) (Vector laboratories, MP-7444) and horseradish peroxidase-labeled polymer from (Dako, K4003) for Gr-1 and CD68 respectively. Gr-1and CD68 cell counts were performed manually in five high-powered field sections of 20x magnification using an Olympus BX41 light microscope. Cell counting was performed in a blinded manner.

Fluorescence lifetime imaging and second harmonic generation imaging

Instrumentation. The autofluorescence lifetime images of the liver sections (5 µm thick) were measured using a modified Olympus FVMPERS (Waltham, MA) microscope equipped with a Spectra-Physics Insight X3 (Milpitas, CA) laser and FastFLIM (ISS, Champaign, IL) acquisition card. The samples were excited with the 740 nm laser line using a 20X air objective (LUCPLFLN 0.45NA, Olympus) applying a two-photon excitation scheme. The fluorescence was collected using the DIVER (Deep Imaging *Via* Enhanced Recovery) detector (19–21) assembly and recorded using a FastFLIM card (ISS, Champaign, IL). The pixel dwell time for the acquisitions was 20 µs, and the images were taken with sizes of 256x256 pixels with a field of view of 318.8 µm (Zoom =2X). To obtain a high signal-to-noise ratio, 16 frames were collected for each area. The data from each pixel were recorded and analyzed using the SimFCS software (Laboratory for Fluorescence Dynamics, University of California, Irvine, CA). The FLIM data were collected using the passive mode, where the raster scanning was done using the Olympus software, and the images were collected using the FLIMBox/FastFLIM system, and the scanning parameters were matched to ensure proper image acquisition. SHG and FLIM images were obtained using two separate filter

assemblies in DIVER and further separated based on their lifetime and phasor position.

Phasor Fluorescence Lifetime Imaging (FLIM) Methodology. The Phasor approach to FLIM is a fit free method of analysis where fluorescence decay information collected at each pixel of an image is transformed to the phasor plot and designated a coordinate based on the lifetime (22–25). Being a fit free method, phasor is a much faster analysis method and is used increasingly in biological fluorescence imaging with a large data set. The phasor transformation results in the formation of a heat map in the phasor plot where each pixel of an image is represented by a single phasor point and segmentation and filtering methods and of image analysis can be applied without loss of image definition of the original intensity images. Recent advances in analysis techniques allow us to quantify the contribution of multiple components and this is applied in this work (26–29).

A brief description of the method follows below. A much more detailed description of the method, along with individual analysis schemes, flowcharts, and assumptions for both phasor-FLIM quantification and SHG analysis is explained in the supplemental information. FastFLIM (ISS, Champaigne, IL) is a frequency domain FLIM imaging instrument. In frequency-domain fluorescence lifetime measurements, the transformation to the phasor plot uses the following relations,

$$g_{i,j}(\omega) = m_{i,j} \cdot cos\left(\phi_{i,j}\right) \quad 3$$

$$s_{i,j}(\omega) = m_{i,j} \cdot sin\left(\phi_{i,j}\right) \quad 4$$

where, $g_{i,j}(\omega)$ and $s_{i,j}(\omega)$ are the X and Y coordinates of the phasor plot, respectively, and $m_{i,j}$ and $\phi_{i,j}$ are the modulation and phase of fluorescence signal at the image pixel *i, j*. The longer lifetime is represented by the larger phase angle in the Phasor plot – movement towards S=0, G=0 around universal semi-circle. The distribution of phasor points originating from FLIM measurements appears on (for mono-exponential decays) or inside (for multi-exponential decays) the universal circle (please refer to SM1 in the phasor supplemental methods). The linear combinations are shown by the blue. If each component has a multi-exponential decay, its location will be represented by phasors not in the universal circle, but the principle of linear combination remains valid. More details can be found in the phasor section of the supplemental methods.

According to this principle, if a pixel of an image has multiple components originating from multiples species, then the position of the corresponding phasor point is inside the polygon whose vertices are occupied by the Phasor points originating from the individual components. The distance of the image phasor point from any of the vertices is reciprocal to the fractional intensity component of that particular component. The higher the fractional intensity contribution of that particular species towards the total intensity of the image pixel, the closer the phasor point of that image pixel is to the corresponding component phasor position (24, 30, 31). For a three component system, an algebraic solution of this system exists, and this allows the breakdown of a Phasor cloud from an image to the individual fractional intensity components (28). Our recent work created a framework where the phasor clouds originating from multiple components can be quantitatively resolved, and their individual fractional intensities can be calculated (26, 28, 29). For a system where the quantum yield can be assumed based on their lifetimes or can be quantified – the fractional intensity ratios can be modified to molar fraction ratios. Please see supplemental methods for additional details of the analysis and stepwise processes.

In this work, the positions of the three original phasor positions were selected based on previously published work. Free and protein bound NADH have a lifetime of 0.4 ns and ~3.4 ns, respectively, and their positions are on universal semicircle (32), and are shown by the blue and green circles, respectively (Figure 3A). The line joining the two cursors is named metabolic trajectory (33). The long lifetime species (LLS) has a lifetime of ~8ns, and the corresponding phasor position is selected by the red circle (26, 27, 33, 34). In the presence of LLS, the autofluorescence FLIM phasor in the NADH channel shifts away from the metabolic trajectory and inside the triangle whose vertices are occupied by the central positions of red, green, and blue circles. As mentioned above and in supplemental methods (Phasor section) – we have used multiple component analysis to obtain the quantitative information about the concentration ratio of free and protein-bound NADH and fractional intensity of NADH.

Targeted lipidomic profiling

Snap-frozen liver tissue was dissolved in 300 µL of extraction buffer (IPA) and subjected to two cycles of freezing and rapid thawing into a 37°C water bath or 90 seconds. Then, tissue samples were sonicated at 30 kHz for 30 seconds and mixed with 100µl of ice-chilled isopropyl alcohol (IPA) with internal standards (IS). Upon 30 minutes of incubation on ice and additional incubation at −20°C for 30 minutes, the tissue in suspension was spun down at 14000xg at 4°C for 20 minutes to collect the supernatant. Targeted LCMS-MS was performed using Xbridge Amide 3.5 µm, 4.6 × 100 mm column (Phenomenex) online with a triple quadrupole mass spectrometer (5500 QTRAP, SCIEX) equipped in the multiple reaction monitoring (MRM) modes. Each metabolite, declustering potential, collision energies, cell exit potential, and entrance potential were optimized to acquire maximum ion intensity using Analyst 1.6.3 software (SCIEX, United States).

To ensure the most intense precursor and fragment ion pair selection, for the MRM-based quantitation, we ranked individual analyte signal intensities for all MRM Q1/Q3 ion pairs of that specific analyte. To obtain metabolite ratio, we used normalized

peak area of endogenous metabolites within samples with normalized IS for every class of lipid molecule. Appropriate measures were taken to randomize sample queue and to assess sample carryover. Pooled quality control (pooled QC) samples were injected periodically to check for instrumental variation and National Institute of Standards (NIST) plasma samples were injected for lipidomic data analysis. Data normalized to QC variance. MultiQuant 3.0.3 (Sciex) software was used to obtain QC normalized data and imputed MRM data. To determine relative quantification values of analytes, the ratio of peak areas of sample transitions normalized to the peak area of the IS specific for every class was computed. Data post-processing statistical analysis including heatmap, volcano plot, and ANOVA was conducted with the software MetaboAnalyst (35). Product numbers for all reagents are listed in Supplemental Table 1.

Cell preparation and polychromatic flow cytometry

The left lobe of the liver was collected into RPMI-1640 culture medium (Gibco). Liver tissues were harvested, passed through a 70-µm cell strainer (Fisher Scientific), and leukocyte fractions were isolated *via* Percoll (Cytiva) density gradient. Samples were centrifuged at 1000g (25°C), without brake for 20 minutes, and the upper layer was carefully discarded. The leukocyte layer was washed and resuspended in 1x PBS (Gibco). Liver leukocytes were stained with the following antibodies (BioLegend, San Diego, CA) for flow cytometry analysis: Alexa Fluor700 conjugated CD45, Brilliant Violet 510 conjugated CD 4, Brilliant Violet 421 conjugated CD8, Brilliant Violet 605 conjugated NK1.1, PE-CD1d-tetramer (NIH Core Tetramer Facility), and Fluorescein isothiocyanate-conjugated CD3. Data were acquired using a BD FACSAria III Cytometer (BD Biosciences) at our Flow Cytometry & Cell Sorting Shared Resource. Any samples with viability of 60% or lower (as determined by staining with live dead marker Zombie NIR™, BioLegend) were excluded from all analyses. FlowJo v10 (BD, Franklin Lakes, NJ) was used for all subsequent data analyses. Product numbers for all reagents are listed in Supplemental Table 1.

Cytokine stimulation and intracellular cytokine staining

Intracellular staining for the detection of cytokines was carried out from liver leukocytes. Approximately 1x10^{6}cells/ml RPMI supplemented with 10% FBS, 1% Penicillin Streptomycin, and 0.5% Gentamycin were cultured for 20 hours at 37°C in a cell culture flask. Recombinant mouse cytokine concentrations used were 10 ng/ml IL-12, 50 ng/ml IL-18, and 50 ng/ml IL-15 (R&D Systems). Cells were stimulated for 4 hours with Cell Activation Cocktail containing phorbol-12-myristate-13-acetate (PMA, 50 ng/ml) and ionomycin, (BioLegend) in the presence of 5 µg/ml brefeldin A (BioLegend). Following stimulation, the cells were stained with the following antibodies to detect cytokines: Brilliant Violet 650™-conjugated anti-IFN-γ (BD Biosciences) and Brilliant Violet 605™-conjugated anti-TNF-α (BioLegend). Cells were fixed (IC Fixation buffer, Invitrogen) and permeabilized (Permeabilization buffer, Invitrogen) according to the manufacturer's instructions.

Real-time polymerase chain reaction

To assess the effect of IRI on mouse-specific cytokines and chemokines, we used the SYBR-green based RT² Profiler™ Polymerase Chain Reaction (PCR) Array Mouse Cytokines & Chemokines (PAMM-150ZC-12, Qiagen) to evaluate the gene expression of 84 different cytokines and chemokines. For this experiment, mice liver specimens collected 24 hours-post sham and IRI surgeries and stored in the Allprotect Tissue Reagent (Qiagen) were used for the total RNA extraction. All tissues were lysed using 1.0 mm Zirconia/Silica beads (BioSpec Products) in FastPrep 24 Tissue Homogenizer (MP Biomedical). We extracted total mouse liver RNA as instructed in the RNeasy Mini kit with RNase-free DNase set (Qiagen). RNA quality and quantity were assessed using 2100 Agilent Bioanalyzer, and RNA samples with RNA integrity number (RIN) ≥ 7 were used for the PCR arrays.

For each RT² Profiler™ PCR Array, 1.25 µg of total RNA was pooled from at least three separate mice livers in an equal proportion. We performed standard procedures to eliminate mouse genomic DNA, synthesize first-strand and set up RT^2 profiler PCR array for cytokines and chemokines. Raw Ct values from the array were analyzed using the GeneGlobe web tool (https://geneglobe.qiagen.com/us/) to check the quality of the PCR arrays, normalize threshold cycle (Ct) values using Beta-2-Microglobulin (B2m) as a housekeeping gene and estimate fold regulation with ND (Sham) as a control group. Unsupervised hierarchical clustering for the $2^{-\Delta\Delta Ct}$ was performed using ClustVis (36) to identify gene clusters specific to sham and IRI groups under two different diet regimens. Venn diagrams for genes with fold upregulation ≥ 2 were created using Venny (37) to identify common genes among all the IRI groups and exclusively diet-specific gene signatures. Product numbers for all reagents are listed in Supplemental Table 1.

Statistical analysis

All data are expressed as mean ± standard error of the mean (SEM). Comparison between groups was performed by a Mann-Whitney U test unless otherwise mentioned in the figure legend. Statistical significance was established at $p<0.05$ with all p-values

being two-sided and stratified in the following order: "*" 0.05 to 0.01, "**"0.01 to 0.001, "***" 0.001 to 0.0001, and "****" <0.0001. Prism Software (GraphPad, Inc. San Diego) was used for all statistical analyses.

Results

NAC supplementation clinically reduced hepatic steatosis and facilitated Eovist® uptake during hepatic MRI

To establish the efficacy of our HFD murine model, we first examined trends in body weight and food consumption within our model. HFD mice gained significantly more weight than ND mice and this effect was significantly reduced with oral NAC supplementation (Supplemental Figure 1A). There were no statistically significant differences in food consumption between HFD and HFD + NAC, although HFD + NAC mice had a trend of higher food consumption. The average NAC water consumption was 139 mL/week/cage of five mice in the HFD + NAC mice and there was no significant difference as compared to ND + NAC water consumption. We further assessed blood glucose measurements; HFD mice had significantly higher blood glucose measurements starting at twelve weeks of age compared to HFD + NAC mice ($p<0.05$) (Supplemental Figure 1B).

We next assessed the adiposity of the liver, the abdomen, and the nuchal areas of mice from each group, *in vivo*, using 3D-RARE MRI. HFD mice presented with a significant accumulation of hepatic steatosis and visceral abdominal fat and accumulation of white adipose tissue (WAT) in the nuchal region. NAC treatment prevented the development of hepatic steatosis and supported the transformation of WAT into brown adipose tissue (BAT) (Supplemental Figure 2). We then correlated these findings with H&E-stained liver sections evaluated by an expert pathologist. Consistently, hepatic steatosis varied between both ND and ND + NAC when compared to HFD mice, with HFD mice demonstrating 80% hepatic steatosis on average ($p<0.0001$). This difference was significantly reduced in mice on NAC supplementation, which resulted in a 50% reduction in hepatic steatosis (Supplemental Figure 3).

Given the profound reduction of hepatic steatosis in the HFD + NAC mice, we next assessed the baseline liver function of our HFD murine model by performing DCE-MRI with Eovist®. HFD fed mice showed a significant decrease in relative liver contrast enhancement as compared to ND mice (Figure 1). These data, expressed as AUC analyses, correlated strongly with other imaging parameters such as *in vivo* and *ex vivo* liver fat content. Corresponding contrast enhancement slopes were calculated during the first 20 minutes post-injection, which represents the transitional phase before the contrast levels begin to plateau during the hepatobiliary phase. These data were strongly correlated with the AUC and overall hepatic relative liver enhancement values, where the rates of T1 enhancement in the HFD group were slower and failed to achieve the signal intensity levels observed in the ND mice. However, the HFD + NAC mice exhibited contrast uptake comparable to that observed in ND mice. It is important to note, that the differences in mean intensity between HFD and all the other groups (ND, ND + NAC and, HFD + NAC) were significant at 18- and 30-minutes post-injection. Collectively, these data indicate the deficits in Eovist uptake in the HFD mice are restored in HFD + NAC mice to a level consistent with ND mice.

Hepatic ischemia-reperfusion injury in a HFD model is attenuated following oral NAC supplementation

Partial warm IRI was induced in mice from all groups. Both ND and HFD groups experienced a significant elevation in serum ALT levels as compared to sham-operated mice ($p<0.0001$ and $p=0.0009$, respectively). However, HFD mice experienced a significantly sharper rise in serum ALT following IRI than did ND mice (79 u/L *vs*. 408 u/L, $p<0.0001$), suggesting a higher degree of injury. We then evaluated the role of NAC supplementation in the prevention of IRI and demonstrated a significant reduction in serum ALT following IRI in HFD + NAC mice as compared to HFD mice alone (201.5 u/L *vs*. 408 u/L, $p<0.0001$), and in fact, there was no significant difference between ND IRI and HFD + NAC IRI groups, suggesting a normalization of injury (Figure 2A).

Representative mice from each group were subjected to T2-weighted MRI prior to the terminal procedure to assess the magnitude, distribution, and bilaterality of hepatic edema and associated inflammation, and pre-and post-IRI T2 maps were generated. Specifically, baseline T2 mapping of the liver was performed on ND and HFD, with and without NAC. Twenty-four hours after partial hepatic IRI surgery, the mice again underwent T2 mapping. The T2 maps were generated, and the T2 values quantified. Pre-IRI T2 values were similar between ND mice and ND + NAC mice, while the T2 values trended towards a slight increase in the livers of mice on HFD (Figure 2B). Ischemia-reperfusion injury exposure did not affect the T2 values of either the ND or ND + NAC livers. Conversely, the hepatic T2 values of mice on HFD were noticeably elevated after IRI, while the T2 values of HFD + NAC were comparable to those observed with ND, both before and after IRI. It is important to note that baseline and post-IRI T2 values were not significantly different between the right and left liver lobes in any group. Overall, the T2 maps enabled the quantification and visualization of

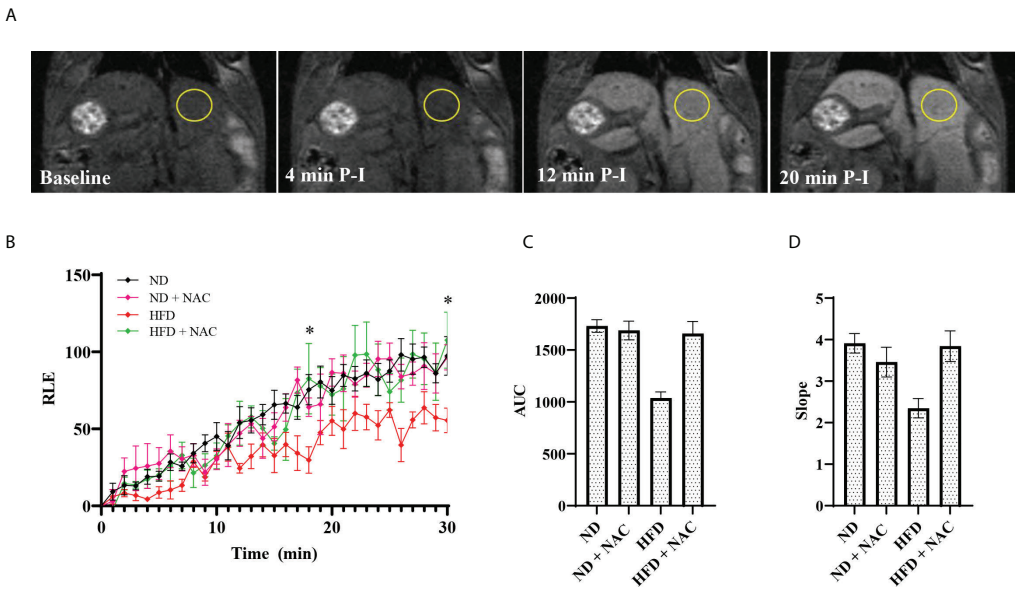

FIGURE 1
Effects of HFD on liver function as assessed by DCE-MRI with the contrast agent Gadoxetate Disodium (Eovist® Bayer). **(A)** Representative images of 26-30 week old male mice undergoing DCE-MRI, showing T1-weighted images performed before Eovist® injection and at 4, 12 and 20 minutes post-injection (P-I). The yellow circle denotes a typical region of interest used to measure mean intensity. **(B)** Time course of relative liver enhanced T1 signal intensities after Eovist® injection, comparing mice on ND (n=4), ND + NAC (n=5), HFD (n=5), and HFD + NAC (n=5). The differences in mean intensity between HFD and all the other groups (ND, ND + NAC and, HFD + NAC) were significant at 18- and 30-minutes post-injection. **(C)** Area under the curve (AUC) calculated from the data in **(B)**. **(D)** The slope of T1 signal intensity increase for each group shown, corresponding to the rates of change within the first 20 min after Eovist® injection. Statistical significance was established using a one-way ANOVA multiple comparisons test. "*" 0.05 to 0.01.

hepatic edema and inflammation resulting from IRI in HFD mice, which demonstrated an increase in hepatic T2 relaxation times in HFD as compared to ND mice. NAC ameliorated the impact of IRI in HFD mice, making T2 values comparable to those seen in the ND + NAC mice.

We further evaluated the liver tissue using immunohistochemistry to evaluate for neutrophil (Gr-1+) and macrophage (CD68+) influx in mice treated with NAC and underwent IRI. We have previously demonstrated that there is a significant increase in Gr-1 and CD68 positive cells in HFD IRI mice compared to ND IRI mice (38). We further established that HFD + NAC IRI mice have an average of a 45% reduction in Gr-1+ cell counts ($p<0.0001$) and an average of a 35% reduction in CD68 cells following IRI ($p<0.0001$) (data not shown). Representative immunohistochemical stained images are shown in Supplemental Figure 3C.

Phasor-FLIM imaging reveals marked differences in glycolysis, successfully corresponding to the degree of hepatic IRI

Given recent advances in Phasor FLIM and SHG imaging of steatotic human and mouse liver tissue (39), we sought to employ this methodology to evaluate the differences in liver tissue following IRI as a novel approach to evaluate liver injury. Samples were examined for glycolysis and lipid oxidation based on the Phasor-FLIM signatures. A higher ratio of free to protein-bound NADH is indicative of increased glycolysis (25, 40–43) and a larger amount of long lifetime species (LLS) is indicative of higher lipid peroxidation (33, 34). The FLIM images (Figure 3A) were colored according to the three cursor positions for bound NADH (green), free NADH (blue), and the LLS (red) selected using the phasor map (Figure 3B).

We first evaluated the models for increased glycolysis, as demonstrated by free NADH (blue). Visually, there is increasing blue color present in all groups following IRI, while the ND, ND + NAC and HFD + NAC groups show more green color, thus more bound NADH. These data, when converted to the concentration ratio of free/bound NADH (Figure 3C), establish that the ratio increases in HFD mice compared to ND mice and this is further exacerbated following IRI, again demonstrating a greater ratio of free/bound NADH ratio in HFD IRI mice compared to ND IRI mice. This increasing ratio correlates to higher glycolytic stress, thus a greater degree of IRI. Importantly, glycolytic stress is significantly reduced in the HFD + NAC IRI mice compared to the HFD IRI mice, suggestive of a protective effect of NAC in the HFD group.

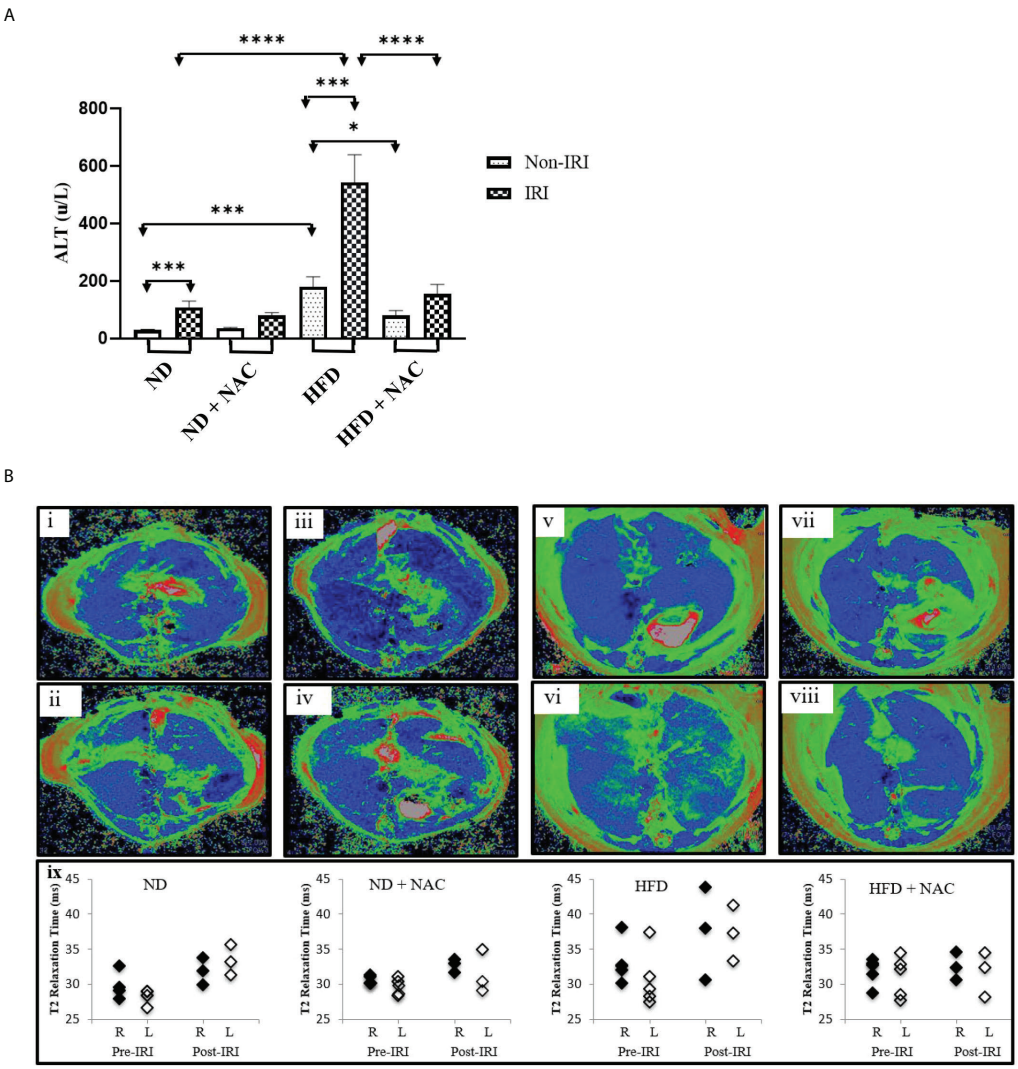

FIGURE 2
HFD Mice are prone to more severe IRI, which is significantly improved with NAC supplementation. **(A)** Serum ALT level following 24 hours of reperfusion. Number of mice per group is as follows: ND=11, ND (IRI)=13, ND + NAC= 5, ND + NAC (IRI)=10, HFD=5, HFD (IRI)=15, HFD + NAC, HFD + NAC (IRI)=8. **(B)** Representative images of baseline T2 mapping of mice on i) ND, iii), ND + NAC, v) HFD and vii) HFD + NAC. Representative images of T2 mapping twenty-four hours after IRI surgery of ii) ND, iv) ND + NAC, vi) HFD and viii) HFD + NAC. Blue represents liver parenchyma while green denotes edema. Graphical representation (xi) of the average of the T2 relaxation times of ROIs placed on the right and left areas of the corresponding livers (n=3-5 per group). "*" 0.05 to 0.01, "***" 0.001 to 0.0001, and "****" <0.0001.

LLS was then evaluated for differences in lipid oxidation between the samples. There was a noticeable increase in LLS in the HFD, as seen by the increasing red color of images, as compared to the ND mice. We then quantified this fractional intensity of LLS (Figure 3D), as described in the supplemental methods. HFD and HFD IRI mice both demonstrate statistically significant higher quantifications of LLS compared to ND and ND IRI mice, respectively.

LLS imaging demonstrates a reduction of lipid droplet size in HFD + NAC mice, which corresponds to a significant reduction of triacylglycerols

Upon establishing that a higher degree of IRI is present on a background of hepatic steatosis, as demonstrated by biochemical, MRI, and glycolytic analysis, we next sought to

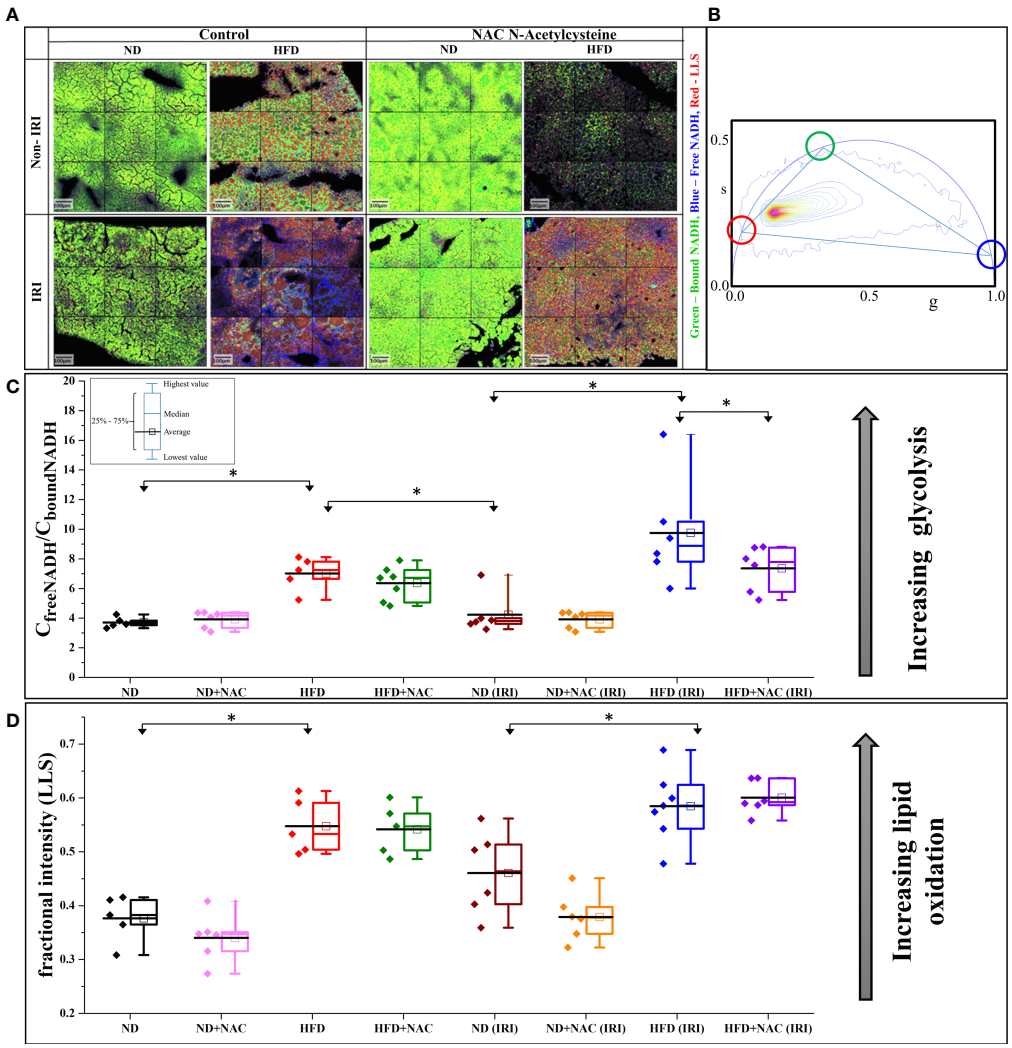

FIGURE 3
IRI results in a higher degree of glycolytic stress in HFD mice. **(A)** Color mapped Phasor FLIM images of the ND and HFD liver samples in the absence (left) and presence (right) of NAC supplementation. The top row shows the sham samples, and the bottom row shows the IRI samples. More green, blue and red color represents more protein-bound NADH, free NADH and long lifetime species (LLS), respectively. **(B)** Phasor plot of autofluorescence FLIM in liver samples – the three colored circles represent the lifetime position of the three components: free and bound NADH, and LLS. **(C)** The concentration ratio of free to bound NADH was calculated from each mouse. The higher value represents more glycolytic stress. There is a higher level of glycolytic stress in HFD and HFD (IRI) samples. This is reduced in the HFD + NAC (IRI) samples, but not the HFD + NAC samples, respective to their HFD counterparts. **(D)** The fractional intensity of LLS calculated using three-component calculations to show the increasing LLS in high fat liver and how that increases with IRI (n=5-7 mice per group for both analyses). "*" 0.05 to 0.01.

quantify hepatic steatosis more accurately within our samples. Phasor FLIM imaging allows us to quantifiably calculate steatosis based on the accumulation of the LLS (27). Selection of the phasor signature of LLS (long lifetime species, red circle in Figure 4A), enables the identification of the lipid droplets in autofluorescence FLIM images, where they are mapped according to the color of the selection (red here). Steatosis is then quantified by calculating the size of the droplets occupying the image. Our data show that droplets are much smaller or are nonexistent in ND diet mice and are much larger in HFD diet mice, both in the IRI and sham samples, which correlates to pathological evaluation of H&E staining. Note that the Y axis is in log scale and shows that exceptionally large droplets are seen in HFD livers in both sham and IRI mice as compared to ND mice. Importantly, while the average size of the lipid droplets increases in both HFD and HFD IRI mice, this is visibly reduced in HFD + NAC and HFD + NAC IRI mice (Figures 4B–D). It is further notable that, while not statistically significant, there is a visible and quantifiable increase in lipid droplet size in ND IRI and HFD IRI mice when compared to the respective ND and

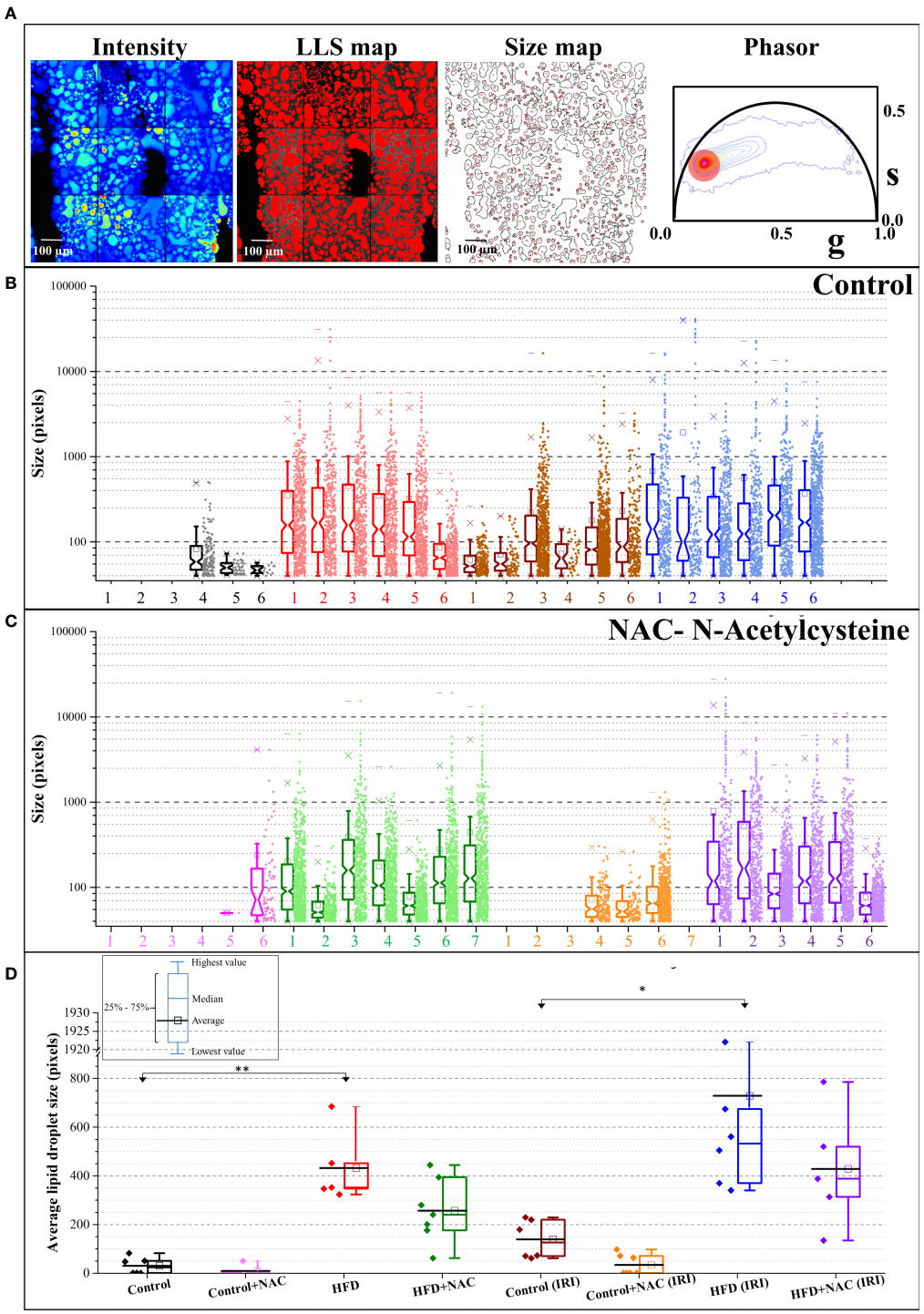

FIGURE 4
NAC treatment significantly reduced hepatic steatosis in HFD mice. **(A)** The fluorescence intensity image, the LLS mapped image, the calculated size distribution maps, and the corresponding phasor plot. The red cursor was used to select the LLS lifetime signature originating from the intensity image and the LLS image was colored according to that phasor signature. The size map was created to show the distribution of the droplets. **(B, C)** The size map was created to show the distribution of the droplets. **(B, C)** The size distribution plots for Control **(B)** and NAC **(C)** treatment. The Y axis is shown in logscale to exemplify the increasing size as a function of diet and IRI. The distribution shows HFD and IRI induce the large lipid droplets and (especially above 10000 pixels) are lower in number in HFD + NAC, groups. (n=5-7 mice per group). **(D)** The average size distribution of lipid droplets from the livers of the animals in different feeding regimen. "*" 0.05 to 0.01, "**"0.01 to 0.001.

HFD counterparts. It is important to note that upon evaluation of the individual distributions of lipid droplet within each sample (Supplemental Figure 4), it demonstrated that a large degree of variation in lipid droplet sizes is seen in each sample.

Prepared snap-frozen liver tissue from sham mice was subsequently subjected to metabolomic profiling of 21 classes of lipid metabolites. We identified significant changes in lipid composition between the tissues, as visible in the heat map (Figure 5A). Of the 21 classes analyzed, triacylglycerols (TAG) were significantly upregulated in HFD mice as compared to normal diet (0.222 normalized intensity *vs.* 6.783 normalized intensity, $p<0.0001$). This was significantly decreased in the HFD + NAC mice, as demonstrated in the volcano plots showing differences in upregulated lipid profile in HFD *vs.* ND and HFD + NAC *vs.* HFD mice (Figure 5B). Interestingly, the HFD + NAC mice had a statistically reduced composition of TAG, as compared to HFD mice (6.281 normalized intensity *vs.* 2.681 normalized intensity, $p<0.0001$; Figure 5C). The reduction of TAG species demonstrated with NAC supplementation was largely global, affecting 149 of the 277 species evaluated. There were no statistically significant reductions in the HFD + NAC mice for the remaining 20 classes of lipids.

IRI results in specific genetic upregulation in HFD mice

In order to identify specific transcriptomic changes that occur in the liver following IRI, we performed array-based PCR transcriptional profiling using the RT^2 profiler PCR array for 84 distinct Chemokine and Cytokines (Qiagen, Germantown, MD). Utilizing an unsupervised hierarchical clustering analysis, we demonstrated a distinct difference in gene expression patterns between HFD mice and those mice that underwent IRI (Figure 6A). We then identified both shared and discrete genes with a minimum of two-fold upregulation amongst the mouse groups that underwent IRI (Figure 6B).

We identified 45 genes of interest that were upregulated within the collective specimens. Among these genes, seven were uniformly upregulated in both ND IRI and HFD IRI groups, including *CSF3, CXCL1, CCL17, CCL19, TNFSF13b* (TNF Superfamily Member 13b), *IL-6* and *IL17a*. Uniquely, HFD IRI mice exhibited an exclusive upregulation of five genes: *TGFβ-2, Pf4* (Platelet Factor 4), *IL-1β, IL-10*, and *IFN-γ*. In comparison, HFD + NAC mice that underwent IRI exhibited significantly lower expression levels of the genes that were exclusively upregulated in HFD IRI and shared between ND IRI and HFD IRI mice.

IFN-γ producing CD3+/NK1.1+ and CD3+/CD1d+ cells drastically contribute to hepatic IRI and are mitigated with NAC treatment

Given the significant upregulation of IFN-γ and its related genes shown by RT-PCR array analysis and the variations in lipidomic analysis, specifically TAGs, we next aimed to specifically evaluate the role of IFN-γ producing NKT cells in hepatic IRI by polychromatic flow cytometry. We first evaluated this using NKT1 cell surrogate markers defined as CD45+/CD3+/NK1.1+ cells. Utilizing this strategy, we first evaluated the sham mice from each group. ND mice harbored NKT cells at an average frequency of 13.65%. This was significantly higher than the HFD mice (6.97%, p=0.004). Interestingly, while there was no significant difference between the HFD and HFD + NAC groups, the ND + NAC mice were shown to harbor a larger frequency of CD45+/CD3+/NK1.1+ cells as compared to ND mice (27.5%, p=0.017).

We then elicited hepatic IRI and evaluated for CD45+/CD3+/NK1.1+ cell changes. ND IRI mice had a significant rise in the percentage of CD45+/CD3+/NK1.1+ cells as compared to the ND sham mice (p=0.0095). There were no significant differences in NKT cells frequencies amongst ND + NAC IRI mice or the ND + NAC sham mice, despite the increased frequencies in ND + NAC mice, as previously demonstrated. Interestingly, following reperfusion injury, HFD IRI mice underwent a drastic rise in CD45+/CD3+/NK1.1+ cells as compared to HFD sham mice (28.9%, p=0.0079), which was statistically similar to that seen in the ND IRI group (Figures 7A, C). This effect was ameliorated following NAC treatment in HFD mice. The HFD + NAC IRI mice showed no significant differences in NKT cell populations as compared to the HFD SHAM counterparts; however, the frequency of NKT cells was drastically reduced when compared to both HFD IRI and ND IRI groups.

We next employed *ex vivo* cell stimulation with PMA from samples obtained from all IRI groups to identify the level of IFN-γ and TNF-α produced from CD45+CD3+ NK1.1+NKT cells, as demonstrated in Supplemental Figure 5. While the level of IFN-γ produced was similar between ND IRI and ND + NAC IRI mice, there was a significantly greater frequency of IFN-γ produced by HFD IRI mice (Figures 7B, D), corresponding to the previously demonstrated cell populations (p=0.0177). This rise in IFN-γ production was ameliorated in the HFD + NAC IRI mice as compared to the HFD IRI mice (p=0.0001). The levels of TNF-α were significantly higher in the ND IRI than the HFD IRI mice, and there was no significant difference between HFD IRI and HFD + NAC IRI mice (Supplemental Figure 6).

Finally, we validated our findings by evaluating the effect of NAC supplementation on the IFN-γ production from CD1d

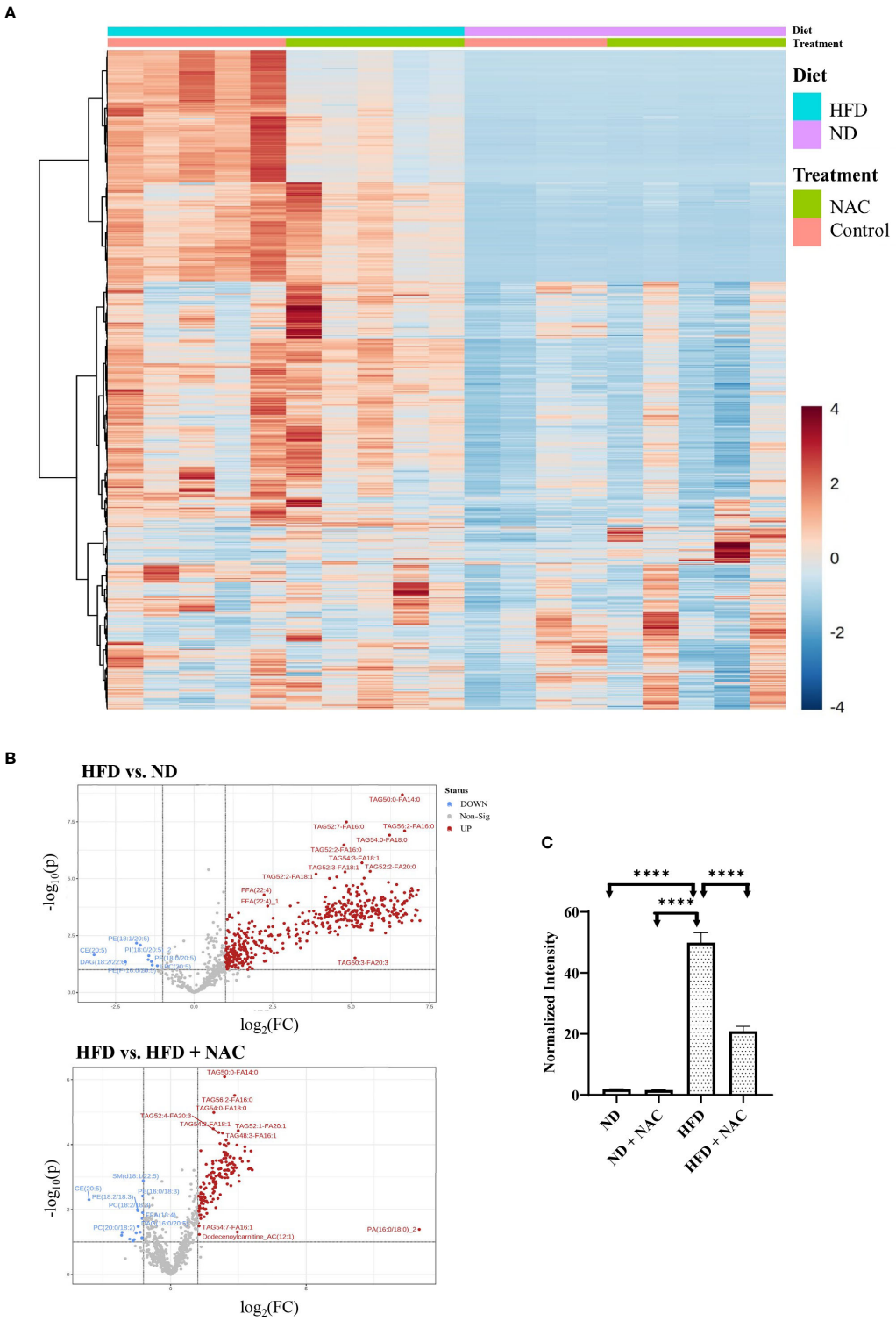

FIGURE 5
NAC treatment in HFD mice significantly altered the lipid profile within the liver. **(A)** Heat map demonstrating the alterations in lipid composition with the respective tissue. **(B)** Volcano plots demonstrating the differences in upregulated lipid species in HFD *vs.* ND and HFD *vs.* HFD + NAC mice, ultimately revealing changes TAG composition within these tissues. **(C)** Histogram representing quantitative differences in TAG composition between the treatment groups. "****" <0.0001.

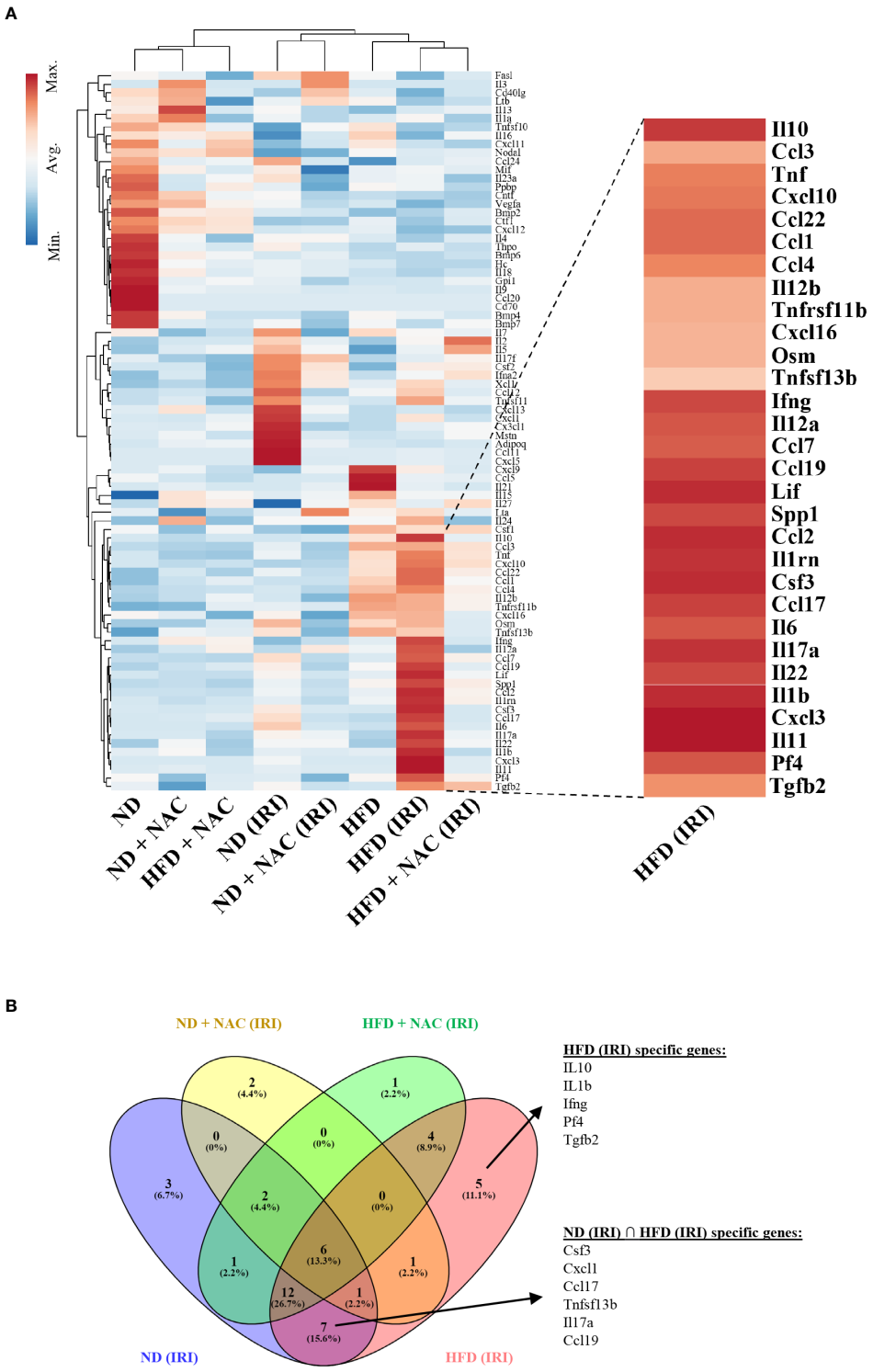

FIGURE 6
IRI induced specific genetic upregulation in HFD mice. RT^2 profiler PCR array for cytokines and chemokines was utilized to examine differences in genetic regulation among treatment groups. Each group represents a single pooled sample from at least three separate liver-tissue specimens. **(A)** Heat map of cytokine and chemokine PCR analysis. **(B)** Venn Diagram demonstrating genes that are upregulated in HFD (IRI) and those shared amongst ND (IRI) and HFD (IRI).

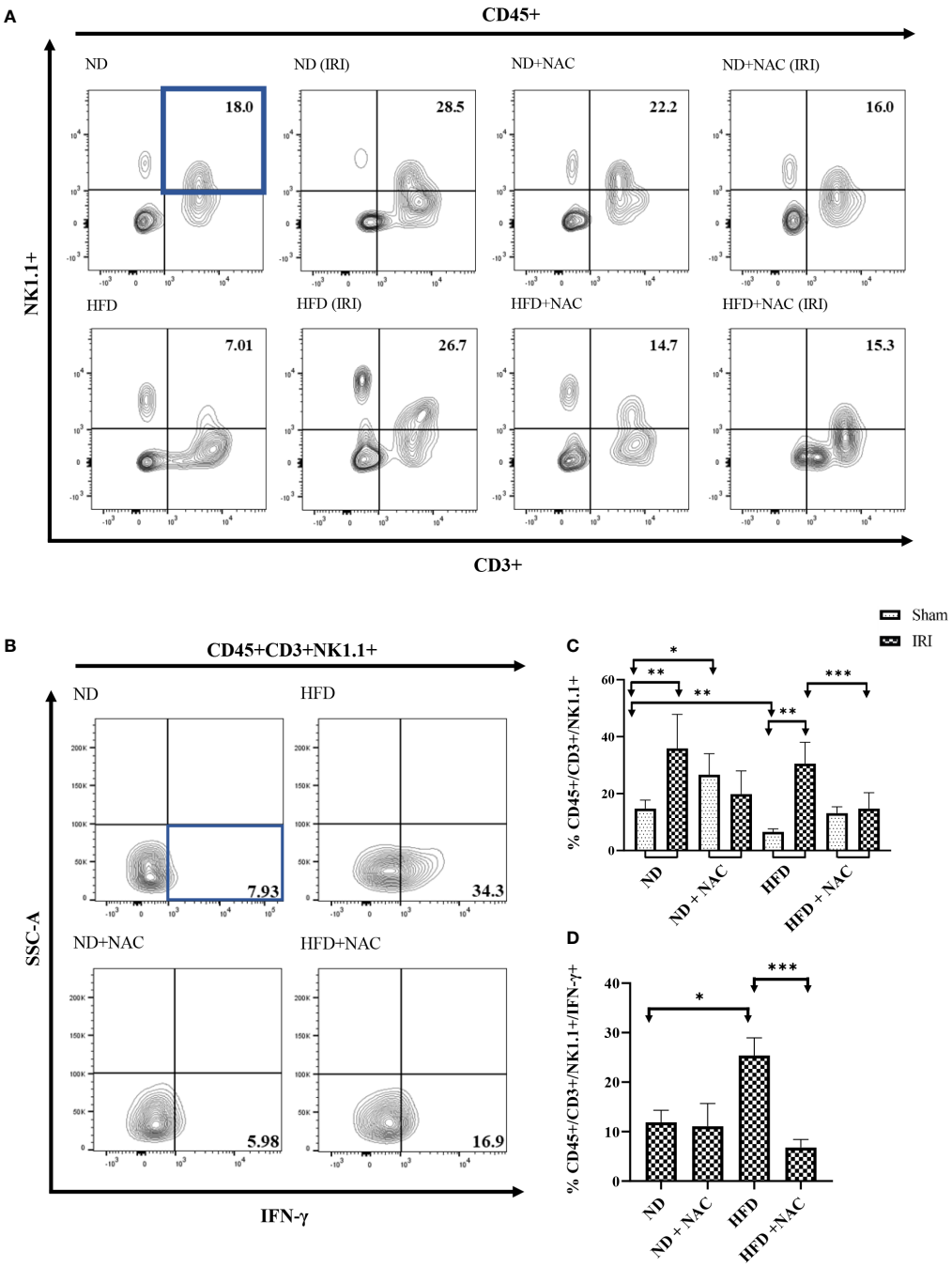

FIGURE 7
IFN-γ producing Hepatic CD3+/NK1.1+ cells are contributors following IRI and successfully ameliorated with NAC supplementation. **(A)** Representative contour plots of the percentage of CD45+/CD3+/NK1.1+ NKT1 cells within Hepatic Mononuclear cells. Number of mice per group is as follows: ND=6, ND (IRI)=5, ND + NAC= 5, ND + NAC (IRI)=11, HFD=5, HFD (IRI)=5, HFD + NAC=5, HFD + NAC (IRI)=10. **(B)** Representative contour plots of the percentage of IFN-γ producing CD45+/CD3+/NK1.1+ NKT cells after IRI. Number of mice per group is as follows: ND (IRI)=5, ND + NAC (IRI)=5, HFD (IRI)=7, HFD + NAC (IRI)=10. **(C)** Histogram demonstrating the percentage of NKT1 cells illustrated in **(A)**. **(D)** Histogram demonstrating the percentage of NKT1 cells illustrated in **(B)**. "*" 0.05 to 0.01, "**"0.01 to 0.001, "***" 0.001 to 0.0001.

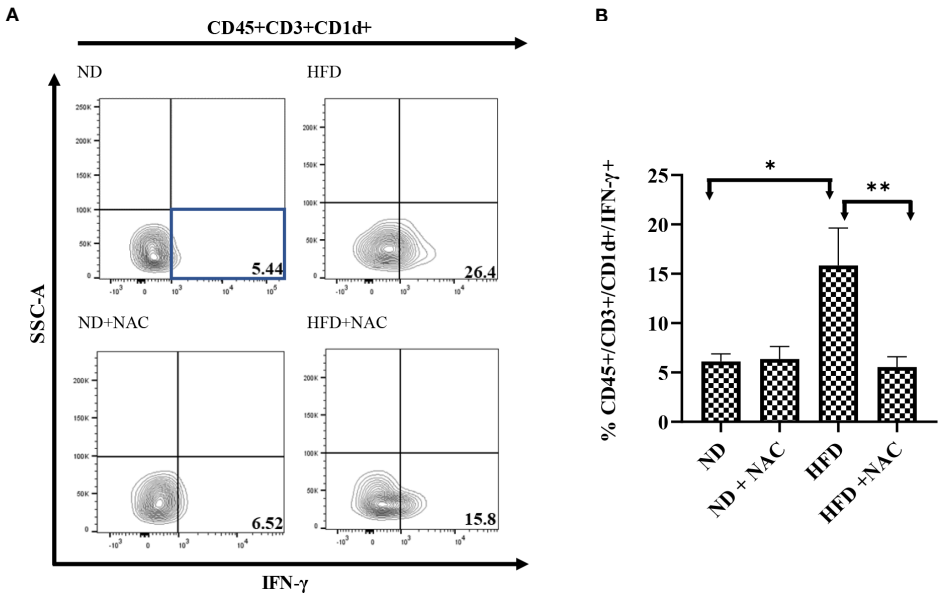

FIGURE 8
IFN-γ producing hepatic CD3+/CD1d+ cells are contributors following IRI and successfully ameliorated with NAC supplementation. **(A)** Representative contour plots of the percentage of IFN-γ producing CD45+/CD3+/CD1d+ NKT cells after IRI. Number of mice per group is as follows: ND (IRI)=5, ND + NAC (IRI)=5, HFD (IRI)=7, HFD + NAC (IRI)=10. **(B)** Histogram demonstrating the percentage of IFN-γ producing CD45+/CD3+/CD1d+ NKT cells illustrated in **(A)**. "*" 0.05 to 0.01, "**"0.01 to 0.001.

bound NKT cells (CD45+/CD3+/CD1d+ cells). HFD IRI mice had a significantly higher frequency of IFN-γ from CD45+/CD3+/CD1d+ cells as compared to ND IRI mice (p=0.017). This effect was significantly reduced in the HFD + NAC IRI mice (p=0.0012) (Figures 8A, B). There were no significant differences in TNF-α production from these cells in the HFD IRI and HFD + NAC IRI mice (Supplemental Figure 6).

Discussion

Nonalcoholic Fatty Liver Disease (NAFLD) remains a significant problem in liver transplantation. Not only can NAFLD progress to cirrhosis/liver failure (44) and contribute to the development of hepatocellular carcinoma (both indications for liver transplantation), but it also affects the potential donor population. In this regard, steatotic allografts experience a greater degree of IRI upon reperfusion, which increases the risk of poor clinical outcomes in decompensated recipients. A key component towards increasing the potential donor population involves effectively preventing, diagnosing, and treating IRI. As such, reliable animal models for the study of hepatic steatosis and the innate immune system response to IRI are paramount. In this work, we demonstrated the effectiveness of a HFD murine model and primary treatment group to highlight novel and noninvasive methods of investigating liver injury, as well as identify a key immune regulatory strategy in the prevention of IRI.

The efficacy of a diet induced-obesity murine model is well established (1, 45). However, potential therapeutics are limited. Intravenous (IV) NAC has previously been successful in the treatment of IRI, both clinically and experimentally, with a well-established role in the reduction of reactive oxygen species (2, 46–48). Recently, oral NAC supplementation was investigated for its use in the treatment of metabolic disorders and was shown to decrease hepatic steatosis *via* a PPAR-γ dependent mechanism and stimulation of thermogenic gene expression (45). Our work has expanded upon these findings, as we have demonstrated that oral NAC treatment decreased hepatic steatosis and increased BAT as detected by T1 weighted MRI. In this sense, BAT is characteristic of high metabolism and thermogenic capacity (49), which supports that NAC alters thermogenic gene expression. We were further able to correlate the decreased hepatic steatosis with improved liver functional capacity using Eovist® DCE MRI, which has emerged as a useful hepatobiliary contrast agent that clinically, and non-invasively, allows for stratification of steatotic liver damage (50). We demonstrated a stark difference in contrast uptake in HFD mice in comparison to the ND mice, which was normalized with NAC supplementation, especially at 18 and 30 minutes post-injection of Eovist®. While the mechanisms by which NAC improves Eovist® uptake in the HFD mice are presently

unknown, previous work in cirrhotic rats suggests alterations in the expression of associated membrane proteins may be a key factor (51), although alternations in hepatic perfusion cannot be ruled out and additional studies are warranted to establish these relationships. Overall, these findings collectively established this HFD model with NAC treatment group as an effective method to study IRI mitigation.

Despite the known effect of IV NAC in IRI, to our knowledge, this is the first study to address the effectiveness of oral NAC supplementation in the prevention of IRI. Utilizing our clinically relevant model, we demonstrated improvement of IRI in HFD mice on NAC supplementation as compared to HFD only using serum ALT and T2 MRI mapping. Interestingly, T2 relaxation times, which correlate with hepatic edema and inflammation (52), show a similar effect in all lobes of the liver. This demonstrates the scope of full liver sequelae following segmental injury in HFD mice, which is significantly reduced in HFD + NAC mice. Previous work has demonstrated the vasodilatory effects of NAC in models *via* Nitric Oxide dependent (46, 47) and Vascular Endothelial Growth Factor (VEGF)/VEGFR2 (47, 48) dependent mechanism, which may offer insight into the reduced edema visualized in our samples. However, this does not provide insight into the key roles of innate immune system cytokine generation and metabolic changes at a cellular level which occur following IRI.

While it is known that NAFLD is associated with significant modulation of metabolic pathways involved in glycolysis (53, 54) and lipid oxidation (55), the alterations in these pathways following IRI are the subject of ongoing research. To elicit some insight into this area, we employed Phasor-FLIM and SHG imaging as a novel approach in the evaluation of hepatic IRI, where we demonstrated increased glycolytic stress and lipid oxidation within our HFD murine model that was worsened following IRI. This is consistent with known requirements of NADPH and FAD metabolism (43). We further determined that NAC supplementation decreased glycolytic stress in HFD mice following IRI, correlating to a less severe degree of injury and inflammation that was corroborated by our previous findings in serum ALT and T2 mapping. Interestingly, we did not appreciate the same changes in lipid oxidation. Additionally, utilizing LLS imaging of lipid droplets, we further appreciate a visual reduction in lipid droplet size in our HFD + NAC mice when compared to HFD mice. However, when an average value was calculated for total image, this resulted in loss of dimensional information and the inherent, visually depicted heterogeneity (Supplemental Figure 4). The actual distribution of the fractional intensity of LLS (red) and free NADH (blue) demonstrate that embedded spatial information is a key component phasor-FLIM auto fluorescent image analysis. This is demonstrated in the composite image of LLS, free and bound NADH and the individual species distribution (Supplemental Figures 4C-F), which demonstrates how different parts of the image have a differential amount of each species. The cumulative graphs from 3 samples show that along with a shift of LLS in HFD IRI samples, there may also be broadening of these distributions. In case of broadening, e.g. HFD + NAC *vs.* ND – the central position of the distribution may not shift appreciably, however more metabolic heterogeneity is seen in the HFD + NAC samples than in the ND diet samples, which is apparent. Further, while previous work had shown a downregulation of genes involved in lipid oxidation in obesity induced mice on NAC supplementation (45), this was not apparent on LLS imaging for lipid oxidation. Importantly, LLS is a complex and incompletely understood representation of lipid oxidation byproducts that depends greatly on the different pathways of oxidation. Thus, absence of changes in LLS does not confidently correlate to a lack of lipid oxidation throughout the tissue (56), which is the subject of ongoing research.

To further classify metabolic changes occurring with NAC supplementation, we performed a quantitative lipid profile analysis of whole liver tissue. To our knowledge, this is first time a full lipidomic profile has been generated from liver tissue of HFD mice on NAC supplementation. This demonstrated significant downregulation of TAGs species when compared to mice on HFD alone. TAG synthesis is known to be regulated *via* a PPAR-γ dependent pathway (57), and previous studies have demonstrated that PPAR-γ activity is downregulated as a result of NAC supplementation (45, 58). Recently, PPAR-γ has also been identified as a key mediator in the synthesis of CD1d (59), which serves a crucial function in priming of NKT cells. This expands on work that previously demonstrated NKT cell activation occurs secondary to lipid excess (7, 14, 60), which has been linked to CD1d expression on adipocytes. It has further been demonstrated that NKT cell activation is secondarily decreased in *ApoE* $^{-/-}$ mice (61). Further work by Downs et al. demonstrated that NAC supplementation can abolish Vα14iNKT cells and IFN-γ signaling in fulminant liver failure (62). Taken together, our findings further suggest that NAC treatment could prevent NKT cell activation by preventing lipid excess and downregulating CD1d.

Our subsequent experiments were formulated around determination of NKT cell activity. RT-PCR array for cytokine and chemokine expression was performed from liver tissue in the maximally affected left lobe. This ultimately eluded to significant upregulation in HFD IRI mice that was not established elsewhere, specifically IFN-γ and its related genes, including IL-12. Upon further analysis, we appreciated significantly upregulated in genes that have been linked to the NF-κB pathway—CXCL1 (63, 64) and CXCL10 (63, 65). This is in line with previous reports that the NAC treatment results in a downregulation of NF-κB (45, 66), and also furthered our suspicion that NKT cells were in fact mediators in the model, as IFN-γ (67) and, more specifically, TCR-β both result in direct activation of the NF-κB pathway (68, 69). Further, IFN-γ also results in NF-κB activation by means of JAK/STAT activation pathways. Finally, we elicited a complete downregulation of

these associated genes in HFD + NAC IRI mice. This ultimately alludes to an injurious effect of IFN-γ that can be, at least partially, alleviated by NAC supplementation. However, we cannot fully exclude other mechanisms, and additional studies will be needed to confirm our findings.

While our flow cytometry findings suggest that NKT cell activation and cytokine production are affected by NAC, additional studies using a CD1d deficient mouse model and adoptive transfer experiments of IFN-gamma-deficient NKT cells into *Ja18*$^{-/-}$ mice are needed within our HFD NAC model for definitive confirmation. Moreover, we observed a significant upregulation of IL-17 within our HFD IRI mice that was subsequently ameliorated by NAC. We have previously demonstrated that IL-17 produced by unconventional RORγt T-cells contribute to hepatic ischemia reperfusion injury (70). More recently, IL-17 producing NKT cells have been described and implicated in inflammatory diseases (71) and may also play a critical role in IRI. Further comparative studies will be needed to identify the role of NAC in IL-17 reduction and the degree of injury prevention, as compared to IFN-γ.

Overall, our work utilized novel methods of hepatic injury identification to demonstrate the effectiveness of oral NAC supplementation in preventing IRI. We further identified potential downstream pathways and targets for future research into the prevention of hepatic IRI. Further work will be required to definitively establish mechanism behind the protective effect of oral NAC supplementation.

Conclusion

Oral N-acetylcysteine supplementation can ameliorate IRI in a HFD mouse model. IFN-γ pathways and NKT cells are largely implicated in this observed effect.

Data availability statement

The original contributions presented in the study are publicly available. This data can be found in NCBI's Gene Expression Omnibus; GEO accession number: GSE209733. Further inquiries can be directed to the corresponding authors.

Ethics statement

The animal study was reviewed and approved by Georgetown University Institutional Animal Care and Use Committee.

Author contributions

JL, JK, and SR equally contributed experiment completion, data analysis, authorship and critical review of this manuscript. AK, JL, JK, SR, OR, KL, DP, YC, KO, BF, SN, BH, YL, DK, WC, KK, HL, and BK acquired, analyzed and/or critically reviewed data. AK, SCR, KK, WC, CA, TF, SR, and ML secured funding, contributed to study design and facilitated critical oversight of the project. All authors contributed to the article and approved the submitted version.

Funding

Funding was provided by NIH R21AI130800 (AK, SCR), with contributions from NIH S10 OD025153 (CA), NIH-P30 CA051008-22 (CA), NIH/NCI P30-CA051008 (Microscopy & Imaging Shared Resource), NIH R01 DK116567 and R01DK127830 (SR and ML), and private funding from the Children's Rare Disease Organization Inc. (AK, JK, KK).

Acknowledgments

Gadoxetate Disodium (Eovist®/Primovist®) was kindly provided by BayerHealthCare *AG, D-51368 Leverkusen, Germany* (CA). The CD1d Tetramer was graciously provided by the National Institute of Health Core Tetramer Facility, Atlanta, GA.All *in vivo* imaging was carried out in the Georgetown-Lombardi Preclinical Imaging Research Laboratory and all flow cytometry analyses were performed in Flow Cytometry & Cell Sorting Shared Resource.

Conflict of interest

Georgetown University filed a patent related to this manuscript. KK, WC, and AK are named as inventors on this application and declare that as a potential conflict of interest. The remaining authors declare that the research was conducted in the absence of any commercial or financial relationships that could be construed as a potential conflict of interest.

Publisher's note

Author's disclaimer

The views expressed in this manuscript reflect the results of research conducted by the authors and do not necessarily reflect the official policy or position of the Department of the Navy, Department of Defense, or the United States Government.

JL is a military service member. This work was prepared as part of official duties. Title 17, USC, Section 105 provides that Copyright protection under this title is not available for any work of the U.S. Government and defines a U.S. Government work as a work prepared by a military service member or employee of the U.S. Government as part of that person's official duties.

Supplementary material

The Supplementary Material for this article can be found online at: https://www.frontiersin.org/articles/10.3389/fimmu.2022.898799/full#supplementary-material

References

1. Zhu H, Zhang Q, Chen G. Cxcr6 deficiency ameliorates ischemia-reperfusion injury by reducing the recruitment and cytokine production of hepatic nkt cells in a mouse model of non-alcoholic fatty liver disease. *Int Immunopharmacol* (2019) 72:224–34. doi: 10.1016/j.intimp.2019.04.021

2. Jegatheeswaran S, Siriwardena AK. Experimental and clinical evidence for modification of hepatic ischaemia-reperfusion injury by n-acetylcysteine during major liver surgery. *HPB (Oxford)* (2011) 13(2):71–8. doi: 10.1111/j.1477-2574.2010.00263.x

3. Patel MS, Mohebali J, Coe TM, Sally M, Groat T, Niemann CU, et al. The role of deceased donor liver biopsy: An analysis of 5449 liver transplant recipients. *Clin Transplant* (2020) 34(5):e13835. doi: 10.1111/ctr.13835

4. Hueper K, Lang H, Hartleben B, Gutberlet M, Derlin T, Getzin T, et al. Assessment of liver ischemia reperfusion injury in mice using hepatic T2 mapping: Comparison with histopathology. *J Magn Reson Imaging* (2018) 48(6):1586–94. doi: 10.1002/jmri.26057

5. Ranjit S, Dobrinskikh E, Montford J, Dvornikov A, Lehman A, Orlicky DJ, et al. Label-free fluorescence lifetime and second harmonic generation imaging microscopy improves quantification of experimental renal fibrosis. *Kidney Int* (2016) 90(5):1123–8. doi: 10.1016/j.kint.2016.06.030

6. Thorling CA, Liu X, Burczynski FJ, Fletcher LM, Gobe GC, Roberts MS. Multiphoton microscopy can visualize zonal damage and decreased cellular metabolic activity in hepatic ischemia-reperfusion injury in rats. *J BioMed Opt* (2011) 16(11):116011. doi: 10.1117/1.3647597

7. Rakhshandehroo M, van Eijkeren RJ, Gabriel TL, de Haar C, Gijzel SMW, Hamers N, et al. Adipocytes harbor a glucosylceramide biosynthesis pathway involved in inkt cell activation. *Biochim Biophys Acta Mol Cell Biol Lipids* (2019) 1864(8):1157–67. doi: 10.1016/j.bbalip.2019.04.016

8. Tsagaratou A. Unveiling the regulation of Nkt17 cell differentiation and function. *Mol Immunol* (2019) 105:55–61. doi: 10.1016/j.molimm.2018.11.013

9. Godfrey DI, Hammond KJ, Poulton LD, Smyth MJ, Baxter AG. Nkt cells: Facts, functions and fallacies. *Immunol Today* (2000) 21(11):573–83. doi: 10.1016/s0167-5699(00)01735-7

10. Arrenberg P, Maricic I, Kumar V. Sulfatide-mediated activation of type ii natural killer T cells prevents hepatic ischemic reperfusion injury in mice. *Gastroenterology* (2011) 140(2):646–55. doi: 10.1053/j.gastro.2010.10.003

11. Richards JA, Wigmore SJ, Anderton SM, Howie SEM. Nkt cells are important mediators of hepatic ischemia-reperfusion injury. *Transpl Immunol* (2017) 45:15–21. doi: 10.1016/j.trim.2017.08.002

12. Dey N, Szczepanik M, Lau K, Majewska-Szczepanik M, Askenase PW. Stimulatory lipids accumulate in the mouse liver within 30 Min of contact sensitization to facilitate the activation of naive inkt cells in a Cd1d-dependent fashion. *Scand J Immunol* (2011) 74(1):52–61. doi: 10.1111/j.1365-3083.2011.02540.x

13. Van Kaer L, Wu L, Joyce S. Mechanisms and consequences of antigen presentation by Cd1. *Trends Immunol* (2016) 37(11):738–54. doi: 10.1016/j.it.2016.08.011

14. Huh JY, Kim JI, Park YJ, Hwang IJ, Lee YS, Sohn JH, et al. A novel function of adipocytes in lipid antigen presentation to inkt cells. *Mol Cell Biol* (2013) 33 (2):328–39. doi: 10.1128/MCB.00552-12

15. van Eijkeren RJ, Krabbe O, Boes M, Schipper HS, Kalkhoven E. Endogenous lipid antigens for invariant natural killer T cells hold the reins in adipose tissue homeostasis. *Immunology* (2018) 153(2):179–89. doi: 10.1111/imm.12839

16. Baker SB, Cohen M, Kuo L, Johnson M, Al-Attar A, Zukowska Z. The role of the neuropeptide Y2 receptor in liporemodeling: Neuropeptide y-mediated adipogenesis and adipose graft maintenance. *Plast Reconstr Surg* (2009) 123 (2):486–92. doi: 10.1097/PRS.0b013e3181954c80

17. Coia H, Ma N, Hou Y, Permaul E, Berry DL, Cruz MI, et al. Theaphenon e prevents fatty liver disease and increases Cd4+ T cell survival in mice fed a high-fat diet. *Clin Nutr* (2021) 40(1):110–9. doi: 10.1016/j.clnu.2020.04.033

18. Kurtz R, Libby A, Jones BA, Myakala K, Wang X, Lee Y, et al. Empagliflozin treatment attenuates hepatic steatosis by promoting white adipose expansion in obese tallyho mice. *Int J Mol Sci* (2022) 23(10):5675. doi: 10.3390/ijms23105675

19. Crosignani V, Dvornikov A, Aguilar JS, Stringari C, Edwards R, Mantulin WW, et al. Deep tissue fluorescence imaging and *in vivo* biological applications. *J Biomed Optics* (2012) 17(11):116023. doi: 10.1117/1.JBO.17.11.116023

20. Crosignani V, Jahid S, Dvornikov AS, Gratton E. A deep tissue fluorescence imaging system with enhanced shg detection capabilities. *Microscop Res Technique* (2014) 77(5):368–73. doi: 10.1002/jemt.22354

21. Dvornikov A, Gratton E. Imaging in turbid media: A transmission detector gives 2-3 order of magnitude enhanced sensitivity compared to epi-detection schemes. *Biomed Optics Expr* (2016) 7(9):3747–55. doi: 10.1364/BOE.7.003747

22. Malacrida L, Ranjit S, Jameson DM, Gratton E. The phasor plot: A universal circle to advance fluorescence lifetime analysis and interpretation. *Annu Rev Biophys* (2021) 50:575–93. doi: 10.1146/annurev-biophys-062920-063631

23. Ranjit S, Malacrida L, Jameson DM, Gratton E. Fit-free analysis of fluorescence lifetime imaging data using the phasor approach. *Nat Protoc* (2018) 13(9):1979–2004. doi: 10.1038/s41596-018-0026-5

24. Digman M, Gratton E. The phasor approach to fluorescence lifetime imaging: Exploiting phasor linear properties. In: *Fluorescence lifetime spectroscopy and imaging* (2014) Boca Raton: CRC Press. p. 235–48.

25. Stringari C, Nourse JL, Flanagan LA, Gratton E. Phasor fluorescence lifetime microscopy of free and protein-bound nadh reveals neural stem cell differentiation potential. *PloS One* (2012) 7(11):e48014. doi: 10.1371/journal.pone.0048014

26. Ranjit S, Datta R, Dvornikov A, Gratton E. Multicomponent analysis of phasor plot in a single pixel to calculate changes of metabolic trajectory in biological systems. *J Phys Chem A* (2019) 123(45):9865–73. doi: 10.1021/acs.jpca.9b07880

27. Ranjit S, Dvornikov A, Dobrinskikh E, Wang X, Luo Y, Levi M, et al. Measuring the effect of a Western diet on liver tissue architecture by flim autofluorescence and harmonic generation microscopy. *BioMed Opt Expr* (2017) 8(7):3143–54. doi: 10.1364/BOE.8.003143

28. Vallmitjana A, Dvornikov A, Torrado B, Jameson DM, Ranjit S, Gratton E. Resolution of 4 components in the same pixel in flim images using the phasor approach. *Methods Appl Fluoresc* (2020) 8(3):035001. doi: 10.1088/2050-6120/ab8570

29. Vallmitjana A, Torrado B, Dvornikov A, Ranjit S, Gratton E. Blind resolution of lifetime components in individual pixels of fluorescence lifetime

images using the phasor approach. *J Phys Chem B* (2020) 124(45):10126–37. doi: 10.1021/acs.jpcb.0c06946

30. Torrado B, Malacrida L, Ranjit S. Linear combination properties of the phasor space in fluorescence imaging. *Sensors* (2022) 22(3):999. doi: 10.3390/s22030999

31. Digman MA, Caiolfa VR, Zamai M, Gratton E. The phasor approach to fluorescence lifetime imaging analysis. *Biophys J* (2008) 94(2):L14–6. doi: 10.1529/biophysj.107.120154

32. Ranjit S, Malacrida L, Stakic M, Gratton E. Determination of the metabolic index using the fluorescence lifetime of free and bound nicotinamide adenine dinucleotide using the phasor approach. *J Biophoton* (2019) 12(11):e201900156. doi: 10.1002/jbio.201900156

33. Datta R, Alfonso-Garcia A, Cinco R, Gratton E. Fluorescence lifetime imaging of endogenous biomarker of oxidative stress. *Sci Rep* (2015) 5:9848. doi: 10.1038/srep09848

34. Datta R, Heylman C, George SC, Gratton E. Label-free imaging of metabolism and oxidative stress in human induced pluripotent stem cell-derived cardiomyocytes. *BioMed Opt Expr* (2016) 7(5):1690–701. doi: 10.1364/BOE.7.001690

35. Chong J, Soufan O, Li C, Caraus I, Li S, Bourque G, et al. Metaboanalyst 4.0: Towards more transparent and integrative metabolomics analysis. *Nucleic Acids Res* (2018) 46(W1):W486–W94. doi: 10.1093/nar/gky310

36. Metsalu T, Vilo J. Clustvis: A web tool for visualizing clustering of multivariate data using principal component analysis and heatmap. *Nucleic Acids Res* (2015) 43(W1):W566–W70. doi: 10.1093/nar/gkv468

37. Oliveros JC. *Venny. an interactive tool for comparing lists with venn's diagrams*. Available at: http://bioinfogp.cnb.csic.es/tools/venny/index.html.

38. Kang J, Liggett JR, Patil D, Ranjit S, Loh K, Duttargi A, et al. Type 1 innate lymphoid cells are proinflammatory effector cells in ischemia-reperfusion injury of steatotic livers *Front Immunol* (2022) 13:899525. doi: 10.3389/fimmu.2022.899525.

39. Yoshihara T, Maruyama R, Shiozaki S, Yamamoto K, Kato SI, Nakamura Y, et al. Visualization of lipid droplets in living cells and fatty livers of mice based on the fluorescence of pi-extended coumarin using fluorescence lifetime imaging microscopy. *Anal Chem* (2020) 92(7):4996–5003. doi: 10.1021/acs.analchem.9b05184

40. Chance B, Nioka S, Warren W, Yurtsever G. Mitochondrial nadh as the bellwether of tissue O2 delivery. *Adv Exp Med Biol* (2005) 566:231–42. doi: 10.1007/0-387-26206-7_31

41. Skala MC, Riching KM, Gendron-Fitzpatrick A, Eickhoff J, Eliceiri KW, White JG, et al. *In vivo* multiphoton microscopy of nadh and fad redox states, fluorescence lifetimes, and cellular morphology in precancerous epithelia. *Proc Natl Acad Sci USA* (2007) 104(49):19494–9. doi: 10.1073/pnas.0708425104

42. Stringari C, Cinquin A, Cinquin O, Digman MA, Donovan PJ, Gratton E. Phasor approach to fluorescence lifetime microscopy distinguishes different metabolic states of germ cells in a live tissue. *Proc Natl Acad Sci USA* (2011) 108 (33):13582–7. doi: 10.1073/pnas.1108161108

43. Kolenc OI, Quinn KP. Evaluating cell metabolism through autofluorescence imaging of Nad(P)H and fad. *Antioxid Redox Signaling* (2019) 30(6):875–89. doi: 10.1089/ars.2017.7451

44. Mehta K, Van Thiel DH, Shah N, Mobarhan S. Nonalcoholic fatty liver disease: Pathogenesis and the role of antioxidants. *Nutr Rev* (2002) 60(9):289–93. doi: 10.1301/002966402320387224

45. Ma Y, Gao M, Liu D. N-acetylcysteine protects mice from high fat diet-induced metabolic disorders. *Pharm Res* (2016) 33(8):2033–42. doi: 10.1007/s11095-016-1941-1

46. Fernando B, Marley R, Holt S, Anand R, Harry D, Sanderson P, et al. N-acetylcysteine prevents development of the hyperdynamic circulation in the portal hypertensive rat. *Hepatology* (1998) 28(3):689–94. doi: 10.1002/hep.510280314

47. Licks F, Hartmann RM, Marques C, Schemitt E, Colares JR, Soares Mdo C, et al. N-acetylcysteine modulates angiogenesis and vasodilation in stomach such as DNA damage in blood of portal hypertensive rats. *World J Gastroenterol* (2015) 21 (43):12351–60. doi: 10.3748/wjg.v21.i43.12351

48. Lee PC, Yang YY, Huang CS, Hsieh SL, Lee KC, Hsieh YC, et al. Concomitant inhibition of oxidative stress and angiogenesis by chronic hydrogen-rich saline and n-acetylcysteine treatments improves systemic, splanchnic and hepatic hemodynamics of cirrhotic rats. *Hepatol Res* (2015) 45 (5):578–88. doi: 10.1111/hepr.12379

49. Herz CT, Kiefer FW. Adipose tissue browning in mice and humans. *J Endocrinol* (2019) 241(3):R97–R109. doi: 10.1530/JOE-18-0598

50. Poetter-Lang S, Bastati N, Messner A, Kristic A, Herold A, Hodge JC, et al. Quantification of liver function using gadoxetic acid-enhanced mri. *Abdom Radiol (NY)* (2020) 45(11):3532–44. doi: 10.1007/s00261-020-02779-x

51. Sheng RF, Wang HQ, Yang L, Jin KP, Xie YH, Fu CX, et al. Assessment of liver fibrosis using T1 mapping on gd-Eob-Dtpa-Enhanced magnetic resonance. *Dig Liv Dis* (2017) 49(7):789–95. doi: 10.1016/j.dld.2017.02.006

52. Guimaraes AR, Siqueira L, Uppal R, Alford J, Fuchs BC, Yamada S, et al. T2 relaxation time is related to liver fibrosis severity. *Quant Imaging Med Surg* (2016) 6(2):103–14. doi: 10.21037/qims.2016.03.02

53. Liu J, Jiang S, Zhao Y, Sun Q, Zhang J, Shen D, et al. Geranylgeranyl diphosphate synthase (Ggpps) regulates non-alcoholic fatty liver disease (Nafld)-fibrosis progression by determining hepatic Glucose/Fatty acid preference under high-fat diet conditions. *J Pathol* (2018) 246(3):277–88. doi: 10.1002/path.5131

54. Horie Y, Suzuki A, Kataoka E, Sasaki T, Hamada K, Sasaki J, et al. Hepatocyte-specific pten deficiency results in steatohepatitis and hepatocellular carcinomas. *J Clin Invest* (2004) 113(12):1774–83. doi: 10.1172/JCI20513

55. Hoebinger C, Rajcic D, Hendrikx T. Oxidized lipids: Common immunogenic drivers of non-alcoholic fatty liver disease and atherosclerosis. *Front Cardiovasc Med* (2021) 8:824481. doi: 10.3389/fcvm.2021.824481

56. Alfonso-Garcia A, Smith TD, Datta R, Luu TU, Gratton E, Potma EO, et al. Label-free identification of macrophage phenotype by fluorescence lifetime imaging microscopy. *J BioMed Opt* (2016) 21(4):46005. doi: 10.1117/1.JBO.21.4.046005

57. Wang Y, Nakajima T, Gonzalez FJ, Tanaka N. Ppars as metabolic regulators in the liver: Lessons from liver-specific ppar-null mice. *Int J Mol Sci* (2020) 21(6). doi: 10.3390/ijms21062061

58. Lin CC, Yin MC. Effects of cysteine-containing compounds on biosynthesis of triacylglycerol and cholesterol and anti-oxidative protection in liver from mice consuming a high-fat diet. *Br J Nutr* (2008) 99(1):37–43. doi: 10.1017/S0007114507793881

59. Szatmari I, Pap A, Ruhl R, Ma JX, Illarionov PA, Besra GS, et al. Ppargamma controls Cd1d expression by turning on retinoic acid synthesis in developing human dendritic cells. *J Exp Med* (2006) 203(10):2351–62. doi: 10.1084/jem.20060141

60. Wu L, Parekh VV, Gabriel CL, Bracy DP, Marks-Shulman PA, Tamboli RA, et al. Activation of invariant natural killer T cells by lipid excess promotes tissue inflammation, insulin resistance, and hepatic steatosis in obese mice. *Proc Natl Acad Sci USA* (2012) 109(19):E1143–52. doi: 10.1073/pnas.1200498109

61. Braun NA, Covarrubias R, Major AS. Natural killer T cells and atherosclerosis: Form and function meet pathogenesis. *J Innate Immun* (2010) 2 (4):316–24. doi: 10.1159/000296915

62. Downs I, Liu J, Aw TY, Adegboyega PA, Ajuebor MN. The ros scavenger, nac, regulates hepatic Valpha14inkt cells signaling during fas mab-dependent fulminant liver failure. *PloS One* (2012) 7(6):e38051. doi: 10.1371/journal.pone.0038051

63. Kircheis R, Haasbach E, Lueftenegger D, Heyken WT, Ocker M, Planz O. Nf-kappab pathway as a potential target for treatment of critical stage covid-19 patients. *Front Immunol* (2020) 11:598444. doi: 10.3389/fimmu.2020.598444

64. Burke SJ, Lu D, Sparer TE, Masi T, Goff MR, Karlstad MD, et al. Nf-kappab and Stat1 control Cxcl1 and Cxcl2 gene transcription. *Am J Physiol Endocrinol Metab* (2014) 306(2):E131–49. doi: 10.1152/ajpendo.00347.2013

65. Yeruva S, Ramadori G, Raddatz D. Nf-Kappab-Dependent synergistic regulation of Cxcl10 gene expression by il-1beta and ifn-gamma in human intestinal epithelial cell lines. *Int J Colorectal Dis* (2008) 23(3):305–17. doi: 10.1007/s00384-007-0396-6

66. Oka S, Kamata H, Kamata K, Yagisawa H. Hirata h. n-acetylcysteine suppresses tnf-induced nf-kappab activation through inhibition of ikappab kinases. *FEBS Lett* (2000) 472(2-3):196–202. doi: 10.1016/s0014-5793(00)01464-2

67. Pfeffer LM. The role of nuclear factor kappab in the interferon response. *J Interferon Cytokine Res* (2011) 31(7):553–9. doi: 10.1089/jir.2011.0028

68. Paul S, Schaefer BC. Visualizing tcr-induced polkadots formation and nf-kappab activation in the D10 T-cell clone and mouse primary effector T cells. *Methods Mol Biol* (2015) 1280:219–38. doi: 10.1007/978-1-4939-2422-6_12

69. Paul S, Schaefer BC. A new look at T cell receptor signaling to nuclear factor-kappab. *Trends Immunol* (2013) 34(6):269–81. doi: 10.1016/j.it.2013.02.002

70. Eggenhofer E, Rovira J, Sabet-Baktach M, Groell A, Scherer MN, Dahlke MH, et al. Unconventional rorgammat+ T cells drive hepatic ischemia reperfusion injury. *J Immunol* (2013) 191(1):480–7. doi: 10.4049/jimmunol.1202975

71. An JN, Ryu S, Kim YC, Yoo KD, Lee J, Kim HY, et al. Nk1.1(-) natural killer T cells upregulate interleukin-17 expression in experimental lupus nephritis. *Am J Physiol Renal Physiol* (2021) 320(5):F772–F88. doi: 10.1152/ajprenal.00252.2020

Advantages of publishing in Frontiers

OPEN ACCESS
Articles are free to read for greatest visibility and readership

FAST PUBLICATION
Around 90 days from submission to decision

HIGH QUALITY PEER-REVIEW
Rigorous, collaborative, and constructive peer-review

TRANSPARENT PEER-REVIEW
Editors and reviewers acknowledged by name on published articles

Frontiers
Avenue du Tribunal-Fédéral 34
1005 Lausanne | Switzerland

Visit us: www.frontiersin.org
Contact us: frontiersin.org/about/contact

REPRODUCIBILITY OF RESEARCH
Support open data and methods to enhance research reproducibility

DIGITAL PUBLISHING
Articles designed for optimal readership across devices

FOLLOW US
@frontiersin

IMPACT METRICS
Advanced article metrics track visibility across digital media

EXTENSIVE PROMOTION
Marketing and promotion of impactful research

LOOP RESEARCH NETWORK
Our network increases your article's readership